

Alma Mater Studiorum - Università di Bologna

DOTTORATO DI RICERCA IN

SCIENZE CHIMICHE

Ciclo XXIV

Settore Concorsuale di afferenza: 03/C1-CHIMICA ORGANICA

Settore Scientifico-Disciplinare: CHIM/06-CHIMICA ORGANICA

**THIOPHENE- BASED MATERIALS
FOR PHOTOVOLTAIC APPLICATIONS**

Presentata da: PASQUALE OLIVELLI

Coordinatore Dottorato

Relatore

Prof.ssa ADRIANA BIGI

Prof. MARCO BANDINI

Esame finale anno 2012

Table of Contents

Aim of the Thesis	v
1 General Introduction	1
1.1 A Brief Survey of Semiconductors	1
1.1.1 Elemental Semiconductors	2
1.1.2 Organic Semiconductors	5
1.2 Conductive π -Conjugated Materials	15
1.2.1 Doping	19
1.3 π -Conjugated Polymers	26
1.3.1 Applications in Organic Electronics	36
1.3.1.1 Rechargeable Batteries	38
1.3.1.2 Electronic Devices	39
1.4 References	54

2	<i>Thiophene- Based Materials in Organic Electronics</i>	58
2.1	Introduction	58
2.2	Oligothiophenes in Organic Electronics	63
2.2.1	Oligothiophenes for OFETs	64
2.2.2	Oligothiophenes for OLEDs	69
2.2.3	Synthetic Procedures for Oligothiophenes	76
2.2.3.1	Copper(II)-Promoted Oxidative Homocoupling	77
2.2.3.2	Metals Catalyzed Coupling Methods	78
2.3	Polythiophenes in Organic Electronics	82
2.3.1	Structure and Optical Properties	85
2.3.2	Polythiophenes for OFETs	89
2.3.3	Polythiophenes for OLEDs	91
2.3.4	Polythiophenes for OECDs	94
2.3.5	Synthetic Procedures for Polythiophenes	96
2.3.5.1	Metals Catalyzed Coupling Polymerizations	97
2.3.5.2	MW-Assisted Synthesis of Polythiophenes	105
2.4	References	108
3	<i>Thiophene- Based Materials in Organic Photovoltaics</i>	116
3.1	The Energy Question	116
3.2	Silicon Solar Cells	121
3.2.1	Physics of Silicon Solar Cells	123
3.3	Organic Solar Cells	126
3.3.1	Operating Principles	129
3.3.2	Electronic Donor-Acceptor Interactions	135

3.3.3	Organic Photovoltaic Device Architectures	138
3.3.4	BHJ Solar Cells Morphologies	144
3.3.4.1	PPV:PCBM in BHJ Solar Cells	145
3.4	Oligo- and Polythiophenes for OPVDs	146
3.4.1	Oligothiophenes for OPVDs	147
3.4.1.1	Alpha-Sexithiophenes	148
3.4.1.2	Oligothiophenes-S-S-Dioxide	156
3.4.1.3	Alternative Oligothiophenes	163
3.4.2	Polythiophenes for OPVDs	164
3.4.2.1	P3HT-PCBM in BHJ Solar Cells	166
3.4.2.2	New Materials for Alternative Approaches	174
3.5	Stability of Organic Solar Cells	175
3.6	References	176

4 A Successful Chemical Strategy to Induce Oligothiophene Self-Assembly into Fibers with Tunable Shape and Function **184**

4.1	Introduction	184
4.2	Results and Discussion	187
4.3	Conclusions	202
4.4	Experimental Part	203
4.4.1	General	203
4.4.2	Materials	206
4.4.3	^1H NMR and ^{13}C NMR	216
4.4.4	UV and PL Spectra of Octamers 9 and 11-13	221
4.4.5	Optical Microscopy of 9,11,12,13 and SEM of 13	222
4.4.6	Fluorescence Microscopy and LSCM images of 12	224

4.4.7	Cyclic Voltametry	224
4.4.8	Electrical Characterizations	227
4.5	References	235
5	BHJ Solar Cells based Head-to-Head Thiophene Hexadecamers	238
5.1	Introduction	238
5.2	Results and Discussion	240
5.3	Conclusions	249
5.4	Experimental Parts	250
5.4.1	General	250
5.4.2	Materials	252
5.4.3	^1H NMR and ^{13}C NMR	256
5.5	References	260
	Conclusions	261

Aim of the Thesis

Thiophene oligomers (**OTs**) and polymers (**PTs**) are currently attracting remarkable attention as organic materials showing semiconducting, fluorescent, nonlinear optical and liquid crystalline properties.

All these properties can be fine-tuned through minor structural modifications.

As a consequence, thiophene oligomers and polymers are among the most investigated compounds for applications in organic electronics, optoelectronics and thin film devices such as field effect transistors (**FETs**), light emitting diodes (**LEDs**) and photovoltaic devices (**PVDs**).¹

Our research aims to explore the self-assembly features and the optical, electrical and photovoltaic properties of a class of thiophene based materials so far scarcely investigated, namely that of oligo- and polythiophenes *head-to-head* substituted with *alkyl* or *S-alkyl* chains.

In particular, we synthesized these compounds in short reaction times, high yields, high purity and environmentally friendly procedures taking advantage of ultrasound (**US**)² and microwave (**MW**)³ enabling technologies in Suzuki-Miyaura cross-couplings.

[1] J. Chen, Y. Cao, *Acc. Chem. Res.*, **2009**, *42*, 1709-1718

[2] V. Paul, A. Sudalai, T. Daniel, K. V. Srinivasan, *Synth. Commun.*, **1995**, *25*, 2401-2405

[3] S. Alesi, F. Di Maria, M. Melucci, D. J. Macquarrie, R. Luque, G. Barbarella, *Green Chem.*, **2008**, *10*, 517-523

1 General Introduction

1.1 A Brief Survey of Semiconductors

A *semiconductor* is usually defined as a material with electrical resistivity lying in the range of 10^{-2} - 10^9 Ω cm.⁴ Alternatively, it can be defined as a material whose *energy-gap* (**Eg**) between the valence band (**VB**) and the conduction band (**CB**) for electronic excitations, lies between zero and about 4 electron volts (eV). Materials with zero **Eg** are metals or semimetals, while those with an **Eg** larger than 3 eV are more frequently known as insulators. There are exceptions to these definitions. For example, terms such as semiconducting diamond (whose **Eg** is about 6 eV) and semi-insulating **GaAs** (with a 1.5 eV **Eg**) are frequently used. **GaN**, which is receiving a lot of attention as optoelectronic material in the blue region, has a **Eg** of 3.5 eV.

The best-known semiconductor is undoubtedly *silicon* (**Si**) even if there are many semiconductors besides **Si**. In fact, many minerals found in nature, such as *zinc-blende* (**ZnS**) *cuprite* (**Cu₂O**) and *galena* (**PbS**), to name just a few, are semiconductors.

Including the semiconductors synthesized in laboratories, the family of semiconductors forms one of the most versatile class of materials known to man.

Semiconductors occur in many different chemical compositions with a large variety of crystal structures. They can be elemental semiconductors, such as **Si**, carbon in the form of C_{60} or nanotubes and selenium (**Se**) or binary compounds such as gallium arsenide (**GaAs**). Many organic compounds, e.g. polyacetylene (**PA**), are semiconductors. Some semiconductors exhibit magnetic (**Cd_{1-x}Mn_xTe**) or ferroelectric (**SbSI**) behavior. Others become superconductors when doped with sufficient carriers (**GeTe** and **SrTiO₃**).

Many of the recently discovered *high-T_c* superconductors have non metallic phases which are semiconductors. For example, **La₂CuO₄** is a semiconductor ($E_g \approx 2$ eV) but becomes a superconductor when alloyed with **Sr** to form **(La_{1-x}Sr_x)₂CuO₄**.

1.1.1 Elemental Semiconductors

The best-known semiconductor is of course the element **Si**. Together with *germanium* (**Ge**), it is the prototype of a large class of semiconductors with similar crystal structures. The crystal structure of **Si** and **Ge** is the same as that of diamond and α -tin (a zero-gap semiconductor also known as "gray" tin). In this structure each atom is surrounded by four nearest neighbor atoms (each atom is said to be four-fold coordinated), forming a tetrahedron. These tetrahedrally bonded semiconductors form the mainstay of the electronics industry and the cornerstone of modern technology. Most of this book will be devoted to the study of the properties of these tetrahedrally bonded semiconductors.

Some elements from the groups **V** and **VI** of the periodical table, such as *phosphorus (P)*, *sulfur (S)*, *selenium (Se)* and *tellurium (Te)*, are also semiconductors (**Figure 1**).

The atoms in these crystals can be three-fold (**P**), two-fold (**S, Se, Te**) or four-fold coordinated. **As** a result, these elements can exist in several different crystal structures and they are also good glass-formers. For example, **Se** has been grown with monoclinic and trigonal crystal structures or as a glass (which can also be considered to be a polymer).

Elemental semiconductors	
Si	Silicon
Ge	Germanium
Compound semiconductors	
AlP	Aluminum phosphide
AlAs	Aluminum arsenide
GaP	Gallium phosphide
GaAs	Gallium arsenide
InP	Indium phosphide

Figure 1. A List of some semiconductor materials.

Summarizing a metal is an excellent conductor of electricity because it is in the presence of a partial overlapping of the **CB** with the **VB**, thus allowing the electrons to move freely throughout the solid, then the conductivity in metals is high because $E_g = 0$.

An insulator is a poor electrical conductor because it has a high E_g between the **VB** and **CB** bands and cannot conduct current, in fact insulators normally cannot promote electrons in sufficient quantity to have acceptable conductivity because $E_g \gg 2.5$ eV (**Figure 2**).

In the case of semiconductors, E_g is not prohibitive (in some cases the order of 1eV) and the promotion can be done with 3 ways:

- by simple heating of the solid so that with increasing temperature and electronic vibration is possible to have electrons in the **CB**
- photoexcitation (irradiation with UV light)
- through chemical doping of the semiconductor with suitable elements that could create in its an excess or electronic gaps (the doped Si with B generates electronic gaps creating a p-type doping while with As the excess electrons are generated creating a n-type doping)

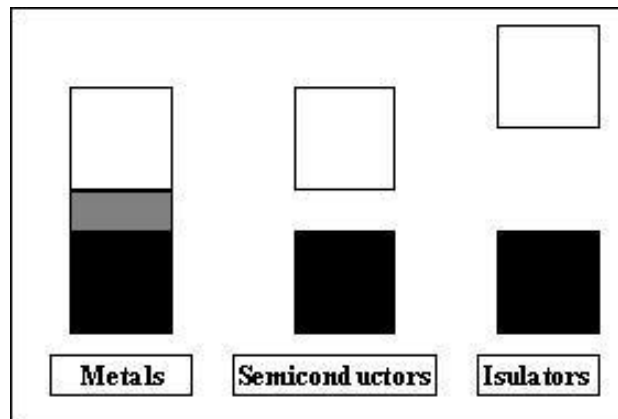


Figure 2. E_g for metals, semiconductor and insulators.

When we speak about semiconductors we think about **Si** or **Ge** which at room temperature show the possibility that some electrons can jump from the **VB** to the **CB**, creating an intrinsic semiconductor. But when we go to drug a semiconductor such as **B** or **As**, respectively we obtain a gap in the electron structure of **Si** achieving a *p-type* doping and in the second case an excess of electrons producing an *n-type* doping, obtained in both cases an extrinsic semiconductor.

1.1.2 Organic Semiconductors

The field of organic electronic is an active emerging technology with immense promise for innovative, convenient and high-performance electronics.^{5,6,7,8} In the late 1970s three researchers found types of plastics capable of being modified to enable them as conducting metal. Conventional plastics are electrical insulators, but the discovery found they also can conduct electricity. It has opened a new era of plastics science and technology to be employed in organic semiconductors.

Inorganic materials are rigid crystalline, which must be extremely pure, and require very precise processing under highly demanding conditions. Organic materials combine novel semiconducting electronic properties with the scope for easy shaping and manufacture of plastics. There is a nearly infinite variety of these organic materials and their properties can be tuned by changing their chemical structure, making them very versatile.⁹

Because of the remarkable properties of these organic materials, they can be used to make a wide range of semiconducting electronic devices, such as *field effect transistors (FETs)*, *light-emitting diodes (LEDs)*, *photovoltaic devices (PVDs)* and even *lasers*.

Organic semiconductor can provide us flat and flexible electronics, and light-emission from these materials is particularly promising when a voltage is applied to a thin film of a semiconducting material to give out light. And it is possible to deposit semiconducting material to greatly simplify the manufacturing process, increase flexibility, and reduce cost.^{10,11,12,13,14,15,16}

Inorganic semiconductor has been widely applied; however, it requires extremely high purity, and needs very precise processing under highly demanding conditions. To overcome those challenges, organic semiconductors are proposed to provide potential solutions. Those advantages are resulted from the great characteristics of organic materials: easy shaping and manufacturing, infinite variety and tunable properties by changing the chemical structure. Organic materials are based on π -conjugated organic oligomers and polymers. In the last decade, organic materials were used to produce plenty of products of devices, because they are large-area, low-cost, plastic substrates and therefore a great of progress have been made in a lot of fields.

Organic semiconductors offer several advantages because of their easy processing, good compatibility with a wide variety of substrates including flexible plastics and opportunities of modifying the structure of organic semiconductor. Also thin films of organic semiconductors are mechanically robust and flexible and possible to get flexible electronics.

The main advantage of organic semiconductor is assembled to a fully flexible insulating film without any substrate. It is possible to expose the gate side of the film to an external medium to apply to any kind of substrate. Compared to *silicon* structures, organic materials have several advantages: low-cost of the technology and possible to achieve fully flexible structures, relatively low voltages, comparable with the performance for solution monitoring and some innovative applications, which are not possible for *silicon* based devices nowadays, for example, system embedded in textiles and smart food packages.

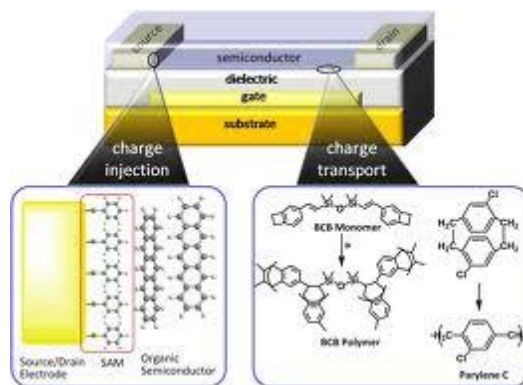


Figure 3. Structure of the organic semiconductor transistor.

The structure of organic semiconductor (**Figure 3**) devices is manufactured by an organic semiconductor uniform and high carrier transport property over a relatively large area. Typical current carriers in organic semiconductors are holes and electrons in π -bonds. Almost all organic solids are insulators. But when their constituent molecules have π -conjugate systems, electrons can move via π -electron cloud overlaps, especially by hopping, tunnelling and related mechanisms.

Mainly due to low mobility, even unpaired electrons may be stable in charge-transfer complexes. Such unpaired electrons can function as current carriers.

This type of semiconductor is also obtained by pairing an electron donor molecule with an electron acceptor molecule.

Charge transport in organic semiconductors is dependent on π -bonding orbitals and quantum mechanical wave-function overlap. In disordered organic semiconductors, there is limited π -bonding overlapping between molecules and conduction of charge carriers (electrons or holes) is described by quantum mechanical tunnelling. Charge transport depends on the ability of the charge carriers to pass from one molecule to another.

Because of the quantum mechanical tunnelling nature of the charge transport, and its subsequent dependence on a probability function, this transport process is commonly referred to as hopping transport.¹⁷ Hopping of charge carriers from molecule to molecule depends upon the energy gap between *HOMO* and *LUMO* levels. Carrier mobility is reliant upon the abundance of similar energy levels for the electrons or holes to move to and hence will experience regions of faster and slower hopping. This can be affected by the temperature and also electric field across the system.

A theoretical study¹⁸ has shown that in a low electric field the conductivity of organic semiconductor is proportional to $T^{-1/4}$ and in a high electric field is proportional to $e^{-(E/aT)}$, where a is a constant of the material. Another study shows that the AC conductivity of the organic semiconductor *pentacene* was frequency-dependent and provided evidence that this behavior was due to its polycrystalline structure and hopping conduction.¹⁹

Organic semiconductors differ from inorganic counterparts in many ways. These include optical, electronic, chemical and structural properties. In order to design and model the organic semiconductors, such optical properties as absorption and photoluminescence need to be characterized.^{20,21}

Optical characterization for this class of materials can be done using UV-visible absorption spectrophotometers and photoluminescence spectrometers. Semiconductor film appearance and morphology can be studied with *atomic force microscopy (AFM)* and *scanning electron microscopy (SEM)*. Electronic properties such as ionization potential can be characterized by probing the electronic band structure with *ultraviolet photoelectron spectroscopy (UPS)*.²²

The charge-carrier transport properties of organic semiconductors are examined by a number of techniques. For example, *time-of-flight (TOF)* and space charge limited current techniques are used to characterize "bulk" conduction properties of organic films. *Organic field effect transistor (OFET)* characterization technique is probing "interfacial" properties of semiconductor films and allows to study the charge carrier mobility, transistor threshold voltage and other **FET** parameters.

OFETs development can directly lead to novel device applications such as organic-based flexible circuits, printable *radio frequency identification tags (RFID)* and active matrix backplanes for displays.²³ Chemical composition and structure of organic semiconductors can be characterized by *infrared spectroscopy*, *secondary ion mass spectrometry (SIMS)* and *X-ray photoelectron spectroscopy (XPS)*.

Modern chemistry enables the synthesis of complex molecules, such as *carbon, hydrogen, oxygen, and nitrogen* atoms. They can be linked together with strong covalent bonds where two neighboring atoms each as addition. *F* or non-covalent interactions, they can be built to complex supramolecular structures.

They can approach nanotechnology; their interactions allow the materials to be tunable and mechanical properties.

Carbon can form four bonds with neighboring carbon atoms or other atoms. Such as *methane (CH₄)*, four valence electrons occupy four *sp³* in and can form four covalent bonds. When two adjacent carbon atoms come together, a bond is formed between two electrons; we call it conjugated where atoms are linked by alternative double bonds.

The contribution of change has been observed in the crystal structure with temperature to the variation of carrier mobility with temperature. With the temperature increasing, there will be slight increase in electron mobility along the crystal direction. Since the changes in crystal lattice dimensions of *anthraquinone* at various temperatures are small, the electronic band structure of organic compounds may be highly structure-sensitive.

Organic semiconductors can be widely classified into two groups on the basis of their molecular weight: conjugated polycyclic compounds of molecular weight less than 1000, and heterocyclic polymers with molecular weight greater than 1000.

There are significant differences between the processing of small molecule organic semiconductors and semiconducting polymers. Thin films of soluble conjugated polymers can be prepared by solution processing methods.

On the other hand, small molecules are quite often insoluble and typically require deposition via vacuum sublimation. Both approaches yield amorphous or polycrystalline films with variable degree of disorder. "Wet" coating techniques require polymers to be dissolved in a volatile solvent, filtered and deposited onto a substrate. Common examples of solvent-based coating techniques include drop casting, spin-coating, doctor-blading, inkjet printing and screen printing.²⁴ Spin-coating is a widely used technique for small area thin film production. It may result in a high material loss. The doctor-blade technique has a minimal material loss and was primarily developed for large area thin film production. Vacuum based thermal deposition of small molecules requires evaporation of molecules from a hot source. The molecules are then transported through vacuum onto a substrate.

Condensation of these molecules on the substrate surface results in thin film formation. Wet coating techniques can be applied to small molecules but to a lesser extent depending on material solubility.

Due to the ease with which they form thin films with large surface area, oligomers and polymers are very useful materials for semiconductors. Small-molecule organic semiconductors may further be classified as linear, two-dimensional fused ring compounds, and heterocyclic oligomers. It is more facile control of charge transport by modifying various molecular parameters.

LED is a semiconductor device that light emits from a solid material, caused by an electrical power source. Its effect is a form of electroluminescence. The composition and condition of the semiconducting material used decide the color of the emitted light also can be infrared, such as visible or near-ultraviolet, infrared emission from *gallium arsenide* (**GaAs**) and other semiconductor alloys.

A phenomenon termed electroluminescence is introduced here. The first **LED** had been born. At that time, the properties of materials were poorly controlled, and the emission process was not well understood. The light-emitting active material was **SiC** crystallites, **GaAs** and **AlGaAs** as used for sandpaper abrasive.

The first example of totally flexible field effect device for chemical detection based on an *organic light-emitting diode* (**OLED**) has been fabricated, which is made by *pentacene* films grown on flexible plastic structures. A similar structure can be used also for detecting mechanical deformations on flexible surfaces, the flexibility of the substrate and the low cost of the employed technology, the production of flexible chemical and strain gauge

sensors can be employed in a variety of innovative applications such as wearable electronics.

Over the last decade, blue **OLEDs** with high efficiencies and advantages have attracted considerable attention for their potential applications to the full color ultra-thin flat panel display. Moreover, blue light can be converted into green or red with the use of proper dyes giving the possibility to generate all colors from the blue emitter. This latter property leads to an important simplification in the design of the **OLEDs** displays. Efficient blue **OLEDs** are doped transport layers in a *p-i-n* type structure.

Below (**Figure 4**) are showed different molecular structures of the organic compounds, while the details (**Figure 5**) of the layer structures belong to two types of devices.

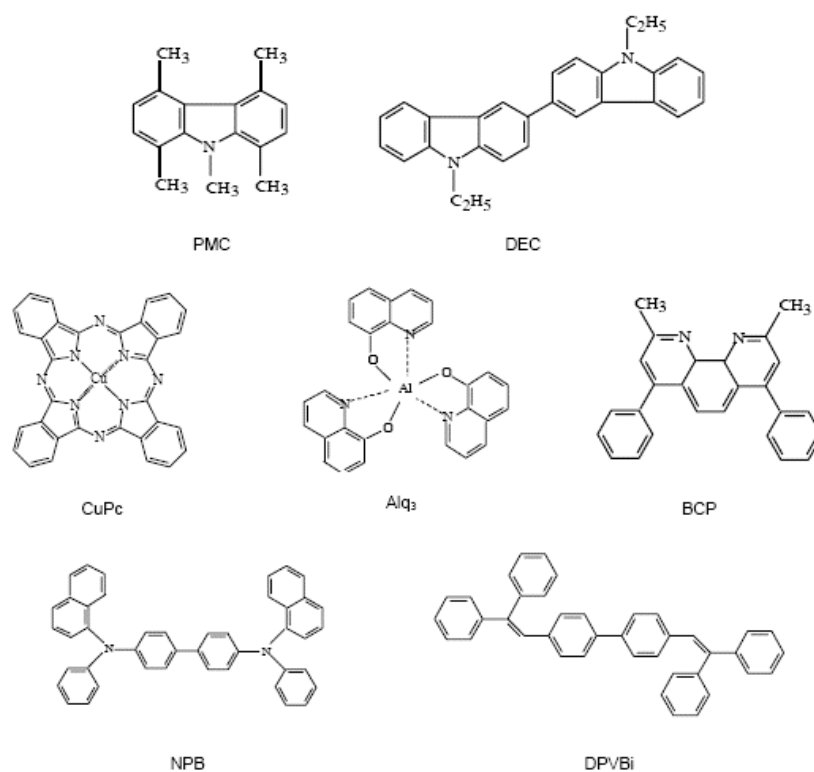


Figure 4. Molecular Structures of the organic materials used for the Blue-OLED.

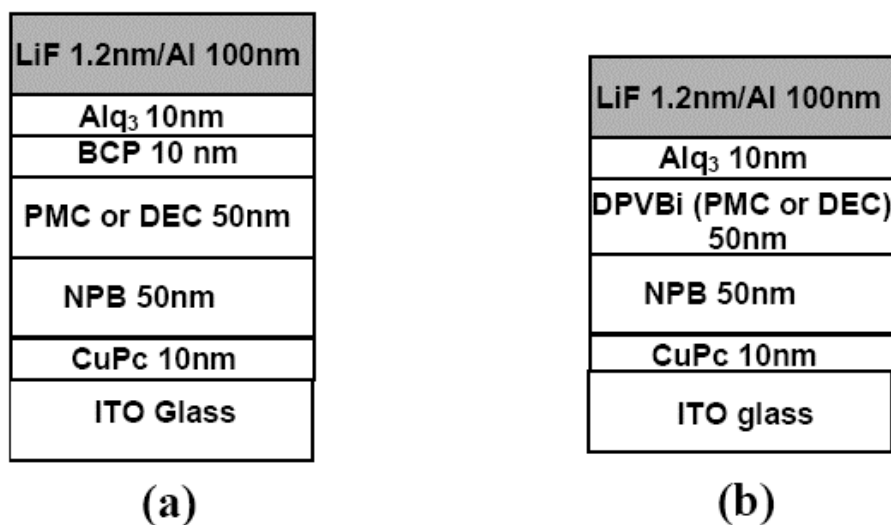


Figure 5. OLED structure with the detail of the thickness and the organic material used in each layers; (a) the emissive layer is DEC or PMC, (b) the emissive layer is DPVBi-doped with DEC or with PMC.

Organic thin-film transistors (OTFTs) use organic semiconductor on organic semiconducting compounds in electronic components, notably computer displays, sensors, smart cards, and *radio-frequency identification (RFID)* tags.

Furthermore organic semiconductors based photoconductors are extensively used in *xerography*; it can add certain combinations of amorphous organic semiconductors replaced amorphous **Si** and **Se** as the active material in this application, which might be considered as the first large scale commercial application of an organic semiconductor. Small molecule and conjugated polymer light-emitting diodes are on the verge of commercialization.

Organic semiconductors pose a range of molecular weight and include small molecules. Because of chemical tenability, organic semiconductors become attractive materials for fabrication of different devices. Organic semiconductors remain the best performance, due to very well ordered structures.

It has been proved that organic materials fabrication is easier and cheaper than *silicon* transistors fabrication, although the carrier mobility is not sufficient fast. In addition, challenges exist in large-scale manufacturing.

Contrary to the *inorganic materials (IMs)*, which have ionic or covalent bonds on entire crystalline solid structure, *organic materials (OMs)* are essentially of independent molecules, and are characterized by weak intermolecular interactions. This implies that an **OM** can be "projected" on molecular scale.

Special attention is paid to *π -conjugated systems*, characterized by the presence of π -molecular orbitals, for their very interesting optical and electronic properties. For different applications in electronics and photonics paths is very important that the **OM** used can be easily processed and deposited in the form of thin film, by evaporation or by solution. Many **OMs** either with low weight that soluble polymers fulfill this demand.

In addition we have that:

- the **OMs** are used as thin film of amorphous structure, thus easily processable on large areas
- the thicknesses used are small (about 100 nm), so the large-scale production is simpler than that of **IMs** (growth of monocrystals, high-temperature processes, etc.)
- all properties (Eg, charge transport, solubility, etc.) can be modified and tuned on the basis to the device to realize, acting on the chemical structure and on the functionality of materials, thanks also to their great variety (polymers, oligomers, dendrimers, organo-metals, pigments, liquid crystals, etc.)

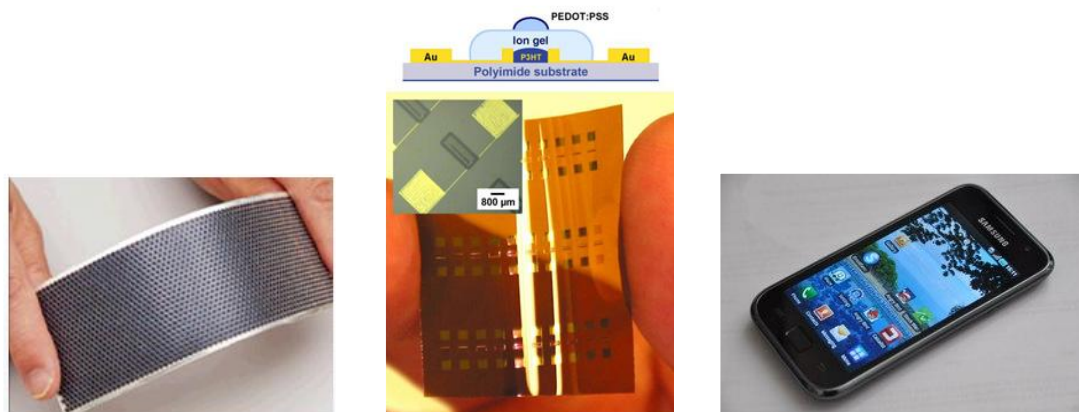


Figure 6. Examples of OMs: solar cell on flexible substrate (left); OFET realized on Polyamide (center); OLED employed on commercial mobile phone (right).

1.2 Conductive π -Conjugated Materials

Usually we tend to think that organic compounds cannot conduct current, and in general we are accustomed to consider its of the insulation. Both electrons and ions can be seen as responsible for the charge carriers' electrical conductivity in solids. Therefore so that a firm can conduct current, is necessary that inside it was available mobile electrons, free to move.

The most notable difference between organic materials and inorganic semiconductors is the electron mobility, which until very recently was dramatically lower in organic compounds than their inorganic counterparts. This difference is diminishing with the invention of new organic materials and the development of new processing techniques.

The interest towards the π -conjugated organic materials as oligomers and polymers for different electronic devices has recently.

The first highly-conductive organic compounds were the *charge transfer* (**CT**) complexes. In the 1950s, researcher reported that polycyclic aromatic compounds formed semi-conducting **CT** complex salts with halogen.²⁵ In the 1954, researchers at *Bell Labs* and elsewhere reported organic **CT** complexes with resistivities as low as $8 \text{ ohms}\cdot\text{cm}$.^{26,27}

The 1964 monograph *Organic Semiconductor*²⁸ cites multiple reports of similar high-conductivity oxidized **PA**.

With notable exception of **CT** complexes (some of which are even superconductors), organic molecules were previously considered insulators or at best weakly conducting semiconductors, so much so that the property of most organic materials, which distinguishes them from metals, is their inability to carry electricity; the insulating properties of organic materials are a significant advantage for many applications of plastics: electrical wires, for example, are protected from shorting by a coating of insulating organic material.

What is the reason of the conductivity into π -conjugated organic molecules?

The answer is that these materials have backbone of contiguous sp^2 hybridized carbon center. One valence electron on each center resides in a p_z orbital, which is orthogonal to the other three sigma-bond; the side overlap of these p_z orbitals produces π -bonds which has a molecular orbitals (π -orbitals) completely different from the overlap of σ -bonds (σ -orbitals) in which the shared electrons are strongly localised.

Therefore the organic compounds which presents only σ -bonds, due to of this electronical immobility, are insulators.

In fact when an organic molecule presents alternated single and double bonds, that one is a conjugated system in which these π -orbitals produce a big, unique and continue π -orbital in whole molecule. This continuity makes the electrons into the π -orbitals strongly delocalised and for this reason have a mobility into the π -conjugated backbone.

The conductivity depends from the electronic structure and it is the result of two important factors:

- numbers of carriers (electrons or holes)
- mobility of charges along the chain

The energy levels of π (bonding) and π^* (antibonding) are separated by an amount of energy, known as **E_g** or **ΔE** (energy-gap), as the number of conjugated double bonds, they create two bands: the **VB** (HOMO) and **CB** (LUMO) (**Figure 7**).

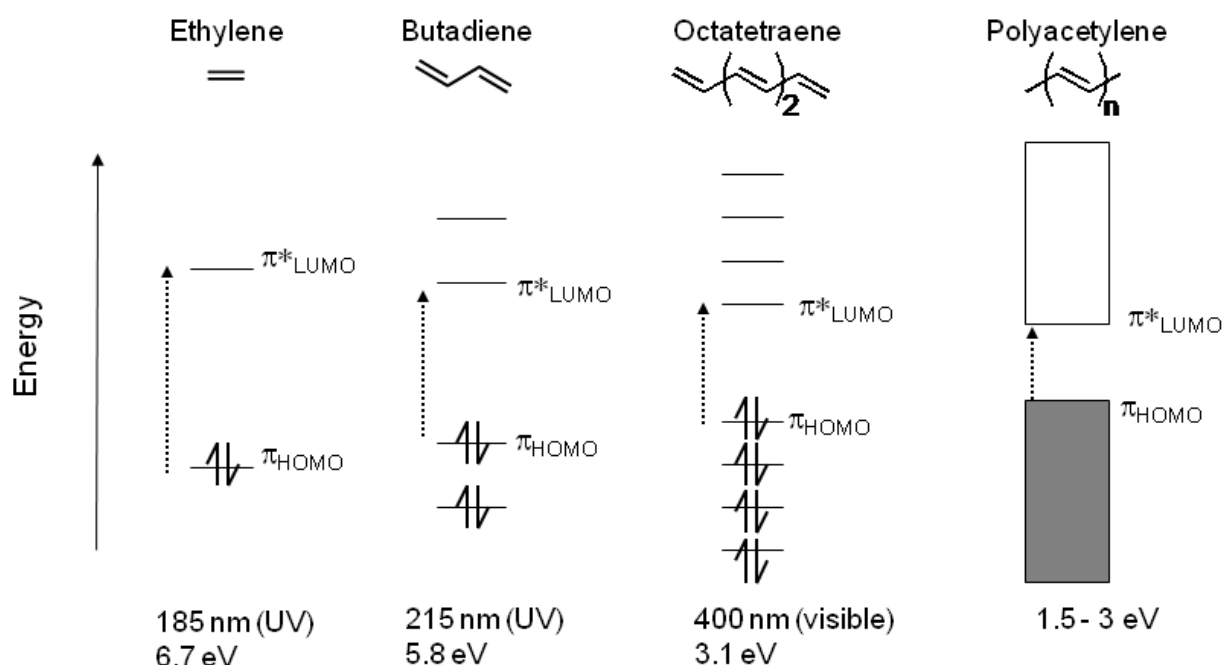


Figure 7. The polyene series with decreasing band gaps and increasing wavelength.

To have a good conductivity, it is necessary to reduce the ΔE between the bands **VB** and **CB**: by so doing, the ΔE tends asymptotically to a limit value, which allows the π -electrons to shift from the neutral state to the excited state and to populate the **CB**.

After the promotion from the **VB** to the **CB** the electrons are free to move under the action of an electric field.

Normally the dimensions of organic material and the π -conjugation degree into its π -backbone, modulate the ΔE between the valence band **VB** and the conduction band **CB**; the ΔE is easily calculable as follow down:

$$\Delta E = h * c / \lambda$$

in which we realise that higher is the π -conjugation degree into the organic material, higher will be the λ value, and for this reason lower will be the ΔE value energy-gap.

However, the conjugation is never very large, because there are structural defects such as: sp^3 hybridized carbon atoms, limited flatness of the chain (often is necessary to modify something to make the polymer actionable) and finally regio-irregularities due to of *head-to-head* or *tail-to-tail* substitutions (see 2.3.1).

1.2.1 Doping

However neutral π -conjugated organic materials are insulators²⁹, and to make these materials electrically conductive (**Figure 8**) we need "to drug" the system introducing species *electron-acceptor* (oxidizing agents) or *electron-donor* (reducing agents); these reagents dopes the π -conjugated compound into its oxidized or reduced form (depends from the organic material typology) making it a charge transporter positive (hole) and negative (electron) respectively.

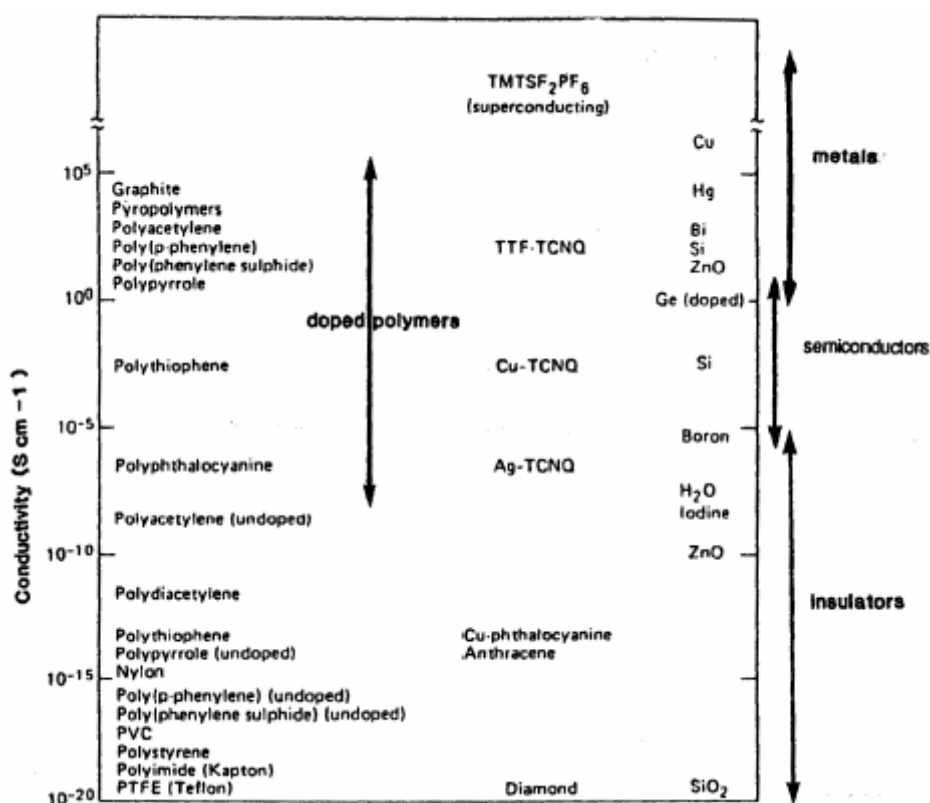


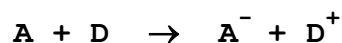
Figure 8. Electronic conductivity of organic polymers, organic molecules and inorganic materials.

The oxidation and reduction reactions with dopant agents which induce high conductivity are termed, using the language of physics semiconductor, *p-doping* and *n-doping* respectively.

An oxidized π -conjugated organic materials will be a *p*-type semiconductor in which the dopant agent modulated the **VB** (HOMO), while a reduced π -conjugated organic materials will be a *n*-type semiconductor in which the dopant agent modulated the **CB** (LUMO). In both cases the energy-gap **VB-CB** (HOMO-LUMO) becomes narrower.

Therefore an organic molecule can conduct current in its, when that electrons (negative charges into *n*-type material) or holes (positive charges into *p*-type material), generated from *n*-doping or *p*-doping respectively, are free to move throughout the π -conjugated backbone. To do that we need that the **VB** and the **CB** had an **Eg** more and less comparable to that of an usual semiconductor, obtaining respectively the **VB** and the **CB** directly from the *HOMO* and from the *LUMO* of the organic molecule.

In the **CT** complex, the *HOMO* derives from the donator electron species, while the *LUMO* from the acceptor electron species:



Generally the features for the *acceptor-electron* species are:

- high electron affinity (LUMO energy of the low)
- presence of *acceptor-electron* groups
- minimum coulombian interactions

while for the *donor-electron* species are:

- low oxidation potential ($D \rightarrow D^{+}$)
- presence of *electron-donor* groups
- maximum polarizability
- small size

However, the process of doping in π -conjugated organic materials is completely different from that used for inorganic materials. In semiconductors doping involves replacing some of the atoms with atoms that have either more or less electrons, while in π -conjugated organic compounds the dopant agent never replace any of the atoms of the molecule; rather they simply act as associates that accept or donate electrons^{30,31} (**Figure 9**):

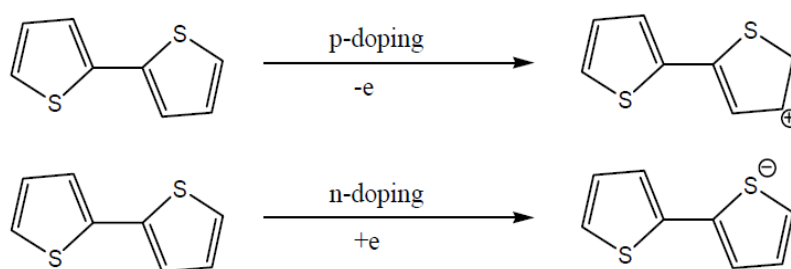


Figure 9. Doping types in bithiophene molecules.

Suitable redox reagents are either chemical *electron acceptors*, or *electron donors* or the process may be electrochemically induced via an electrochemical cell. Because of the redox reaction the material chain is negatively charged in the case of reduction and positively charged in the case of oxidation. To maintain electro-neutrality, appropriate counter ions diffuse in to the material during charging and out of the material during discharging.

In conductive π -conjugated polymers is generated a *cation* or a *cation-radical* for oxidation (oxidative polymerization) of an electron-rich organic system or an *anion* or *anion-radical* for reduction of an electron-poor organic system.

In fact by removing electrons from the π -conjugated polymer (p-doping), or adding electrons into the π -system (n-doping), a charged unit is formed.

The charged unit moves up and down the polymer π -backbone, and is responsible for the macroscopically observed conductivity of the material. Simultaneous oxidation of the conducting polymer and introduction of counter ions, *p-doping*, can be accomplished electrochemically or chemically. Reduction of the conducting polymer, *n-doping*, is much less common than *p-doping*.

When one electron is removed from neutral polymer a polaron is formed having only one charge. Removing a second electron from the polymer segment results not in two polarons, but in the bipolaron, which is predicted to be energetically more favored than the polaron. The reason is that the bipolaron is considerably greater than that for the polaron. The ionization energy required to remove a second electron decreases, or the electron affinity for taking up a second electron increases.

For example the polaron and bipolaron formation of the polythiophene (PT) is shown below (**Figure 10**):

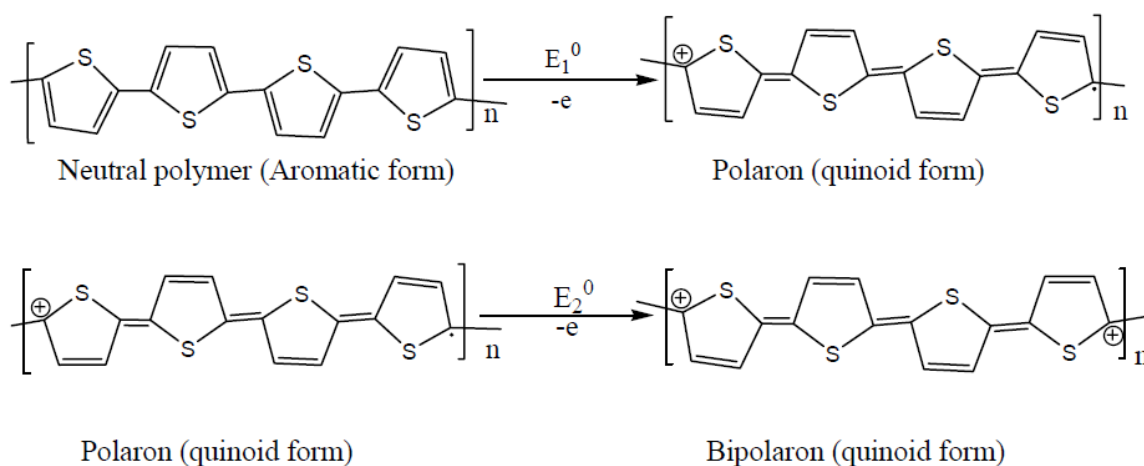


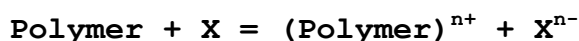
Figure 10. Polaron and Bipolaron formations in polythiophene.

The neutral π -conjugated polymers has full **VB** (HOMO) and empty **CB** (LUMO) separated by an **Eg**.

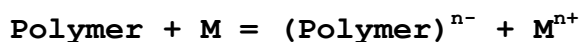
The generation of polarons and bipolarons creates two localized electronic levels, which are energetically separated in the **Eg**.

For polarons the discrete level within the gap is singly charged while for bipolarons it is all empty or all full depending on the doping type. Finally the doping process of conducting polymer can be represented as follows:

For an oxidation process:



For a reduction process:



Where **X** is the oxidizing agent and **M** is the reducing agent. X^{n-} and M^{n+} are the dopant counter *anion* and *cation*, respectively. The oxidizing agents can be **I₂**, **Br₂**, **Cl₂**, **AsF₅**, **FeCl₃**, and **NOPF₆**, and reducing agents like **Li**, **Na**, and **K**. *P-type* doping is more common than *n-type* doping because of the interference of oxygen in the *n-doping* process and also *p-doping* gives higher conductivity and better stability than *n-doping*.

Summarizing the doping effects are multiple; firstly, there is the formation of charge carriers (polaron and bipolaron species on the polymeric skeleton), which move under the influence of the electric field, and the counter ion, secondly, there is a reorganization of the physical structure of the polymer, because the transition from the aromatic structure to that chinoide increases the planarization and results an increase in volume as

the counterions have generally larger dimensions of the repetitive unit creeping themselves between the inner chains.

Finally, the doping is accompanied by a color change. In the doped form, the polymer has a higher conjugations in the chain (due to increased planarization), so it tends to absorb at higher wavelengths (red-shift) and to take blue-green color; in a neutral form it has an absorption toward shorter wavelengths (blue shift) and a red-orange coloration.

The doping is a reversible process. The reversibility of the process is crucial, especially in terms of industrial applicability: for example the creation of rechargeable batteries, where the polymer and the counter ion (the electrolyte itself) participate at more redox cycles of charging and discharging.

By doping, the electrical conductivity increases greatly: polymers such as the **PT**, increase their electrical conductivity of nine orders of magnitude when they are subjected to doping.

In fact generally π -conjugated molecules in their undoped pristine state are insulators and as much the **Eg** *HOMO-LUMO* could be $> 2\text{eV}$, which is too great for thermally activated conduction. Therefore undoped organic materials, such as **PT**, **PA** and others, have a low electrical conductivity of around 10^{-10} to 10^{-8} S/cm. Even at a very low level of doping ($< 1\%$), electrical conductivity increases several orders of magnitude up to values of around 0.1 S/cm.

The electrical properties of conventional materials depend on how the bands are filled. When the bands are filled or empty, no conduction occurs. If the energy-gap *HOMO-LUMO* is narrow, at room temperature thermal excitation of electrons from the **VB** to the **CB** gives rise to conductivity.

When the **E_g** HOMO-LUMO is too wide, thermal excitation at room temperature is insufficient to excite electrons across the gap and become an insulator. The high conductivity of metals is due to a zero band gap (**Figure 11**).

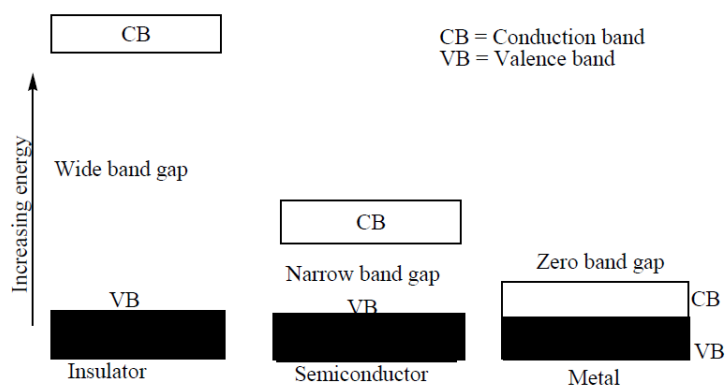


Figure 11. Eg diagram for insulators, semiconductors, and metals.

In the case of conducting materials when an electron is removed from the top of the **VB** (HOMO) of a π -conjugated material a vacancy (hole or radical cation) is created that does not delocalize completely. Only partial delocalization occurs, extending over several monomeric units and causing them to deform structurally. The energy level associated with this *radical cation* represents a destabilized bonding orbital and thus has a higher energy than the energies in the **VB**. In other words, its energy is in the **E_g** HOMO-LUMO.

Despite intensive research, the relationship between morphology, chain structure and conductivity is still understood. Even if generally is assumed that the conductivity should be higher for the higher degree of crystallinity and better alignment of the chains, however this could not be confirmed for materials like *poly(3,4-ethylenedioxythiophene)* (**PEDOT**) and **PT** which are largely amorphous.

1.3 π -Conjugated Polymers

The replacement of inorganic semiconductors by polymers, is considered as highly appealing due to the ease of processing and interesting mechanical properties of the final material.

Polymers are large molecules, or macromolecules, produced by the union of many monomers or smaller repeating units. Conducting polymers have some similarities to conventional polymeric materials, but it is clearly the extensive main chain π -conjugation and its implicit stiffness with respect to chain bending and twisting that most influences the overall physical behavior. In other words conducting polymers contain high conjugation, which may not present in other polymers.

As a novel and very promising class of materials, conjugated semiconducting polymers combine the optical and electronic properties of semiconductors with the processing advantages and special mechanical properties of polymers.

As a result, the research devoted to the synthesis of conjugated oligomers and polymers has experienced a dramatic increase in the past years.^{32,33,34,35,36,37}

The development of substituted conjugated polymers has been the focus of much synthetic research and allows fortuning of the electronic properties by molecular engineering. The synthetic flexibility, the potential ease of processing, e.g. after attaching solubilizing side chains and the possibility of an exact tailoring of the electronic and mechanical properties to accomplish a desired function makes semiconducting organic oligomers and polymers attractive candidates for future applications in electronic devices.^{38,39,40,41,42,43,44}

Variation of the conjugated backbone structure of *poly(para-phenylene)s* (**PPPs**), *poly(paraphenylenevinylene)s* (**PPVs**), *polythiophenes* (**PTs**) or *polyfluorenes* (**PFs**) has been shown to dramatically influence the polymers electronic properties.

For instance, a large number of **PTs** with varying side chain structure have been synthesized and structure-property relationships investigated with a focus on solubility and processability issues and the environmental stability (**Figure 12**).

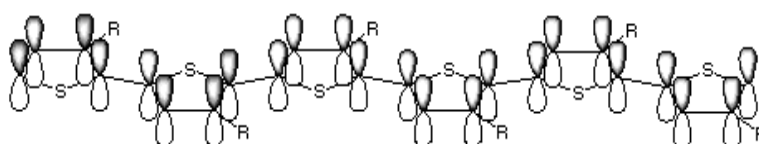


Figure 12. π -backbone of PT, σ bonds and π -orbitals.

Minor changes in the design of the polymeric backbone as well as the structure of the side chains can dramatically influence the characteristics of the polymer. Changes in the substituents are often made to make the materials more suitable for applications, e.g. in polymer electronic devices such as **OFET**,^{45,46} **OLED**,^{47,48} and **OPVD** (**Figure 13**).^{49,50,51,52}

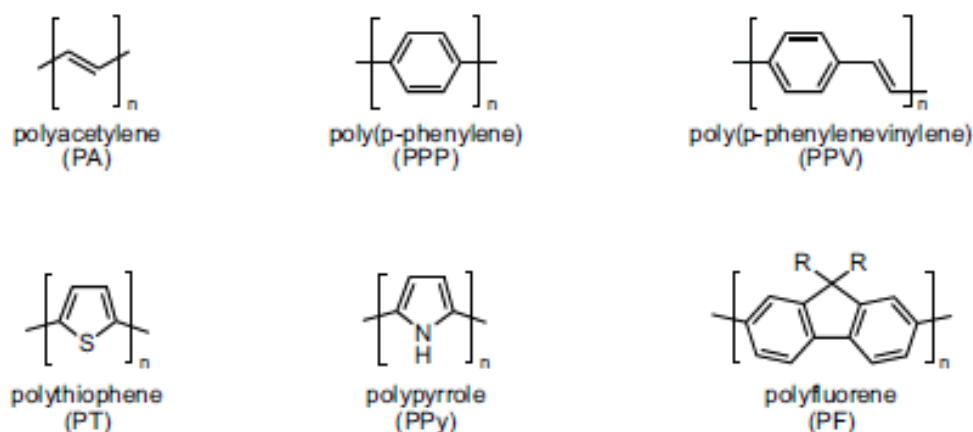


Figure 13. Chemical structure of some common π -conjugated polymers.

Special attention is paid to the **E_g** as it is considered to be a crucial factor in tuning the intrinsic electronic and optical properties.

Therefore, it is of particular importance to understand the evolution of the **E_g** of π -conjugated materials based on their chemical structure.

Conducting polymers have some similarities to conventional polymeric materials, but it is clearly the extensive main chain π -conjugation and its implicit stiffness with respect to chain bending and twisting that most influences the overall physical behavior.

In other words conducting polymers contain high conjugation, which may not present in other polymers.

As conjugated polymers have their electrons organized in bands rather than in discrete energy levels and their ground state energy bands are either completely filled or completely empty, organic semiconductors hardly differ from inorganic semiconductors with respect to their electronic energy levels.

The band structure of conjugated polymers originates from an interaction of the π -orbitals within the repeat unit throughout the main chain, which was shown by theoretical studies comparing the calculated energy levels as a function of oligomer length for **OTs** with $n=1-4$ and **PTs**.⁵³

Starting from a single "monomer" unit addition of each new repeat unit causes additional hybridization of the energy levels until the overlap of the energetic levels results in bands rather than discrete levels (**Figure 14**).

As is the case for inorganic semiconductors, previously we said that the highest occupied band is called the **VB**, while the lowest unoccupied band is called the **CB**, originating from the *HOMO* and the *LUMO* levels of the monomer units respectively, while the energy difference **E_g** is called the band-gap.

Due to the delocalization of the π -electrons, conjugated polymers display semiconducting properties in their electro-neutral state and the ability to support the transport of charge carriers. When the molecular structure is considered, both oligomers and polymers with a narrow band gap (1.5-3.0 eV) represent a fruitful approach towards novel materials for electronic applications.⁵⁴

A versatile variation of the **E_g** can be obtained by smart modification of the macromolecular structure, e.g. by tuning the electronic properties a) towards small band gaps suitable for so-called synthetic metals or infrared emitting polymers, or b) towards a larger **E_g** for a use as UV or blue emitting polymers.

By changing subtle structural features of the oligomer or polymer, like the regioregularity or arrangement and distribution of the chromophoric units, it is possible to design a broad range of polymers with different band gap energies from a basic conjugated structure.

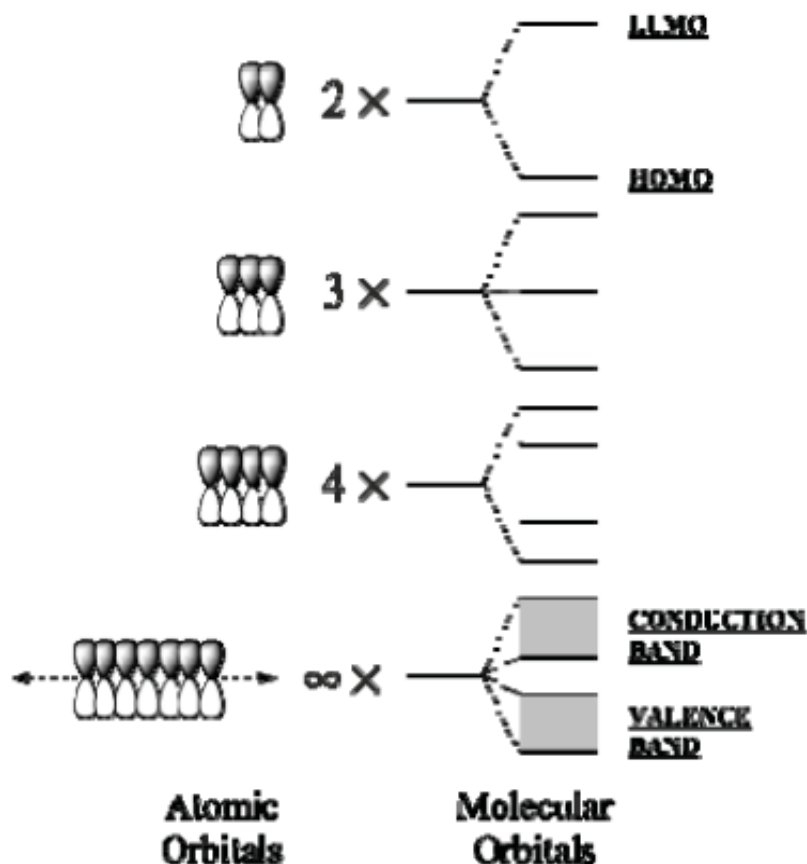


Figure 14. Energy band structure of conjugated polymers emerging from the energetic splitting upon addition of an increasing number of atomic orbitals.

Finally the strong π -electrons delocalization along the polymer chain, generated by the overlap of π -orbitals, is the first step so that a polymer was a semiconductor potential, which through its oxide or reduced forms by doping will become conductive.

The delocalization can also be generated by the interaction of π -electrons with not-bonded electrons furnished from heteroatoms such as *sulfur* and *nitrogen* present in the polymer chains, in this way we understand the electrochemical polymerization of aromatic compounds such as *thiophene*, *pyrrole*, *carbazole*, etc.

In addition to the imminent influence of substituents, the so-called effective conjugation length is an important factor determining the electronic and electrochemical properties of organic semiconductors.

Extended conjugation implies wider bands and a narrower **E_g** in the resulting semiconducting polymer. Therefore, the absorption of a conjugated polymer is red-shifted with an increasing *degree of polymerization (DP)* up to a certain **DP** above which no further red-shift is observed. This threshold is described as the effective conjugation length. The convergence of the **E_g** for **OTs** was investigated by *Bauerle et al* amongst others.

They observed no further changes of the optical properties once the chain had reached 16 repeat units.^{55,56}

Furthermore, the band gap energy is strongly dependent on the so-called *bond length alternation (BLA)*, which refers to the energetic difference between single and double bonds.^{57,58,59,60,61}

As a result, polyaromatic polymers differ from their non-aromatic counterparts $(CH)_x$ as they have a non degenerate ground state. The competing benzoic and quinoid energy states are energetically inequivalent, resulting in a smaller resonance energy for the quinoid form. Stabilization of the quinoid resonance structure of conjugated oligomers and polymers is of particular importance since it underlies most of the attempts to synthesize low **E_g** polymers (**Figure 15-16**).

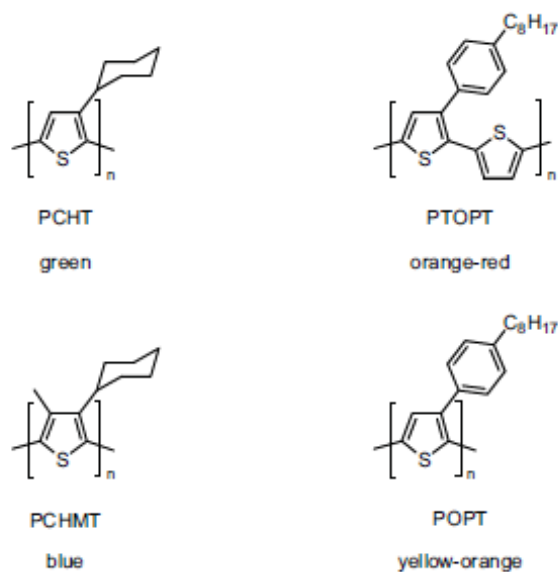


Figure 15. Examples of band gap energy tuning for PTs (the photoluminescence emission color of the polymers is given underneath).

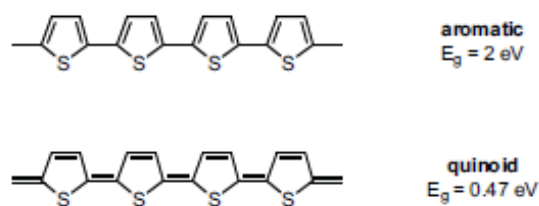


Figure 16. The aromatic form allows the thiophenes to rotate with a certain degree of rotational freedom while the quinoid form forces the rings to align in a planar conformation.

One of the factors determining the energy levels of conjugated polymers is the rotation between neighboring aromatic units around the single bonds with its distinct influence on the effective conjugation length. In the aromatic resonance state (ground state), the repulsion of (bulky) *ortho-side* groups often leads to a non-planar backbone. The consequent reduced overlap of the π -orbitals, which is proportional to the cosine of the twist angle (σ), results in an increased band **Eg**.^{62,63}

A second factor is the aromaticity of the monomeric units, which results in a competition between confinement of the π -electrons within the aromatic rings and delocalization along the π -conjugated chain.⁶⁴

Therefore, to obtain a low band gap energy it is desirable to induce coplanarity of the building blocks along the π -conjugated chain, which can be achieved by an appropriate choice of substituents, fused ring systems (**Figure 17**), or the introduction of additional covalent bonds to rigidify the conjugated backbone in so-called step-ladder or ladder-type structures.

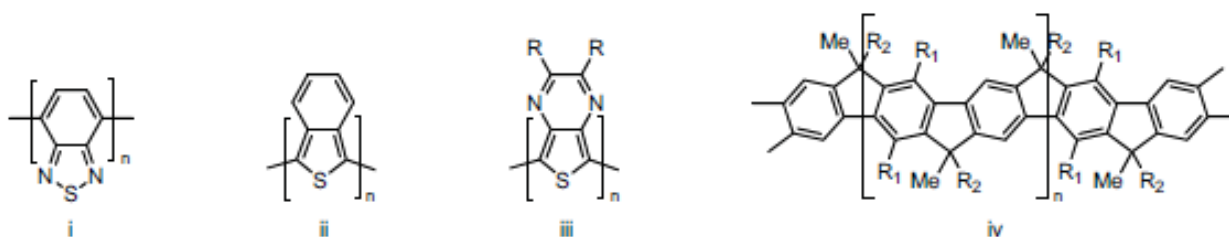


Figure 17. Common fused-ring systems for low band-gap polymers: (i) poly(benzothiadiazole), (ii) poly(isothianaphthalene) (PITN), (iii) poly(thienopyrazine), as well as a ladder-type poly(para-phenylene): (iv) methyl-substituted ladder-type poly(para-phenylene) (MeLPPP).

These type of π -conjugated polymers represent a class of *intrinsic conductive polymers (ICPs)*.

It was in 1977 that Heeger, McDiarmind and Shirakawa found that the **PA**, properly treated, had a conductivity comparable to that of a metal.

In fact among all the organic molecules applied in molecular electronics π -conjugated polymers have attracted strong interest and were nicknamed "materials of the future", for the new generations of optical and electronic devices.

The **ICPs** are organic polymers that conduct electricity;⁶⁵ such compounds may have metallic conductivity or can be semiconductors.

The biggest advantage of conductive polymers is their processability, mainly by dispersion. Conductive polymers are generally not plastics, i.e. they are not thermoformable. But, like insulating polymers, they are organic materials.

They can offer high electrical conductivity but do not show mechanical properties as other commercially used polymers do. The electrical properties can be fine-tuned using the methods of organic synthesis and by advanced dispersion techniques.

The linear-backbone "polymer blacks" (polyacetylene, polypyrrole, and polyaniline) and their copolymers are the main class of conductive polymers. Historically, these are known as melanins. *Poly(p-phenylene vinylene)* (**PPV**) and its soluble derivatives have emerged as the prototypical electroluminescent semiconducting polymers.

Today, the *poly(3-alkylthiophenes)* (**P3HT**) are the archetypical materials for **OPVDs**, **OFETs**, **OLEDs** and other organic devices.

In addition, the ability to insert different monomers in the desired points in the molecules has opened the way for the use of these compounds, by taking advantage of the low density, mechanical strength, ease manufacturing, stability, corrosion resistance, flexibility in low-cost project design.

Disappointing π -conjugated polymers, characterized by the main feature of regular alternation of single and double/triple bond in their polymeric backbone, are generally insoluble and infusible materials.

This insolubility is not surprising since these polymers tend to be conformationally rigid in order to maintain the conjugation of the π -electrons in the backbone. In order to increase the solubility and to control the material properties, many of these **ICPs** have been substituted.

Since most conductive polymers require oxidative doping, the properties of the resulting state are crucial. Such materials are salt-like (polymer salt), which diminishes their solubility in organic solvents and water and hence their processability.

Furthermore, the charged organic backbone is often unstable towards atmospheric moisture. Compared to metals, organic conductors can be expensive requiring multi-step synthesis.

The poor processability for many polymers requires the introduction of solubilizing or substituents, which can further complicate the synthesis.

Experimental and theoretical thermodynamical evidence suggests that conductive polymers may even be completely and principally insoluble so that they can only be processed by dispersion.

The **PA** is the organic material with higher conductivity, but its high sensitivity to air and to moisture does not make it suitable for practical use although it is still being studied as a basic model of this class of compounds.

Other materials, particularly those based thiophene (oligomers and polymers), are much more stable both in neutral and in the electro-conductive form.

1.3.1 Applications in Organic Electronics

The **PTs** and other conducting polymers can be used in many applications and the conductivity is only one parameter that determines whether a material can have practical use. Not surprisingly, the considerable research interest in respect of these polymers, because they permit to combine the conductive properties, usually typical of metallic materials, with those intrinsic of polymers.

That means:

- good mechanical properties
- low density
- thermal and chemical stability
- semiconductor properties if neutral
- conductivity after doping
- processability
- easy and low cost synthesis
- low environmental impact

When the polymers were synthesized for the first time, it was thought that some of their physico-chemical properties could limit their technological applications. Many of them decomposed in air, were insoluble and infusible, but today following the development of new synthetic processes, the possible applications of conducting polymers have multiplied.

The physico-chemical properties must be perfectly adapted to each application, to obtain products that have commercial success.

The conducting polymers possess a combination of properties that place them as an alternative attractive to certain materials currently used in microelectronics.

The potential applications in this field are many, due to their easy chemical manipulation, the wide range of conductivity according to the nature and the amount of dopant agent, their lightness, flexibility and workability.

The most studied and used polymers are **PTs**, *polyaniline (PANI)* and *polypyrrole (PPy)*, and several research works are in the field of lithography, in the dissipation of electrical charges and the creation of conductive tracks on the insulating matrix formed from the polymer self.

In addition, these conductive polymers are applied in so called "metallization", i.e. creation of interconnections between the various electronic components of an integrated circuit. Very important is the property of conducting polymers to absorb electromagnetic radiation at low frequencies: this allows to use them as electromagnetic shields to eliminate the escape of radiation from terminals computers.

Finally, concerning the electronics, the polymers doped are employed in diodes, transistors, conductive tracks of printed circuit and in junction replacing at conventional semiconductor.

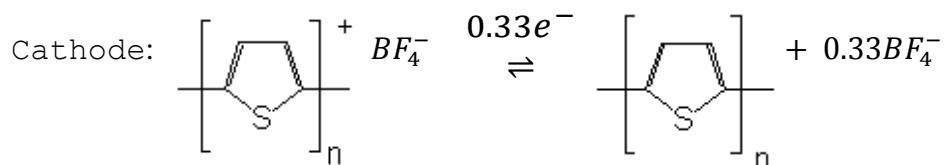
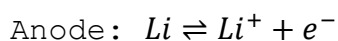
Currently, these devices do not have the same reliability as their forefathers *silicon*, although someday might be very important, in order to replace the limited development of silicon technology.

1.3.1.1 Rechargeable Batteries

From the commercial point of view, this chemistry is exploited very much for the rechargeable batteries.⁶⁶

In the discharging process, the electrons flow from the negative electrode to the positive and reduce the **PPy** from neutral to the doped form. During the charging cycle, however a opposite potential is applied to the electrodes: the polymer is oxidized and takes the electrolyte's anions, *tetrafluoroborate* as counter ions, while to the other electrode, *lithium ions*⁶⁷ are deposited.

Following the same principle can be create a rechargeable *lithium-polythiophene* battery, whose half-reactions are as follows:



The innovations, which determined the success are the possibility to model the geometry of the battery and the extreme lightness of the same.

For years, there are rechargeable button batteries *Li-polymers* for watches, with high capacity and cyclability, manufactured by *Bridgestone-Seiko*, batteries, or folding (in sheets) batteries, created by *Varta-BASF*, extremely versatile, because they vary their capacity by extending or shortening the length of the "roll".

1.3.1.2 Electronic Devices

▪ *Electrochromic Devices*

The electrochromic is a phenomenon of change in color, induced in a material by reversible electrochemical processes: in other words, there are changes in the visible spectral region, associated with a reversible process of doping-dedoping.⁶⁸ This is made possible by the fact that in the **ICPs** the two oxidation states have different **Eg**, hence different color (**Table 1**).

Polymer	Emission
PT (not doping)	Red
PT (doping)	Blue
PPy (not doping)	Yellow-green
PPy (doping)	Blue-Black
PA (not doping)	Yellow
PA (doping)	Green-Blue
PPV (not doping)	Colorless
PPV (doping)	Black

Table 1. Emission of different conductive polymers.

The application of an external potential in the conducting polymers makes move them from the conductive to the insulator with a great chromatic contrast. An electrochromic device is essentially an electrochemical cell in which a liquid or solid electrolyte separates the two electrodes. These are devices that are used in electro-optical systems such as "display" or smart windows.

Important factors for the validity of the final device are:

- optical contrast (color difference between a neutral and doped)
- response time (10-300 ms)
- number of charging-discharging cycles (up to 10^5)

They are used commercially in the manufacture of obfuscate windows car for buildings, cars and car accessories (for example, the rearview mirror that dims at night, when the vehicle behind using lights too high) (**Figure 18-19**).

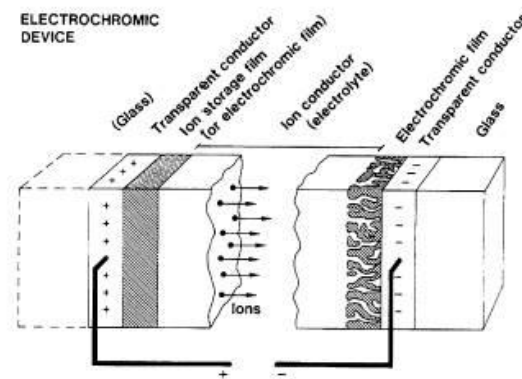


Figure 18. Schematic system of an electrochromic device.

A small device, sold over two million copies, is the battery tester life: it is based on the electrochemical transition of a thin film of PPV, due to a weak potential difference.



Figure 19. Electrochromic device of PPV applied on a battery.

▪ Optical Information Storage

Some polymeric materials are excellent for the manufacture of optical discs of digital video or audio.⁶⁹ The information is transferred to the polymer by means of monochrome laser printers.

The most widely technique used is the ablation technique (hole burning): it creates on the surface of the polymer a series of small holes, which have different length and frequency spacing.

Information can be obtained by measuring the intensity and the modulation of the light reflected by the "pattern" that these holes create on the surface of the disc (**Figure 20**).

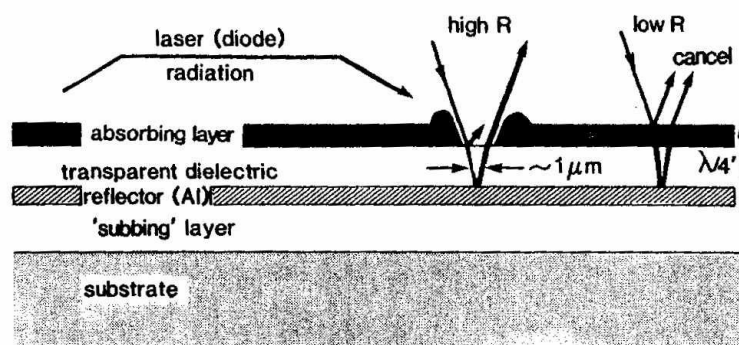


Figure 20. Section of digital optical disc.

The substrate must be optically transparent and is generally made of *polycarbonate (PC)*, *polymethylmethacrylate (PMMA)* or *polyethylene terephthalate (PET)*.

It is covered with a smooth layer that acts as a support for a metal reflector, usually *aluminum* which is covered by a dielectric layer of transparent *poly(alpha-methylstyrene)*; finally is possible to add an absorbent layer where are created the holes are previously mentioned.

The absorbent layer may be formed by a metallic or polymeric composite or molecules dispersed in a polymer matrix.

It is protected by a transparent layer of *polydimethylsiloxane* (**PDMS**): in this way produces a hard "not-erasable", the so-called *DRAW* disk (direct read after write).

The reading is done according to a binary code depending of the time t .

T is the transparent polymeric support (**Figure 21**), R is the metal that acts as a reflective, PC is the protection, P is the cavity created by the laser.

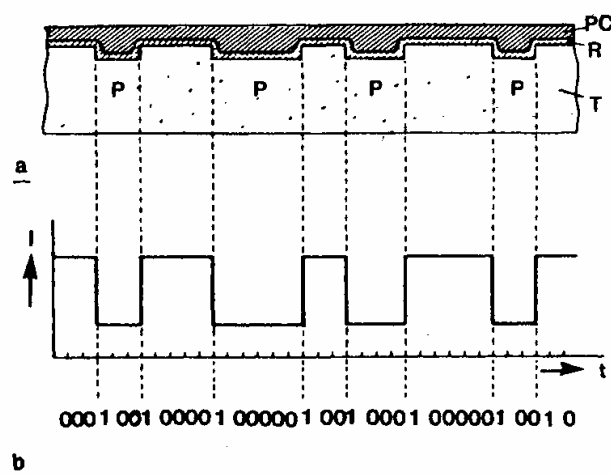


Figure 21. Binary reading of an optical disc.

The polymers can be used also to produce lenses and television screens. In this purpose is used the **PMMA** usually mixed with glass (to keep under control the thermal expansion of the polymer).

▪ Field Effect Transistor (FETs)

A typical device of a polymeric material is the field effect transistor (**Figure 22**), also so called **PFET**.

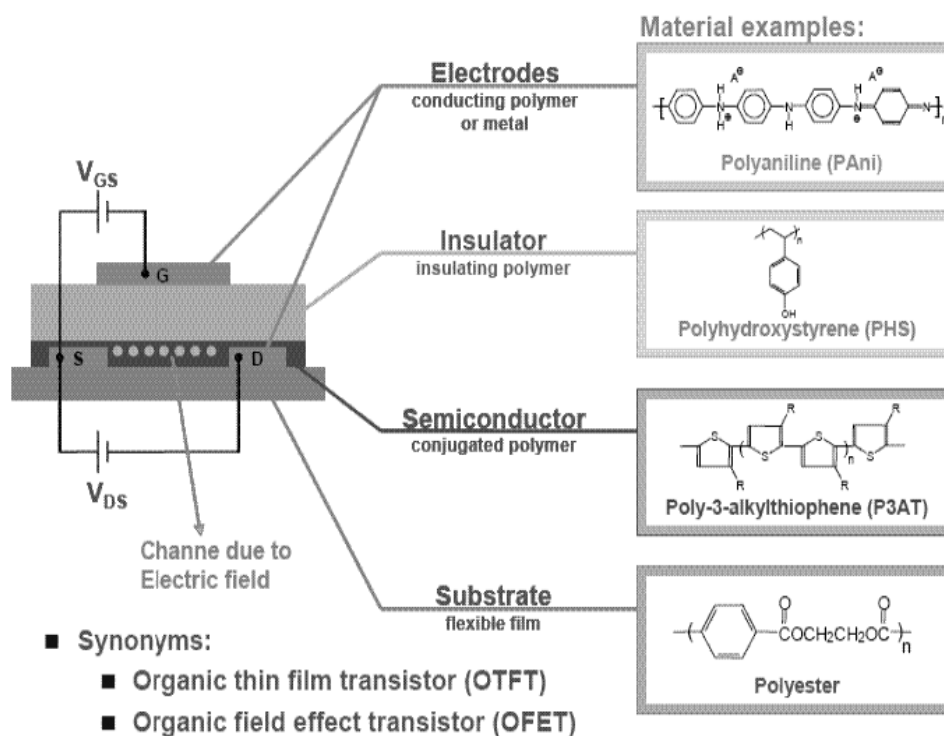


Figure 22. FET that uses organic polymers.

It consists of four electrodes, which make up the *gate (G)*, the *source (S)*, the *drain (D)* and the substrate (not showed). In this case, the gate, the source and the drain are in **PANI**, a conducting polymer.

The conducting channel between source and drain is made of a polymer semiconductor. If the module of the voltage between gate and source (V_{GS}) is above a certain threshold (V_{th}),⁷⁰ between source and drain there is a conducting channel of positive charges.

Applying a voltage between drain and source (V_{DS}) then creates a current between them.

The value of the current (I_{DS}) is controlled by the voltage V_{GS} . The following figure shows the characteristic curves of the **PFET**.

We can see how the intensity I_{DS} varies as a function of the d.d.p and of d.d.p. V_{GS} (**Figure 23**).

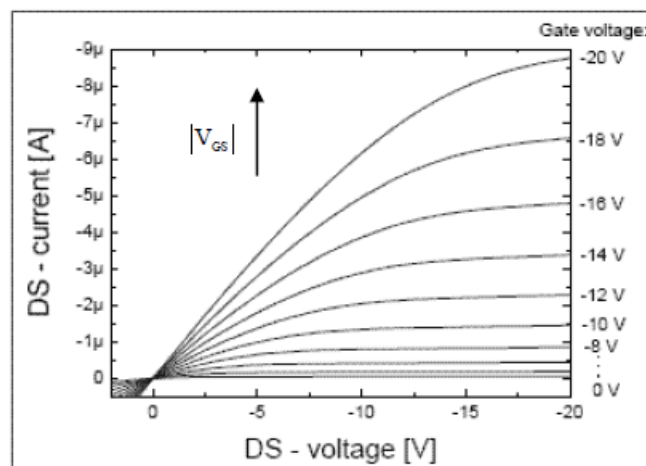


Figure 23. PFET Graph current-voltage.

Furthermore we can see also how the intensity augment when increases the voltage module applied to the gate, while there is a saturation effect when increase V_{DS} .

- **Light Emission Diodes (LEDs)**



Figure 24. LEDs commercially available.

The **LEDs** (**Figure 24**) are part of optoelectronic components, which are generally made of gallium compounds. They change their electrical characteristics, interacting with electromagnetic waves of λ between 1 micron and 0.3 microns.

The **LEDs**, are devices *p-n junction* made with special semiconductors: these semiconducting polymers, when they are crossed by the current, they emit electromagnetic radiations in the VIS-IR spectrum. In particular, when they emit light in the visible spectrum (pink, yellow, green, blue), are known as **LEDs** or **VLEDs**, instead are called **IREDS**, when they emit in the infrared spectrum.

The emission of electromagnetic radiations is due to the high number of recombinations between holes and electrons, by the passage effect of the electrons from the **CB** to the **VB**.

The radiation emitted by the **LED** increases with augmenting of the injected current and with the decreasing of the temperature.

Its spectrum is limited by a narrow band around a specific wavelength, called wavelength peak, which characterizes the color of the emitted radiation.

The **LEDs** are employed as viewers elements and, in particular, in the creation of alphanumeric indicators, i.e. the display, due to the small size achievable, low power absorbed and fast response.

The **OLEDs** are currently used to fabricate thin screens, bright, with low power and cost.

The cathode ray tube screens, however, still offer excellent image quality, but they are bulky, heavy and cannot be used for portable equipments.

Concerning **LCDs** (liquid crystal displays), which are the dominant technology in the field of flat panel displays, they are not very bright and easily readable front only.⁷¹ Only **OLEDs** do not have these disadvantages. The phenomenon on which the **OLEDs** devices are based is in the emission of electromagnetic radiation caused by an electric field applied to a solid (electroluminescence). The radiation is usually in the visible region, but are also possible in the near UV and IR regions (**Figure 25**).

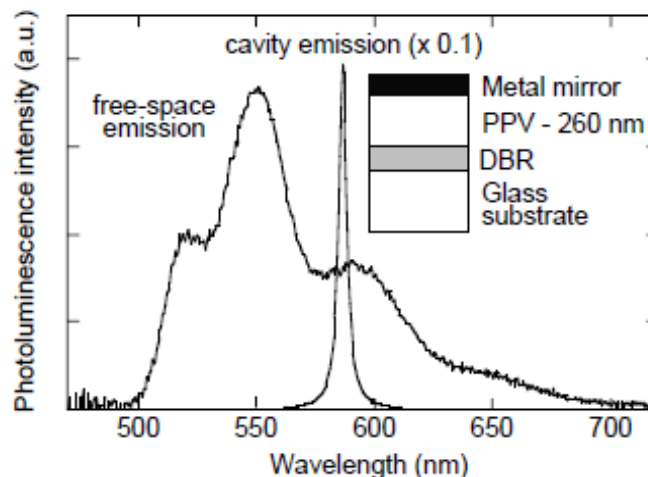


Figure 25. Photoluminescence spectrum of del PPV in which is showed the EL misured for a film on a glass substrate and for micro cable structure (OLEDs devices).

The electroluminescence (**EL**) is, the direct conversion of electrical energy into light energy by means electron transitions between levels. The same phenomenon in solution is defined electrochemiluminescence.

This phenomenon has been observed and studied for the first time in inorganic semiconductors: the first report on **EL** dates back around 1920, when it got light applying an electric field to a sample of **SiC**.⁷²

The interest on a possible application in organic solids was in 1987, when *Van Slik*, belongs to the *Kodak*, published the construction of an organic **LED** that operated at low voltage (< 10 V).

Low voltage operation was possible only when it have reached a technology to prepare uniform layers of organic compounds, having a thickness of a few tens of nanometers.

In 1990 there was the first report on an electroluminescent polymer, the **PPV**. There are many reasons very promising for applications in organic-based devices:

- the almost unlimited possibilities to draw appropriate molecular structures
- the modulation of chemical and physical properties (ionization potentials, electron affinities, etc.)
- the peculiar mechanical properties, which allow to build flexible polymers
- manufacturing technologies easier and less expensive than those needed for organic **LEDs**

Not surprisingly, in the last decade, the research in this field was very wide and, in short time has led to the development of devices that have very comparable performance to that of inorganic **LEDs**. The **OLEDs** devices consist of one or more organic layers, the thickness of a few tens of nanometers, between two electrodes of which at least one is transparent.

The color of the light emitted is characteristic of the chemical species on which occurs after the application of an electric potential. The process is divided into a series of events:

- injection of charges from the electrodes (electrons vacancy)
- transportation charges up to their recombination
- generation of an electronically excited state
- final light emission

All this happens in few microseconds.

In order to optimize the performances and to achieve emissions of various colors, was important the activity of synthesis of new materials. The most important trend is that of the synthesis and of the study of polymers.

As already mentioned, the first polymer used in **OLEDs** was **PPV**. The device, also known as **PLEDs**, consisted of a single layer of **PPV** with a thickness about 70 nm, between a *tin-doped indium oxide* (**ITO**) and an *aluminum* electrodes. The **PPV** is an insoluble polymer in some solvents, a its soluble precursor the makes it film, which with appropriate treatment at high temperature and reactive atmosphere forms the **PPV** (**Figure 26**).

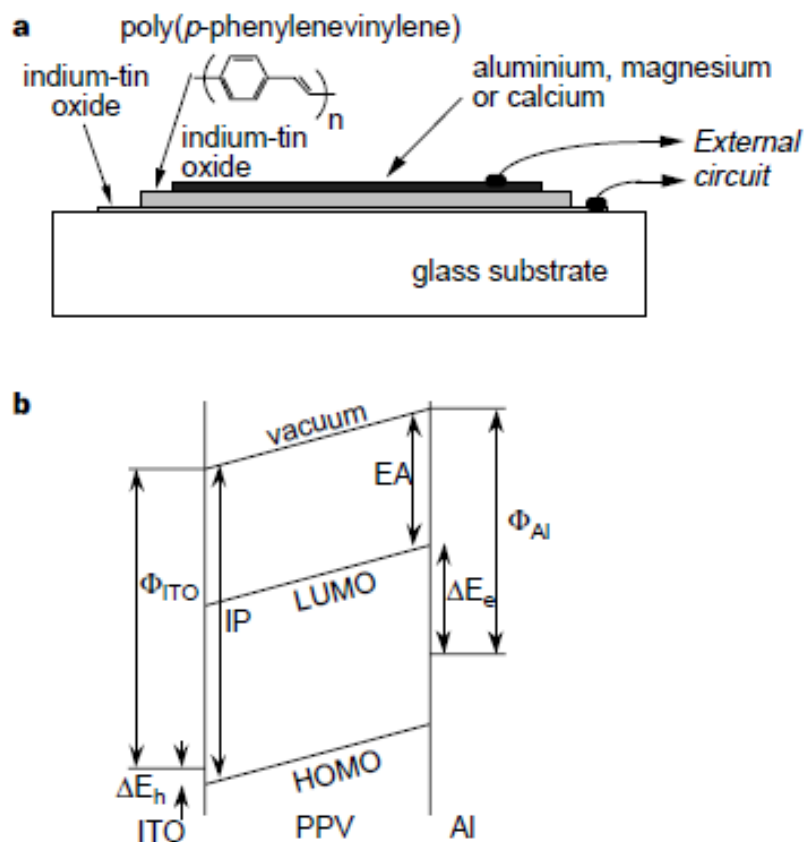


Figure 26. a. Device structure b. Schematic diagram of energy levels of an LED ITO / PPV / Al, which shows the ionization potential (IP) and electron affinity (EA) of the PPV, the ITO electrode work function and metallic (Al) (Φ_{ITO} and Φ_{Al}) and electron injection barriers and vacancies (ΔE_e and ΔE_h).

Today in the field of macromolecules, several organic derivatives for **OLEDs** devices was synthesized, in order to modify the electronical properties and to increase their solubility.

The introduction of functional *electron withdrawing group* (**EWG**) or *electron donating groups* (**EDG**) on the polymeric skeleton alters the ionization potential and the electron affinity, which allow better exchange of electrons between the electrodes.

For example the replacing on *phenylene* ring produces distortion of conjugation, which vary the emission spectrum, while the solubility is increased by long alkyl side chains.

Finally, recent studies are as main subject an enormous variety of copolymers that include either units with an emitter functions either unit that involves the charge transport.

Even if there is something to improve, in particular the duration, the **OLEDs** are emerging as a leader technology for the manufacture of next generation displays.

Summarizing the **OLEDs** devices present these features:

- high brightness
- colored
- high emission
- low consume (they work at low potency)
- 180° view angle
- excellent contrast
- controllable at necessary frequency for a video

Several laboratories, academics and industrials, have achieved considerable improvements in the quality and in the durability of these devices.

The first commercial **OLEDs** were introduced on the japanese market by *Pioneer* in 1997 as a radio panels. A second generation of color displays for radio is recently produced, always by the same company, while *Motorola* and *Sanyo* have recently introduced **OLEDs** screens in the mobile phones, while *Kodak* has marketed a digital camera **OLEDs** display.

There is no doubt that the market for **OLEDs** displays will include a vast range of consumer electronics products, as phones, palmtops, laptops and cameras.

Other classes of interesting π -conjugated organic materials are the oligomers and the polymers based-thiophene, which have excellent conductive properties and for this reasons used in many electronic and electrochromic devices.

▪ **Photovoltaic Cells (PVCs)**

The photovoltaic (**PV**) effect observed for the first time by *Alexandre Edmond Becquerel* in 1839, was an indirect evidence of the corpuscular nature of electromagnetic waves.

This phenomenon occurs when an electron in the **VB** of a material (usually semiconductor) pass to the **CB** due to an absorption of a photon which strike the material.⁷³

Photovoltaic cells (PVCs), take advantage of the photoelectric effect to produce electricity. **PVCs** are the building blocks of all **PV** systems because they are the devices that convert sunlight to electricity.

Commonly known as *solar cells*, individual **PVCs** are electricity-producing devices made of semiconductor materials. **PVCs** come in many sizes and shapes, from smaller than a postage stamp to several inches across.

They are often connected together to form **PV modules** that may be up to several feet long and a few feet wide.

Crystalline *silicon* **PVCs** are the most common photovoltaic cells in use today. They are also the earliest successful **PV** devices, and therefore, crystalline silicon solar cells provide a good example of typical **PV** cell functionality (**Figure 27**).

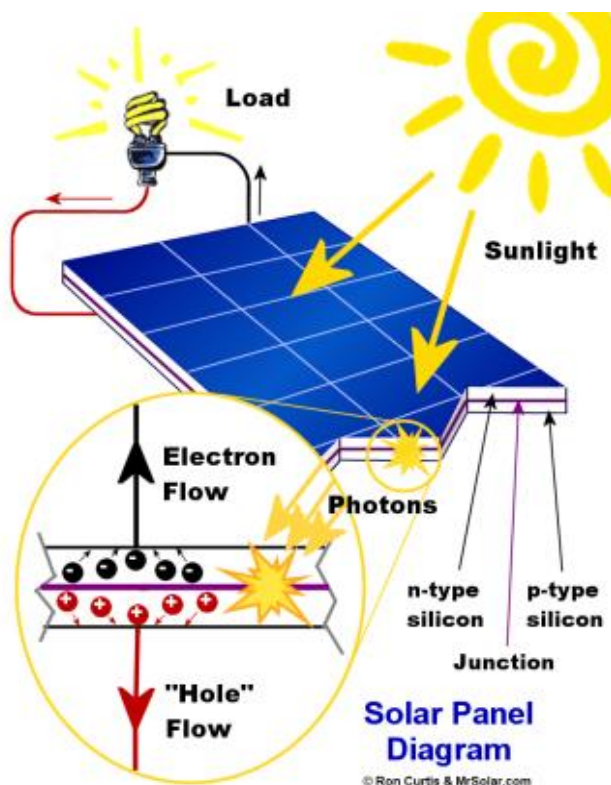


Figure 27. Silicon solar-photovoltaic system.

A notable success has been achieved with the so-called *bulk-heterojunction solar cells* (**BHJ-PVCs**) that exploit the semiconductive properties of these organic materials.⁷⁴

Typical *organic photovoltaic devices* (**OPVDs**) are obtained by mixing of two materials: a polymer *electron-donor* (**D**) *p-type*, which forms the active layer picture, and an polymer *electron-acceptor* (**A**) *n-type*, which must be soluble so that penetrate in the polymer layer electron-donor; all located between two electrodes, one positive **ITO** and a negative **Al**.

Given that in the photovoltaic effect an electron is promoted from **VB** to **CB** by means photon absorbing, therefore it is very important to synthesize a material capable of capturing electromagnetic radiation of the incident photon (the ideal is to have organic materials that cover the range of the wavelengths from UV to near IR, thus having a E_g very narrow).

Furthermore the *p-type* and *n-type* organic materials must have a good match of the electronic levels, in the sense that the *LUMO* of the donor must have an energy higher than the *LUMO* of the acceptor, and the *HOMO* of the acceptor must also have a lower energy of the *HOMO* donor to impede that there was a holes transfer from the donor to the acceptor.

Overall the work functions of cathode and anode, which should facilitate the collection of the electrons and of the holes respectively from the acceptor and from the donor, must therefore have an energetic value compatible with the energy levels *HOMO* and *LUMO* of the organic species (donor and acceptor), and this means that the work functions must have an energetic value between the *HOMO* and the *LUMO* of the donor, and higher than the *HOMO* of the acceptor (**Figure 28**).

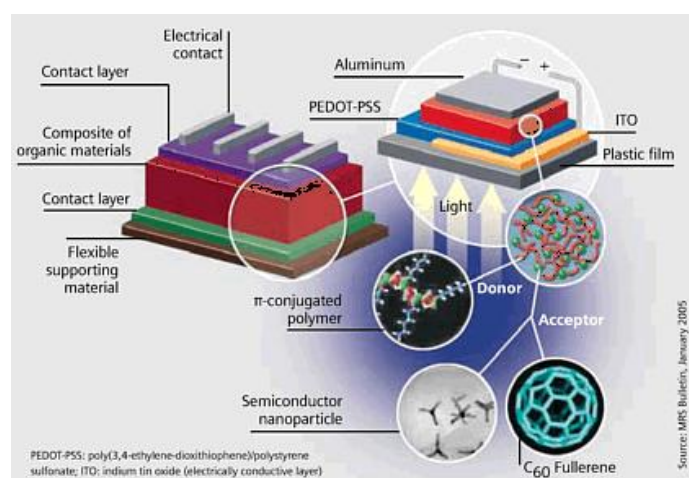


Figure 28. Representative BHJ-PVC design.

The *n*-type organic material more used is a derived of the fullerene, the [6.6]-phenyl C_{61} -butyrric acid methyl ester (**PCBM**), which has better solubility in different organic solvents compared to the fullerene C_{60} . A ideal *p*-type organic material, as for example the **P3HT** or **PPV**, are those which have a lowest **E_g** with high mobility of the positive charges (holes mobility).

Generally the best performance in the **BHJ-PVCs** are obtained by mixing of **P3HT/PCBM** that carry out up to **7-8%** of efficiency, but more details concerning *Organic Photovoltaics*, will be discuss in the *Chapter III*.

1.4 References

-
- [4] P. Y. Yu, M. Cardona, *Fundamentals of Semiconductors*, Springer, **2005**
- [5] H. E. Katz, Z. Bao, and S. J. Gilat, *J. Acc. Chem. Res.*, **34**, **2001**, 359
- [6] N. Madhavan, *Small-molecule organic semiconductors*, **2002**
- [7] A. Dodabalapur, *The future of organic semiconductor devices*, **2000**, 11-14
- [8] J. M. Shi, and C. W. Tang, *Appl. Phys. Lett.*, **2002**, 80
- [9] C. D. Dimitrakopoulos, and D. J. Mascaro, *Organic thin-film transistors: A review of recent advances*, *IBM J. Res. & Dev.*, **45**, **2001**
- [10] C. Reese, M. Roberts, M. M. Ling, and Z. Bao, *Organic thin film transistors, materials today*, 2004, 20-27
- [11] Z. Q. Gao, C. S. Lee, I. Bello, S. T. Lee, R. M. Chen, T. Y. Luh, J. Shi, C. W. Tang, *Appl. Phys. Lett.*, **1999**, 74
- [12] A. P. Kulkarni, A. P. Gifford, C. J. Tonzola, and S. A. Jenekhea, *Appl. Phys. Lett.*, **2005**, 86
- [13] D. Gebeyehu, *et al.*, *Synth. Met.*, **2005**, 148-205
- [14] C. Hosokawa, H. Higashi, H. Nakamura, and T. Kusumoto, *Appl. Phys. Lett.*, **1995**, 67
- [15] C. H. Liao, *et al.*, *Appl. Phys. Lett.*, **2005**, 86
- [16] Y. Z. Wu, *et al.* *Appl. Phys. Lett.* **2003**, 83
- [17] J. Hirsch, *Journal of Physics C: Solid State Physics*, **1979**, **12**, 321

-
- [18] L. Li, G. Meller, H. Kosina, *Microelectronics Journal*, **2007**, *38*, 47-51
- [19] R. Daniel, A. Southard, M. S. Fuhrer, *Applied Physics Letters*, **2009**, *94*
- [20] Brütting, Wolfgang, *Physics of organic semiconductors*, **2005**
- [21] B. Masenelli, S. Callard, A. Gagnaire, J. Joseph, *Thin Solid Films*, **2000**, *364*, 264-268
- [22] W. R. Salaneck,; A. Kahn, *Conjugated polymer and molecular interfaces*, **2002**
- [23] R. Dost, A. Das, M. Grell, *Journal of Physics D: Applied Physics*, **2007**, *40*, 3563-3566
- [24] H. Sirringhaus, C. W. Sele, T. Von Werne, C. Ramsdale, *Semiconducting polymers: Chemistry, Physics and Engineering*, **2007**
- [25] H. Naarmann, *Polymers, Electrically Conducting*, Ullmann's Encyclopedia of Industrial Chemistry, **2002**, Wiley-VCH, Weinheim
- [26] Y. Okamoto, and W. Brenner, *Organic Semiconductors*, **1964**
- [27] H. Akamatsu, H. Inokuchi, and Y. Matsunaga, *Nature*, **1954**, *173*, 168
- [28] Y. Okamoto, and W. Brenner, *Organic Semiconductors*, **1964**, 125-158
- [29] R. D. McCullough, *Adv. Mater.*, *10*, **1998**, 93-116
- [30] M. A. Jean; J. Delhalle; and J. L. Bredas, *Quantum Chemistry Aided Design of Organic Polymers*, World Scientific Publishing, Singapore, **1991**
- [31] H. Lund; and O. Hammerich, *Organic Electrochemistry*, 4th ed., Marcel Dekker Publishers, **2001**
- [32] A. C. Grimsdale, K. Mullen, *Macromol.*, **2007**, *28*, (17), 1676
- [33] V. Coropceanu, J. Cornil, D. A. da Silva, Y. Olivier, R. Silbey, J. L. Bredas, *Chem. Rev.*, **2007**, *107*, 926
- [34] J. Gierschner, J. Cornil, H. J. Egelhaaf, *Adv. Mater.*, **2007**, *19*, 173
- [35] M. H. Chang, M. J. Frampton, H. L. Anderson, L. M. Herz, *Phys. Rev. Lett.*, **2007**, *98*, 027402
- [36] H. Mart, *Des. Monom. Polym.*, **2006**, *9*, 551
- [37] M. Gholami, R. R. Tykwinski, *Chem. Rev.*, **2006**, *106*, 4997
- [38] J. Roncali, P. Leriche, A. Cravino, *Adv. Mater.*, **2007**, *19*, 2045
- [39] L. G. Li, G. H. Lu, X. N. Yang; E. L. Zhou, *Chin. Sci. Bull.*, **2007**, *52*, 145
- [40] D. S. Bag, K. U. B. Rao, *J. Polym. Mater.*, **2006**, *23*, 225
- [41] J. Roncali, *Macromol. Rapid Commun.*, **2007**, *28*, 1761
- [42] Y. Y. Liang, H. B. Wang, S. W. Yuan, Y. G. Lee, L. P. Yu, *J. Mater. Chem.*, **2007**, *17*, 2183
- [43] A. R. Murphy, J. M. J. Frechet, *Chem. Rev.*, **2007**, *107*, 1066

- [44] A. Facchetti, *Materials Today*, **2007**, *10*, 28
- [45] A. Bilge, A. Zen, M. Forster, H. B. Li, F. Galbrecht, B. S. Nehls, T. Farrell, D. Neher, U. Scherf, *J. Mater. Chem.*, **2006**, *16*, 3177
- [46] Y. D. Park, J. A. Lim, H. S. Lee, K. Cho, *Materials Today*, **2007**, *10*, 46
- [47] S. Grigalevicius, L. Ma, Z. Y. Xie, U. Scherf, *J. Polym. Sci.*, **2006**, *44*, 5987
- [48] N. Koch, *Chem. Phys. Chem.*, **2007**, *8*, 1438
- [49] S. Gunes, H. Neugebauer, N. S. Sariciftci, *Chem. Rev.*, **2007**, *107*, 1324
- [50] M. Koppe, M. Scharber, C. Brabec, W. Duffy, M. Heeney, I. McCulloch, *Adv. Funct. Mater.*, **2007**, *17*, 1371
- [51] A. Tsami, T. W. Bunnagel, T. Farrell, M. Scharber, S. A. Choulis, C. J. Brabec, U. Scherf, *J. Mater. Chem.*, **2007**, *17*, 1353
- [52] C. Waldauf, M. Morana, P. Denk, P. Schilinsky, K. Coakley, S. A. Choulis, C. J. Brabec, *Appl. Phys. Lett.*, **2006**, *89*
- [53] U. Salzner, J. B. Lagowski, P. G. Pickup, R. A. Poirier, *Synth. Met.*, **1998**, *96*, 177
- [54] B. C. Thompson, Y. G. Kim, J. R. Reynolds, *Macromolecules*, **2005**, *38*, 5359
- [55] P. Bauerle, T. Fischer, B. Bidlingmeier, A. Stabel, J. P. Rabe, *Angew. Chem.*, **1995**, *34*, 303
- [56] P. Bauerle, *Adv. Mater.*, **1992**, *4*, 102
- [57] Q. T. Zhang, J. M. Tour, *J. Am. Chem. Soc.*, **1997**, *119*, 5065
- [58] A. Ajayaghosh, *Chem. Soc. Rev.*, **2003**, *32*, 181
- [59] M. Karikomi, C. Kitamura, S. Tanaka, Y. Yamashita, *J. Am. Chem. Soc.*, **1995**, *117*, 6791
- [60] J. Kastner, H. Kuzmany, D. Vegh, M. Landl, L. Cuff, M. Kertesz, *Macromolecules*, **1995**, *28*, 2922
- [61] T. T. Hung, S. A. Chen, *Polymer*, **1999**, *40*, 3881
- [62] R. S. Mulliken, C. A. Rieke, W. G. Brown, *J. Am. Chem. Soc.*, **1941**, *41*
- [63] J. L. Bredas, G. B. Street, B. Themans, J. M. Andre, *J. Chem. Phys.*, **1985**, *83*, 1323
- [64] V. Hernandez, C. Castiglioni, M. Delzoppo, G. Zerbi, *Phys. Rev. B*, **1994**, *50*, 9815
- [65] G. Inzelt, *Conducting Polymers: A New Era in Electrochemistry*, Springer, **2008**, 265-269

- [66] D. Linden, T. B. Reddy, *Handbook Of Batteries 3rd Edition*, McGraw-Hill, New York, **2002**
- [67] K. E. Aifantis et al, *High Energy Density Lithium Batteries: Materials, Engineering, Applications*, Wiley-VCH, **2010**
- [68] B. Lamontagne, P. Barrios, C. Py, and S. Nikumb, *The next generation of switchable glass: the Micro-Blinds*, **2009**, 637-639
- [69] M. Albert, and P. López, *Science*, **2011**, 332, 60-65
- [70] J. P. Colinge, C. A. Coling, *Physics of Semiconductor Devices*, Springer, **2002**, 233
- [71] D.J.R. Cristaldi, S. Pennisi, F. Pulvirenti, *Liquid Crystal Display Drivers - Techniques and Circuits*, Springer, **2009**
- [72] R. Khormaei, et al., *High Resolution Active Matrix Electroluminescent Display*, Society for Information Display Digest, **1994**, 137
- [73] R. W. Collins, A. S. Ferlauto, G. M. Ferreira, C. Chen, J. Koh, R. J. Koval, Y. Lee, J. M. Pearce, C. R. Wronski, *Solar Energy Materials and Solar Cells*, **2003**, 78, 143-180
- [74] R. Po, R. Fusco, L. Meda, F. Ferrazza, *Le celle fotovoltaiche organiche e polimeriche*, **2008**, 24-39

2 Thiophene- Based Materials in Organic Electronics

2.1 Introduction

Oligo- and polythiophenes (**OTs** and **PTs**) are among the best investigated and most frequently used π -conjugated materials, in particular as active components in organic electronic devices, molecular electronics and photonic field.^{75,76}

Since the discovery that π -conjugated oligomers and polymers can be successfully implemented as active component in organic electronic devices, **OLEDs** and lasers, **OFETs**, integrated circuits and **OPVDs**, the field of organic conjugated materials and organic electronics literally exploded in this area and a tremendous development took place.

The vision to produce cheap (printable) electronics also on a large scale triggered extensive research in academia and even more in industry, expecting huge markets and many emerging companies and divisions worldwide.

The most prominent and frequently used materials are doubtless *poly(3,4-ethylenedioxythiophene)-poly(styrenesulfonate)* (**PEDOT-PSS**),^{77,78,79} in conducting and hole-transport layers of **OLEDs** and **OPVDs** and also the so-called regioregular or *head-to-tail* coupled **P3HT**,^{80,81,82} as a semiconductor in **OFETs** and **OPVDs**.

Both are rather rare examples of commercially produced conjugated polymers (**Figure 29**).

Parallel to the remarkable development of π -conjugated polymers with applications in the conducting and semiconducting state, a renaissance of **OTs** was launched in 1989 when *Garnier and co-workers* found that also shorter conjugated oligomers such as α -*sexithiophene* (**6T**) can be used as a material and active semiconductor in **OFETs**.^{83,84}

Later, the implementation of structurally defined *end-capped oligothiophenes* (**EC5T-EC7T**) in **OLEDs**⁸⁵ was demonstrated in 1993 and of α -*quinque* (**5T**) and *octithiophene* (**8T**) in **OSCs**⁸⁶ in 1995 (**Figure 30**).

Furthermore, it turned out that the structurally defined and monodisperse oligomers are excellent model compounds for the corresponding polydisperse polymers which include chain length distributions, defects and interruptions of the conjugated chains.⁸⁷

The monitoring of various properties as a function of the chain length allows the establishment of valuable structure-property relationships and extrapolations to the polymer.⁸⁸

For nearly all basic conjugated polymers, manifold series of corresponding oligomers have been produced and finally this development led to a division of organic electronics into two worlds or philosophies.

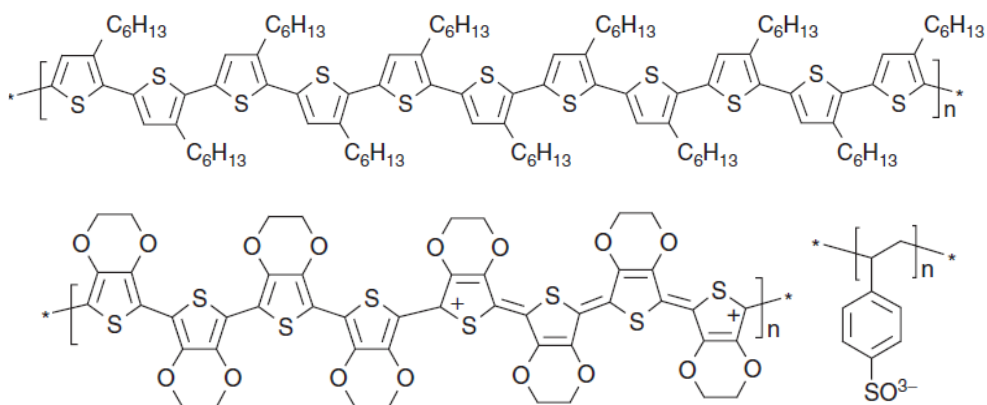


Figure 29. P3HT and PEDOT:PSS thiophene-based materials.

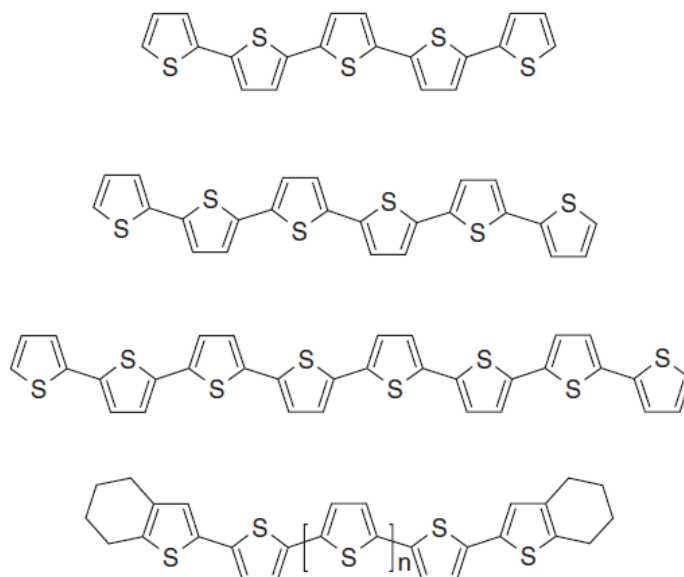


Figure 30. Different oligothiophenes used in organic electronics.

On one side conjugated polymers are used which can be produced fairly simply and cheaply by polymerization of monomers and processed from solution, but include the disadvantage of less defined molecular structures, consequently resulting in less defect-free thin films.

On the other side, there is the field of defined conjugated oligomers which must be synthesized and built up *step-by-step* and typically are processed by more costly evaporation techniques, but guarantee more defect-free layers.

As stated above, among the basic π -conjugated systems, thiophene-based materials, in particular **OTs** and **PTs**, have attracted intense interest among researchers all over the world and have actually been advanced to be the most frequently investigated structures. Two key reasons account for this development.

Thiophene chemistry is well established and has been under development for a long time. There are uncountable methods to modify the core molecule,⁸⁹ but more importantly, thiophenes are ideal building blocks in transition metal-catalyzed cross-coupling reactions which have been developed enormously in the past 10-20 years and nowadays provide the basis for the synthesis of most **OTs** and **PTs**.⁹⁰

In addition to the enormous and attractive potential of structural variations which allow tuning of the electronic properties over a wide range, the second reason why these materials are so successful is their outstanding chemical and physical properties. They are typically stable, both in the conducting and in the semiconducting state, and can be readily characterized by many methods.

Their unique electronic, optical, redox, charge transport and self-assembling properties are intriguing, in addition to their unique arrangement and stacking properties on solid surfaces and in the bulk, which make them useful candidates for organic electronics.

Finally, the high polarizability of sulfur atoms in thiophene rings leads to a stabilization of the conjugated chain and to excellent charge transport properties, which are one of the most crucial assets for applications in organic and molecular electronics.

Also in biological path, π -conjugated **OTs** and **PTs** have been used to couple *analyte/receptor* interactions, as well as non-specific interactions, into observable responses (**Figure 31-32**).⁹¹

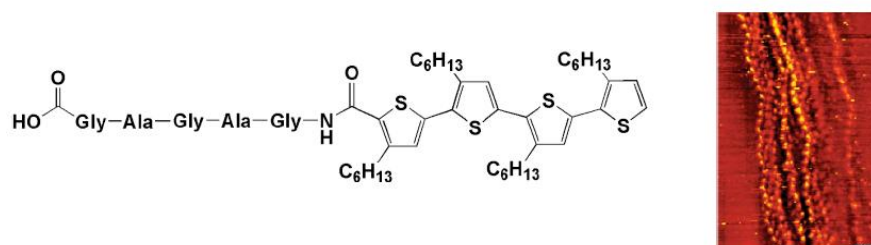


Figure 31. Molecular structure and STM image of the supramolecular organization of biohybrid quaterthiophene.

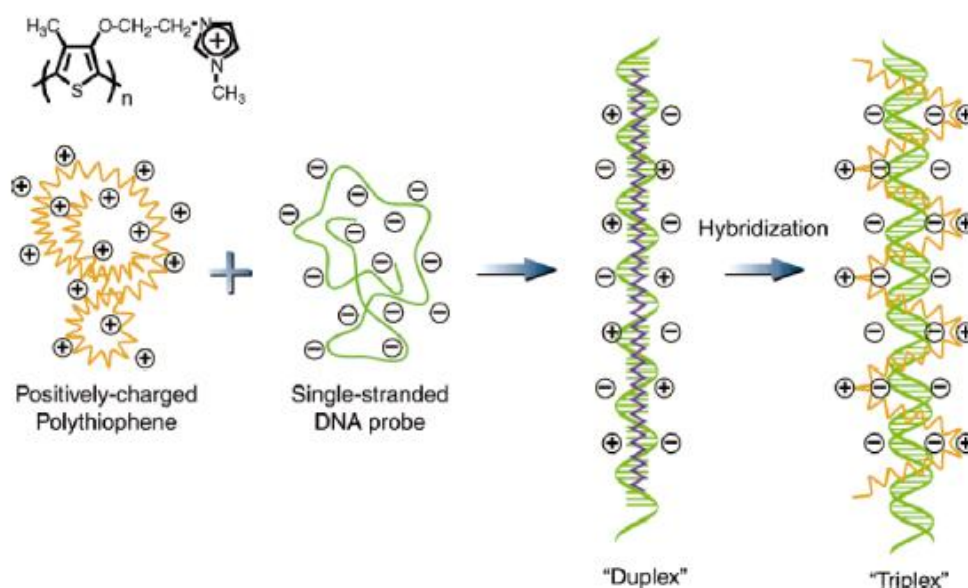


Figure 32. Schematic description of the formation of the polythiophene/single-stranded nucleic acid duplex and the polythiophene/hybridized nucleic acid triplex.

2.2 Oligothiophenes in Organic Electronics

Functional **OTs** have attracted comprehensive interest among researchers all over the world and have actually been advanced to be among the most frequently used *π -conjugated materials*, in particular as active components in organic electronic devices and molecular electronics.

In the last 5-10 years, the number of publications about functionalized **OTs**, which can be considered as a third generation of advanced conjugated materials, dramatically increased.

It was recognized that with functional groups additional and novel properties to those of the *π -conjugated systems* can be created which are important for many applications.

Furthermore, novel molecular architectures having more complicated conjugated structures and sophisticated topologies other than linear systems have emerged as a consequence of increased versatility of thiophene chemistry and currently represent a most interesting and quickly spreading field of research.

In general, the increase of dimensionality in *π -conjugated systems* can lead to different superstructures in the solid state and to multidirectional charge transport.

2.2.1 Oligothiophenes for OFETs

During the past two decades, the number of research groups exploring the field of organic electronics has expanded considerably due to the potential use of organic semiconductors as a low-cost alternative to traditional inorganic materials.

Among the organic semiconductor classes used in **OFETs**, oligo- and polythiophenes are among the most extensively investigated due to their chemical/electrochemical stability and ready functionalization.^{92,93}

Typical **OFET** (**Figure 33**) (or more appropriate thin film transistor) structures. The **OFET** consists of a gate electrode, a dielectric insulating layer and an organic semiconducting material sandwiched between the source and drain electrodes.

Note that the organic semiconductor used in **OFETs** should not be intentionally doped and consequently, the semiconductor carrier concentration is very low, usually $< 10^{14} \text{ cm}^{-3}$.

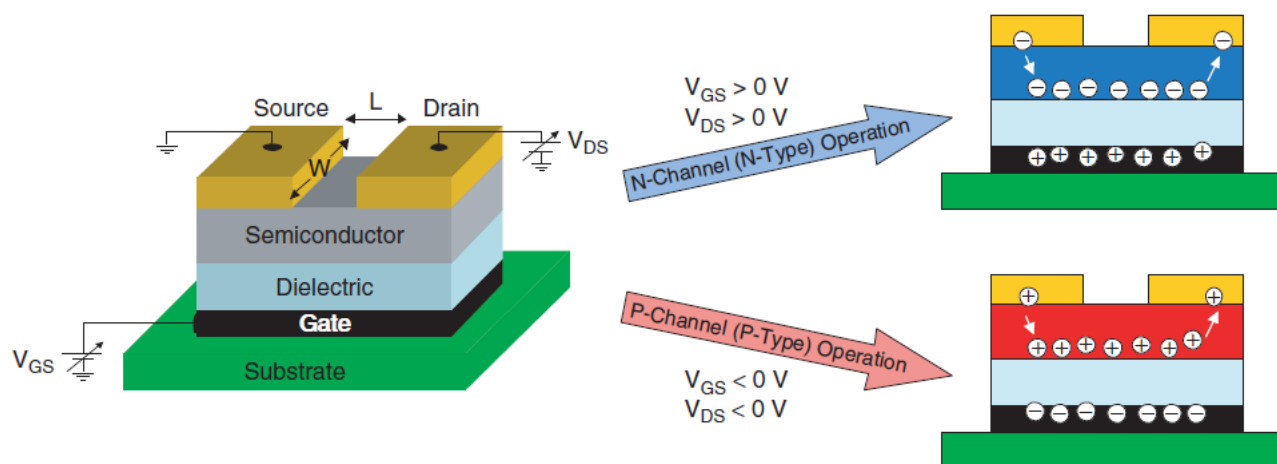


Figure 33. Organic field effect (thin-film) transistor structure with highlighted accumulation of electrons and holes for n- and p-channel semiconductors, respectively.

For inorganic semiconductors such as **Si** and **GaAs**, the solid-state structure is formed by strong covalent or ionic bonds holding the atoms in a well-defined lattice.

In contrast, organic semiconductors are composed of individual molecules or polymeric chains that are only weakly bound through *van der Waals/dipole*, hydrogen-bonding and π - π interactions resulting in small/fragile single crystals or disordered/polycrystalline solids.

Charge delocalization can only occur along the conjugated backbone of a single molecule/polymer or between the π -orbitals of adjacent units. Therefore, charge transport in organic materials mainly occurs by charge hopping from these localized states and can be described as an electron transfer between a charged oligomer and an adjacent neutral oligomer.

For an ideal organic semiconductor in a crystal lattice, the individual *HOMO* and *LUMO* energy levels would blend to form bands analogous to the conduction and valence bands in inorganic materials.

Although most organic semiconductors do not form ideal lattices, charge injection can still be made by matching the work function of the injecting electrode to either the **VB** (*HOMO*) for hole injection or the **CB** (*LUMO*) for electron injection.

P-Type organic semiconductors typically have *HOMO* levels between -4.9 and -5.5 eV, resulting in ohmic contact with high work function metals such as **Au** (5.1 eV) and **Pt** (5.6 eV) while *n-type* materials typically have *LUMO* levels between -3 eV and -4 eV and should have better contact with low work function metals such as **Al** and **Ca**, but these metals are highly reactive and degrade rapidly with air exposure.

Generally solid-state charge transport in organic semiconductors is generally highly anisotropic, hence it occurs preferentially along the π - π stacking direction from overlapping orbitals of adjacent molecules. Therefore the degree of molecular organization within the semiconductor film and orientation of the molecule with respect to the insulator surface greatly affect the efficiency of **FET** charge transport. Chemical modifications affecting solid-state molecular packing and variation/optimization of the film deposition conditions can drastically affect the film morphology and microstructure. Therefore to realize highly efficient organic semiconductor films it is important first to predict/optimize molecular ordering and staking within the single crystal and then film microstructure.

OTs (α nTs, **Figure 34**) are one of the most often investigated organic semiconductor families for optoelectronic devices and the key advantage of well-defined oligomers over their parent polymers is the high degree of molecular and crystalline ordering they can achieve. Polycrystalline and highly oriented thin films can be easily prepared from solution or by vacuum deposition.

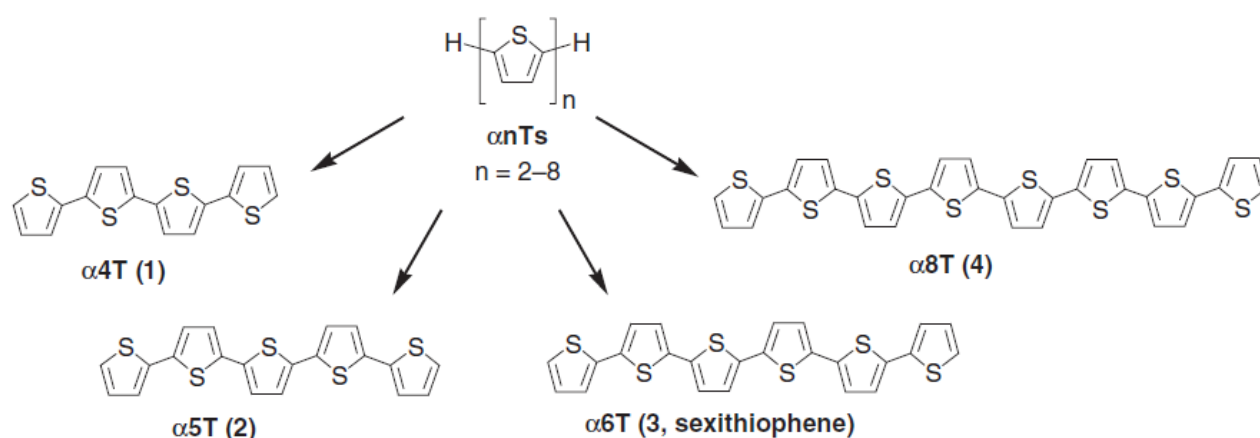


Figure 34. Structure of unsubstituted oligothiophenes.

Except for **α 2T**, **α 3T** and derivatives which do not possess the appropriate electronic properties.

The oligomers **α 4T** and **α 5T** exhibit mobilities up to 0.006 and 0.08 cm² V⁻¹ s⁻¹, respectively, while for **α 8T** the highest reported mobility is 0.33 cm² V⁻¹ s⁻¹ for film deposition at 120°C.⁹⁴

The **α 6T** derivative is the most investigated oligomer in this series and it exhibits a field effect mobility of \approx 0.03 cm² V⁻¹ s⁻¹ in bottom-contact **Si/SiO₂ FETs**, whereas single-crystalline grains of this oligomer exhibit mobilities up to 0.075 cm² V⁻¹ s⁻¹.⁹⁵

Since **OFET** charge transport occurs near the interface with the gate dielectric, *Loi et al.*⁹⁶ investigated the supramolecular organization of **α 6T** ultra-thin films on **SiO₂** dielectric by confocal spectroscopy and microscopy and they demonstrated that **α 6T** sub-monolayer films are composed of mixed regions where the molecules stand on and lie flat on the substrate surface.

Importantly, they discovered that only after the first monolayer is completed, all the **α 6T** molecules stand on the substrate.

For films thicker than two monolayers, the photoluminescence spectra of standing molecules show a molecular *H-like* aggregation as in the single crystal.

Therefore, it was concluded that for **α 6T** films only the two monolayers next to the dielectric interface dominate the charge transport.

Most of the π -conjugated planar organic molecules and all unsubstituted **OTs** crystallize into a *herringbone structure (HB)*, typical in many aromatic hydrocarbon, in which the molecules minimize orbital repulsion by adopting an *edge-to-face* motif.⁹⁷

Theoretical studies have suggested that enforcing the oligomers to adopt a *face-to-face* arrangement, by appropriate substitution or doping, it would increase the π - π orbital overlap, enhancing the field effect mobility by maximizing electronic coupling between adjacent molecules.

However, the addition of substituents (α,ω - and β,β' -alkyl- and perfluoroalkyl-substituted) to the conjugated core (**Figure 35**) can affect the crystal structure, and hence the field effect mobility.^{98,99}

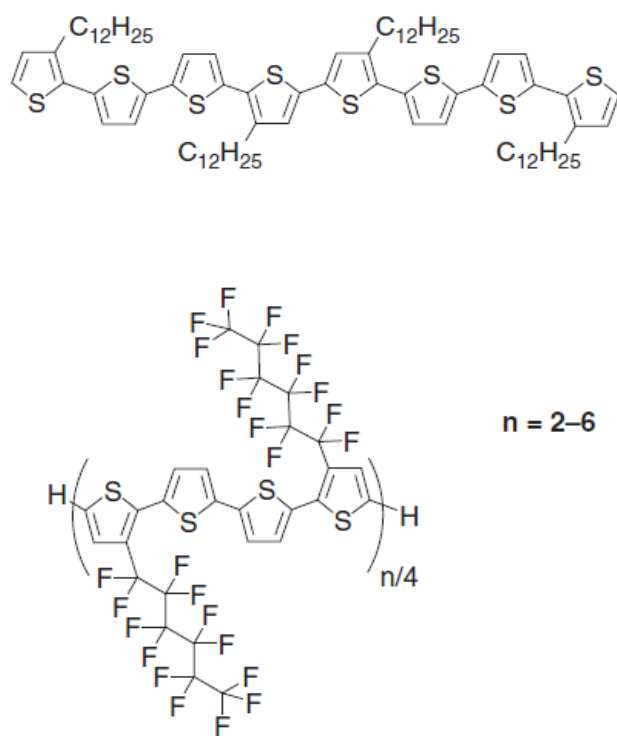


Figure 35. Chemical structure of various alkyl- and perfluoroalkyl-substituted oligothiophenes.

2.2.2 Oligothiophenes for OLEDs

One of the key developments in the advance of organic **LED** (**Figure 36**) technology was the discovery of electrophosphorescence which lifts the upper limit of the internal quantum efficiency of devices from 25% to nearly 100%.¹⁰⁰

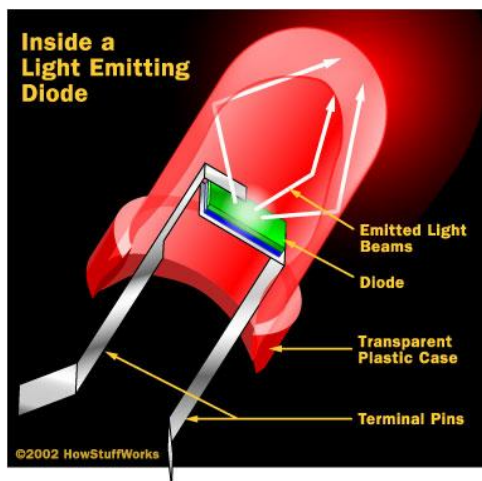


Figure 36. A typical LED device.

Indeed, one of the factors contributing to device efficiency is the ratio of the radiatively recombining excitons (from injected holes and electrons) to the total number of excitons formed. With fluorescent emitters, statistically (parallel spin pairs will recombine to triplet excitons while antiparallel spin pairs will recombine to singlet and triplet excitons) only 25% of the generated excitons can recombine through a radiative pathway, causing an intrinsic limitation on the external quantum efficiency of the **OLED** while in phosphorescent materials-complexes containing heavy metals - strong spin-orbit coupling leads to singlet-triplet state mixing which removes the spin-forbidden nature of the radiative relaxation from the triplet state giving an internal

quantum efficiency up to 100% because phosphorescent emitters both singlet and triplet excitons can radiatively recombine.

However the fluorescent compounds have higher chemical and electrical stability and moreover most fluorescent materials can be deposited without dispersing them in a matrix, instead the phosphors need to be deposited into a wide gap material to avoid self quenching.

Finally the problem of self-quenching together with the wide absorption band of phosphors implies that the host material must have a gap wider than those of the emitters, so the minimum voltage that it is possible to apply to the device is high compared to the voltage of devices based on fluorescent compounds.

For these reasons a great number of laboratories are still working on fluorescent compounds, including those based thiophene oligomers which by appropriate functionalization may increase both electron affinity,¹⁰¹ and photoluminescence efficiency in the solid state,¹⁰² allows to achieve high *p*- and *n*-type charge carrier mobilities,¹⁰³ may lead to white electroluminescence via spontaneous self-assembly of a single oligomer,¹⁰⁴ may allow the realization of optically pumped lasers,¹⁰⁵ and very bright electroluminescent diodes;¹⁰⁶ all this potentialities makes of these **OTs** a great candidates for the next generations of organic devices like light-emitting transistors or diode-pumped lasers.

Surely the **EC6T**, an end capped *sexithiophene*, was the first one to get efficiencies in the range $1-8 \times 10^{-5}$ (**Figure 37**).

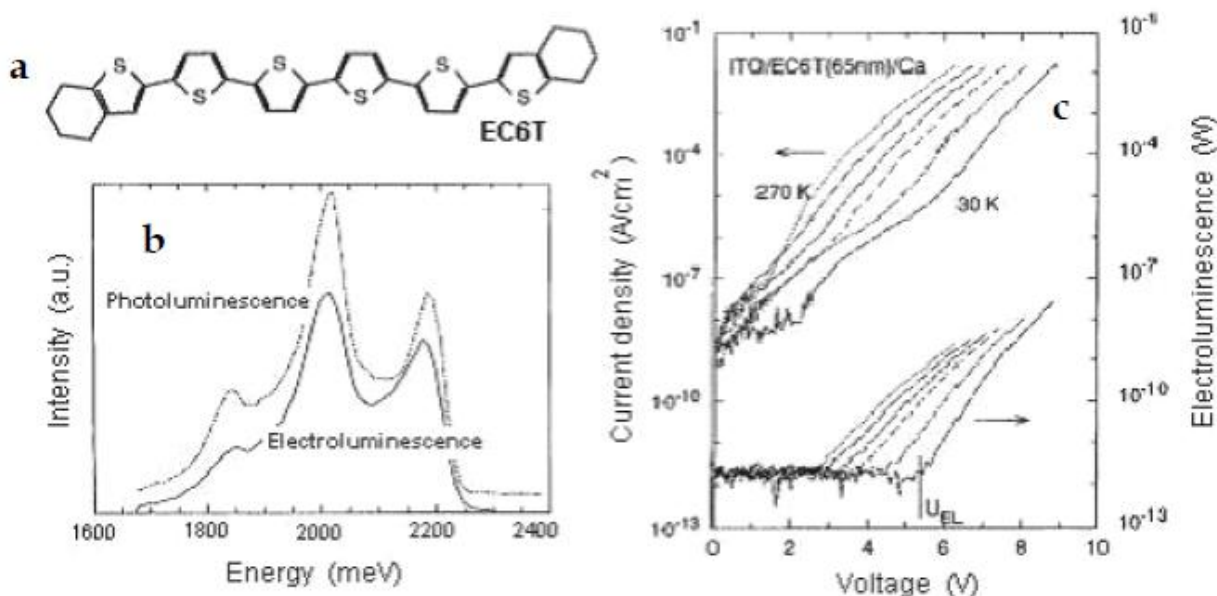


Figure 37. a) Molecular structure of EC6T; b) Photoluminescence and electroluminescence spectra at 4 and 20 K, respectively; c) $I - V$ curves (top, left-hand scale) and EL- V curves (bottom, right-hand scale) of a ITO/EC6T/Ca OLED (thickness 65 nm) as a function of temperature (30, 90, 120, 150, 210, and 270 K from right- to left).

Unluckily two of the main drawbacks of conventional **OTs** such as **EC6T** for applications in **OLEDs** are the low *electron affinity* (**EA**) and the non-radiative phenomena induced by packing causing the quenching of *photoluminescence* (**PL**) in the solid state.

In fact conventional **OTs** are easy to oxidize but difficult to reduce and in light emitting devices the low electron affinity generates a huge energy barrier between the cathode and the organic layer. In consequence, only a small number of electrons are injected, resulting in poor electron-hole balancing.

The low **PL** efficiency in the solid state is largely determined by the intermolecular interactions governing the supramolecular organization.

The analysis of conformation and packing modalities in oligothiophene single crystals has pointed out the existence of numerous intra- and intermolecular interactions, such as *van der Waals*, π - π stacking, weak *CH-S* and *CH- π* hydrogen bondings and *S-S contacts*.¹⁰⁷

Intermolecular interactions induce additional non-radiative channels so that the photoluminescence efficiency of **OTs** is lower in the solid state than in solution.

Owing to low photoluminescence efficiency caused by non-radiative phenomena induced by packing and to intrinsically low electron affinities, conventional **OTs** display very poor electroluminescence characteristics.

For this reason a considerable improvement in solid-state **PL** and electron affinity values was achieved via chemical modification of the thiophene rings through functionalization of the *sulfur* atom with *oxygen*.

Indeed, in thiophene, *sulfur* has unshared lone-pair electrons which can be exploited to form chemical bonds with *oxygen*.

In this way, a new class of oligomeric thiophene materials namely *oligothiophene-S,S dioxides*, in which two *oxygen* atoms are linked to one or more thienyl *sulfurs* was synthesized.¹⁰⁸

By using this approach, compounds with greater electron affinities and photoluminescence efficiencies in the solid state became available and proved to be useful for applications in electroluminescent diodes,¹⁰⁹ and photovoltaic devices.¹¹⁰

Oxidation and reduction potentials are related to *HOMO* and *LUMO* orbital energies hence to ionization energies and electron affinities, respectively and in this purpose the oxygen atoms cause the de-aromatization of the thiophene ring and allow the frontier orbitals to shift towards lower energies, causing in particular a sizeable increase in electron affinities.

The reduction and oxidation potentials of *quinquethiophene* (Figure 38-39) can be tuned by changing the number and the position of the oxygenated units.

In particular, it can be seen that the oligomer with alternating oxidized and non-oxidized thiophene rings is easier to reduce than to oxidize, opposite to the precursor *quinquethiophene*.

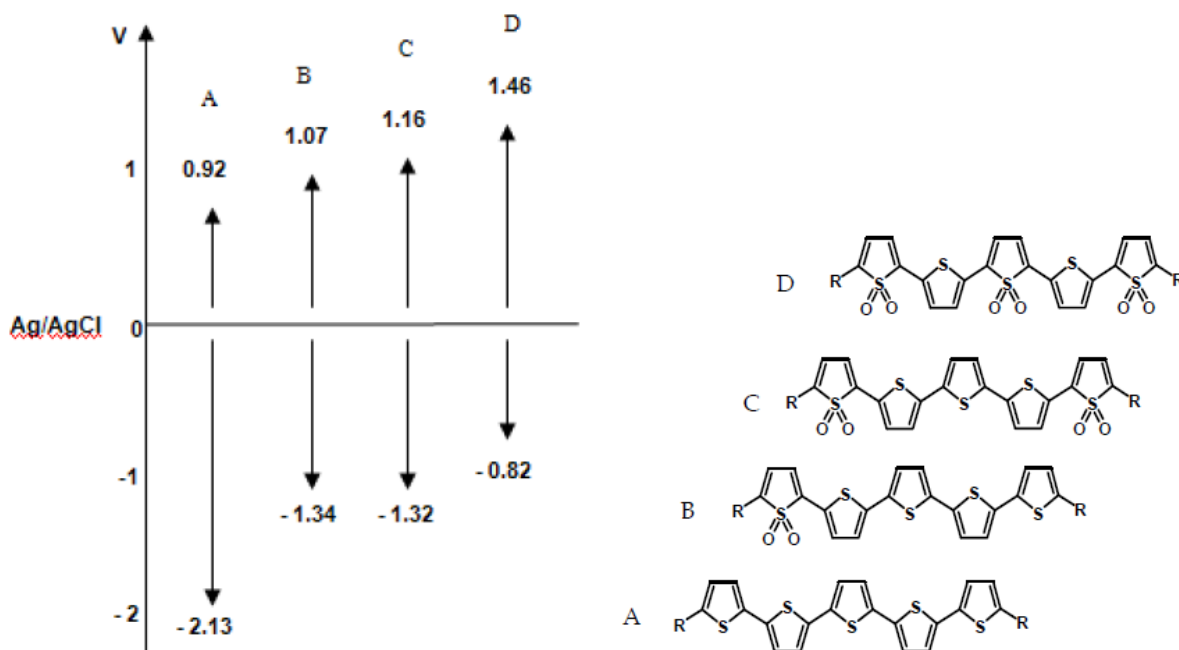


Figure 38. Reduction and oxidation potentials of selected quinquethiophene-S,S-dioxides. R= Si(CH₃)₃C(CH₃)₃.

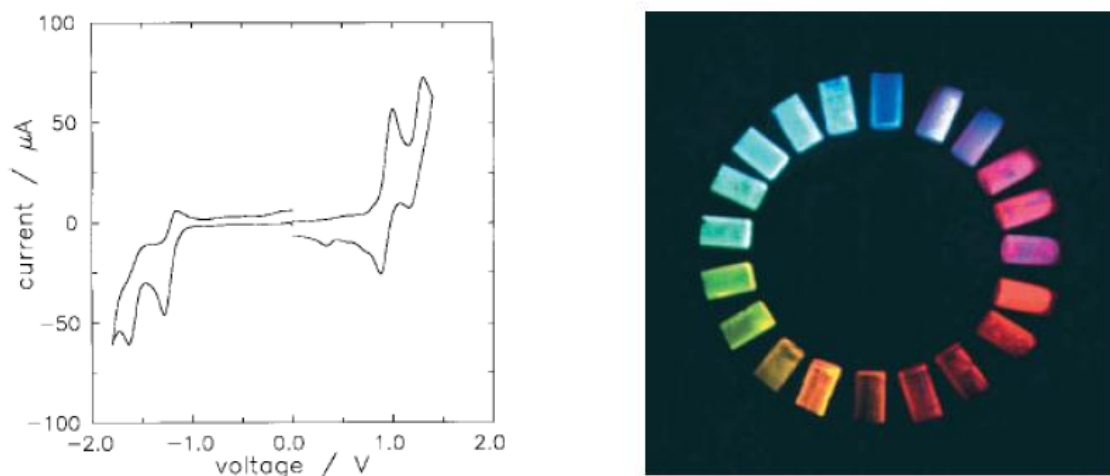


Figure 39. Cyclic voltammogram (200 mV/s, 1 mM in $\text{CH}_2\text{Cl}_2/\text{Et}_4\text{NBF}_4$ 0.2 M. V vs. Ag/AgCl) of quinquethiophene-S,S-dioxide (left); emission of cast-film of different OTs under UV irradiation (right).

Time-Dependent Density Functional Theory (TD-DFT) indicated that the oxidation of the thiophene ring leads to the formation of new interactions in the *LUMO* orbital.

The kinetic energy of the electrons in this orbital is lowered, while the energy of the electrons in the *HOMO* orbital is almost unchanged. As a consequence, the electron affinity of the whole molecule is increased.

The functionalization with oxygen obliges the molecules to pack far apart from each other in the solid state thus preventing the photoluminescence quenching caused by the close packing of non oxidized **OTs**.¹¹¹

Consequently, the *PL quantum yield (PLQY, η* , the number of photons re-emitted radiatively as a percentage of the number of photons absorbed) is increased, by an amount up to one order of magnitude.

Different chemical modifications in the aromatic skeleton as functionalization of the thienyl groups with methyl substituents in the *head-to-head* orientation does not modify the **PLQY** value in solution, but further enhances that in the solid state, which reaches a very significant 37%.

One of the highest **PLQY** values, about 50%, measured in the solid state for an *oligothiophene-S,S-dioxide* was shown by the 'rigid-core' oligomer (**Figure 40**) 3,5-dimethyl-2,3'-bis(3-methylthiophene)-dithieno[3,2-b;2',3'-d]thiophene-4,4-dioxide, (**DTTOMe₄**):

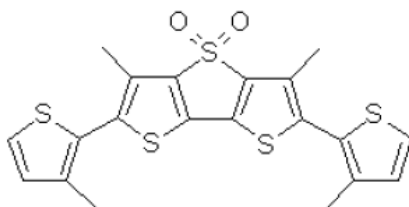


Figure 40. 3,5-Dimethyl-2,3'-bis(3-methylthiophene)-dithieno[3,2-b;2',3'-d]thiophene-4,4-dioxide (DTTOMe₄).

DTTOMe₄ belongs to a class of *oligothiophene-S,S-dioxides* characterized by high photoluminescence efficiency both in solution and in the solid state, contrary to conventional thiophene oligomers and conformationally flexible *oligothiophene-S,S-dioxides*.¹¹²

The increased electron affinities and PL quantum efficiencies of *oligothiophene-S,S-dioxides* in the solid state, combined with the optical and chemical stability of these compounds, allowed the fabrication of electroluminescent devices with much better characteristics than those obtained with conventional **OTs**.

Furthermore these compounds represent one of few *n*-type materials belong to the thiophene's family, used not only for **OLEDs** devices but even in **OPVDs** (see 3.4.1.2).

2.2.3 Synthetic Procedures for Oligothiophenes

Functional **OTs** may be synthesized by α -C-C-linkage via two different routes, either by oxidative homocoupling (lithiation followed by addition of CuCl_2 or $\text{Fe}(\text{acac})_3$), or by metal-catalyzed C-C-coupling, such as *Kumada*,¹¹³ *Suzuki*,^{114,115} *Sonogashira*¹¹⁶, *Stille*,¹¹⁷ and *Negishi*,¹¹⁸ type reactions.¹¹⁹

Surely the technique most used to synthesize **OTs** exploits oxidative cross-coupling of different *organo-metals* (copper, tin, boron, magnesium, zinc) with *transition metals* (palladium or nickel) which catalyze the reaction according a catalytic cycle (**Figure 41**).

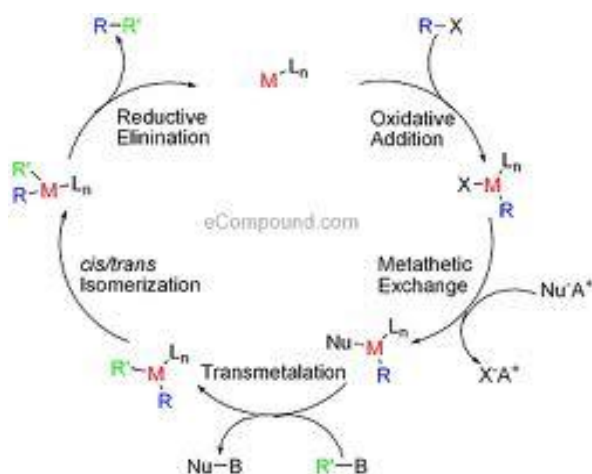


Figure 41. General catalytic cycle.

The first step in this the oxidative addition of the organohalide (**R-X**) to the transition-metal (palladium or nickel) that gives a *cis* intermediate which rapidly isomerizes to the *trans* intermediate. The second step is the *transmetalation* with the organo-metal (copper, tin, boron, magnesium, zinc) to form an intermediate which produces the desired product (**R-R'**) and the gives back the active transition metal (palladium or nickel) species after *reductive elimination*.

The oxidative addition and reductive elimination retain the stereochemical configuration of the respective reactants.

Regioisomeric **OTs** including β -linkages have a strongly decreased conjugation and are only discussed to a minor extent.

2.2.3.1 Copper(II)-Promoted Oxidative Homocoupling

The oxidative coupling of organolithium compounds with cupric chloride¹²⁰ was the first reaction that was found. Thus, the reaction of monothiophene **H-T-H** with *n*-butyl-lithium (**n-BuLi**) followed by the addition of one equivalent of **CuCl₂** afforded **H-T₂-H** in discrete yield (Figure 42).^{121,122}

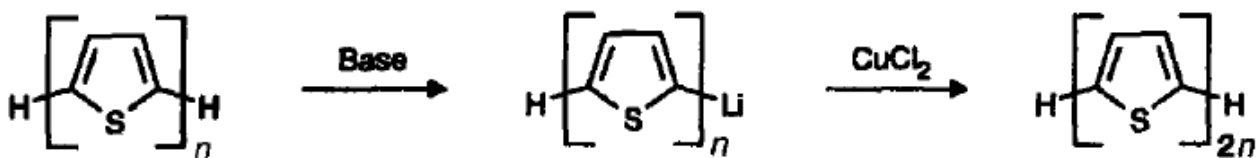


Figure 42. Oxidative coupling of R-Li with **CuCl₂**.

Obviously later this reaction was improved furnishing yield up to 85% and used to synthesize not only *bithiophenes* but applied to higher, even-numbered **OTs** up to α -sexithiophene **H-T₆-H**.

2.2.3.2 Metals Catalyzed Coupling Methods

▪ *The Ulmann Reaction*

This procedure consist in two steps: first, in the preparation of an, e.g. *thienyl-copper* derivative followed by the treatment with different *aryl-halides*. *2-Thienylcopper*, for example, is prepared from the corresponding **Li-T-H** or *Grignard* derivative and a *copper(I)-halide* and is then reacted with *iodo- or bromoarenes* in pyridine or quinoline.

By this procedure e.g. **H-T₂-H** is formed in 42% yield by the reaction of **Cu-T-H** and *2-iodothiophene* (**Figure 43**).¹²³

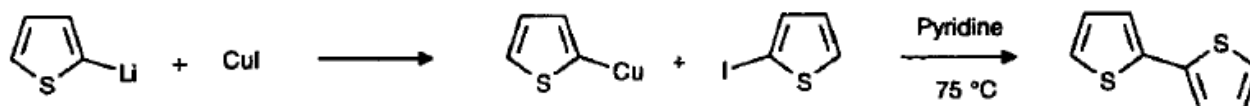


Figure 43. Ulmann cross-coupling reaction.

▪ *The Kumada Reaction*

Nickel- and palladium-catalyzed this type of cross coupling reaction which became the most frequently used method in the synthesis of various types of thiophenes. **OTs** are most effectively and conveniently prepared by the reaction of the *Grignard* reagent; for example the *2-bromothiophene* with various *bromo- or dibromothiophenes* by adding of the *Grignard* solution to a mixture of the organic halide and catalytic amounts of *nickel-complexes* (0.1-1 mol.%) in ether solution, the reaction proceeds under very mild conditions and gives the coupling product in high yields (**Figure 44**).



Figure 44. Kumada cross-coupling reaction.

The reaction's mechanism is basically valid also for other reactions catalyzed by transition metals and follows the catalytic cycle (see 2.2.3).

The reaction is applicable to various types of Grignard reagents (e.g. aryl, alkyl) and organic halides bearing a carbon sp^2 (e.g. aryl, vinyl). The reactivity order of the halide component was found to be $Ar-I > Ar-Br > Ar-Cl > Ar-F$.

Grignard reagents are equally prepared either in Et_2O or in THF, however, the reaction proceeds considerably faster in Et_2O than in THF and the dehalogenation product is formed in larger amount in THF. However, in some cases where these Ni-catalysts are not very reactive or side reactions occur, the analogous Pd-complexes gave much better results¹²⁴ because generally the Pd-complexes even if are less reactive, are more selective.

▪ The Stille Reaction

The palladium-promoted coupling of *organotin* compounds turned out to be especially fruitful because of the possible use of various organic electrophiles, the mild reaction conditions, the regioselectivity, and the tolerance of many functional groups (e.g. CO_2R , CN , OH , CHO , NO_2). General aspects of this so-called 'Stille reaction' and of its applicability have been extensively reviewed.^{125,126}

However, Crisp describes the synthesis of **H-T₂-H** (80%) and **H-T₃-H** (61%) by the **Pd(PPh₃)₂Cl₂** catalyzed coupling of *tributyl(2-thienyl)tin* with **I-T-H** and *2,5-diiodothiophene* **I-T-I** respectively (Figure 45).¹²⁷

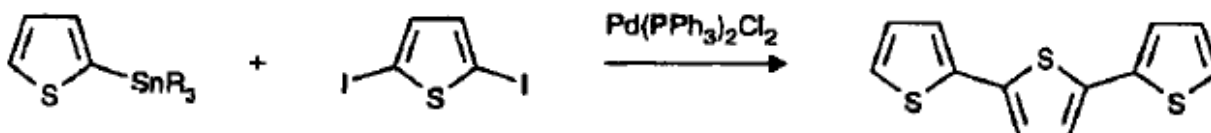


Figure 45. Stille cross-coupling reaction.

The yields are somewhat lower than for the corresponding *nickel-catalyzed* coupling reactions, the catalytic cycle is basically similar to that of the *Ni-catalyzed* 'Kumada reaction' and many different types of *Pd-catalyst* have been investigated to improve this cross-coupling methodology.

▪ **The Suzuki Reaction**

These cross-couplings which use the less electropositive boron instead of magnesium or tin proceed with good to excellent yields even in sterically demanding positions. Gronowitz *et al.* modified the *palladium-catalyzed* 'Suzuki coupling' so that it became useful to the heterocyclic series.¹²⁸

This *carbon-carbon* coupling method, as does the 'Stille-coupling', tolerates a variety of functional groups both in the organometallic reagent and in the heterocyclic halide.

In the series of OTs, 2-thiopheneboronic acid, easily prepared from Li-T-H and boronic acid trimethylester, reacts with Br-T-Br to H-T₃-H in 40% yield (Figure 46).

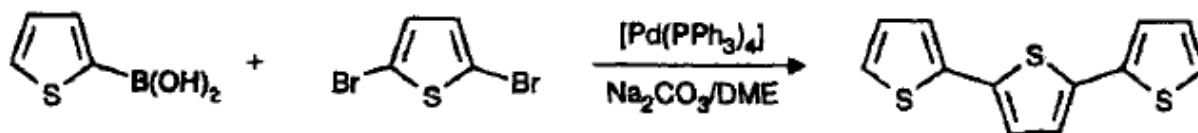


Figure 46. Suzuki cross-coupling reaction.

Furthermore without any necessary precautions against oxygen, to the contrary of the prior cross-coupling reactions seen which demands reduced atmosphere under N₂ or Ar₂, the Suzuki reaction is performed in a mixture of organic solvent and aqueous sodium bicarbonate, using Pd(PPh₃)₄ as catalyst.

Typically, an excess of 20% boronic acid is used in the coupling reaction. Less excess results in the formation of mono-coupled by-products which are difficult to separate.

Only few examples are known in which organozinc (Negishi cross-coupling) or organomercuric derivatives instead of the more reactive Grignard reagents are used in palladium catalyzed heteroaryl/heteroaryl-coupling reactions.

In most cases, they are used for couplings of substituted thiophenes¹²⁹ or mixed thiophene/(hetero)arene compounds.¹³⁰

Herein we described a brief survey about the main synthetic procedures for OTs, therefore for a more details is necessary to consult the *Handbook of Oligo- and Polythiophenes*.

2.3 Polythiophenes in Organic Electronics

PTs represent one of the most important classes of π -conjugated polymers for organic electronic in different devices, because they meet the essential requirements of solubility and processability and offer the possibility of structural modifications by incorporation of a wide variety of side-chain functionalities.¹³¹

Furthermore, they exhibit an acceptable environmental stability (**Figure 47**).

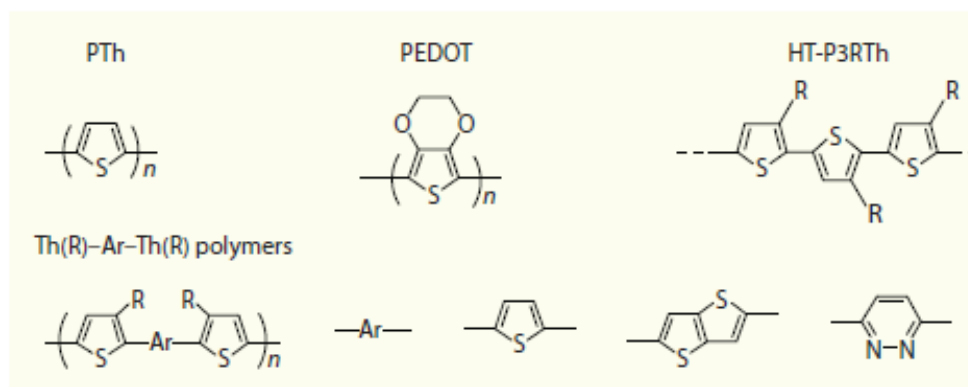


Figure 47. Examples of polythiophenes. PTh, poly(thiophene-2,5-diyl); PEDOT, poly(ethylenedioxythiophene); HT-P3RTh, regio-regular head-to-tail poly(3-alkylthiophene-2,5-diyl).

As mentioned in the *Chapter I*, the **Eg** of **PTs** is strongly influenced by the molecular structure (geometry) and favoring the quinoid resonance structure of **PTs** leads to an increasing rigidification and planarization of the backbone since the rotation between the rings becomes more and more restricted.

The extent of the effective π -conjugation along the *PT-backbone* is also much dependent on the length and structural regularity of the polymer chain.^{132,133,134,135,136,137,138,139,140}

Its **Eg** can be tuned throughout the whole UV/Vis spectrum from the UV to the near IR (NIR) by variation of the substituents attached in 3 and/or 4-position of the thiophene ring, depending on the inductive/mesomeric effects towards the main chain.^{141,142}

However the major drawback concerning oxidative polymerization methodologies to synthesize different **PTs** consists of the formation of regioirregular *poly-alkylthiophenes* (**PATs**) (by substitution on the β -position of thiophene units), i.e. **PTs** in which the *head-to-head* (**HH**), *tail-to-tail* (**TT**) and *head-to-tail* (**HT**) couplings are randomly present in the polymer backbone (**Figure 48**).

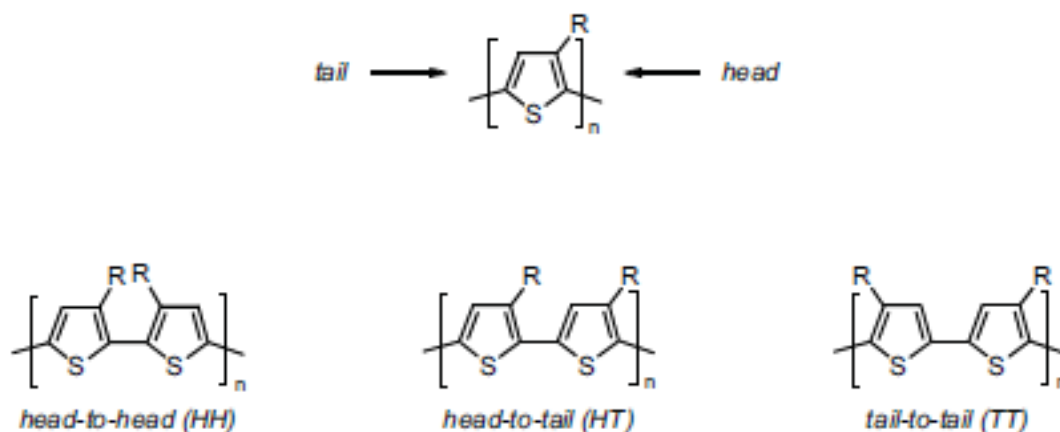


Figure 48. Regiochemical dyads of regioregular poly(alkylthiophene)s.

The coupling **HH** or **TT** disadvantage the coplanarity of the polymer: due to of the side chains, which generate a steric hindrance preventing free rotation around C-C bonds, resulting the loss of π -conjugation, at the expense of electrical and electronic properties of the **PTs**.

By contrast, we can tune the polymer properties and the order of **PTs** by changing properties of the substituent such as *sterical hindrance, electronic effect and hydrophilicity*.

Generally the **PTs** that contain only pairs **HT** have a greater conformational order, greater flatness and greater long-range order, which determines high crystallinity; all these are necessary demands for their application organic electronic devices (OFETs, OLEDs, OPVDs, etc).

However the organization of irregular **PTs** is difficult to predict and therefore to control, and synthetic strategies have been developed to attain regioregular structures (see 2.3.5) and the ability of molecular architects to understand how to gain control over the structure properties and function in **PTs** continues to make their synthesis a critical subject in development of new advanced materials.

Synthesis can help to determine the magnitude of π -overlap along the backbone and eliminate structural defects. Materials assembly (and/or processing) determines interchain overlap and dimensionality.

Finally in functional **PTs** structural order over many length scales can be created in self-organizing materials by the presence of molecular interactions including *solvophobic and solvophilic effects, hydrogen bonding, coulombic interactions and Van der Waal forces*.¹⁴³

2.3.1 Structure and Optical Properties

PT is the main aromatic polyheterocycle, in which the rings are linked in the α -position. In the neutral state, it is stable up to 350°C in air and 900°C in an inert atmosphere: this depends on the high redox potential ($E^{\circ} = 0.70\text{ V}$). It has high conductivity ($10\text{-}100\text{ S cm}^{-1}$) and stability, accompanied by low cost of synthesis.

Industrially the **PT** is obtained from a monomer at low cost whereas the thiophene can be synthesized from *alkynes* and *butane*, or recovered as a byproduct of the distillation of *petroleum*, in the *hamlet BTX* ($T_{\text{eb}} = 84^{\circ}\text{C}$).¹⁴⁴

The **PT** is insoluble, infusible (decomposes before melting) and for this reason it is not workable. To make it processable, it is necessary to functionalize, in order to reduce the packing and, therefore, the interaction between the **PT** chains.

The easiest way is to introduce the alkyl chains in β -position (**Figure 49**).

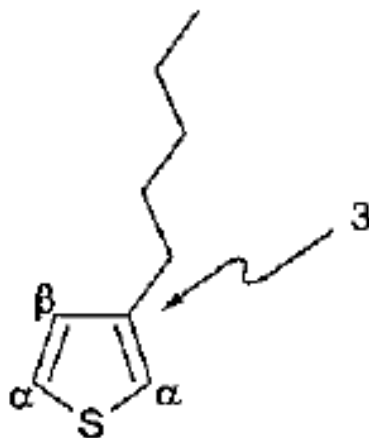


Figure 49. Thiophene with a hexyl group in β -position.

The first **PATs** synthesized were the *poly-3-methylthiophene*, *poly-3-ethylthiophene*, *poly-3-butylthiophene* and *poly-3-octylthiophene*. These polymers are soluble in common organic solvents, thus easily processable, except for the *poly-3-methylthiophene* in which the solubility is determined by the length of the side chain, which generally must be length at least four carbon atoms.

Insertion of long and flexible alkyl chains on the monomer leads also other effects, as the reduction of β -linkages, favoring α - α couplings between the repeating units; the methylene groups decouple, except for a weak +I effect; finally it has the appearance of chromism which is observed both in solution and in solid state.¹⁴⁵

The **PT** in the solid state, it is important the thermochromism, which is the color changing by means temperature variations; in fact increasing the temperature, it has the main chain transition from a planar and ordered conformation to a partially rotated and distorted, in which increases the disorder of the side chains decreasing the conjugation. The conformational transition derives from **Eg** which is inversely proportional to the extension of conjugation. When the temperature decreases, increases the conjugation at the expense of the **Eg**; finally the promotion of electrons into the excited state (LUMO), provokes a color change of the polymer.

The same result is obtained in solution, solvatochromism, by adding of a not-solvent: in this case the polymeric backbone desolvated and reaches an ordered and planar conformations at energy lower.¹⁴⁶

Furthermore when it presents in a side chain a chiral substituent (**Figure 50**) optical activity is induced in the main chain. The study of the chiroptical properties of an optically active polymer is carried out using techniques such as *optical rotary dispersion (ORD)* and *circular dichroism (CD)*.¹⁴⁷

These techniques are very useful to obtain information also on the tertiary structure of biopolymers. Conjugated polymers bearing chiral side chain substituents or chiral dopants show optical activity associated to the absorption attributed to the electronic transition $\pi \rightarrow \pi^*$.

Optical activity, however, is evident only when the polymer forms an ordered aggregate. Today, there have been several studies that demonstrate the importance that have the regioregularity, the solvent effect and the temperature.

As regards the regioregular structure, several studies have shown that an unregioregular **PTs** optically active has a lower optical property than that of a regioregular polymers.

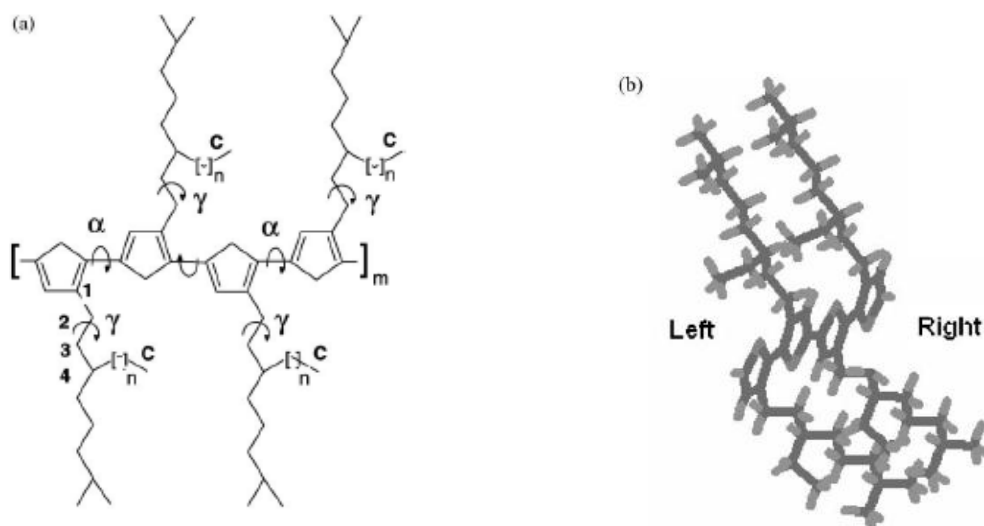


Figure 50. a) Structure of PTs used in calculations; b) Position of side chains with respect to the main chain.

The solvent effect has been studied, dissolving the polymer in a good solvent and adding known amounts of a bad solvent, causing the formation of chiral micro-aggregates, which can be studied by **CD**. The examination of the spectra led to the conclusion that the optical activity is not observed if the polymer is dissolved in a good solvent, but only if it is in aggregate form or in film.

Studies concerning the effect of temperature showed, finally, that no optical activity is observed at room temperature, but only at low temperatures. Decreasing the temperature, the macromolecules tend to aggregate each other, but they do that only by means an precise order given from the chirality of the side chains; in this way the elevate order intrachain gives optical activity to the polymer itself.

Today, the nature and the molecular origin of these chiroptical effects are unclear and are matters of debate. The optical and electronic properties depend strongly from the chemical structure, in the first place, and from the structural intrachain-interchain organization in second place.

Other hypothesis on **PTs**, demonstrated that these polymers in solid state and in solution, adopt an helical conformation of the main backbone. Some theoretical calculations have predicted that the helical conformation is the most stable, with a small energy difference between the cysoidal form and that transoidal. However, they are no yet experimental evidences that support this theory.¹⁴⁸

Other studies have been performed on single chains of substituted **PTs**, but there was observed a wide variety of conformations of the chains: straight, flat, curved, and helical.

Therefore, the interpretation of the high optical activity of the π -conjugated polymers must consider not only the organization of a intramolecular single chain, but also intermolecular organizations between the adjacent rigid and planar chains, which package each other to form a supramolecular assemblage (π -stacked).

It is very important to underline that there is not yet a clear interpretation on the structural origin of the chiral induction.

However, the main interpretations appeal to the cholesteric liquid crystals theories; for example has been compared the direction of the helix with the absolute configuration of the chain and the distance from the chiral center of the chain itself; this is an empiric rule in agree for liquid-crystalline systems.

2.3.2 Polythiophenes for OFETs

Achieving solution-deposited semiconductor films exhibiting large **OFET** charge carrier mobilities and environmental stability by *roll-to-roll processing* is an ultimate goal in organic electronics. This can be achieved by developing solution-processable polymer semiconductors, since polymers have the advantage of being more readily solution processable than small molecules because of the superior solution viscosity and rheological properties.

Poly(3-substituted thiophene)s (**Figure 51**), are one of the most studied polymer families for (semi)conductor/optical applications.^{149,150} These systems have the advantage that the presence of the *3-substituent* strongly enhances solubility and processability.

The properties of regioregular *head-to-tail* poly(3-alkylthiophene)s are found to be very different from those of their corresponding regiorandom polymers, in agreement with theoretical calculations, which predicted that *head-to-head* couplings prevent efficient π -conjugation and inhibit intrachain charge mobility.¹⁵¹

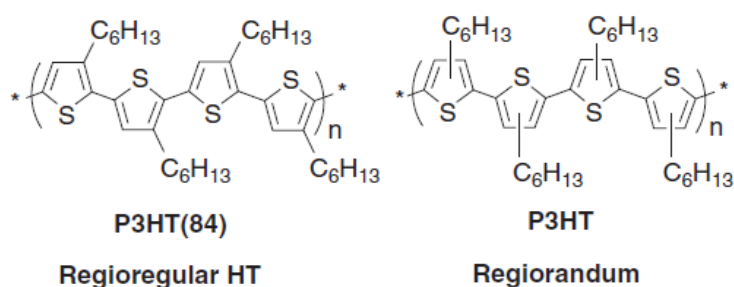


Figure 51. Chemical structures of regioregular head-to-tail (HT) poly(3-hexylthiophene) and regiorandom (or regioirregular) poly(3-hexylthiophene).

Indeed, *head-to-tail* regioregularity decreases **Eg**, improves microstructural ordering and crystallinity in the solid state and substantially improves electrical conductivities. Drop-cast films of highly regioregular **P3HT** self-orient into a well-ordered lamellar structure with an *edge-on orientation* of the thiophene rings relative to the substrate. Spin-coated films of regioregular **P3HT** are also well ordered with an *edge-on orientation* (π - π stacking direction in the plane of the substrate); in fact when regioregular **P3HT** consisting of >90% or more *head-to-tail* linkages is used to fabricate **FETs**, a dramatic increase in mobility is observed relative to regiorandom poly(3-alkylthiophene)s.

P3HT films prepared by drop casting from a *chloroform* solution exhibit lamellar structures and mobilities as high as $0.045 \text{ cm}^2 \text{ V}^{-1} \text{ s}^{-1}$.¹⁵² In contrast, spin-coated films of **P3HT** with lower regioregularity (81% HT linkages) consist of lamellae having

a *face-on orientation* (π - π stacking direction perpendicular to the substrate) and exhibit low mobilities of $\approx 10^{-4} \text{ cm}^2 \text{ V}^{-1} \text{ s}^{-1}$.

This study demonstrated that in addition to the degree of order in the polymer, film microstructure and electrical performance depend strongly on the film deposition method. This is reasonable since the *edge-on* lamellar structure ensures that delocalized intermolecular states are formed in the direction parallel to the substrate, which is the transport direction in **FET** devices.

The mobility of regioregular **P3HT** has also been found to vary substantially depending on the solvent used for the deposition and substrate pretreatment. The apolar nature of these groups apparently attracts the *hexyl* side-chains of **P3HT**, favoring lamellae with an *edge-on orientation*. Mobilities of 0.05-0.1 $\text{cm}^2 \text{ V}^{-1} \text{ s}^{-1}$ from highly regioregular **P3HT** have been attributed to this surface modification process.¹⁵³

2.3.3 Polythiophenes for OLEDs

Large numbers of different classes of light-emitting conjugated polymers have been developed, e.g., *poly(fluorene)s* (**PFs**) and *poly(phenylene)s* (**PPVs**) are still the leader materials for **LEDs** devices, the top polymeric green and blue-light emitters.

Usually the **PTs** emit orange-red light, consistent with their **E_g** of ca. 2 eV; often the luminescence in the solid state^{154,155} is much lower than that of **PPVs** and **PFs**. In fact the **PL** efficiency of *poly (3-alkylthiophene)s* decreases from 30-40% to 1-4% passing from the solution to the solid state, due to the increased contribution of non-radiative decay via interchain interactions (this feature is an advantage of **PTs** in **OFETs**) and intersystem

crossing caused by heavy-atom effect sulfur.¹⁵⁶ For the same reason the thiophene-based polymers have stronger spin-orbital coupling than benzene-based polymers, and hence triplet-state processes plays a great role in their photophysics.¹⁵⁷

We said (see 2.3.1) that another feature of **PTs** is the phenomenon of thermochromism,^{158,159} which shifts the planar structure of chains at low temperature to a random-coil conformation when the temperature is increased, forcing the polymer backbone out of planarity. All this leads to a decreased orbital overlap and shorter effective conjugation length,¹⁶⁰ resulting in a **Eg** increase and blue-shifted polymer absorbances (from red to purple or purple-blue).

PT Leds were first *Ohmori* in 1991¹⁶¹ (prepared by oxidation of 3-alkylthiophenes with FeCl_3 in CH_2Cl_2) as red-orange-light emitting materials in single layer *ITO/PT/Mg:In* devices. Shortly there were different **PTs** prepared by different synthetic polymerization methodologies (see 2.4) that increased the **PL** efficiency quantum yield (**Figure 52**).^{162,,163,164,165,166,167,168,169,170}

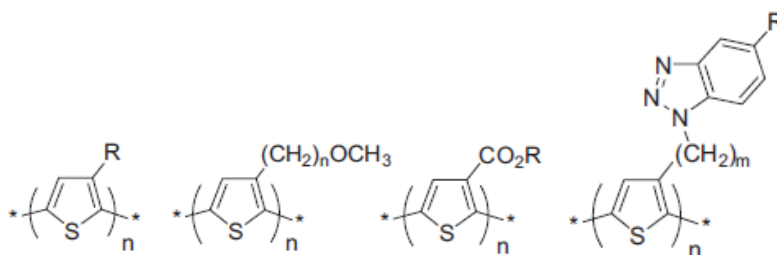


Figure 52. Different PTs for OLED applications.

The above-mentioned aspect of regioregularity in **PTs** plays an important role in their *HOMO-LUMO Eg* control, very important for the electron affinities and **PL** quantum efficiencies, two necessary demands for their application in **OLEDs** devices.

We showed (see 2.2.2) that the *n*-type **OTs** materials incorporating *thiophene-s-s-dioxide* units possess good **PL** properties both in solution and in solid state, as well as high **EL** efficiency.

Hence the alternating *donor-acceptor* **PTs** obtained by chemical polymerization of **OTs** *thiophene-s-s-dioxide* showed **PL** in the NIR region c.a. 900 nm. Furthermore *thiophene-s-s-dioxide* copolymers, reported by Berlin et al.,¹⁷¹ absorbed at 535nm and emitted at 650nm (**Figure 53**).

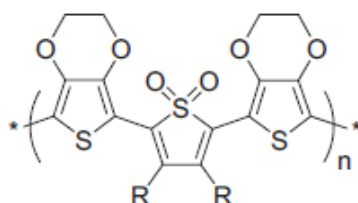


Figure 53. Thiophene-s-s-dioxide copolymers used for OLEDs.

The *Barbarella's* research about **OTs** *thiophene-s-s-dioxide* stimulated many researchers towards incorporation of the *thiophene-s-s-dioxide* unit into various polymers and copolymers used for **OLEDs** applications.

Other copolymers, as *thiophene-phenylene* and *thiophene-fluorene*, reported high efficiencies for thiophene-based **LEPs** (**Figure 54**).

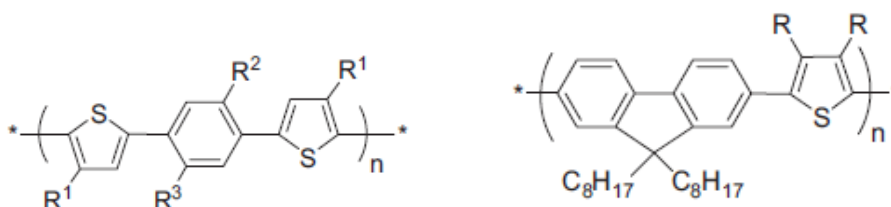


Figure 54. Thiophene-phenylene and thiophene-fluorene for LEPs.

2.3.4 Polythiophenes for OECDs

In 1932, the term 'electrochromism' was used to describe the physical phenomena of *Franz-Keldish and Stark's effects*. Since the mid-1970s, the term 'electrochromic materials' has become applicable to the family of polymers and small molecules which exhibit color changes under various types of electrochemical or chemical stimuli.¹⁷² A number of conjugated polymers exist that are colored in both the oxidized and neutral states (**Table 2**), as their **E_g** corresponds to absorption maxima which lie within the visible region.

The intensity of the π - π^* transition decreases via oxidation, resulting in two low-energy transitions, which emerge to produce a second color. Tuning of the **E_g** of organic conjugated polymers has now been established for several systems, such as the **PTs**.

PTs are of particular interest as electrochromic materials owing to their chemical stability, ease of synthesis and processability. For the most part, current research has been focused on composites, blends and copolymer formations of several conjugated polyheterocyclics, **PT** and its derivatives, especially **PEDOT** (**Figure 55**).

Other examples, **PEDOT/poly(2-acrylamido-2-methyl-1-propanesulfonate)** (**PAMPS**) composite films were prepared by *Sonmez et al.* for alternative electrochromic applications¹⁷³ in which thin composite films comprised of **PEDOT/PAMPS** were reported to switch rapidly between oxidized and neutral states, in less than 0.4 s, with an initial optical contrast of 76% at λ_{max} , 615 nm.

Nanostructured blends of electrochromic polymers such as **PPy** and **PEDOT** were developed via self-assembly by *Inganäs et al.* for application as an electrochromic window.¹⁷⁴

Unur *et al.* developed a graft-type electrochromic copolymer of polythiophene and polytetrahydrofuran for use in electrochromic devices,¹⁷⁵ while two EDOT-based copolymers were developed by Aubert *et al.* as other good candidates for **OECDs**.¹⁷⁶

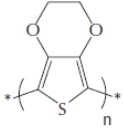
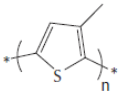
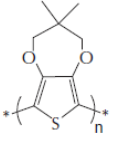
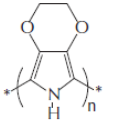
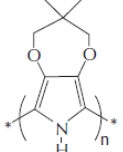
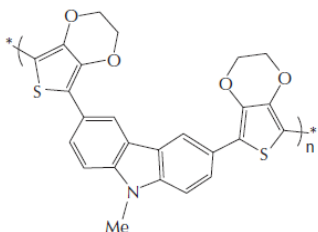
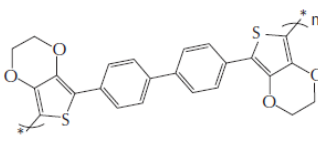
Electrochromic polymer	Chemical structure	Color	
		Undoped	Doped
PEDOT		Dark blue	Light blue
PMT		Bordeaux red	Light blue
PProDOT-(CH ₃) ₂		Light blue	Blue
PEDOP		Pink	Light blue
PProDOP-(CH ₃) ₂		Red-orange	Light blue
PBEDOT-NMeCz		Yellow	Blue
PBEDOT-BP		Brown	Black

Table 2. Colors from electroactive polymers: electrochromic, electroluminescent and laser devices based on organic materials.

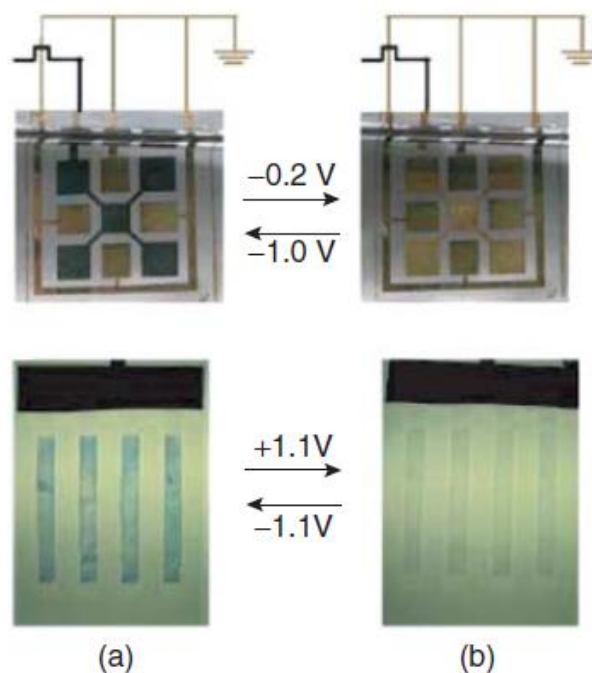


Figure 55. ECD device design with PEDOT on interdigitated ITO-plastic electrodes using (a) cross-patterning and (b) line-patterning methods.

2.3.5 Synthetic Procedures for Polythiophenes

Generally the **PTs** are obtained from α - and β substituted thiophene monomers by different polymerization methodologies in which the polymerization routes can be seen as an extension of different cross coupling reactions (see 2.2.3).

Surely the most common way to polymerize thiophene derivatives is to use the oxidative coupling. The oxidation may be done chemically or electrochemically, but the mechanisms are essentially the same. The first step is the one-electron oxidation of the monomer, resulting in a *radical cation*.

The quantum chemical calculations show in fact that for thiophene, the spin densities are high at the positions 2 and 5 consequently the reactivity is highest at these positions.

The *radical cation* reacts with a non-oxidized monomer molecule to form a *dimer*.

The extra protons disturb the aromaticity and conjugation of the system and thus the deprotonation is energetically favorable. Once formed, the *dimer* is oxidized more easily than the monomer and in this manner a *polymer* is formed.

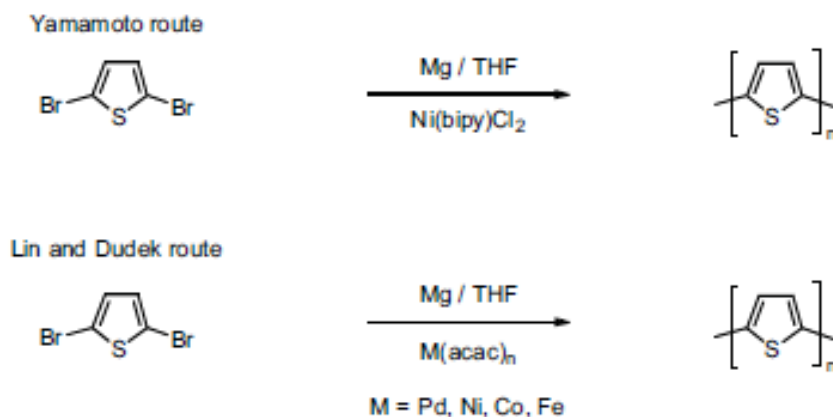
2.3.5.1 Metals Catalyzed Coupling Polymerizations

While much early effort was devoted to optimize the processes for electrochemical polymerization of thiophenes,^{177,178,179,180,181,182,183,184} most of the now commercially available **PTs** are prepared by a wide variety of chemical pathways utilizing metal-catalyzed coupling strategies.

In 1980 two research groups reported independently on the first chemical preparation of unsubstituted **PTs**.^{185,186}

Both groups used an extension of the *Kumada* coupling of Grignard reagents with *aryl halides*,¹⁸⁷ treating *2,5-dibromothiophene* with stoichiometric amounts of **Mg** in THF to yield the appropriate mono-Grignard reagent followed by subsequent homo-coupling of the difunctional intermediate utilizing a) **Ni (bipy)Cl₂** as a catalyst in the route proposed by *Yamamoto et al.* or b) **Ni (acac)₂**, **Pd (acac)₂**, **Co (acac)₂**, or **Fe (acac)₃** as reported by *Lin and Dudek*.

These routes gave unsubstituted **PTs** with only the low molecular weight fraction being soluble in common organic solvents and significant amounts up to 3% of residual metal impurities (**Scheme 1**).



Scheme 1. The first chemical synthesis of unsubstituted polythiophene.

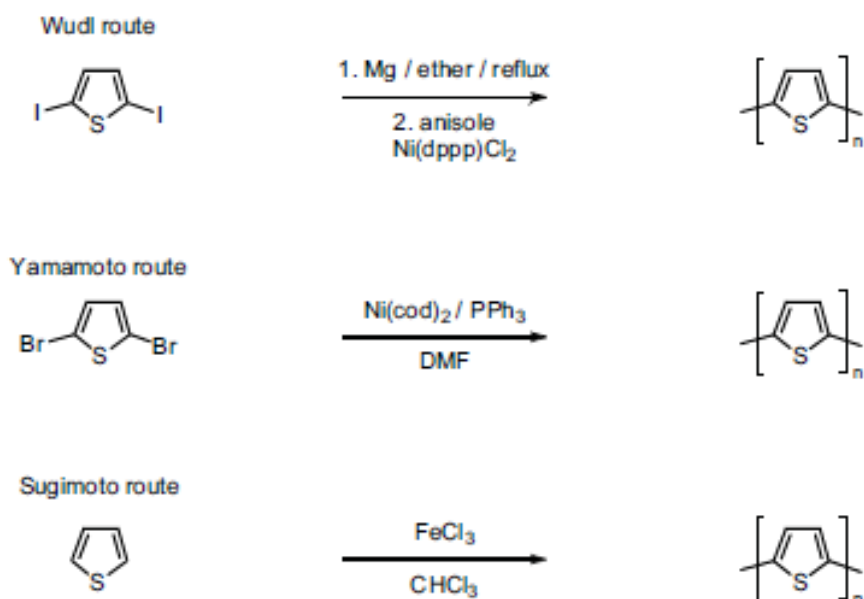
Much work was then undertaken to improve the purity and molecular weight by variation of the solvent and reagents' concentrations, catalysts and reaction conditions.^{188,189,190,191,192,193}

A major improvement was reported by *Wudl et al.* as the poorly soluble Grignard reagent was simply isolated and afterwards redissolved in hot anisole to carry out the *Kumada-type* reaction utilizing **Ni (dppp) Cl₂** as a catalyst.¹⁹⁴

A second approach to minimize the metal content was carried out using a *Yamamoto-type* coupling reaction starting from *2,5-dibromothiophene* and *Ni(COD)₂/triphenylphosphine* as the catalytic system in DMF.

Both strategies gave **PTs** in good yields and high purities with less than 50 ppm residual metal.

However, the applied reaction conditions led to a certain amount of desulfurization which then resulted in a significant drop of the conductivity for solid **PTs** films (**Scheme 2**).



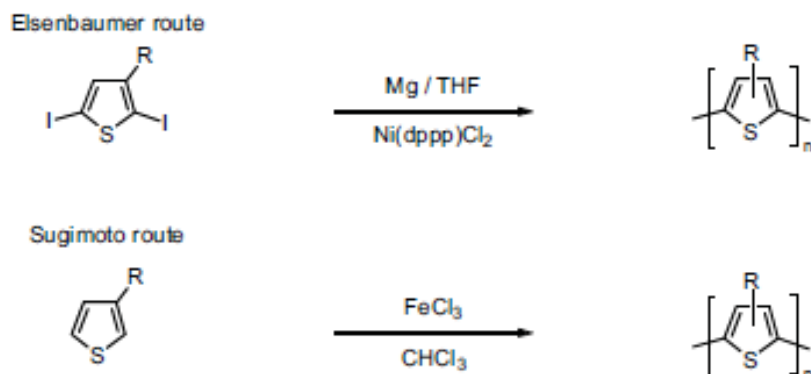
Scheme 2. Additional approaches towards unsubstituted polythiophene.

To increase the solubility and, therefore, improve the molecular weight and processability, the introduction of solubilizing side chains longer than butyl was necessary.^{195,196,197}

The first successful synthesis of **PATs** was reported by *Elsenbaumer et al.* (**Scheme 3**) and again achieved via a *Kumada*-type cross-coupling protocol similar to the previously described methods used for unsubstituted **PTs**.

A second approach was reported by *Sugimoto et al.* via oxidative polymerization of unsubstituted, as well as *3-alkyl-substituted*, thiophene monomers, utilizing **FeCl₃** as oxidizing agent in chloroform and subsequent dedoping of the material after isolation.^{198,199,200}

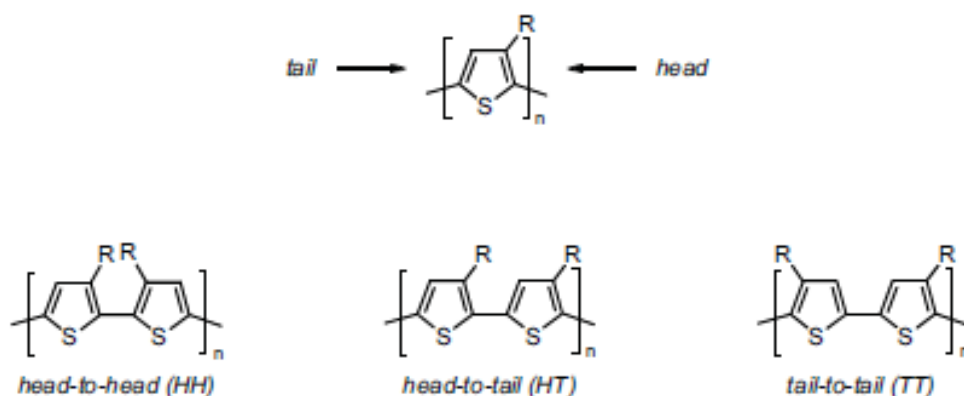
Although, this strategy produces soluble **PATs** in moderate yields and high molecular weight with sufficient purity, the oxidative coupling method did not show good reproducibility.



Scheme 3. Synthetic pathways towards poly(3-alkylthiophene).

Further structural investigations revealed that the methods described above produce *2,5-linked PATs*, exclusively, which should lead to high performance conjugated materials without *2,4-links* as structural defects, which interrupt the main-chain conjugation. As *3-alkylthiophene* is not a symmetrical molecule, three variations of the relative orientation of the building blocks are possible for the coupling of two *3-alkyl-thiophene* rings.

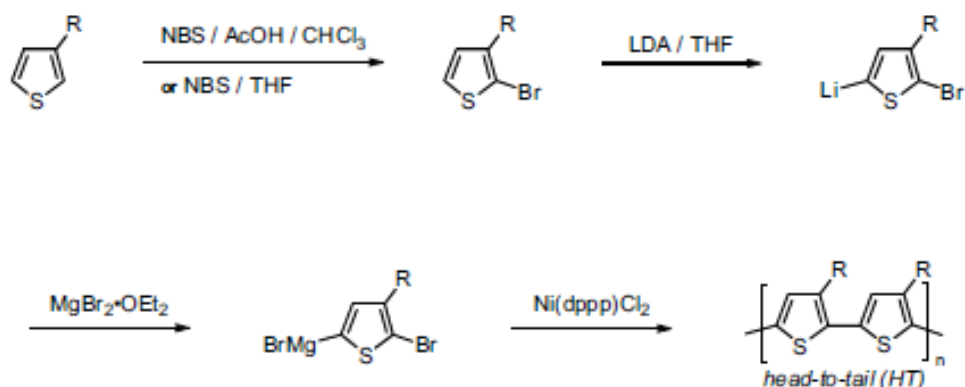
In a stereoirregular coupling, the resulting polymer randomly contains *head-to-head (HH)*, *head-to-tail (HT)*, and *tail-to-tail (TT)* coupled repeat units (**Scheme 4**).^{201,202}



Scheme 4. Regiochemical dyads of regioregular poly(alkylthiophene)s.

Furthermore electrochemical polymerization experiments using *alkylthiophene dimers* with predefined substitution patterns performed by *Wudl et al.* revealed that a higher degree of regioregularity within the resulting **PATs** is superior in its electronic performance (electrical conductivity of doped polymers) over the irregular material.²⁰³ The results were explained by a minimization of the sterical repulsion of *ortho*-substituents resulting in a less-twisted polymer backbone and therefore, as mentioned before, a higher degree of π -conjugation along the main chain.^{204,205,206}

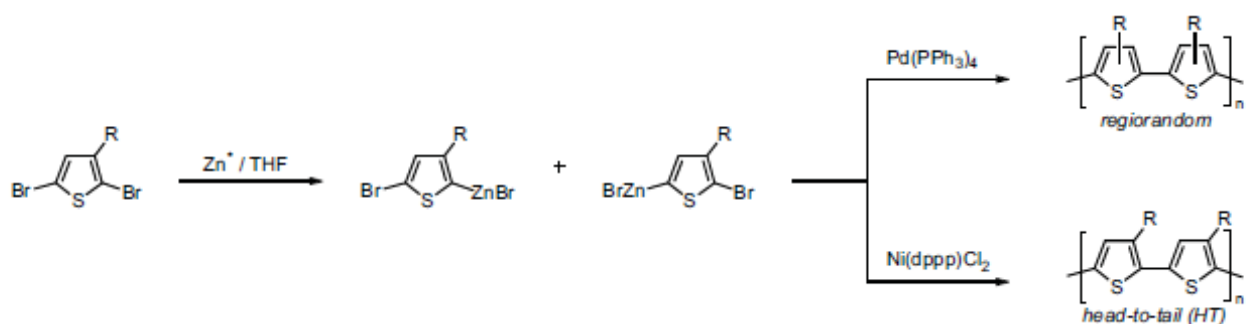
Consequently, fully *HT-coupled PATs*, denoted as regioregular **PATs** or poly(3-alkylthiophene)s (**P3ATs**), should be preferred over stereoirregular **PATs** to give a coplanar conformation (**Scheme 5**).^{207,208}



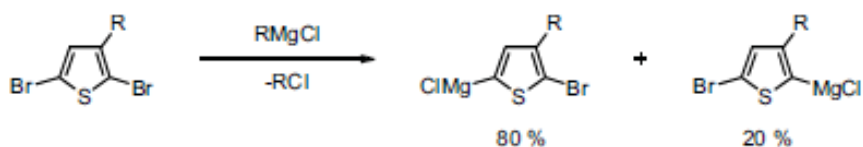
Scheme 5. The first method for the synthesis of regioregular poly(3-alkylthiophene)s after McCullough et al.

The generation of regioregular **PATs** has been demonstrated in the pioneering work of *McCullough et al.*, who reported their first synthesis via a generation of region-defined 2-bromo-5-(bromomagnesio)-3-alkylthiophene followed by a *Kumada-type* cross-coupling protocol, resulting in **P3ATs** with nearly 100 % *HT coupled*

repeat units.²⁰⁹ Further attempts were published by *Rieke et al.* by modifying the organometallic substituent utilizing activated "Rieke-zinc" (**Zn**) as metalating agent.^{210,211,212,213} The choice of the catalyst used in the *aryl-aryl-coupling* can either lead to regiorandom **Pd(PPh₃)₄** or regioregular **Ni(dppe)Cl₂** **PATs** (Scheme 6).²¹⁴



Scheme 6. The Rieke method produces either regiorandom or HT-PATs depending on the choice of the utilized catalyst.



Scheme 7. Halogen-metal exchange reaction in the Grignard metathesis (GRIM) procedure after McCullough *et al.*

To overcome the drawbacks of these methods (multistep procedure in the case of the McCullough method, use of dangerous "Rieke-zinc" in the Rieke method) *McCullough et al.* developed the so called *GRIM* (Grignard metathesis) which allows for the generation of regioregular **PATs** with high molecular weight (Mn up to 40,000 g/mol) and narrow polydispersity in a relatively simple fashion.^{215,216,217}

Similar to the *Rieke* method, the *GRIM* procedure starts from *2,5-dibromo-3-alkylthiophene*, which undergoes a *halogen-metal* exchange reaction when treated with 1 eq. of *RMgCl* (R = alkyl) (**Scheme 7**).

The reaction proceeds with a moderate degree of regioselectivity (80:20) at room temperature regardless of the Grignard reagent employed.

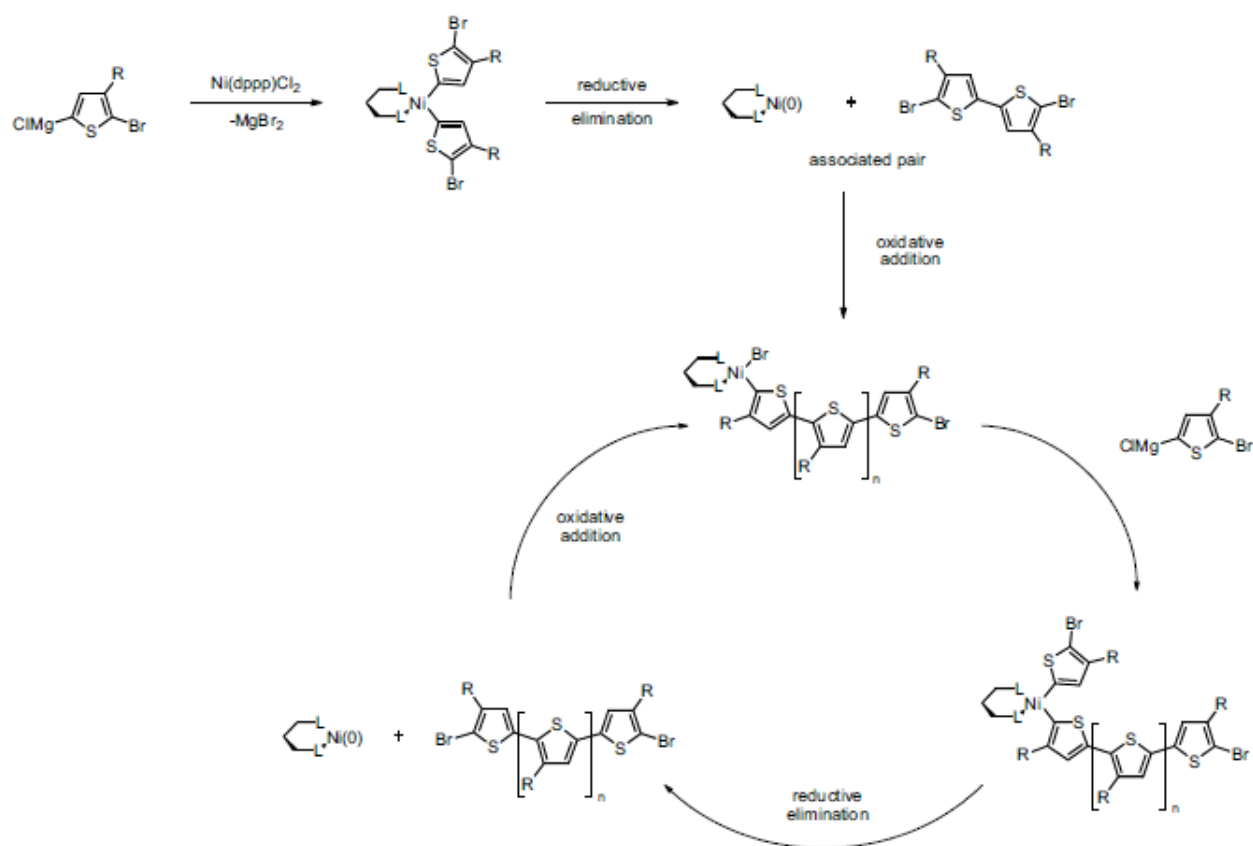
Further studies revealed that only the Grignard reagent metalated in the *5-position* is involved in the polymerization sequence while the other isomer is not consumed.

Utilizing a *nickel-based* coupling catalyst and bulky ligands favors the transformation of the less sterically hindered *5-position* and results in 95-99% *HT-couplings*.

In the initial reaction step of the catalytic cycle *2-bromo-5-chloro-magnesium-3-alkylthiophene* undergoes reductive elimination resulting in the formation of *5,5'-dibromobithienyl* (*TT-coupling*) and **Ni(0)** (**Scheme 8**).

The dimer undergoes a fast oxidative addition to a **Ni(0)** center followed by *transmetallation* with another molecule of the Grignard reagent and chain-forming reductive elimination.

Due to the highly regioselective *HT-type* fashion of the *GRIM* reaction, the formation of the initial *TT-dyad* remains the only structural defect within a single polymer chain.



Scheme 8. Mechanism of the so-called Grignard metathesis (GRIM) coupling in the synthesis of regioregular poly(3-alkylthiophene).

Finally for the synthesis of **PTs**, other synthetic procedures, as Suzuki and Stille-type reactions are exploited, in which is used Pd-catalyst rather than Ni-catalyst.

However these procedures don't succeed, on comparison to that showed for OTs (see 2.2.3.2), to carry out the synthesis of **PTs** in good yields.

2.3.5.2 MW-Assisted Synthesis of Polythiophenes

Within the last years, the use of microwave radiation as a heat source has become increasingly popular in organic synthesis,²¹⁸ since the first successful syntheses were reported in 1986 by the groups of *Giguere* and *Gedye*.^{219,220}

Especially in the field of polymer synthesis, speeding up the reaction time from hours or days to minutes to produce the polymeric materials in high yields with a minimized rate of side products by employing microwave radiation is an undeniable advantage over conventional methods.

The use of modern monomode microwave reactors that allow monitoring of temperature, pressure, stirring, and radiation levels has proven superior over multimode microwave sources in respect of controlling the reaction and furthermore, increasing security and reproducibility. A schematic setup of the monomode microwave reactor "Discoverc" fabricated by *CEM* (**Figure 56**).

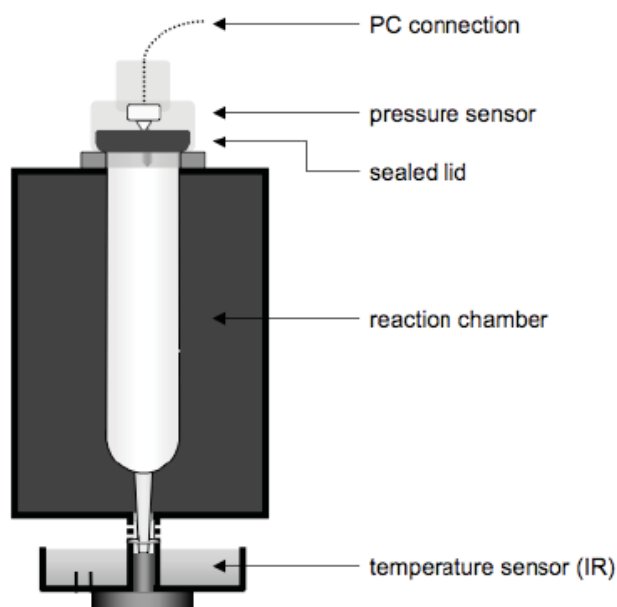


Figure 56. Schematic design of a monomode microwave reactor.

Microwave assisted chemistry gives access to high operating temperatures and elevated pressures that can be reached within a fraction of the time needed by conventional heating. Sealed vessels allow the reaction to be driven under conditions well above the boiling temperature of the solvent under atmospheric conditions.

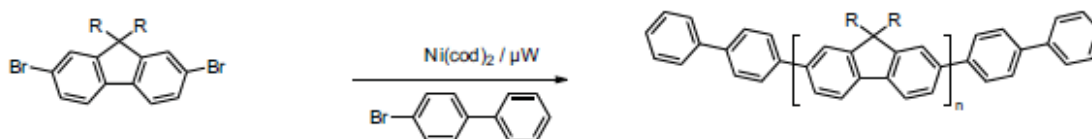
The method allows a broad variety of common organic solvents that are well established in the conventional procedures to be utilized, as long as they are amenable to microwave heating, which is determined by their (high) dielectric constant.²²¹ The response to microwave heating can also be increased by polar additives like ionic liquids or, if the reaction conditions allow, simply water.²²²

To prevent the formation of "hot nuclei" and therefore, non-uniform heating within the vessel efficient stirring is essential.

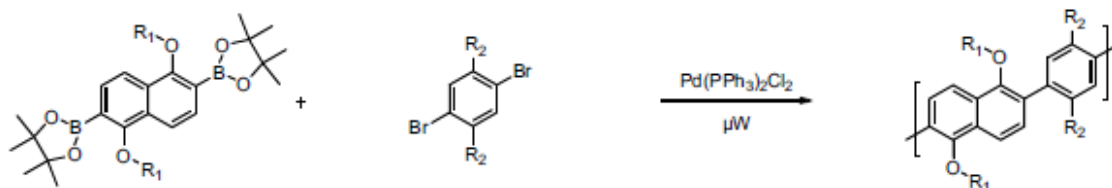
The first microwave-assisted *aryl-aryl coupling* reaction was published in 2002 by *Ken Carter et al.* *2,7-Dibromo-9,9-dihexylfluorene* was reacted in a **Ni**(0) mediated *Yamamoto-type* coupling protocol and gave the polymer [*poly(9,9-dihexylfluorene)*] with high molecular weights (M_n up to 100,000 g/mol) in a very short reaction time of only 10 min.²²³

For comparison, the conventional synthesis utilizes reaction times of several days. Later optimizations by the groups of *Yamamoto* and *Scherf* achieved a further improvement in molecular weights by changing the solvent from DMF to THF.^{224,225} In 2004 *Scherf et al.* reported the first synthesis of aromatic polymers via Pd catalyzed *Suzuki-type* and *Stille-type* cross-coupling reactions utilizing a microwave reactor as a heat source (**Scheme 9**).

Yamamoto-type coupling, Carter, 2002



Suzuki-type coupling, Scherf, 2004



Stille-type coupling, Scherf, 2004



Stille-type coupling, McCulloch, 2005



Scheme 9. First examples of microwave-assisted cross-coupling reactions via modification of the standard cross-coupling protocols.

They demonstrated that the modified reaction conditions had no effect on the quality of the produced materials.²²⁶

McCulloch et al. extended this method to the synthesis of soluble **PTs** in 2005. The procedure allowed the polymer to be obtained in higher molecular weight (>15,000) and narrower polydispersity when compared to conventional heating methods without a loss of the material's performance in **OFETs** devices.²²⁷

2.4 References

- [75] D. Fichou, *Handbook of Oligo- and Polythiophenes*, Wiley-VCH Verlag GmbH, Weinheim, **1999**
- [76] K. Müllen, and G. Wegner, *Electronic Materials: the Oligomer Approach*, Wiley-VCH Verlag GmbH, Weinheim, **1998**
- [77] L. B. Groenendaal, J. Friedrich, D. Freitag, H. Pielartzik, and J. R. Reynolds, *Adv. Mater.*, **2000**, *12*, 481-494
- [78] L. Groenendaal, G. Zotti, P. H. Aubert, S. M. Waybright, and J. R. Reynolds, *Adv. Mater.*, **2003**, *15*, 855-879
- [79] S. Kirchmeyer, and K. Reuter, *J. Mater. Chem.*, **2005**, *15*, 2077-2088
- [80] T.-A. Chen, and R. D. Rieke, *J. Am. Chem. Soc.*, **1992**, *114*, 10087-10088
- [81] T.-A. Chen, R. A. O'Brien, and R. D. Rieke, *Macromolecules*, **1993**, *26*, 3462-3463
- [82] R. D. McCullough, R. D. Lowe, M. Jayaraman, and D. L. Anderson, *J. Org. Chem.*, **1993**, *58*, 904-912
- [83] G. Horowitz, D. Fichou, X. Peng, Z. Xu, and F. Garnier, *Solid State Commun.*, **1989**, *72*, 381-384
- [84] F. Garnier, G. Horowitz, X. Peng, and D. Fichou, *Adv. Mater.*, **1990**, *2*, 592-594
- [85] F. Geiger, M. Stoldt, H. Schweizer, P. Bäuerle, and E. Umbach, *Adv. Mater.*, **1993**, *5*, 922-925
- [86] N. Noma, T. Tsuzuki, and Y. Shirota, *Adv. Mater.*, **1995**, *7*, 647-648
- [87] F. Garnier, G. Horowitz, and D. Fichou, *Synth. Met.*, **1989**, *28*, 705-714
- [88] P. Bäuerle, *Adv. Mater.*, **1992**, *4*, 102-107
- [89] S. Gronowitz, *Thiophene and its derivatives*, in *The Chemistry of Heterocyclic Compounds*, ed. A. Weissberger and E. C. Taylor, John Wiley & Sons, Inc., New York, **1985-1992**, *44*, Parts 1-5
- [90] F. Diedrich, and P. J. Stang, *Metal Catalyzed Cross-coupling Reactions*, Wiley-VCH Verlag GmbH, Weinheim, **2006**
- [91] (a) H. Korri-Youssoufi, F. Garnier, P. Srivastava, P. Godillot, A. Yassar, *J. Am. Chem. Soc.*, **1997**, *119*, 7388-7389. (b) K. Faïd, M. Leclerc, *J. Am. Chem. Soc.*, **1998**, *120*, 5274-5278. (c) M. Baek, R. C. Stevens, D. H. Charych, *Bioconjugate Chem.*, **2000**, *11*, 777-788. (d) L. Kumpumbu-Kalemba, M. Leclerc, *Chem. Commun.*, **2000**, 1847-1848

- [92] (a) H. Akimichi, K. Waragai, S. Hotta, H. Kano, and H. Sakaki, *Appl. Phys. Lett.*, **1991**, *58*, 1500. (b) F. Garnier, A. Yassar, R. Hajlaoui, G. Horowitz, F. Deloffre, B. Servet, S. Ries, and P. Alnot, *J. Am. Chem. Soc.*, **1993**, *115*, 8716
- [93] (a) H. Sirringhaus, N. Tessler, and R. H. Friend, *Science*, **1998**, *280*, 1741. (b) Z. Bao, A. J. Dodabalapur, and A. J. Lovinger, *Appl. Phys. Lett.*, **1996**, *69*, 4108
- [94] (a) M. E. Hajlaoui, F. Garnier, L. Hassine, F. Kouki, and H. Bouchriha, *Synth. Met.*, **2002**, *129*, 215. (b) Y. Y. Noh, J. J. Kim, Y. Yoshida, and K. Yase, *Adv. Mater.*, **2003**, *15*, 699
- [95] G. Horowitz, F. Garnier, A. Yassar, R. Hajlaoui, and F. Kouki, *Adv. Mater.*, **1996**, *8*, 52
- [96] M. A. Loi, E. Da Como, F. Dinelli, M. Murgia, R. Zamboni, F. Biscarini, and M. Muccini, *Nat. Mater.*, **2005**, *4*, 81
- [97] (a) D. Fichou, *J. Mater. Chem.*, **2000**, *10*, 570. (b) J. Cornil, D. Beljonne, J.-P. Calbert, and J.-L. Bredas, *Adv. Mater.*, **2001**, *13*, 1053
- [98] G. Barbarella, M. Zambianchi, L. Antolini, P. Ostojja, P. Maccagnani, A. Bongini, E. A. Marseglia, E. Tedesco, G. Gigli, and R. Cingolani, *J. Am. Chem. Soc.*, **1999**, *121*, 8920
- [99] G. Barbarella, P. Ostojja, P. Maccagnani, O. Pudova, L. Antolini, D. Casarini, and A. Bongini, *A. Chem. Mater.*, **1998**, *10*, 3683
- [100] Y. Kawamura, K. Goushi, J. Brooks, J. J. Brown, H. Sasabe, C. Adachi, *Appl. Phys. Lett.*, **2005**, *86*
- [101] G. Barbarella, L. Favaretto, M. Zambianchi, O. Pudova, C. Arbizzani, C.; A. Bongini, M. Mastragostino, *Adv. Mater.*, **1998**, *10*, 551
- [102] G. Barbarella, L. Favaretto, G. Sotgiu, M. Zambianchi, A. Bongini, C. Arbizzani, M. Mastragostino, M. Anni, G. Gigli, R. Cingolani, *J. Am. Chem. Soc.*, **2000**, *122*, 11971
- [103] M. H. Yoon, C. Kim, A. Facchetti, T. J. Marks, *J. Am. Chem. Soc.*, **2006**, *128*, 12851
- [104] M. Mazzeo, V. Vitale, F. Della Sala, M. Anni, G. Barbarella, L. Favaretto, G. Sotgiu, R. Cingolani, G. Gigli, *Adv. Mater.*, **2005**, *17*, 34
- [105] M. Zavelani-Rossi, G. Lanzani, S. De Silvestri, M. Anni, G. Gigli, R. Cingolani, G. Barbarella, L. Favaretto, *Appl. Phys. Lett.*, **2001**, *79*, 4082
- [106] M. Mazzeo, V. Vitale, F. Della Sala, D. Pisignano, M. Anni, G. Barbarella, L. Favaretto, A. Zanelli, R. Cingolani, G. Gigli, *Adv. Mater.*, **2003**, *15*, 2060

- [107] E. A. Marseglia, F. Grepioni, E. Tedesco, D. Braga, *Mol. Cryst. Liq. Cryst.*, **2000**, 348, 137
- [108] G. Barbarella, L. Favaretto, G. Sotgiu, M. Zambianchi, L. Antolini, O. Pudova, A. Bongini, *J. Org. Chem.*, **1998**, 63, 5497
- [109] G. Barbarella, L. Favaretto, G. Sotgiu, M. Zambianchi, V. Fattori, M. Cocchi, F. Cacialli, G. Gigli, R. Cingolani, *Adv. Mater.*, **1999**, 11, 1375
- [110] N. Camaioni, G. Ridolfi, V. Fattori, L. Favaretto, G. Barbarella, *Appl. Phys. Lett.*, **2004**, 84, 1901
- [111] L. Antolini, E. Tedesco, G. Barbarella, L. Favaretto, G. Sotgiu, M. Zambianchi, M. D. Casarini, G. Gigli, R. Cingolani, *J. Am. Chem. Soc.*, **2000**, 122, 9006
- [112] G. Barbarella, L. Favaretto, G. Sotgiu, L. Antolini, G. Gigli, R. Cingolani, A. Bongini, *Chem. Mater.*, **2001**, 13, 4112
- [113] K. Tamao, K. Sumitani, Y. Kiso, M. Zembayashi, A. Fujioka, S. Kodama, I. Nakajima, A. Minato, M. Kumada, *Bull. Chem. Soc. Jpn.*, **1976**, 49, 1958-1969
- [114] A. Suzuki, *Pure Appl. Chem.*, **1991**, 63, 419-422
- [115] S. Kotha, K. Lahiri, D. Kashinath, *Tetrahedron*, **2002**, 58, 9633-9695
- [116] K. Sonogashira, Y. Tohda, N. Hagihara, *Tetrahedron Lett.*, **1975**, 16, 4467-4470
- [117] J. K. Stille, *Angew. Chem. Int. Ed.*, **1986**, 25, 508-524
- [118] M. Miyasaka, A. Rajca, *Synlett*, **2004**, 177-181
- [119] R. Chinchilla, C. Nájera, M. Yus, *Chem. Rev.*, **2004**, 104, 2667-2722
- [120] Y. Ito, T. Konoike, T. Harada, T. Saegusa, *J. Am. Chem. Soc.*, **1977**, 99, 1487
- [121] S. Gronowitz, H.-O. Karlson, *Arkiv Kemi*, **1961**, 17, 89
- [122] T. Kauffmann, *Angew. Chem.*, **1974**, 86, 321
- [123] P. E. Fanta, *Synthesis*, **1974**, 9
- [124] K. Tamao, S. Kodama, I. Nakajima, M. Kumada, *Tetrahedron*, **1982**, 38, 3347
- [125] J. K. Stille, *Angew. Chem.*, **1986**, 98, 504
- [126] V. N. Kalinin, *Synthesis*, **1992**, 413
- [127] G. T. Crisp, *Synth. Commun.*, **1989**, 19, 307
- [128] S. Gronowitz, D. Peters, *Heterocycles*, **1990**, 30, 645
- [129] (a) E. Negishi, F. T. Luo, R. Frisbee, H. Matsuchita, *Heterocycles*, **1982**, 18, 117. (b) T. Frejd, T. Klingstedt, *Synthesis*, **1987**, 40

- [130] A. Minato, K. Tamao, T. Hayashi, K. Suzuki, M. Kumada, *Tetrahedron Lett.*, **1980**, 845
- [131] T. A. Skotheim, *Handbook of Conducting Polymers.*, 2nd ed.; Marcel Dekker: New York, 1997
- [132] Y. Furukawa, M. Akimoto, I. Harada, *Synth. Met.*, **1987**, 18, 151
- [133] D. Delabouglise, R. Garreau, M. Lemaire, J. Roncali, *New J. Chem.*, **1988**, 12, 155
- [134] J. Roncali, F. Garnier, *New J. Chem.*, **1986**, 10, 237
- [135] J. Roncali, A. Yassar, F. Garnier, *Chem. Commun.*, **1988**, 9, 581
- [136] A. Yassar, J. Roncali, F. Garnier, *Macromolecules*, **1989**, 22, 804
- [137] S. Hotta, *Synth. Met.*, **1987**, 22, 103
- [138] M.-A. Sato, S. Tanaka, K. Kaeriyama, *Synth. Met.*, **1986**, 14, 279
- [139] J. L. Sauvajol, D. Chenouni, J. P. Lere-Porte, C. Chorro, B. Moukala, J. Petrissans, *Synth. Met.*, **1990**, 38, 1
- [140] J. Roncali, M. Lemaire, R. Garreau, F. Garnier, *Synth. Met.*, **1987**, 18, 139
- [141] M. Granstrom, O. Inganas, *Appl. Phys. Lett.*, **1996**, 68, 147
- [142] J. Roncali, *Chem. Rev.*, **1997**, 97, 173
- [143] M. Muthujumar, C. K. Ober, E. L. Thomas, *Science*, **1997**, 277, 1225
- [144] E. Ruckenstein, J. Park, *Synthetic Metals*, **1991**, 44, 293
- [145] R. D. McCullough, and R. D. Lowe, *J. Chem. Soc., Chem. Commun.*, **1992**, 70-72
- [146] X. Wu, T.-A. Chen, and R. D. Rieke, *Macromolecules*, **1996**, 29, 7671-7677
- [147] M. Lemaire, D. Delabouglise, R. Garreau, A. Guy, J. Roncali, *Journal of the Chemical Society, Chemical Communications*, **1988**, 10, 658
- [148] H. Goto, Y. Okamoto, E. Yashima, *Macromolecules*, **2002**, 35, 4590
- [149] A. Pron, and P. Rannou, *Prog. Polym. Sci.*, **2002**, 27, 135
- [150] I. F. Perepichka, D. F. Perepichka, H. Meng, and F. Wudl, *Adv. Mater.*, **2005**, 17, 2281
- [151] J.-L. Bredas, *J. Chem. Phys.*, **1985**, 82, 3809
- [152] Z. Bao, A. Dodabalapur, and A. Lovinger, *Appl. Phys. Lett.*, **1996**, 69, 4108
- [153] H. Sirringhaus, N. Tessler, and R. H. Friend, *Science*, **1998**, 280, 1741
- [154] N. C. Greenham, I. D. W. Samuel, G. R. Hayes, R. T. Phillips, Y. A. R. R. Kessener, S. C. Moratti, A. B. Holmes, R. H. Friend, *Chem. Phys. Lett.*, **1995**, 241, 89

- [155] F. Chen, P. G. Metha, L. Tajiff, R. D. McCullough, *J. Mater. Chem.*, **1996**, *6*, 1763
- [156] H. Saadeh, T. Goodson, L. Yu, *Macromolecules*, **1997**, *30*, 4608
- [157] a) B. Kraabel, D. Moses, A. J. Heeger, *J. Chem. Phys.*, **1995**, *103*, 5102. b) D. Belyonne, Z. Shuai, G. Pourtois, J.-L. Bredas, *J. Phys. Chem. A*, **2001**, *105*, 3889
- [158] a) S. D. D. Rughooputh, S. Hotta, A. J. Heeger, F. Wudl, *J. Polym. Sci.*, **1987**, *25*, 1071. b) O. Inganäs, W. R. Salaneck, J.-E. Österholm, J. Laakso, *Synth. Met.*, **1988**, *22*, 395. c) O. Inganäs, G. Gustafson, W. R. Salaneck, *Synth. Met.*, **1989**, *28*, 377
- [159] a) M. Leclerc, K. Faïd, *Handbook of Conducting Polymers*, **1998**, 695. b) O. Inganäs, G. Gustafson, *Synth. Met.*, **1990**, *37*, 195
- [160] G. Zerbi, B. Chierichetti, O. Inganäs, *J. Chem. Phys.*, **1991**, *94*, 4646
- [161] Y. Ohmori, M. Uchida, K. Muro, K. Yoshino, *Jps. J. Appl. Phys.*, **1991**, *30*, 1938. b) Y. Ohmori, M. Uchida, K. Muro, K. Yoshino, *Solid State Commun.*, **1991**, *80*, 605
- [162] D. Braun, G. Gustaffson, D. McBranch, A. J. Heeger, *J. Appl. Phys.*, **1992**, *72*, 564
- [163] M. Uchida, Y. Ohmori, C. Morishima, K. Yoshino, *Synth. Met.*, **1993**, *55-57*, 4168
- [164] N. C. Greenham, A. R. Brown, D. D. C. Bradley, R. H. Friend, *Synth. Met.*, **1993**, *57*, 4134
- [165] A. Bolognesi, C. Botta, Z. Geng, C. Flores, L. Denti, *Synth. Met.*, **1995**, *71*, 2191
- [166] A. Bolognesi, W. Porzio, G. Bajo, G. Zannoni, L. Fanning, *Acta Polym.*, **1999**, *50*, 151
- [167] A. Bolognesi, C. Botta, L. Cecchinato, *Synth. Met.*, **2000**, *111-112*, 187
- [168] M. Pomerantz, H. Yang, Y. Cheng, *Macromolecules*, **1995**, *28*, 5706
- [169] S.-H. Ahn, M.-Z. Czae, E.-R. Kim, H. Lee, S.-H. Han, J. Noh, M. Hara, *Macromolecules*, **2001**, *34*, 2552
- [170] A. Bolognesi, W. Porzio, F. Provasoli, T. Ezquerra, *Makroml. Chem.*, **1993**, *194*, 817
- [171] A. Berlin, G. Zotti, S. Zecchin, G. Schiavon, M. Cocchi, D. Virgili, C. Sabatini, *J. Mater. Chem.*, **2003**, *13*, 27
- [172] N. Leventis, *Polym. News*, **1995**, *20*, 5

- [173] G. Sonmez, P. Schottland, J. R. Reynolds, *Synth. Met.*, **2005**, *155*, 130
- [174] O. Inganäs, T. Johansson, S. Ghosh, *Electrochim. Acta*, **2001**, *46*, 2031
- [175] E. Ünür, L. Toppare, Y. Yagci, F. Yilmaz, *Mater. Chem. Phys.*, **2005**, *91*, 261
- [176] P. Aubert, M. Knipper, L. Groenendaal, L. Lutsen, J. Manca, D. Vanderzande, *Macromolecules.*, **2004**, *37*, 4087
- [177] J. Roncali, *J. Mater. Chem.*, **1999**, *9*, 1875
- [178] B. Ballarin, R. Seeber, L. Tassi, D. Tonelli, *Synth. Met.*, **2000**, *114*, 279
- [179] C. Zanardi, R. Scanu, L. Pigani, M. I. Pilo, G. Sanna, R. Seeber, N. Spano, F. Terzi, A. Zucca, *Electrochim. Acta*, **2006**, *51*, 4859
- [180] H. Brisset, A.-E. Navarro, F. Moggia, B. Jousseme, P. Blanchard, J. Roncali, *J. Electroanal. Chem.*, **2007**, *603*, 149
- [181] B. Ballarin, M. Lanzi, L. Paganin, G. Cesari, *Electrochim. Acta*, **2007**, *52*, 7849
- [182] M. Talu, M. Kabasakaloglu, F. Yildirim, B. Sari, *Appl. Surf. Sci.*, **2001**, *181*, 51
- [183] D. Demeter, P. Blanchard, M. Allain, I. Grosu, J. Roncali, *J. Org. Chem.*, **2007**, *72*, 5285
- [184] A. Galal, E. T. Lewis, O. Y. Ataman, H. Zimmer, H. B. Mark, *J. Polym. Sci.*, **1989**, *27*, 1891
- [185] J. W. P. Lin, L. P. Dudek, *J. Polym. Sci.*, **1980**, *18*, 2869
- [186] T. Yamamoto, K. Sanechika, A. Yamamoto, *J. Polym. Sci.*, **1980**, *18*, 9
- [187] K. Tamo, K. Sumitani, M. Kumada, *J. Am. Chem. Soc.*, **1972**, 4376
- [188] C. Z. Hotz, P. Kovacic, I. A. Houry, *J. Polym. Sci.*, **1983**, *21*, 2617
- [189] T. Yamamoto, T. Maruyama, Z. H. Zhou, Y. Miyazaki, T. Kanbara, K. Sanechika, *Synth. Met.*, **1991**, *41*, 345
- [190] T. Yamamoto, A. Morita, T. Maruyama, Z. H. Zhou, T. Kanbara, K. Sanechika, *Polym. J.*, **1990**, *22*, 187
- [191] T. Yamamoto, K. Osakada, T. Wakabayashi, A. Yamamoto, *Makromol. Chem. - Rapid Commun.*, **1985**, *6*, 671
- [192] T. Yamamoto, A. Morita, Y. Miyazaki, T. Maruyama, H. Wakayama, Z. Zhou, Y. Nakamura, T. Kanbara, S. Sasaki, K. Kubota, *Macromolecules*, **1992**, *25*, 1214
- [193] I. Colon, G. T. Kwiatkowski, *J. Polym. Sci.*, **1990**, *28*, 367
- [194] M. Kobayashi, J. Chen, T. C. Chung, F. Moraes, A. J. Heeger, F. Wudl, *Synth. Met.*, **1984**, *9*, 77

- [195] K. Y. Jen, G. G. Miller, R. L. Elsenbaumer, *Chem. Commun.*, **1986**, 1346
- [196] T. R. Jow, K. Y. Jen, R. L. Elsenbaumer, L. W. Shacklette, M. Angelopoulos, M. P. Cava, *Synth. Met.*, **1986**, *14*, 53
- [197] R. L. Elsenbaumer, K. Y. Jen, R. Oboodi, *Synth. Met.*, **1986**, *15*, 169
- [198] R. Sugimoto, S. Takeda, K. Yoshino, *Chem. Express*, **1986**, 635
- [199] K. Yoshino, S. Hayashi, R. Sugimoto, *Jpn. J. Appl. Phys.*, **1984**, *23*, 899
- [200] M. Pomerantz, J. J. Tseng, H. Zhu, S. J. Sproull, J. R. Reynolds, R. Uitz, H. J. Arnott, M. I. Haider, *Synth. Met.*, **1991**, *41*, 825
- [201] M. A. Sato, H. Morii, *Polym. Commun.*, **1991**, *32*, 42
- [202] M. A. Sato, H. Morii, *Macromolecules*, **1991**, *24*, 1196
- [203] R. M. S. Maior, K. Hinkelmann, H. Eckert, F. Wudl, *Macromolecules*, **1990**, *23*, 1268
- [204] H. Sirringhaus, P. J. Brown, R. H. Friend, M. M. Nielsen, K. Bechgaard, B. M. W. Langeveld-Voss, A. J. H. Spiering, R. A. J. Janssen, E. W. Meijer, P. Herwig, D. M. De Leeuw, *Nature*, **1999**, *401*, 685
- [205] R. D. McCullough, *Adv. Mater.*, **1998**, *10*, 93
- [206] G. Barbarella, A. Bongini, M. Zambianchi, *Macromolecules*, **1994**, *27*, 3039
- [207] R. D. McCullough, R. D. Lowe, M. Jayaraman, D. L. Anderson, *J. Org. Chem.*, **1993**, *58*, 904
- [208] R. D. McCullough, R. D. Lowe, M. Jayaraman, P. C. Ewbank, D. L. Anderson, S. Tristramnagle, *Synth. Met.*, **1993**, *55*, 1198
- [209] G. Barbarella, M. Zambianchi, A. Bongini, L. Antolini, *Adv. Mater.*, **1994**, *6*, 561
- [210] X. M. Wu, T. A. Chen, R. D. Rieke, *Macromolecules*, **1995**, *28*, 2101
- [211] T. A. Chen, R. D. Rieke, *J. Am. Chem. Soc.*, **1992**, *114*, 10087
- [212] T. A. Chen, R. A. Obrien, R. D. Rieke, *Macromolecules*, **1993**, *26*, 3462
- [213] T. A. Chen, R. D. Rieke, *Synth. Met.*, **1993**, *60*, 175
- [214] T. A. Chen, X. M. Wu, R. D. Rieke, *J. Am. Chem. Soc.*, **1995**, *117*, 233
- [215] M. C. Iovu, E. E. Sheina, R. R. Gil, R. D. McCullough, *Macromolecules*, **2005**, *38*, 8649
- [216] R. L. Loewe, P. C. Ewbank, J. S. Liu, L. Zhai, R. D. McCullough, *Macromolecules*, **2001**, *34*, 4324
- [217] R. S. Loewe, S. M. Khersonsky, R. D. McCullough, *Adv. Mater.*, **1999**, *11*, 250
- [218] D. Adam, *Nature*, **2003**, *421*, 571

- [219] R. J. Giguere, T. L. Bray, S. M. Duncan, G. Majetich, *Tetrahedron Lett.*, **1986**, 27, 4945
- [220] R. Gedye, F. Smith, K. Westaway, H. Ali, L. Baldisera, L. Laberge, J. Rousell, *Tetrahedron Lett.*, **1986**, 27, 279
- [221] D. V. Stass, J. R. Woodward, C. R. Timmel, P. J. Hore, K. A. McLauchlan, *Chem. Phys. Lett.*, **2000**, 329, 15
- [222] J. M. Pringle, M. Forsyth, D. R. MacFarlane, K. Wagner, S. B. Hall, D. L. Officer, *Polymer*, **2005**, 46, 2047
- [223] K. R. Carter, *Macromolecules*, **2002**, 35, 6757
- [224] T. Yamamoto, Y. Fujiwara, H. Fukumoto, Y. Nakamura, S. Y. Koshihara, T. Ishikawa, *Polymer*, **2003**, 44, 4487
- [225] F. Galbrecht, X. H. Yang, B. S. Nehls, D. Neher, T. Farrell, U. Scherf, *Chem. Commun.*, **2005**, 2378
- [226] B. S. Nehls, U. Asawapirom, S. Fuldner, E. Preis, T. Farrell, U. Scherf, *Adv. Funct. Mater.*, **2004**, 14, 352
- [227] L. McCulloch, C. Bailey, M. Giles, M. Heeney, I. Love, M. Shkunov, D. Sparrowe, S. Tierney, *Chem. Mater.*, **2005**, 17, 1381

3 Thiophene- Based Materials in Organic Photovoltaics

3.1 The Energy Question

The energy question has become one of most major and worrying problem of the modern society. The worldwide demand for energy has grown dramatically over the last century as consequence of the increase in the industrialization of the world. The need for energy is likely to grow even more in the 21st century with the improvements in living standards across the planet; moreover, the economic develop of Asiatic nation, like *China* and *India*, has emphasized the problem of energy demand (**Figure 57**).

This high demand of energy, the pollution generated by energy sources currently used and the depletion of natural resources bring into question.

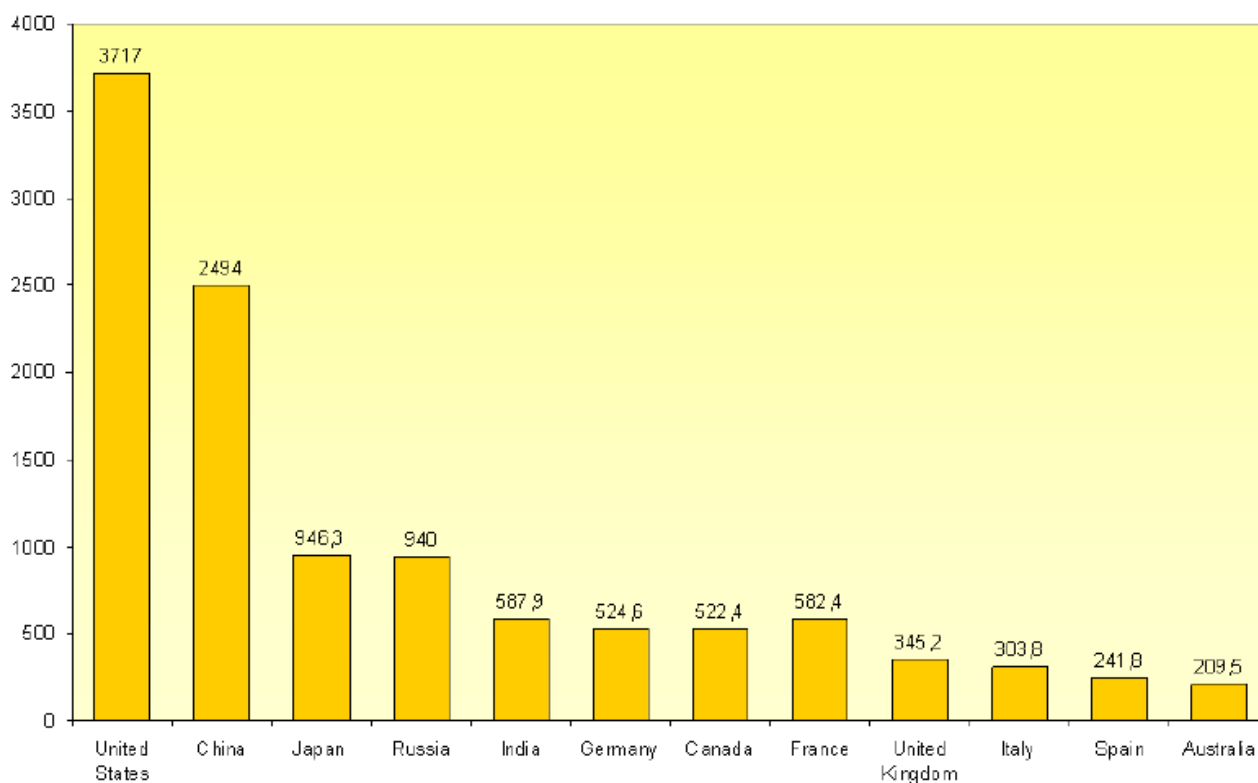


Figure 57. Total energy consumed annually in the most important country.

Oil gas and coal are usually referred to as fossil fuels. The percentage of energy production that is from fossil fuels (oil, coal, and natural gas) was actually still high, more than 70% in the *US* in 2010 and nearly 80% in *Italy* (**Figure 58**).

The production of electric power and heat is achieved by the combustion of fossil fuels.

Carbon dioxide (CO_2) and sulfur compounds like SO_2 are the product of this process. While the former is related to the greenhouse effect leading to global warming and the rise in sea level, the latter is a cause of acid rain harming the environment.

Moreover, everybody knows that the earth's resources of oil, coal, and natural gas are limited and will deplete sooner or later.

Was *M. King Hubbert* the first to predict in 1956 the Peak oil, the point in time when the maximum rate of global petroleum extraction is reached. After this peak, the rate of production enters terminal decline, as shown in his famous Hubbert curve (**Figure 59**).

Most of analyses indicate that the worldwide Hubbert peak would reach in the second decade of 21st century, between 2010 and 2020. This suggests that within 15 years oil and natural gas production rates will start to decrease.

With these prospects, new sources of energy must be implemented that do not rely on depleting resources.

The energy sources that use natural resources without depleting them and with no harmful side effects for the environment are called *Renewable Sources*. Wind energy, energy from water (hydroelectricity), biomass, geothermal and solar energy are the most renowned examples.

The most interesting source for its availability, is the sun. The sun has produced energy for billions of years. Solar energy is the sun's rays (solar radiation) that reach the earth.

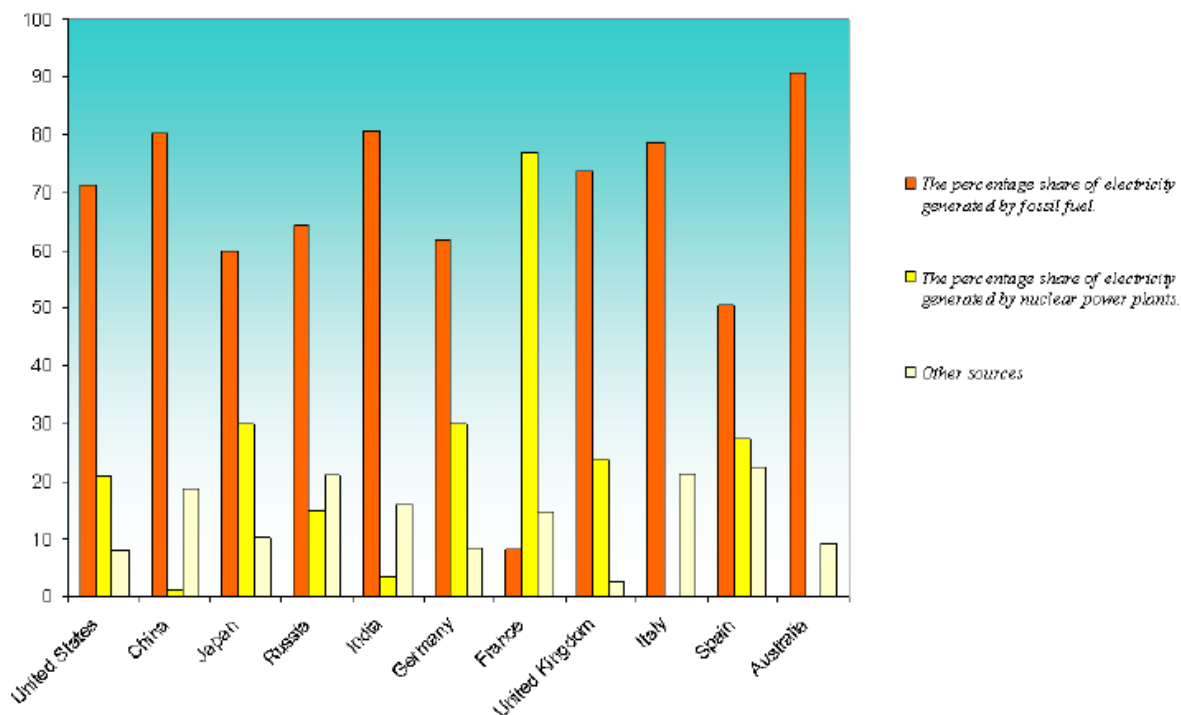


Figure 58. The percentage share of electricity generated by different sources.

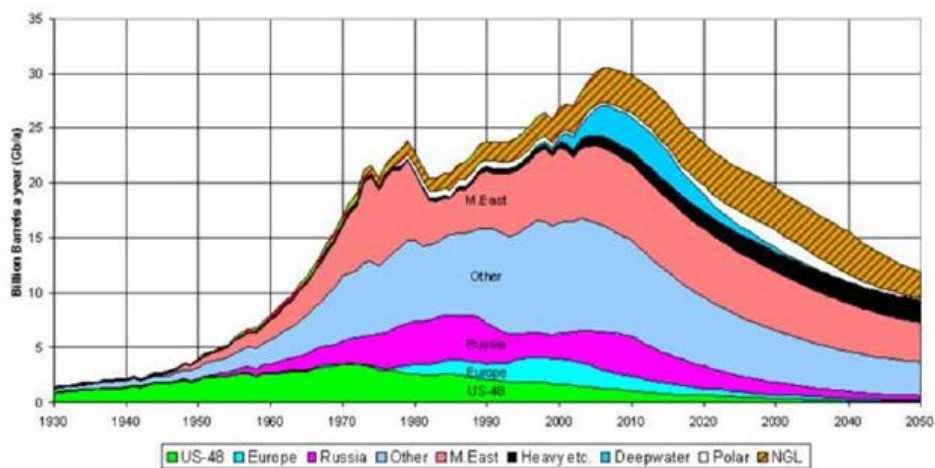


Figure 59. The Hubbert's curve.

The amount of energy available from the sun outside the Earth's atmosphere is approximately 1367 W/m^2 ; obviously, some of the solar energy is absorbed as it passes through the Earth's atmosphere.

As a result, on a clear day the amount of solar energy available at the Earth's surface in the direction of the sun is typically 1000 W/m^2 . The high power reaching every day all regions of our planet makes this primary source the most interesting between the renewable energy sources.

Two are the most important way to exploit sun energy: the solar collector systems, which permit to heat water, or the direct conversion into electric energy in photovoltaic devices. The first technology is quite mature, and already finds a large use also in domestic employment.

Unfortunately, at the moment, the second one cannot produce energy at the low cost that conventional fossil fuel power plants can. The R&D focalizes its attention to improve the efficiencies of the *photovoltaic devices* (**PVDs**) making this technology more convenient (also in term of cost) in respect of those based on fossil fuel.

The governs are fortunately investing in this technology, as demonstrate the high photovoltaic capacity installed in some European country, *Germany* in the lead (**Figure 60**) because the organic materials are characterized by the possibility of fast, simple, low-cost and high-volume processing.

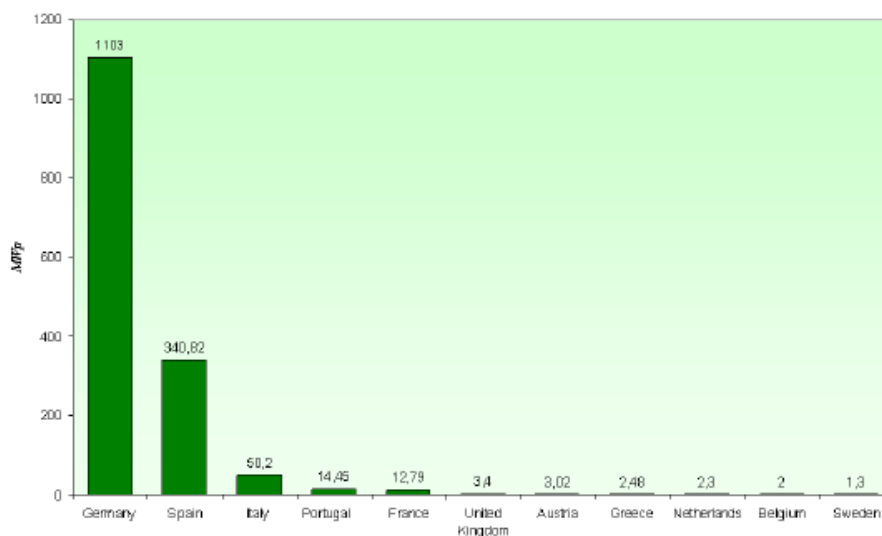


Figure 60. Photovoltaic capacity installed in Europe.

In fact from an industrial viewpoint, this very attractive feature has resulted in finding a new, exciting application of such materials in the field of photovoltaic (**PV**) or, in other words, creating a new generation of organic solar cell devices.

3.2 Silicon Solar Cells

The *silicon* based **PVDs** are the most diffused system to convert sun energy in electricity: they dominate the photovoltaic market by 80%.

The first *silicon solar cell* (**SSCs**) was developed by *Chapin, Fuller and Pearson* at the *Bell Telephone Laboratories* in the mid 1950's, and it had already about 6% efficiency which was rapidly increased to 10%.

Solar cell technology benefited greatly from the high standard of *silicon* technology developed originally for transistors and later for integrated circuits and the best research-cells efficiencies are displayed below (Figure 61).

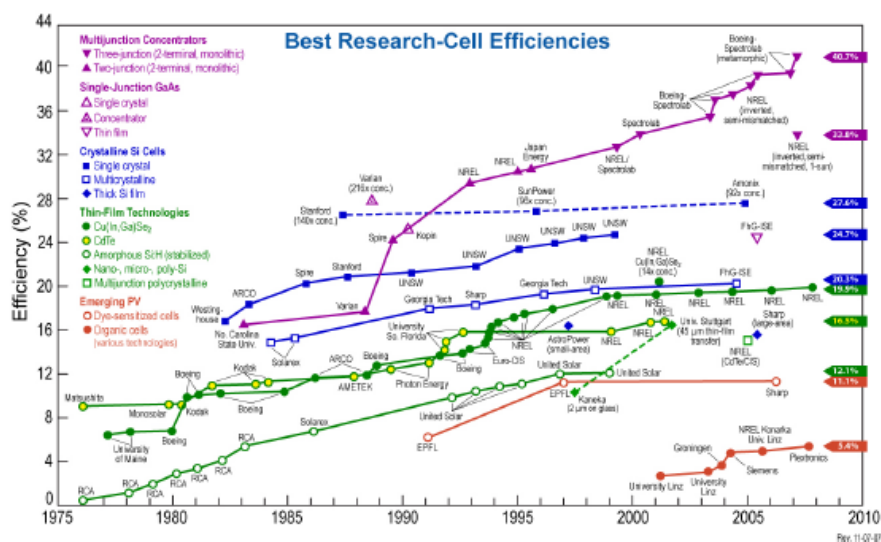


Figure 61. Reported timeline of solar cell energy conversion efficiencies.

This applied also to the quality and availability of single crystal *silicon* of high perfection. In the first years only *Czochralski (Cz)* grown single crystals were used for solar cells. This material still plays an important role.

Polycrystalline material in the form of fragments obtained from highly purified poly-silicon is placed in a quartz crucible which itself is located in a graphite crucible and melted under inert gases by induction heating.

A seed crystal is immersed and slowly withdrawn under rotation. At each dipping of the seed crystal into the melt, dislocations are generated in the seed crystal even if it was dislocation free before.

To obtain a dislocation free state, a slim crystal neck of about 3 mm diameter must be grown with a growth velocity of several millimeters per minute. The dislocation free state is rather stable and large crystal diameters can be grown despite the high cooling strains in large crystals.²²⁸

SSCs has benefited from the fast development in the integrated circuit industry (**Figure 62**), and this means that it is now possible to produce *SSCs* with efficiencies as high as 25%, and at a much lower cost than previously.²²⁹

The prices for solar cell power today lies between \$ 10 and 12W^{-1} , based on today prices on the internet.²³⁰



Figure 62. A *SSC* made from a mono-crystalline silicon wafer.

3.2.1 Physics of Silicon Solar Cells

SSCs solar cells are based on the physical principles described by *Planck's* law. This law states that the energy of a single photon is equal to $h\nu$, where h is *Planck's* constant and ν is the frequency of the light. The energy is thus proportional to the frequency and inversely proportional to the wavelength.

When light, with a frequency corresponding to an energy larger than the **E_g**, hits a semiconductor like *silicon* some of the electrons are excited into higher energy levels.

Only if the energy of the photons are larger than the **E_g**, the electron can be excited.

If the energy is much larger than the **E_g** the electron can be ejected from the material. This is known as the photoelectric effect. In these excited states the electrons are more free to move, and can thus lead a current if a potential difference is imposed across the cell.

This potential difference arises from a built in asymmetry in the cell. **SSCs** are built from several different layers, two of them being *n-type silicon* (negative - excess of electrons) and *p-type silicon* (positive - excess of holes). Naturally found *silicon* has 14 electrons, 4 of them being valence electrons.

In the solid state *silicon* forms covalent bonds with four neighboring *silicon* atoms, and this forms the crystal lattice. To create *n-type* and *p-type silicon*, impurities are introduced into the crystal lattice. This controlled and on purpose contamination of *silicon* is known as doping. *N-type silicon* can be created by doping with *phosphorus*.

Phosphorus is incorporated into the crystal lattice where it occupies a lattice point which would otherwise be occupied by a *silicon* atom. Because phosphorus contains five valence electrons, and only four of them are used for bonding, there is one excess electron per unit cell.

Similarly, to create *p-type silicon*, atoms with three valence electrons, for example *boron*, are incorporated into the lattice producing an excess amount of holes. When *p-type* and *n-type silicon* are brought together a *p/n junction* is formed at the interface.

Because of the excess of electrons on one side, and the excess of holes on the other side electrons and holes recombine at the junction, creating an insulating junction which is termed the depletion zone.

When electrons flow from the *n-type* side towards the junction, excess positive charge is left behind. Similarly, excess negative charge is left behind when holes flow to the junction. This excess charge is not free to move because it is part of the chemical bonds between atoms.

As a result an electric field directed from the *n-type* side to the *p-type* side is established (**Figure 63**).

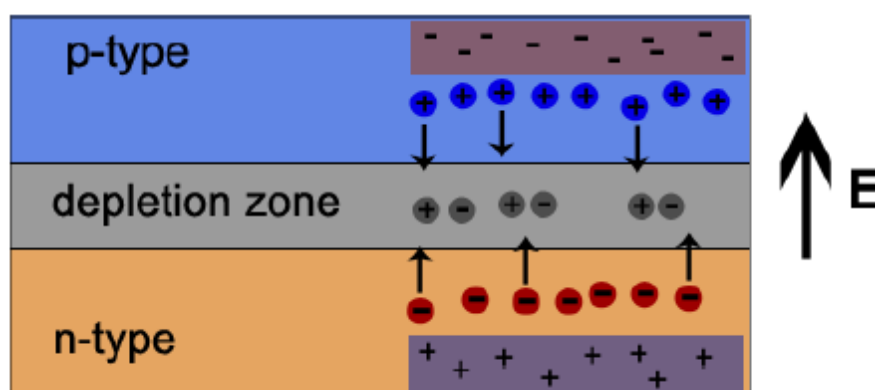


Figure 63. Illustration of the depletion layer. When the p-type and n-type layer are brought together, electrons from the n-type side recombine with holes from the p-type side at the depletion layer. The depletion layer is therefore an insulating layer because there are no free charge carriers.

A basic **SSC** unit produces a photovoltage of between 0.5 and 1.0 volt and a photocurrent of some tens of milliamps per cm^2 when illuminated by the sun.

This voltage is too small for most applications and therefore multiple cells are connected in series into modules.²³¹

3.3 Organic Solar Cells

Fossil fuel alternatives, such as solar energy, are moving to the forefront in a variety of research fields. Polymer-based organic photovoltaic systems hold the promise for a cost-effective, lightweight solar energy conversion platform, which could benefit from simple solution processing of the active layer.

The function of such excitonic solar cells is based on photoinduced electron transfer from a donor to an acceptor. The most effective solar cells or so-called bulk heterojunctions (**BHJ**) currently achieve an efficiency of about 8%, thus significant advances in the fundamental understanding of the complex interplay between the active layer morphology and electronic properties are required if this technology is to find viable application.

Organic solar cells (**OSCs**) belong to the class of photovoltaic cells known as excitonic solar cells, which are characterized by strongly bound electron-hole pairs (excitons) that are formed after excitation with light.²³² Strongly bound excitons exist in these materials as a consequence of the low dielectric constants in the organic components, which are insufficient to affect direct electron-hole dissociation, as is found in their high dielectric inorganic counterparts.

In excitonic solar cells, exciton dissociation occurs almost exclusively at the interface between two materials of differing electron affinities (and/or ionization potentials): the electron donor (or simply donor), a *p-type organic material*, and the electron acceptor (or simply acceptor), a *n-type organic material*.

To generate an effective photocurrent in these organic solar cells, an appropriate donor-acceptor pair and device architecture must be selected.

Two main approaches have been explored in the effort to develop viable devices: the *donor-acceptor bilayer*,^{233,234,235} commonly achieved by vacuum deposition of molecular components,²³⁶ and the so-called bulk heterojunction (**BHJ**),^{237,238} which is represented in the ideal case as a bicontinuous composite of *donor* and *acceptor* phases, thereby maximizing the all-important interfacial area between the *donors* and *acceptors*.

Polymer-based photovoltaic systems which can be processed in solution, and which generally take the form of **BHJ** devices, most closely conform to the ultimate vision of organic solar cells as low-cost, lightweight, and flexible devices.

The real advantage of these **BHJ** devices, which can be processed in solution, over vacuum deposition is the ability to process the composite active layer from solution in a single step, by using a variety of techniques that range from inkjet printing to spin coating and roller casting.

However, regardless of the method of preparation, one feature that extends across all classes of organic solar cells is the almost ubiquitous use of *fullerenes-C₆₀* as the electron accepting component; the high electron affinity and superior ability to transport charge make *fullerenes* the best acceptor component currently available for these devices.

The solubility of simple *C₆₀* is limited. *Wudl et al.* synthesized a soluble derivative of *C₆₀*, **PCBM** (*1-(3-methoxycarbonyl) propyl-1-phenyl[6,6]C₆₁*),²³⁹ which has been widely used in polymer/fullerene solar cells due to its solubility.

Important representatives of hole conducting donor-type semiconducting polymers on the other side are (a) derivatives of phenylene vinylene backbones such as poly[2-methoxy-5-(3,7-dimethyloctyloxy)]-1,4-phenylenevinylene) (**MDMOPPV**), (b) derivatives of thiophene chains such as poly(3-hexylthiophene) **P3HT**, and (c) derivatives of fluorine backbones such as (poly(9,9'-dioctylfluorene-co-bis-N,N'-(4-butylphenyl)-1,4-phenylenediamine) (**PFB**) (**Figure 64**).

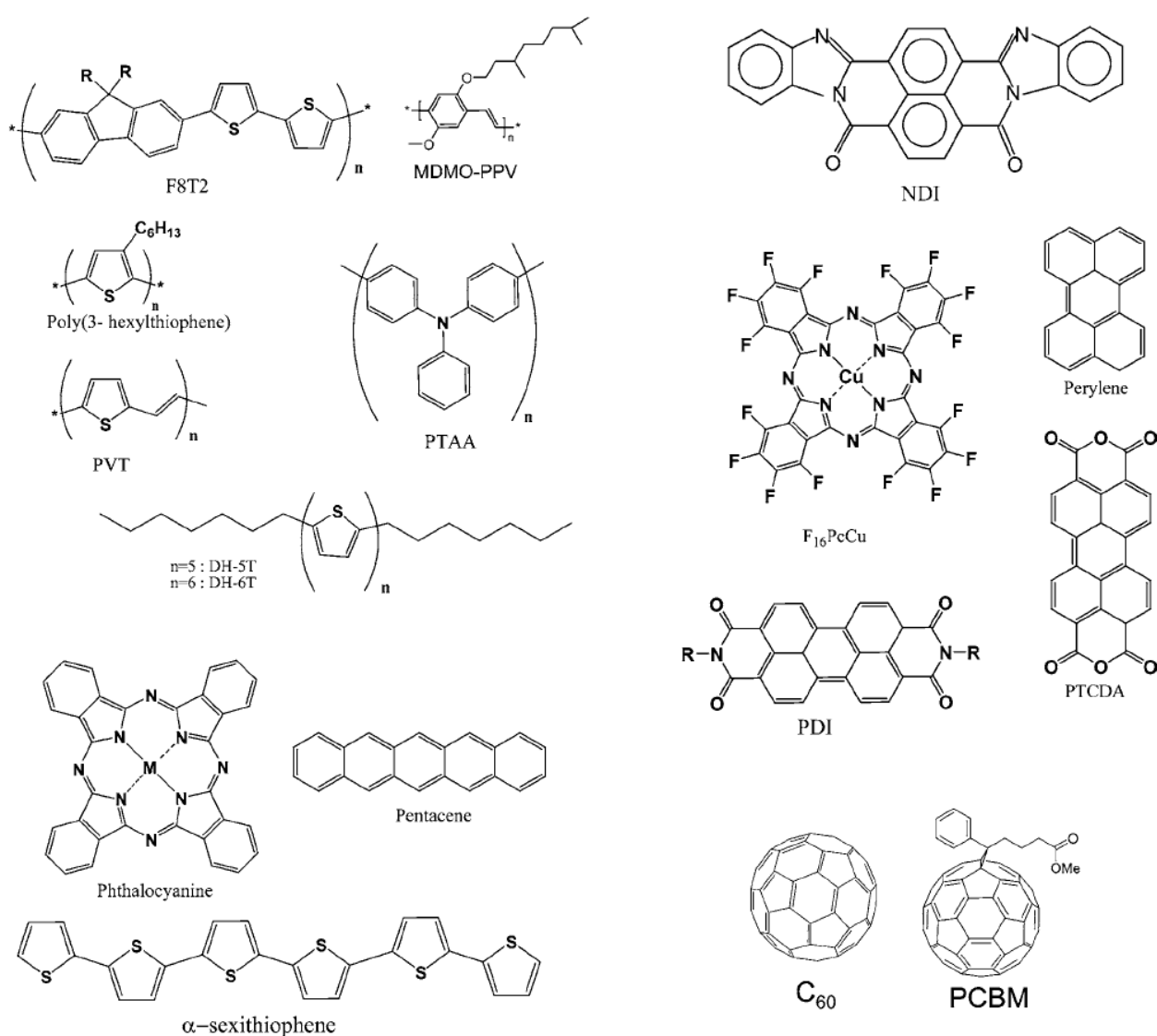
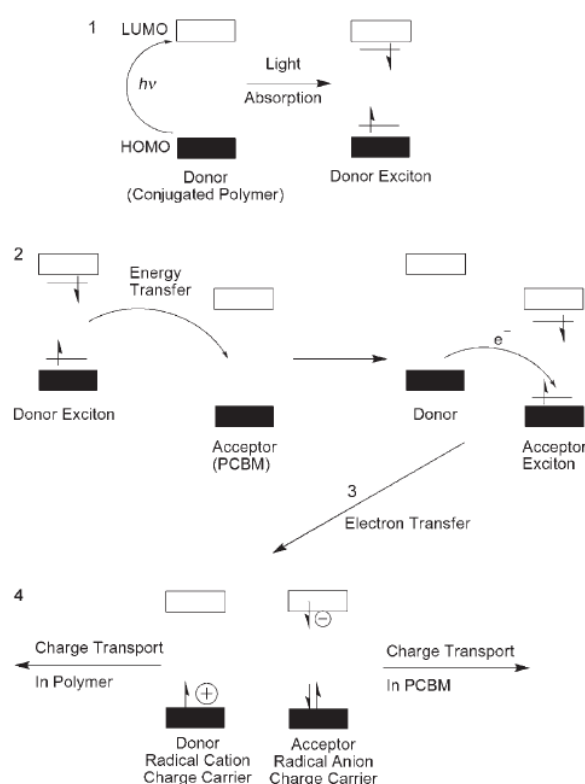


Figure 64. P- and n-type semiconductors used in organic solar cells.

To attain efficiencies approaching 10% in such organic solar cells, much effort is required to understand the fundamental electronic interactions between the polymeric donors and the fullerene acceptors as well as the complex interplay of device architecture, morphology, processing, and the fundamental electronic processes.

3.3.1 Operating Principles

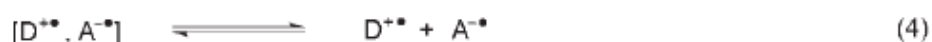
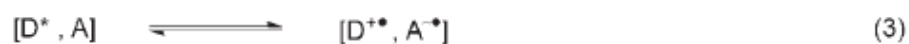
Efforts to optimize the performance of organic solar cells should find their basis in the fundamental mechanism of operation. (Scheme 10) illustrates the mechanism by which light energy is converted into electrical energy in the different organic PVDs (see 3.3.3)



Scheme 10. Mechanism for photo-energy conversion in excitonic solar cells.

In organic semiconductors, absorption of photons leads to the creation of bound electron hole pairs (excitons) rather than free charges and these excitons carrying energy but no net charge may *diffuse* to dissociation sites where their charges can be separated.

The separated charges then need to travel to the respective device electrodes, holes to the anode and electrons to the cathode to provide voltage and be available for injection into an external circuit (**Scheme 11**).



Scheme 11. Elementary steps in the process of photoinduced charge separation for a donor (D) and an acceptor (A): 1) photoexcitation of the donor; 2) diffusion of the exciton and formation of an encounter pair; 3) electron transfer within the encounter pair to form a geminate pair; 4) charge separation.

The process of conversion of light into electricity by an organic solar cell can be schematically described by the following steps:²⁴⁰ absorption of a photon leading to the formation of an excited state, that is, the bound electron-hole pair (exciton) creation; exciton diffusion to a region where exciton dissociation, that is, charge separation occurs; and charge transport within the organic semiconductor to the respective electrodes.

Because of the large **E_g** in organic materials, only a small portion of the incident solar light is absorbed (**Figure 65**).

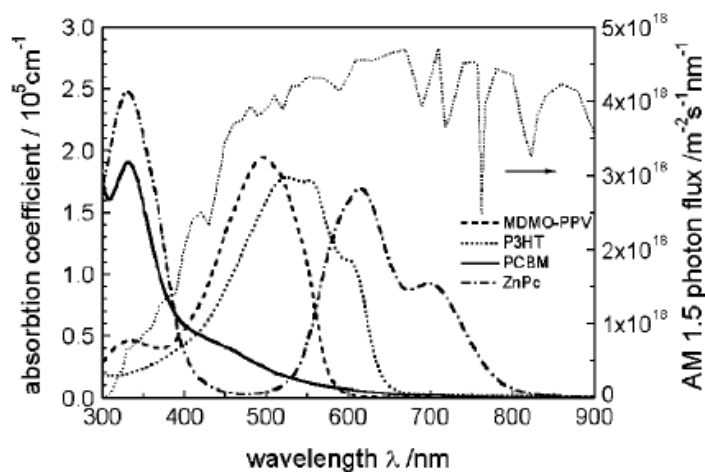


Figure 65. Absorption coefficients of films of commonly used materials are depicted in comparison with the standard AM 1.5 terrestrial solar spectrum.

A **E_g** of 1.1 eV (1100 nm) is capable of absorbing 77% of the solar irradiation on earth. However, the majority of semiconducting polymers have band gaps higher than 2 eV (620 nm), which limits the possible harvesting of solar photons to about 30%.

On the other hand, because the absorption coefficients of organic materials are as high as 10^5 cm^{-1} , only 100 nm thickness is enough to absorb most of the photons when a reflective back contact is used.

This brings the problem to the point: we need a better “spectral” harvesting of solar photons via lower **E_g** polymers and/or using energy-transfer cascades. The thicknesses of the films are not the bottleneck.

The primary photoexcitations in organic materials do not directly and quantitatively lead to free charge carriers but to coulombically bound electron-hole pairs, called excitons.

It is estimated that only 10% of the photoexcitations lead to free charge carriers in conjugated polymers.²⁴¹

For efficient dissociation of excitons, strong electric fields are necessary. Such local fields can be supplied via externally applied electrical fields as well as via interfaces.

At an interface, where abrupt changes of the potential energy occur, strong local electrical fields are possible ($E = -\text{grad } U$). Photoinduced charge transfer can occur when the exciton has reached such an interface within its lifetime. Therefore, exciton diffusion length limits the thicknesses of the bilayers.²⁴²

Exciton diffusion length should be at the same order of magnitude as the donor acceptor phase separation length. Otherwise, excitons decay via radiative or nonradiative path ways before reaching the interface, and their energy is lost for the power conversion. Exciton diffusion lengths in polymers and in organic semiconductors are usually around 10-20 nm.

Blending conjugated polymers with electron acceptors, such as fullerenes, is a very efficient way to break apart photoexcited excitons into free charge carriers. Ultrafast photophysical studies showed that the photoinduced charge transfer in such blends happens on a time scale of 45 fs.

This is much faster than other competing relaxation processes (photoluminescence usually occurs around 1 ns).²⁴³ Furthermore, the separated charges in such blends are metastable at low temperatures (**Scheme 11**).

For efficient **PVDs**, the created charges need to be transported to the appropriate electrodes within their lifetime. The charge carriers need a driving force to reach the electrodes.

A gradient in the chemical potentials of electrons and holes (quasi Fermi levels of the doped phases) is built up in a *donor-acceptor* junction. This gradient is determined by the difference between the highest occupied molecular (HOMO) level of the *donor* (quasi Fermi level of the holes) and the lowest unoccupied molecular orbital (LUMO) level of the *acceptor* (quasi Fermi level of the electrons).

This internal electrical field determines the maximum *open circuit voltage* (V_{oc}) and contributes to a field-induced drift of charge carriers. Also, using asymmetrical contacts (one low work-function metal for the collection of electrons and one high work-function metal for the collection of the holes) is proposed to lead to an external field in short circuit condition within a *metal-insulator-metal* (**MIM**) picture.²⁴⁴

Another driving force can be the concentration gradients of the respective charges, which lead to a diffusion current. The transport of charges is affected by recombination during the journey to the electrodes, particularly if the same material serves as transport medium for both electrons and holes.

Transport in conjugated polymers is dominated by disorder and was treated in many different studies before.^{245,246,247}

As a last step, charge carriers are extracted from the device through two selective contacts. A transparent **ITO** matches the *HOMO* levels of most of the conjugated polymers (hole contact). An evaporated aluminum metal contact with a work function of around 4.3 eV matches the *LUMO* of *acceptor* **PCBM** (electron contact) on the other side.

The key point is that electron transfer is not simple.

The process must be energetically favorable to form the geminate pair in *step 3* (**Scheme 11**) and an energetic driving force must exist to separate this coulombically bound electron-hole pair.

It is apparent that the active layer *donor-acceptor* composite governs all aspects of the mechanism, with the exception of charge collection, which is based on the electronic interface between the active layer composite and the respective electrode.

Besides the fundamental mechanistic steps, the V_{oc} is also governed by the energetic relationship between the *donor* and the *acceptor* (**Figure 66**) rather than the work functions of the cathode and anode, as would be expected from a simplistic view of these diode devices.

Specifically, the energy difference between the *HOMO* of the donor and the *LUMO* of the acceptor is found to most closely correlate with the V_{oc} value.^{248,249}

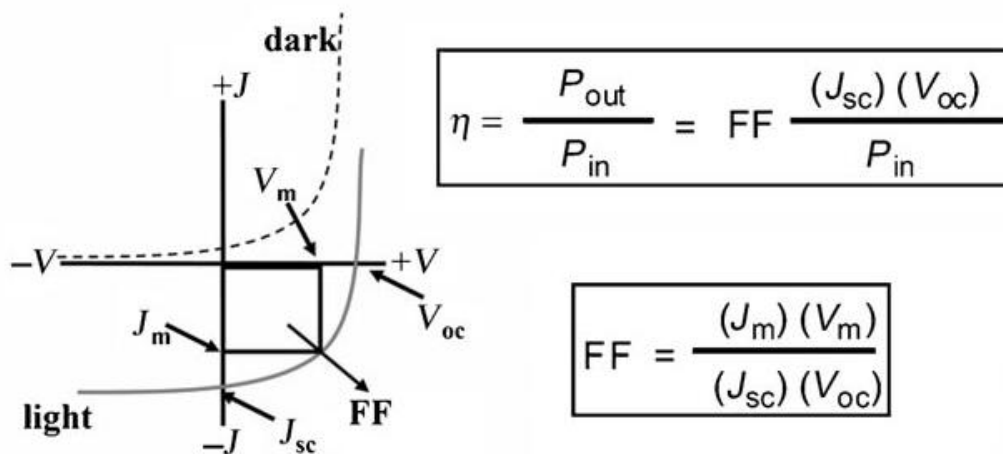


Figure 66. The typical current-voltage characteristics for dark and light current in a solar cell illustrate the important parameters for such device ship.

It is therefore apparent that the choice of the components in the active layer as well as its morphology, which governs the physical interaction between the *donor* and *acceptor*, are the primary factors affecting the performance of the device.

Furthermore architectural modification (such as the use of buffer layers) or the choice of electrodes are also critical aspects which will be viewed as a second level of device optimization in our discussion (see 3.3.3)

3.3.2 Electronic Donor-Acceptor Interactions

The optimization of organic solar cell is based on fine-tuning the electronic properties and interactions of the *donor* and *acceptor* components so as to absorb the most light, generate the greatest number of free charges, with minimal concomitant loss of energy, and transport the charges to the respective electrodes at a maximum rate and with a minimum of recombination.

Therefore it is necessary to know the ideal electronic characteristics that each component should have for the design of the next generation, high-efficiency photovoltaic systems.

The two components required in these devices for electronic optimization are a soluble *fullerene* (generally a C₆₀ derivative) *acceptor* and a polymeric *donor* that can be processed in solution.

Fullerenes are currently considered to be the ideal acceptors for organic solar cells for several reasons; first, they have an energetically deep-lying *LUMO*,²⁵⁰ which endows the molecule with a very high electron affinity relative to the numerous potential organic donors.

MDMO-PPV (*poly[2-methoxy-5-(3,7-dimethyloctyloxy)-1,4-phenylen]-alt-(vinylene)*) and **P3HT**, are two of the most commonly used donor polymers (**Figure 67**).

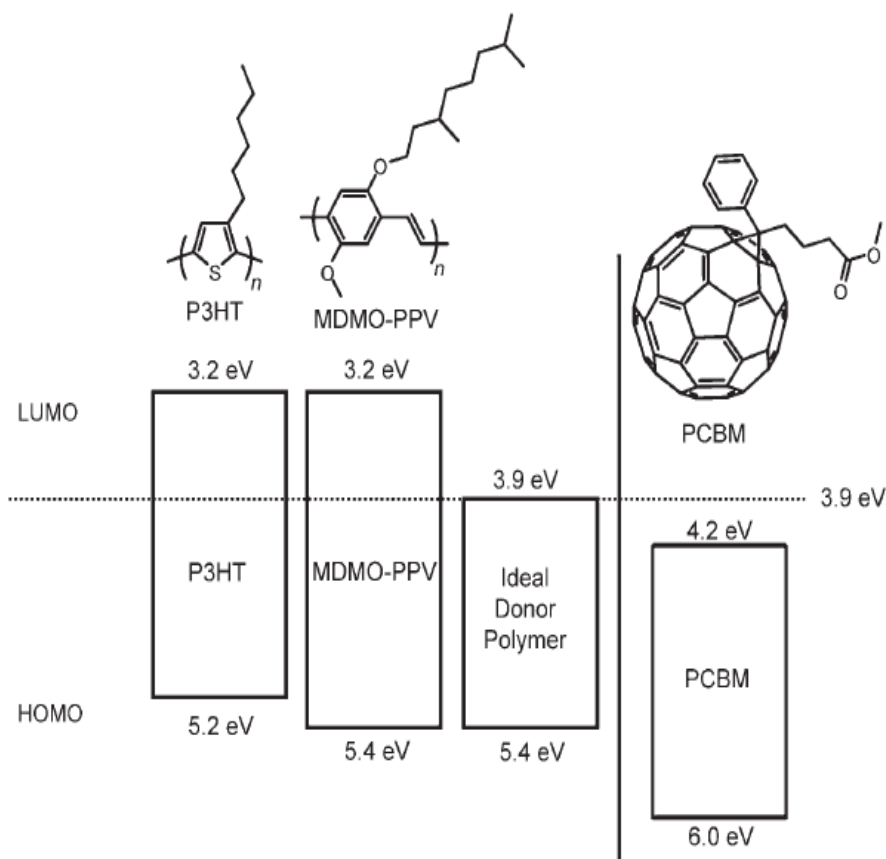


Figure 67. Band structure diagram illustrating the HOMO and LUMO energies of MDMO-PPV, P3HT, and an "ideal" donor relative to the band structure of PCBM. Energy values are reported as absolute values relative to a vacuum.

The first constraint is that the donor must be capable of transferring charge to the fullerene upon excitation (**Scheme 10**). A downhill energetic driving force is necessary for this process to be favorable and the driving force must exceed the exciton binding energy. This binding energy is the coulombic attraction of the bound electron-hole pair in the *donor*, and typical values are estimated to be 0.4-0.5 eV.²⁵¹

The energetic driving force effects the dissociation of the exciton with the formation of a geminate pair (step 3, **Scheme 11**).

Empirically, the overall energetic driving force for a forward electron transfer from the *donor* to the *acceptor* is represented by the energy difference (offset) between the *LUMOs* of the *donor* and *acceptor*.

It appears that a minimum energy difference of 0.3 eV is required to affect the exciton splitting and charge dissociation.^{252,253} Furthermore, an energy difference between the *LUMOs* that is larger than this minimum value does not seem to be advantageous, and indeed results in wasted energy that does not contribute to the device performance.²⁵⁴

The ideal polymer would have a minimum energy difference between the *LUMOs*; in this way wasted energy upon exciton splitting would be avoided and the **E_g** of the polymer would be minimized so as to maximize the absorption of light.

Thus, the *LUMO* of an ideal polymer would reside at approximately 3.9 eV, since the *LUMO* energy for **PCBM**, the most commonly and successfully employed soluble fullerene derivative, is 4.2 eV.

The *HOMO* energy of the ideal donor polymer would then be determined by considering the **E_g** of the polymer, and hence the absorption of light, as well as the influence on the **V_{oc}**.

The lower the energy of the *HOMO*, the greater the maximum theoretically attainable **V_{oc}** value, but the larger the **E_g**, the poorer the spectral overlap with the photon flux from the sun, which has a maximum at 1.8 eV (ca. 700 nm).

A compromise is found by considering that a **E_g** of about 1.5 eV is an optimal value for a polymer absorber.²⁵⁵ This gives a *HOMO* energy of about 5.4 eV, which corresponds to a maximum attainable **V_{oc}** value of 1.2 V. The optimal **E_g** value of 1.5 eV has been determined through a detailed analysis that balances the attainable **V_{oc}** value and the *donor E_g*.²⁵⁶

3.3.3 Organic Photovoltaic Device Architectures

The general structure used for organic solar cells is similar to the **OLEDs**. The devices are fabricated in sandwich geometry (**Figure 68**). This type of polymer solar cell consist of five layers: *glass, ITO, PEDOT:PSS, active layer, calcium and aluminum*.

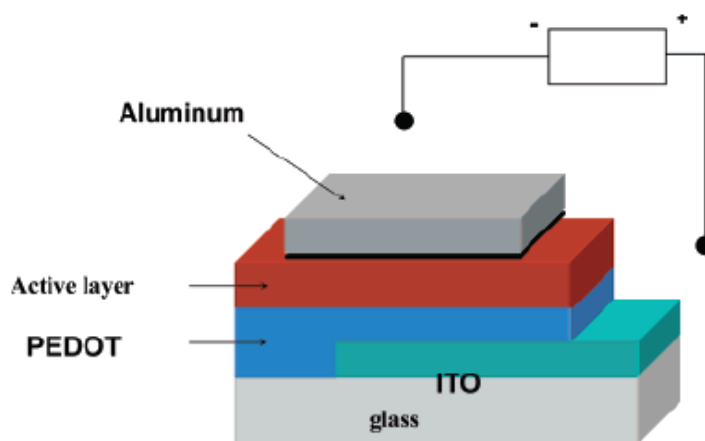


Figure 68. Schematic device structure for polymer/fullerene bulk heterojunction solar cells. The active layer is sandwiched between two contacts: an indium-tin-oxide electrode coated with a hole transport layer PEDOT:PSS and an aluminum top electrode.

The glass serves as a supporting layer for the solar cell and the only demand glass has to fulfill is that it does not absorb light in the visible area, since the solar cell uses this light to generate power. Other and more flexible types of supporting layers, like transparent polymers, can also be used.

ITO and *aluminum* serves as the electrodes in the solar cell. Beyond that, the **ITO** and *aluminum* are also used to generate a built-in electric field caused by the difference in the metals' work functions.

This electric field is used dissociate the excitons, which are generated when the active layer absorbs light, and afterwards to pull the charge carriers out from the active layer. Like glass the **ITO** layer is transparent in the visible area.

PEDOT:PSS and *calcium* are two materials which are introduced into the solar cell in order to increase the built-in electric field and thereby improve the performance of the solar cell.²⁵⁷

The *active layer* in this polymer solar cell consists of a blend between the conjugated polymer and the modified *fullerene PCBM*.²⁵⁸

The polymer is the absorbing part of the *active layer* and **PCBM** is introduced into the layer to make the dissociation of the excitons more effective (**Figure 69**).

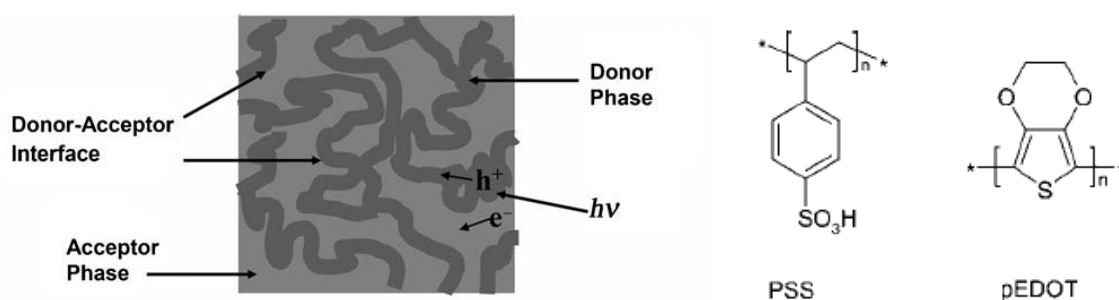


Figure 69. Area showing the bicontinuous morphology of the active layer. ITO is indium tin oxide and PEDOT-PSS is poly(3,4-ethylenedioxythiophene)-polystyrene sulfonate.

In order to meet these specific requirement for efficient photon to charge conversion different device architectures have been developed in the past.

▪ **Single Layer Cells**

Single layer structures consist of only one semiconductor material and are often referred to as *Schottky* type devices or *Schottky diodes* since charge separation occurs at the rectifying (Schottky) junction with one electrode. The other electrode interface is supposed to be of ohmic nature. The structure is simple but absorption covering the entire visible range is rare using a single type of molecule.

The photoactive region is often very thin and since both positive and negative photoexcited charges travel through the same material recombination losses are generally high.

▪ **Double Layer Cells**

In a bilayer heterojunction device, *p-type* and *n-type* semiconductors are sequentially stacked on top of each other. Such bilayer devices using organic semiconductors were realized for many different material combinations.^{259,260,261,262,263,264,265,266,267}

In such devices, only excitons created within the distance of 10-20 nm from the interface can reach the heterojunction interface. This leads to the loss of absorbed photons further away from the interface and results in low quantum efficiencies.²⁶⁸

The efficiency of bilayer solar cells is limited by the charge generation 10-20 nm around the donor-acceptor interface (**Figure 70**).

Using thicker films creates optical filter effects of the absorbing material before the light gets to the interface, resulting in a minimum photocurrent at the maximum of the optical absorption spectrum.²⁶⁹

Also, the film thicknesses have to be optimized for the interference effects in the multiple stacked thin film structure.^{270,271}

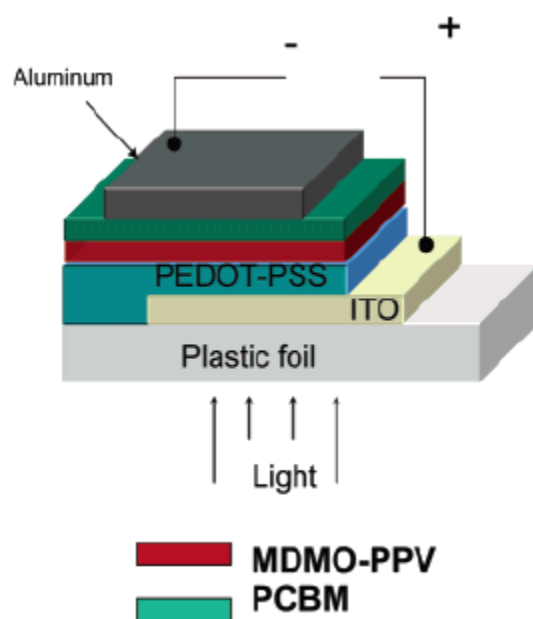


Figure 70. Bilayer configuration in organic solar cells.

▪ **Bulk Heterojunction Devices**

Bulk Heterojunction (**BHJ**) is a blend of the *donor* and *acceptor* components in a bulk volume (**Figure 71**). It exhibits a *donor-acceptor* phase separation in a 10-20 nm length scale. In such a nanoscale interpenetrating network, each interface is within a distance less than the exciton diffusion length from the absorbing site.

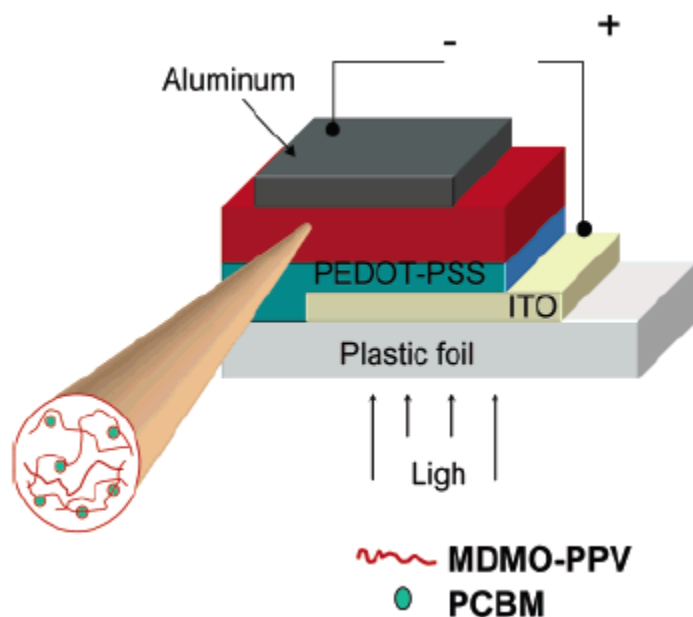


Figure 71. Bulk heterojunction configuration in organic solar cells.

The bulk heterojunction concept has heavily increased (orders of magnitude) the interfacial area between the *donor* and *acceptor* phases and resulted in improved efficiency solar cells.²⁷²

While in the *bilayer heterojunction* the *donor* and *acceptor* phases are completely separated from each other and can selectively contact the anode and cathode, in the **BHJ** both phases are intimately intermixed.

This mixture has a priori no symmetry breaking in the volume. There is no preferred direction for the internal fields of separated charges; that is, the electrons and holes created within the volume have no net resulting direction they should move.

Therefore, a symmetry breaking condition (like using different work-function electrodes) is essential in **BHJ**. Otherwise, only concentration gradient (diffusion) can act as driving force.

Furthermore, separated charges require percolated pathways for the hole and electron transporting phases to the contacts.

In other words, the *donor* and *acceptor* phases have to form a nanoscale, bicontinuous, and interpenetrating network.²⁷³ Therefore, the **BHJ** devices are much more sensitive to the nanoscale morphology in the blend, and they can be achieved by co-deposition of *donor* and *acceptor* pigments^{274,275,276,277} or solution casting of either polymer/polymer^{278,279} polymer/molecule^{280,281} or molecule/molecule^{282,283} *donor-acceptor* blends.²⁸⁴

▪ **Laminated Devices**

This relatively recent type represents the successful attempt to unify the advantages of the two structures above.

Charge separation occurs in the blend layer in the middle that is obtained after laminating the two separate layers together and charge transport can only occur via the correct transport layer.

This structure (**Figure 71**) also features the useful options to treat each layer separately (e.g. doping, physical/chemical conversion) before forming the blend layer and instant encapsulation between the two substrates.

The drawback is that certain mechanical properties of the organic semiconductors are required (low glass transition temperature) to form the intermixed layer.

The laminated device can be seen as a hybrid between the last two devices.

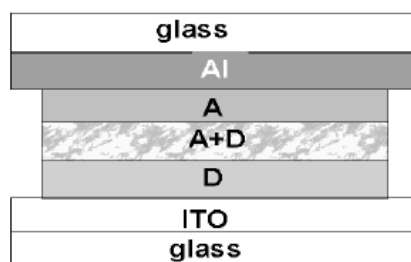


Figure 71. Laminated device configuration in organic solar cells.

3.3.4 BHJ Solar Cell Morphologies

Photoinduced electron transfer from *donor-type* semiconducting polymers onto *acceptor-type* polymers or molecules, such as C_{60} ,²⁸⁵ is utilized in these organic solar cells. Bilayers of semiconducting polymers with fullerenes show low photovoltaic conversion efficiency.

Significant improvement has been achieved by using phase-separated composite materials. Controlling the nanomorphology of the phase separation in an interpenetrating network **BHJ** has increased the power conversion efficiency of solar cells made from **MDMO-PPV/C₆₀** and mostly from **P3HT/C₆₀** significantly.^{286,287}

Typical dimensions of phase separation have to be within the exciton diffusion length (on the order of 10 nm). On the other hand, bicontinuous, undisturbed pathways have to be ensured for transport of charge carriers to the electrodes.²⁸⁸

To enhance charge carrier transport in organic and polymeric materials, we have to increase the mesoscopic order and crystallinity. Hence, a nanoscale interpenetrating network with crystalline order of both constituents seems a desirable architecture for the active layer of polymer **PVDs**.

Eventually, the electronic E_g of the materials in the photoactive layer should be tuned to harvest more light from the solar spectrum.

3.3.4.1 PPV:PCBM in BHJ Solar Cells

2.5% efficient solar cells can be obtained from soluble derivatives of *phenylene-vinylenes*, for example **MDMO-PPV** mixed with soluble **PCBM**. *Shaheen et al.* showed that a power conversion efficiency of 2.5% under AM 1.5 conditions can be obtained by using *chlorobenzene* as a solvent for spincoating in the weight ratio of 1:4 for **MDMO-PPV:PCBM**.

Changing the solvent from *toluene* to *chlorobenzene* increases the efficiency by nearly a factor of 3, which was assigned to originate from the changes in the nanomorphology (**Figure 72**).

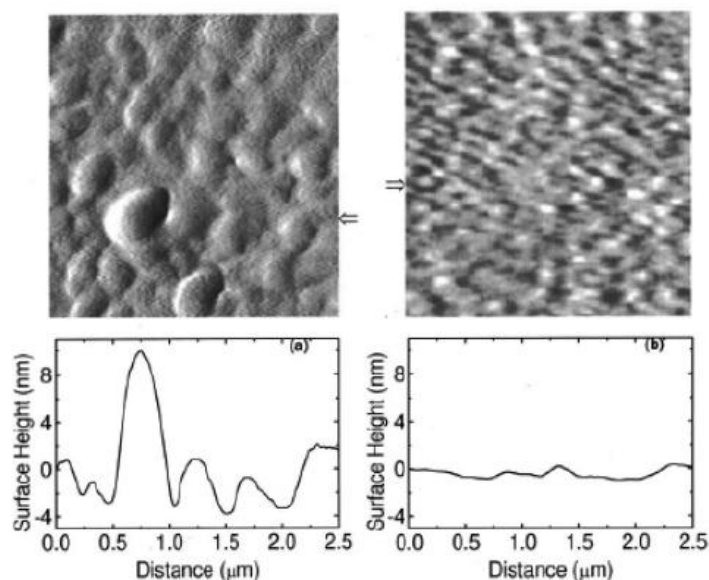


Figure 72. AFM images showing the surface morphology of MDMO-PPV:PCBM (1:4 by wt) blend films spin-coated from (left) toluene and (right) chlorobenzene solutions. The films cast from chlorobenzene have a smoother surface as compared to films cast from toluene.

Such **BHJ** solar cells have 80 wt % **PCBM**. However, the polymer **MDMO-PPV** is supposed to be the main light absorber in these solar cells, because **PCBM** has almost no absorption in the visible-near-infrared region. Therefore, it is better to increase the volume concentration of **MDMO-PPV** for better absorption of solar light.²⁸⁹

The electron mobility of pure **PCBM**²⁹⁰ was reported to be higher ($\approx 10^{-3}$ cm²/V*s) than the hole mobility of pure **MDMO-PPV** (10^{-4} cm²/V*s). The interesting observation is also that the mobility of the holes in the mixture is increasing with increasing fullerene loading. This is counterintuitive because the admixture of fullerene should have introduced more defects and lowered the hole mobility.^{291,292,293,294,295,296,297}

To study the relation between morphology and performance in bulk heterojunction solar cells, **MDMO-PPV/PCBM** blends were investigated in detail^{298,299,300,301} even if the best performance in **BHJ** solar cells belongs to **P3HT-PCBM** blends.

3.4 Oligo- and Polythiophenes for OPVDs

Owing to their efficient light harvesting, structural versatility and intrinsic charge transport behavior, thiophene-based *p-conjugated systems* have attracted much attention in developing high performance organic photovoltaic solar cells.

In fact during the last decade, there have been countless studies devoted to the synthesis of different organic materials and among these, thiophene based oligomers and polymers for photovoltaic applications and various photoconversion efficiencies ranging from 0.1 to 8% have been reported for devices based on such materials.

The state-of-the-art in the field of organic photovoltaics is currently represented by **BHJ** solar cells based on **P3HT** and the **PCBM**, with reproducible efficiencies approaching 9%.^{302,303}

For this reason the **P3HT** and the **PCBM** represent in the organic photovoltaic panorama, materials respectively *p*- and *n*-type, which offer today the best performance for **OPVDs**.

3.4.1 Oligothiophenes for OPVDs

The exploration of donor materials has been centered on *p*-type conjugated small molecules and polymers that own strong absorption of sunlight spectra covering an extensively broad range, ease of film formation, good charge mobility and suitable frontier orbital energy levels.

From the view of these points, thiophene-based *p*-conjugated oligomers are among the most promising materials for **OSCs**.³⁰⁴

In comparison to the relevant conjugated polymers that are used as active materials in **PVDs**, conjugated oligomers and in this case the **OTs** possess some critical advantages; in fact the introduction of electron-withdrawing or electron-donating building blocks into **OTs** has been later revealed to be the most straightforward way to construct new oligomers with well-defined structures and tunable *HOMO* and *LUMO* energy levels.

The *donor-acceptor* (D-A) conjugated **OTs** systems can serve as excellent *donor* components in organic photovoltaics due to their unique features: (1) the well-defined structures make them synthetically reproducible; (2) the light-absorbing regions can be enlarged to cover low-energy long-wavelength spectra; (3) the strong intermolecular interactions arising from the D-A moieties

can favor the self-organization of the oligomers into ordered structures and close packing with increasing *p-p* orbital overlap; (4) both vacuum-deposited and solution-processable methods can be applicable to fabricate devices. In the last few years, several new families of D-A oligomers consisting of electron-donating thiophenes/oligothiophenes have been developed as donor materials in high-performance **OSCs**.

Hence the basic advantages of these materials are its good hole transport and the possibility of controlling mobility, energy level, packing, and ordered structure by changing the number of thiophen rings, and making chemically modifications and substitutions, its characteristics relevant to **PV** applications.

However it has been difficult to fabricate films of *oligothiophene-fullerene blends* with suitable morphology by using the common co-evaporation method, because **OTs** crystallize easily during film deposition.

3.4.1.1 Alpha-Sexithiophene

Surely alpha-sexithiophene (**6T**) as the oligothiophene material because it is well known to exhibit high field-effect hole mobility, and a representative material in the oligothiophene family.

Conversely, a problematic issue arises when high mobility materials are applied to **PV** cells. But there is one issue regarding mobility when it is applied to **PV** cells. Usually longer axis of **6T** molecule is oriented vertically against the substrate, and mobility of vertical direction is lower than horizontal one; for this reason it's important to consider molecular orientation.

Below (**Figure 73**) is showed basic device structure of bilayer heterojunction **PV** cells, chemical structure of **6T** and C_{60} and energy band diagram of a bilayer type **PV** cell.

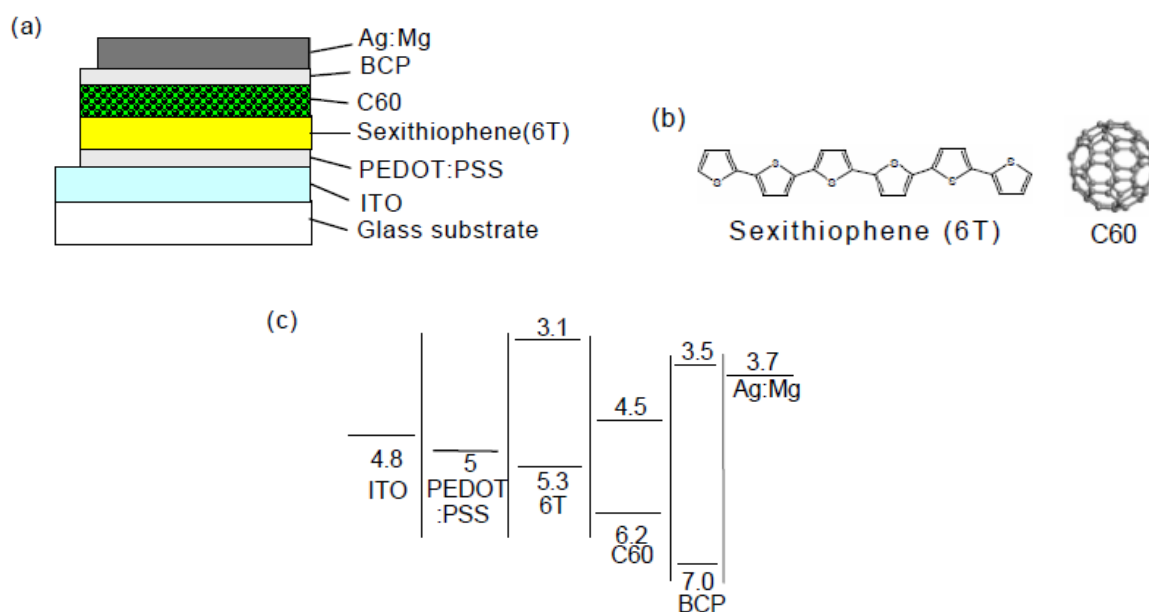


Figure 73. (a) Schematic device structure of 6T/C60 bilayer heterojunction PV cell (b) Chemical structure (c) Energy flat band diagram of a device.

The peak absorption coefficient value of **6T** is as high as **Pc**, ($10^5/\text{cm}$ order) but peak wave length of 6T is less than 400nm. So the mismatch to solar light spectrum is large; therefore we can't expect high short circuit current in this system (**Figure 74**).

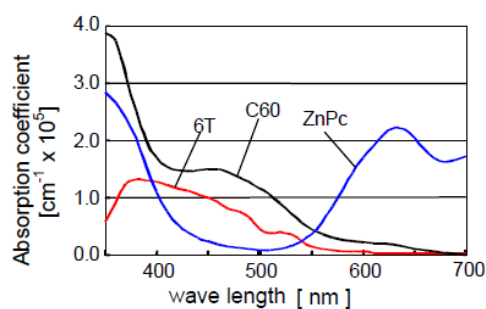


Figure 74. Photo Absorption spectrum of 6T, C_{60} and ZnPc.

▪ 6T/C60 Bilayer Heterojunction PV cells

The characteristic of **6T/C₆₀** bilayer **PV** cell (**Figure 75**) showed excellent **PV** characteristics: **PCE** of 0.75%, **Jsc** of 3.9mA/cm², **V_{oc}** of 0.35V, **FF** of 0.55 at **AM 1.5G** 100mW/cm². **6T/C₆₀** system was proved to be good combination for heterojunction.

But **V_{oc}** is not so high in view of an **E_g** between **HOMO** of **6T** and **LUMO** of **C₆₀** (0.8V).

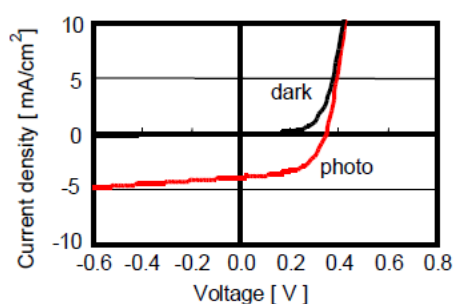


Figure 75. Current-Voltage characteristics under AM 1.5G, 100 mW/cm² for 6T/C₆₀ bilayer PV cell.

After that we investigated film thickness dependence in the **6T/C₆₀** bilayer **PV** cells. Optimum thickness of **6T/C₆₀** active layer was expected to become thicker than **Pc/C₆₀** active layer.

Optimum thickness in **6T/C₆₀** extended into 150nm, while **ZnPc/C₆₀** was around 50nm. This result is probably caused by improvement of hole transport property (**Figure 76**).

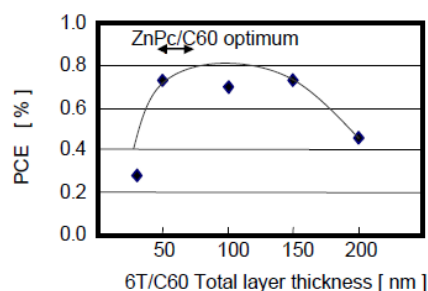


Figure 76. PCE vs total thickness of 6T/C₆₀ active layer.

▪ 6T/C60 Bulk Heterojunction PV cells

A bulk heterojunction PV cells composed of 6T and C₆₀ was prepared by co-evaporation (Figure 77).

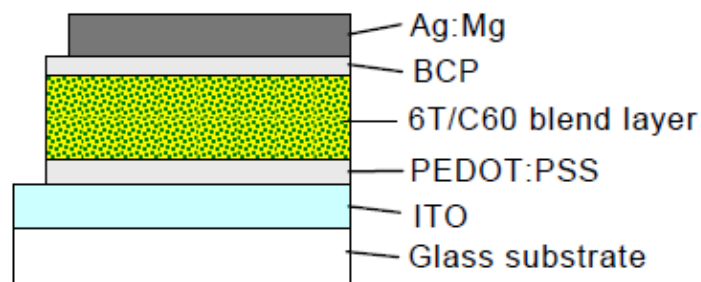


Figure 77. Schematic device structure of 6T/C₆₀ bulk heterojunction PV cell.

First was deposited 6T/C₆₀ blend layer on condition that blend ratio is 1:1. In this study, blend ratio is defined as the ratio of each film thickness monitor value.

In the metal Pc and C₆₀ system, PV characteristics were dramatically improved due to BHJ with equal blending.

But in the 6T/C₆₀ system, contrary to our expectation, PV characteristics with equal blending were not good and inferior to the bilayer heterojunction cells.

Dotted line (Figure 78) shows I-V characteristics: PCE of 0.52%, J_{sc} of 2.8 mA/cm², V_{oc} of 0.4V, FF of 0.46 at AM 1.5G 100mW/cm². When we observed surface, surface roughness of bulk heterojunction was larger than one of bilayer.

It is likely that carrier transport network is not enough due to phase separation.

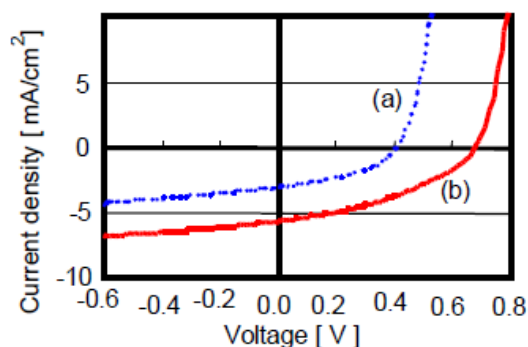


Figure 78. Current-Voltage characteristics under AM1.5, 100 mW/cm² for 6T/C₆₀ bulk heterojunction cell. (a) 6T:C₆₀=1:1 (b) 6T:C₆₀=1:5.

After that, we investigated the influence of some deposit conditions. As a result, it has become clear that blend ratio of **6T/C₆₀** impacts blend morphology. In particular when the blend ratio is around **6T/C₆₀**=1/5, both **J_{sc}** and **V_{oc}** dramatically increased.

Solid line shows I-V characteristics in blend ratio 1/5: **PCE** of 1.5%, **J_{sc}** of 5.6 mA/cm², **V_{oc}** of 0.68V, FF of 0.39 at **AM 1.5G** 100mW/cm².

We compared blend morphology between blend ratio: 1/1 and 1/5. Below is showed (**Figure 79**) significantly different morphologies. In case of 1/1, small grains like rod shape (about 200nm length, 40nm diameter) with some branches were scatteringly deposited.³⁰⁵

On the other hand, in case of 1/5, there were no grains and homogeneous film was deposited.

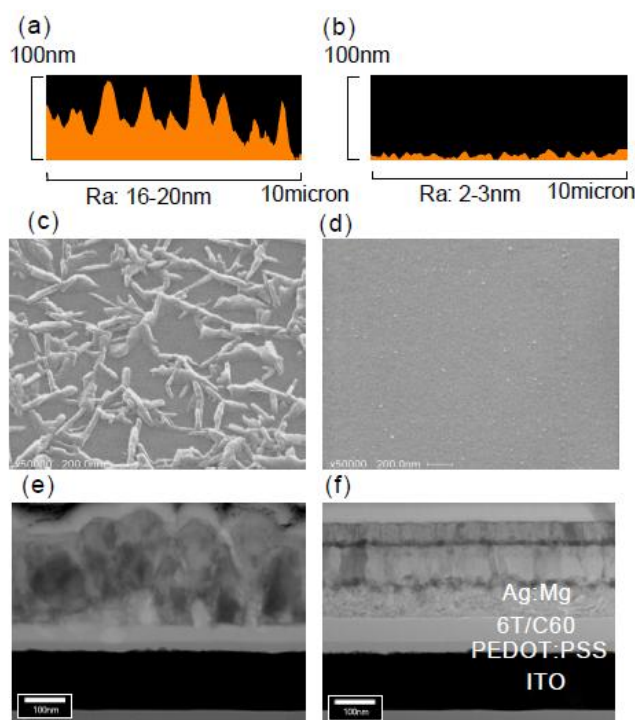


Figure 79. AFM surface profile of blend layer (a) 6T:C₆₀=1:1 (b) 6T:C₆₀=1:5 SEM Images (surface of blend layer) (c) 6T:C₆₀=1:1 (d) 6T:C₆₀=1:5 Cross section TEM Images (e) 6T:C₆₀=1:1 (f) 6T:C₆₀=1:5.

Furthermore (**Figure 80**) from the images below, **6T** and **C₆₀** comprise small grains and they were deposited on the **6T/C₆₀** blend layer. In case of blend ratio 1/1, since carrier transport network was not formed sufficiently, **PV** characteristics was low.

On the other hand, in case of 1/5, it is clear that excess **C₆₀** blend led to the formation of homogeneous film and desirable network, and this led to improvement of **J_{sc}**.

As for increasing **V_{oc}**, it may be presumed that **V_{oc}** of this device approach maximum value estimated *HOMO LUMO* difference or built-in potential increase by forming *schottky* barrier between **C₆₀** and **PEDOT:PSS** layer.

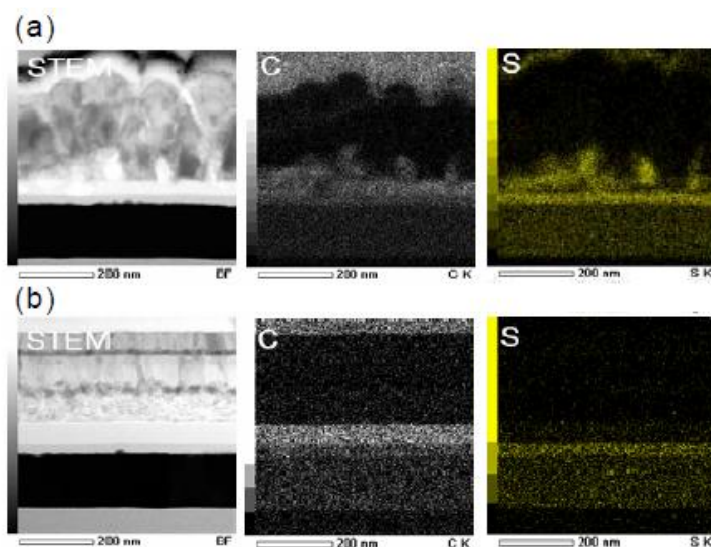


Figure 80. Cross section TEM-EDAX images (a) 6T:C₆₀=1:1 (b) 6T:C₆₀=1:5.

▪ **MIN type (metal-intrinsic-n type) 6T/C60 BHJ PV cells**

In the metal **Pc/C₆₀** bulk heterojunction **PV** cells, pin structure is effective to improve **PV** characteristics.³⁰⁶ We tried to apply pin structure to **6T** and excess **C₆₀** (1/5) bulk heterojunction **PV** cells. But this device didn't show rectification properties.

Alternatively, new device inserted only **C₆₀** layer between blend layer and **BCP** (Min type); Min device: **PCE** of 2.0%, **J_{sc}** of 5.6mA/cm², **V_{oc}** of 0.7V, **FF** of 0.51. **FF** is significantly improved compare to without **C₆₀** layer.

The reason why improvement of **FF** is that **C₆₀** works electron transport layer with hole blocking effect and reduce interface resistance. Below is showed the *external quantum efficiency (IPCE)* of Min device; photo carrier generation seem to occur mainly in **C₆₀**. (**Figure 81**).

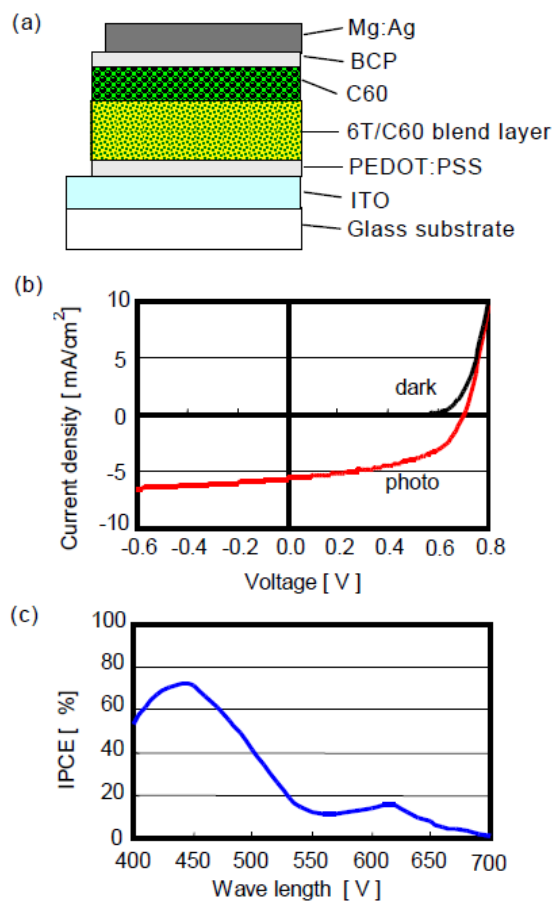


Figure 81. (a) Schematic device structure of 6T/C₆₀ Min type bulk heterojunction PV cell (b) Current-Voltage characteristics under AM1.5 100 mW/cm² for 6T/C₆₀ Min type bulk heterojunction (c) IPCE spectrum of Min type bulk heterojunction.

Finally **6T/C₆₀** bulk heterojunction **PV** cells with **C₆₀** excess blend layer showed excellent PV characteristics; furthermore concerning **6T/C₆₀** bulk heterojunction **PV** cells these represent a very promising devices for higher efficiency cells.³⁰⁷

3.4.1.2 Oligothiophene-S-S-Dioxide

Fullerene derivatives have proven to be good acceptors and have shown high efficiency in organic solar cell devices. These compounds possess a low-lying lowest unoccupied molecular orbital (LUMO) energy level, which favorably accept electrons transferred from the donor material in a range of femto-second time scale, which is faster than the radiative decay of photoexcitation or electron recombination by several orders of magnitude.

These features are favorable for electron hopping from *donor* molecules to *fullerene derivatives*, leading to efficient charge separation and collection.

Moreover, acceptor materials should be able to create effective phase separation from donor species upon blending which allows for charge separation and facilitates charge transport.

Currently, some non-fullerene acceptors have been developed which show significant improvements in spectral absorption, photostability and electron transport. Nevertheless, these acceptors still cannot compete with fullerene derivatives in terms of morphology control upon mixing with donor moieties. The advantage of thiophene units for the construction of new *n-type electron-transport* materials consists of the readily available chemical modification protocols that allows for tuning the *HOMO* and *LUMO* energy levels.

In this purpose the *thiophene-S,S-dioxide* derivatives are among the most promising *n-type* motifs due to their favorable *LUMO* energy, good optical properties and facile chemical functionalization,³⁰⁸ and therefore these materials are proposed not only as a class of *electron-acceptor* materials for **OLED** (see 2.2.2), but also for **OPVDs**.

Generally unsubstituted oligothiophenes are *p*-type, hole-transporting materials but the chemical stability of **OTs** and their easy functionalization, allow the fine tuning of relevant properties.

In this case the chemical transformation of one of the thienyl rings into the corresponding *thienyl-S,S-dioxide*,^{309,310} increases the electron affinity of **OTs** by the dearomatization of the oxidized thiophene ring, which leads to very stable oligomers with increased electron delocalization and with dramatically increased electron affinity (see 2.2.2) (**Figure 82**).³¹¹

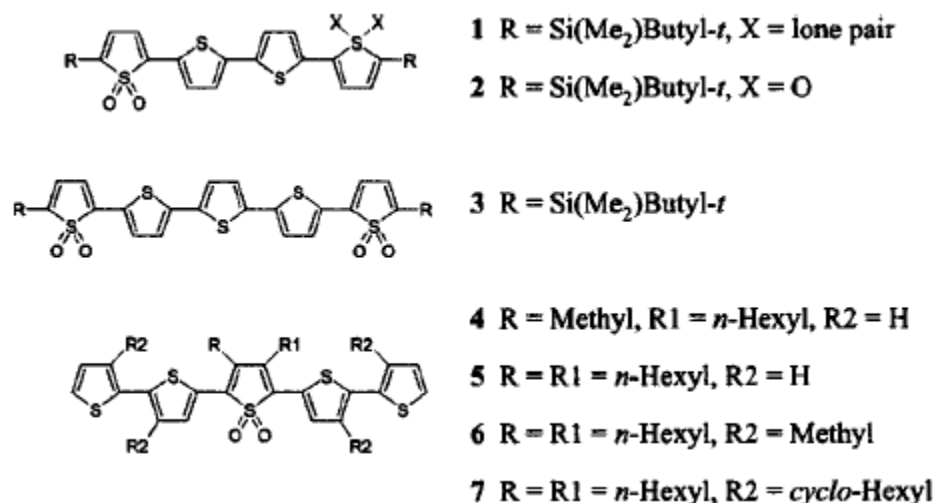


Figure 82. Molecular structures of the oligothiophene-*S,S*-dioxides used in this investigation.

Evidence for charge transfer in blends between regioregular **P3HT** from *Sigma-Aldrich* and the *oligothiophene-S,S-dioxides* was obtained from *photoluminescence PL* measurements. The **PL** efficiencies of three blends (1:1 weight ratio) along with those of the pure components (**Figure 83**).

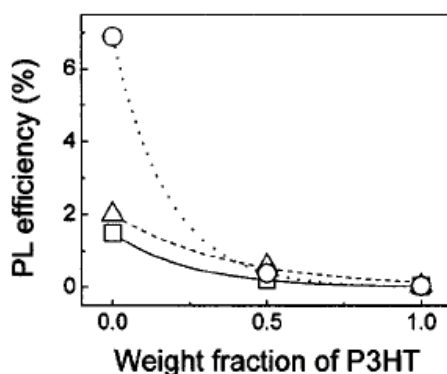


Figure 83. Dependence of the photoluminescence efficiency on the composition of the systems: P3HT:3 (squares); P3HT:4 (triangles); P3HT:5 (circles). PL efficiencies have been evaluated with respect to a reference film of known efficiency. The films (100 nm thick) were spin-coated from chloroform onto quartz substrate. Excitation wavelength: 430 nm.

Oligothiophene-S,S-dioxides are photoluminescent materials and their **PL** is quenched when they are blended with the polymer. This suggests that photoinduced charge separation occurs, preventing the **PL** emission event.

PL quenching of **P3HT** in the blends is not much evident in since the high *oligothiophene-S,S-dioxide's* **PL**, even if quenched, overrides the poor light emission from **P3HT**.

Further evidence for the dissociation of excitons comes from the characterization of photovoltaic cells based on *P3HT/oligothiophene-S,S-dioxides* blends. The weight ratio between the *donor* and *acceptor* component was kept constant (1:1 w/w).

Photovoltaic cells were prepared, at ambient conditions, by spin coating the active layer from chloroform solutions onto **ITO** substrates covered with a film of *poly(ethylenedioxythiophene)* doped with *polystyrene sulfonic acid* (PEDOT:PSS, from Bayer AG) and depositing an *aluminum* top electrode in vacuum.

The junctions were illuminated with white light of 80 mWcm^{-2} intensity through the **ITO** electrode. The electrical characterization was performed under a pressure of 10^{-3} mbar.

The photovoltaic parameters (**Table 3**) measured or calculated for the blended device are reported and compared with the ones of the cells based on the pristine donor.

Active layer	j_{sc} (A cm^{-2})	V_{oc} (V)	FF	η (%)
P3HT	5.5×10^{-6}	0.40	0.31	9.1×10^{-4}
P3HT:1 (1:1)	5.9×10^{-5}	0.61	0.21	9.6×10^{-3}
P3HT:2 (1:1)	1.9×10^{-5}	0.44	0.22	2.3×10^{-3}
P3HT:3 (1:1)	2.2×10^{-5}	0.47	0.21	2.8×10^{-3}
P3HT:4 (1:1)	2.4×10^{-4}	0.93	0.21	6.0×10^{-2}
P3HT:5 (1:1)	1.2×10^{-4}	0.77	0.18	2.3×10^{-2}
P3HT:6 (1:1)	9.3×10^{-5}	0.74	0.20	1.8×10^{-2}
P3HT:7 (1:1)	8.8×10^{-5}	1.00	0.19	2.2×10^{-2}

Table 3. Summary of the photovoltaic parameters (values averaged over three cells). j_{sc} : short-circuit current density; V_{oc} : open-circuit voltage; FF:fill factor; η : power conversion efficiency. White light irradiation of intensity 80 mW cm^{-2} . Active layer thickness: 90-100 nm.

Independent of the active layer morphology and of the molecular structure of the acceptors, an enhancement of the photovoltaic performance of the blended device, with respect to that of cells made of pristine **P3HT**, was observed for all the investigated *D/A systems* (**Figure 84**).

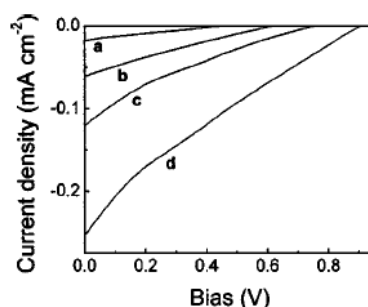


Figure 84. Current-voltage curves (fourth-quadrant only) of cells based on: P3HT:2 (a); P3HT:1 (b); P3HT:5 (c); P3HT:4 (d). Donor/acceptor weight ratio: 1:1. White light irradiation power: $\approx 80 \text{ mW cm}^{-2}$.

An increase of V_{oc} , short-circuit current density (j_{sc}), and power conversion efficiency (η) was obtained with the P3HT/oligothiophene-*S,S*-dioxide active layers. A gain of about 66 was achieved for η in the case of P3HT:4, despite the lack of optimization of both blend morphology and composition.

It is worth noting that the sixty-fold increase in the power conversion efficiency of P3HT:4 devices is comparable to that observed, upon fullerene addition, in diodes made of a blend between MEH-PPV and a functionalized derivative PCBM.³¹²

Furthermore, the photovoltaic performance of D/A blended devices is greatly dependent on the donor component,³¹³ as well as on the D/A weight ratio.

A detailed comparison of all the data (Table 3) cannot be done at this stage. First of all, because of the differences in the molecular structures of the acceptors (substituents, length of the oligomers, number and position of the *S,S*-dioxides).

Second, different morphologies were exhibited by the blended films, likely due to different solubilities or self-organization properties of the oligomers. For example, macroscopic differences in the film morphology were observed between the blends based on acceptors with two thienyl-*S,S*-dioxides units and all the other ones (Figure. 85).

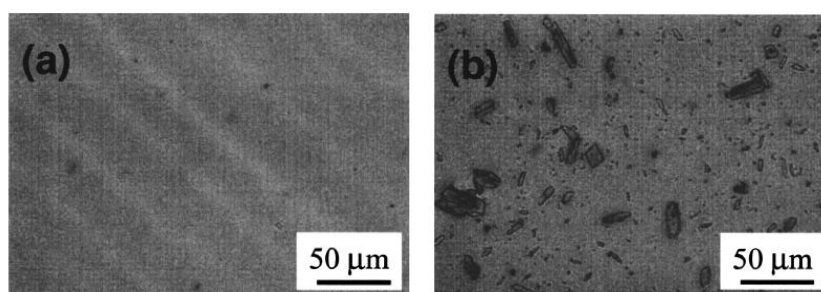


Figure 85. Optical micrographs of P3HT:1 (a) and P3HT:2 (b) films spin-coated from chloroform.

P3HT:2 and **P3HT:3** films presented a much rougher mixture, with respect to that obtained with the other blends. Furthermore, because of the too high roughness exhibited in the former case, it was not possible to compare the different blend morphologies by **AFM** (**Figure 85**).

The figure above shows that oligomer **(2)** (**Figure 82**) forms crystalline aggregates, whereas phase separation was not observed, on the investigated scale, in the **P3HT:1** blend. **P3HT:3** films showed the same morphological properties for **P3HT:2** whereas the image is representative of the morphology observed, on the same scale, for the blends in which the acceptor contains only one *thienyl-S,S-dioxide* unit.

The lower photovoltaic performance exhibited by the devices based on the oligomers containing two *thienyl-S,S-dioxide units*, with respect to that achieved with oligomers bearing only one *thienyl-S,S-dioxide* unit, could be likely ascribed to the less uniform mixing of the blend constituents.

For example, comparing the parameters of devices based on **(2)** and **(3)** as acceptors, an effect of the oligomer length on the cell performance could be hypothesized.

However, given the fact that the photovoltaic parameters are actually relatively close in magnitude for the two devices, this conclusion cannot be drawn at this stage. Also, comparing the performance of devices based on compounds **(4-7)**, which only differ for the nature of the substituent groups, it could be recognized a dependence of the photoresponse on the ''amount'' of substituting groups.

However, it can be objected that the different side groups in structures (4-7) can affect the oligomer solubility and therefore the blend morphology.

The small variation observed in the performance of cells based on acceptors (5-7) could be reasonably explained in terms of both blend morphology and side group effect on the electrical properties.

A deeper investigation is clearly required in order to elucidate the effect of the molecular structure of *oligothiophene-S,S-dioxides* on their photoresponse and blend morphology.

In summary, the *oligothiophene-S,S-dioxides* represent an interesting class of *electron-acceptor* materials for photovoltaic applications and the interaction of the oligomers with the polymer results in an enhanced charge separation.

Blending **P3HT** with oligothiophene (4) a sixty-fold increase of the power conversion efficiency was achieved, with respect to the pristine device in which the polymer was the active layer. The important comparison here is the relative performance.

A successive optimization of both blend composition and design of *oligothiophene-S,S-dioxide* structures could greatly enhance the photoinduced charge-transfer process leading to much better device performance.

Furthermore, the important feature of such materials is the chemical ``compatibility`` with a common class of *donors* such as **PTs**. The functionalization of *oligothiophene-S,S-dioxides* with suitable substituents, conferring good solubility and improving the miscibility with the donor component, could be a method for avoiding the typical problems of phase segregation in blends between two materials of different chemical nature.

3.4.1.3 Alternative Oligothiophenes

Obviously, by selective changes at the α -, β -positions or even sulfur atoms of heterocycle rings into *oligothiophenic system*, we can have different versatile useful structures for **OPVDs**.

For example other typologies of *n-type materials* (**Figure 86**) are possible by appropriate functionalization of different **OTs** systems:

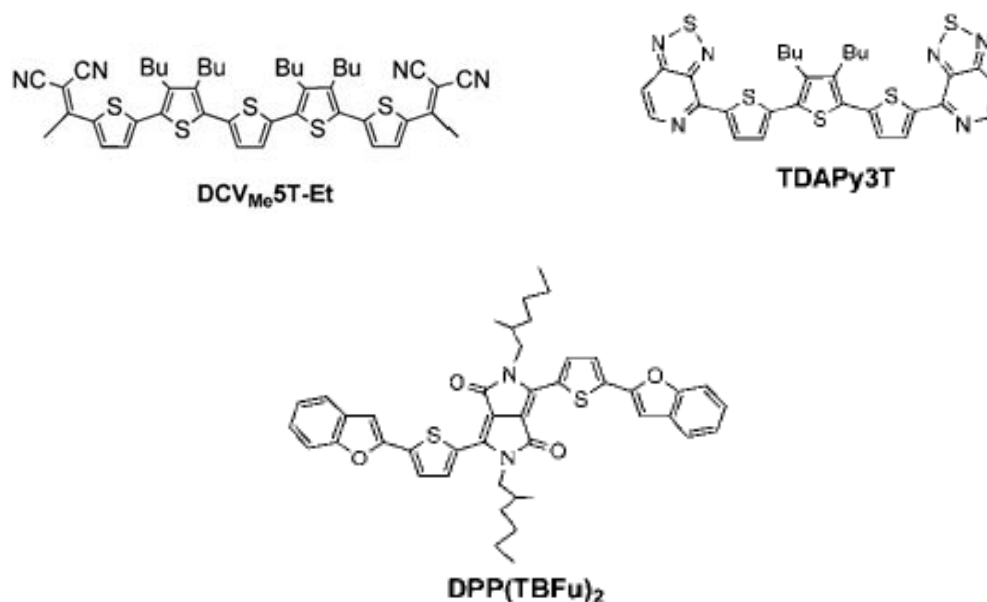


Figure 86. Molecular structures of DVC, BTDA and DPP-containing oligomers.

Furthermore the incorporation of *donor* and *acceptor* moieties into one molecular or polymeric structure may provide a means to adjust the phase separation at the nanometer scale by tailor-made synthesis.

In this purpose several copolymers consisting of **OTs** and *fullerene* or *perylene diimide* as *donor* and *acceptor* building blocks, respectively, have been reported.³¹⁴

While **OSC** devices using polymers as single active component only afforded very poor efficiency, mostly due to their polydispersity (**PDI**) and rigid nature.

Therefore a different approach by Geng *et al.* offers a series of *D-A* type co-oligomers comprising *oligo(fluorine-alt-bithiophene)s* as donor and *perylene diimide* as acceptor segment respectively (**Figure 87**),³¹⁵ providing an high **PCE** up to 1.5%, which is among the highest device efficiencies of single-molecular **OSCs** with **OTs**.

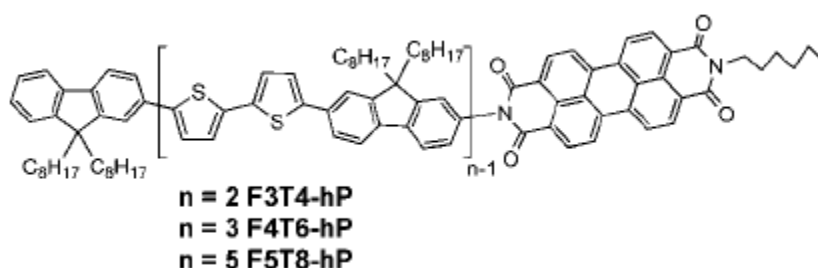


Figure 87. Molecular structure of a representative D-A block co-oligomer.

3.4.2 Polythiophenes for OPVDs

Interest in conjugated polymers picked up significantly after the discovery in 1976 that they can be made highly electrically conducting following a redox chemical treatment,³¹⁶ and discovery of thiophene-based polymers further accelerated the *progress of polymer solar cells (PSCs)*.

PTs have a number of advantages over other materials, which make them good candidates for photovoltaic applications:

- The solubility and/or fusibility of these polymers allow the formation of thin films of optical quality; they also

allow the formation of complex morphologies due to phase separation and supramolecular organization^{317,318}

- It is easy to tailor their optical properties by modifying the **PTs** via simple substitution on the main chain, at least for **E_g** varying from 1 to 3 eV.^{319,320} The chemical control of **E_g** is not easily achieved for the **PPV**³²¹ or *poly(p-phenylene)* (**PPP**)³²² systems that represent two of the other processable polymer families
- The enhanced photochemical stability of **PTs** compared with **PPVs** and **PPPs** make them more attractive for photoconversion. Still, the photochemical stability is limited by photochemistry in the presence of *oxygen, water* or chemical species remaining after synthesis^{323,324,325,326,327,328,329}

Already in the early 1980s there were reports on the conductivity and photovoltaic properties of thin films based on **PT** and its derivatives.^{330,331,332,333}

Glenis et al. prepared and characterized *Al-polymer-Al* devices using **PT** and *poly(3-methylthiophene)* (**P3MT**), but the efficiency of such devices was still poor. Nevertheless, the interest in **PTs** rose and resulted in the intensive study and synthesis of many new derivatives of **PT** with various device performance qualities.

P3HT belongs to this group and has brought the **PTs** to a leading position among all the organic materials for photovoltaic applications. Currently, devices based on a blend of **P3HT** and **PCBM** represent the 'state of the art' in the field of **PSCs**, with reported device efficiencies of about 8-9%,^{334,335} and **P3HT** is the most commonly used material for **PSCs** studies at present.

3.4.2.1 P3HT:PCBM in BHJ Solar Cells

P3ATs are conjugated polymers with good solubility, processability, and environmental stability.^{336,337}

Regioregular **P3ATs**, **P3HT**, *poly(3-octylthiophene)* (**P3OT**), and *poly(3-dodecylthiophene)* (**P3DDT**) are used as *electron-donors* in *polymer:fullerene BHJ* solar cells with record power conversion efficiencies up to 8-9%.³³⁸

*Al Ibrahim et al.*³³⁹ investigated the influence of the alkyl side chain length of regioregular **P3HT**, **P3OT**, and **P3DDT** on the electrochemical and optical properties. Energy levels for **P3OT**,³⁴⁰ for **P3HT**,^{341,342} and for **P3DDT** were almost the same with the optical **E_g** energy around 1.9 eV.

With longer side chain length, their electrochemical **E_g** were slightly increased. The absorption coefficient undergoes a systematic decrease by longer side chain **PTs** due to chromophore dilution (i.e. conjugated segments in ratio to non-conjugated segments decrease upon increasing the side chain length).

We previously said that **P3HT:PCBM** has reported an efficiency as high as 8-9%, which is unusual in the organic cell material (**Figure 88**).

PCBM is a fullerene derivative and because of high hole mobility, it plays the role of electron acceptor in many organic cells. **P3HT** is among the polythiophene family which is a kind of main conducting *p-type* polymer.

It is the excitation of the *π -orbit* electron in **P3HT** that gives the photovoltaic effect in the blend.³⁴³

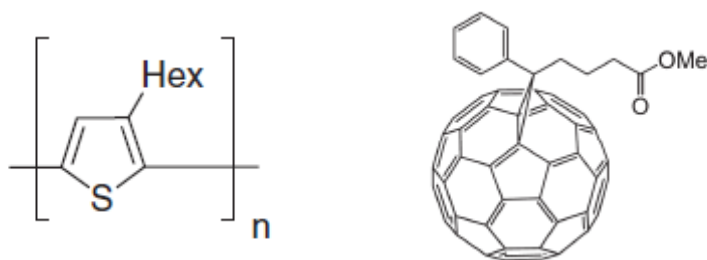


Figure 88. Chemical structure of P3HT (left) and PCBM (right).

▪ Absorption Spectrum

Organic polymers have wider **E_g** than semiconductors. Thus they give an efficient absorption at near UV part. So is **PH3T:PCBM** blends.

The gap of the blend is approximately 1.8eV. So the longest absorption wavelength should be around 650 nm (**Figure 89**).³⁴⁴

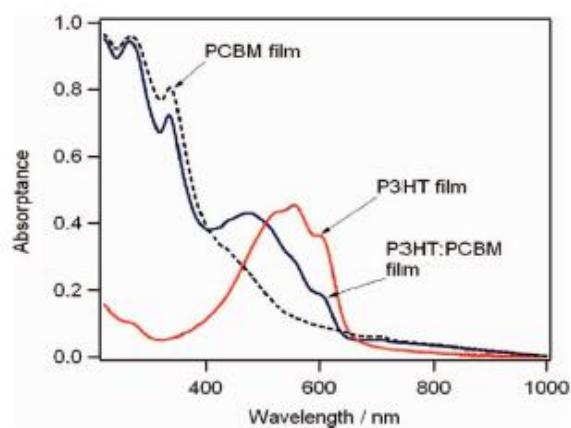


Figure 89. Absorbance spectrum of P3HT film, PCBM film, and P3HT:PCBM film.

One of the interesting features of organic polymer is that the **E_g** can easily be altered without changing its chemical components. It has been discovered that a *head-to-tail* alignment of **P3HT** has narrower gap than a *head-to-head* alignment.

It has also been discovered that in several materials, the different arrangement in lateral chains can also result in different **E_g** structures. Moreover, changing the ratio of **P3HT:PCBM** can change the gap as well.

▪ **Charge Generation**

Like in many other **OSC** materials, **BHJ** structure has been adopted in the **P3HT:PCBM** blends so that the *donor-acceptor* interface is enlarged.

Ultrafast studies have been carried out to study the charge-generation mechanism in the material. It is shown that in the presence of **P3HT**, the PCBM excitons are effectively split quite fast and produced $P3HT^+$ and $PCBM^-$.

The rate of charge transfer is faster than other possible decaying of the **PCBM** in excited state, which means the excitons got separated before the recombination of electron and hole.

From the measured rate of charge transfer, the *Gibbs* free energy change during splitting can be calculated using the *Marcus-Hush theory*. It is approximately 1eV, i.e. over half of the absorbed photon energy (~1.8eV). This is also larger than the binding energy of the excitons (~0.3-0.5eV), indicating that a large portion of photon energy is wasted in heat.

Thus, charge generation would be impeded or even completely stopped due to a fast transfer rate. This challenge points out a possible direction to further increase the efficiency that materials with similar structure but less transfer rate can be exploited.

▪ **Increasing Efficiency: Morphology and Others Ways**

Nanoscale morphology is important in improving cell efficiency. Experiments show that when **P3HT:PCBM** blends adopts an organized morphology, the cell's performance is improved. It is found that the absorption spectra is widened, **I_{sc}** increases, while **V_{oc}** slightly decreases.

Moreover, surface resistivity decreases. There are several advantages taking this more organized morphology, where all **P3HT** aligns parallel and **PCBM** adopts nanocrystal structure. Firstly, probably the gap is narrowed and the absorption spectrum is consequently widened. This is in agree with a lowered **V_{oc}**.

But the change in **V_{oc}** is insignificant compared with the change in absorption spectrum. It is likely to be a result from change in both donor and acceptor's band structures. This is supported by the fact that when applying electric field in synthesizing the organized structure, an increase in **V_{oc}** is achieved, indicating certain kind of polarized structure occurs in the material.

With a widened absorption spectrum, more excitons can be produced. Moreover, this morphology gives a large interface, increasing separate percentage. And experiment have also shown that there's a preferred orientation, which provides charge carrier channel, enhancing charge mobility, and decreases surface resistivity.

This factors above combined give an increased **I_{sc}**. The power conversion can achieve as high as 8-9%, a record for **OSCs** materials (**Figure 90**).³⁴⁵

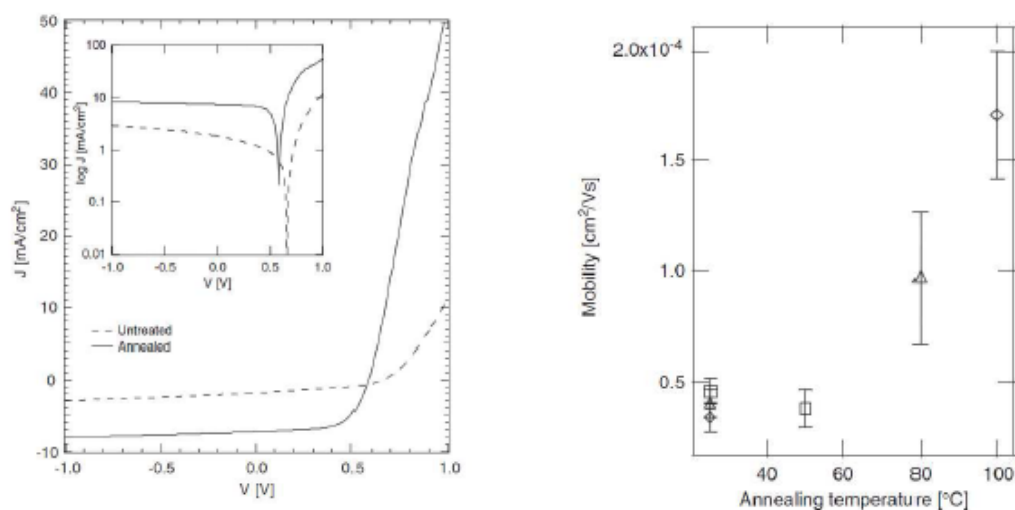


Figure 90. I-V curve (left) of P3HT:PCBM blends before and after annealing and hole mobility (right), as-produced and after annealing.

Thermal annealing is a method commonly used to optimize the material's morphology. Experiments show that after thermal annealing, the **P3HT:PCBM** blends adopts a better-organized structure.

P3HT forms long and thin fibers while **PCBM** crystalline become more homogeneous (**Figure 91**).³⁴⁶

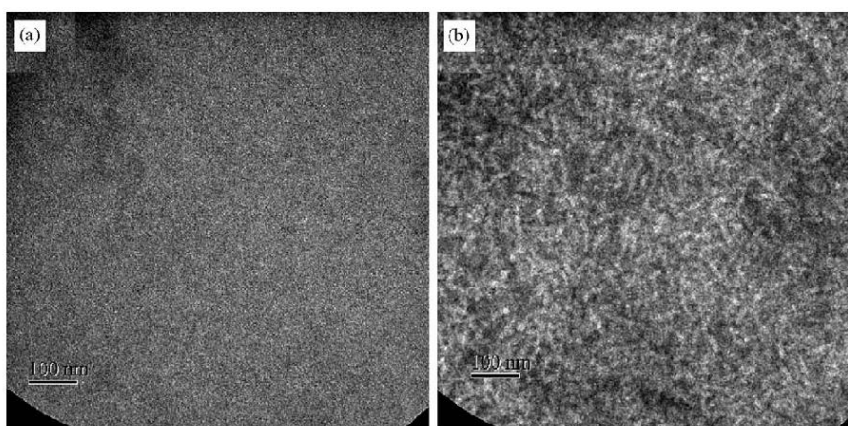


Figure 91. TEM images of a P3HT:PCBM 1:1 blend (a) before and (b) after annealing at 100 °C for 5 min.

A study on the phase diagram of the blends³⁴⁷ gives that the change of conformation occurs as a single glass transition, where T_g is associated with the concentration of **PCBM** and this T_g gives lowest annealing temperature.

Actually, the crystallization of the two components are inhibited at the presence of each other, and by thermal annealing, they resume better crystalline structures.

However, the phase diagram also indicates instability at working temperature. Moreover, when **P3HT** chains are crystallized, nucleation sites were provided for **PCBM**.³⁴⁸

Then the components of the blends grow through a self-organization process. Thus, the growth of such ordered conformation on a larger area is possible.

Besides morphology, various approaches have been tried to enhance the cell's efficiency. Dye has been introduced to increase near IR region photoconversion.³⁴⁹ With proper dye concentration (**Figure 92**), the absorption at long wavelength region of the material increases. But when the concentration goes too high, the efficiency decreases because the efficient charge separation rate has go down.

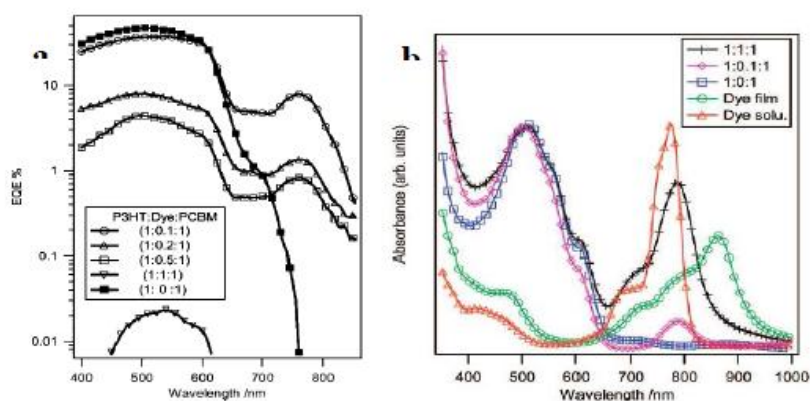


Figure 92. External quantum efficiency with different dye concentration (left); absorption spectra (right).

Hole-extraction layer has been applied.^{350,351,352} **ITO** anode, **PEDOT:PSS** modifier and anode, and carbon nanotube have been used. So far, **ITO** anode provides good efficiency and is highly transparent. And the other two has shown no significant advantage in efficiency but would probably be a good alternative when the cost of **ITO** is kept high by limited source of tin.

Buffer layer between the active layer and the electrodes has been tried, as well.^{353,354}

A buffer layer at the cathode can increase R_{Shunt} by preventing diffusion of the cathode material into the active layer. A buffer layer at the anode plays an optical role, increasing the intensity at the active layer.

However, these do not show significant success.

▪ **Stability of P3HT:PCBM BHJ Solar Cells**

Despite the prediction from the phase diagram, the **P3HT:PCBM** module is quite stable.

Experiments show that under accelerated light soaking conditions in the laboratory, it remains good light stability, and over a year of outdoor exposure.

Ratio of components, morphology, and cathode material would affect stability.³⁵⁵ Besides higher efficiency, a more ordered microscopic structure also gives better stability.³⁵⁶

With **Ca/Ag** cathode the blend film can retain its sufficiency for a significantly longer time than using **LiF/Al** cathode. Moreover, inspired by biological structures, a special family of organic materials, efforts on self-repair and defect-tolerating materials have been done.³⁵⁷

▪ **Synthesis**

The construction of a piece of **BHJ** solar cell (**Figure 93**).

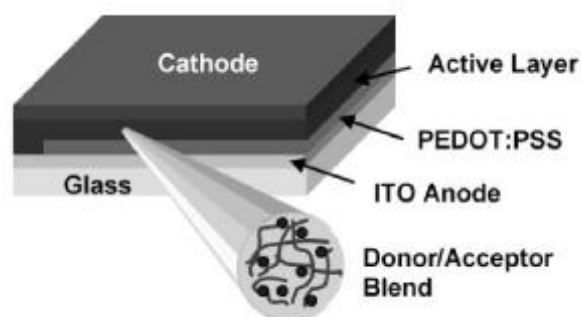


Figure 93. Schematic of a P3HT/PCBM BHJ.

To construct organic thin films, wet processing, is useful. Methods such as *spin coating*, *Knife-over-edge coating*, *spray coating*, *slot-die coating*, *rotogravure printing*, and *screen printing* were introduced.^{358,359,360}

These approaches provides possible ways to process low-cost large-area cells. Designed patterns can easily be reproduced by these highly repeatable methods. This can lead to mass-integrated cells where identical units were arranged in one piece.³⁶¹

Moreover, there're technical reasons adopting these wet processing methods. First of all, many organic polymers have poor heat stability.³⁶² They might decompose before evaporate. So the choice of solvent becomes important for these technique.

Additionally, it is also shown that different solvent can even give different efficiency and stability, probably ligands have played a role in crystallization process. Another reason is that drying process provides conditions for annealing to optimize morphology.

Moreover, the required condition is not so strict. Experiments showed that even a contaminated environment can the printing procedure be operated.

3.4.2.2 New Materials for Alternative Approaches

A variety of other approaches have been used to overcome some limitation as for example the absorption of the solar photon due to limited spectra breath that many polymers have.

The **P3HT** for example, succeeds to capture only the 46% of the available solar photon,³⁶³ therefore expanding the spectral breadth by use of low **E_g** polymers, it would allow absorption of 77% of all the solar photon.³⁶⁴

Below are showed (**Figure 94**) two different polymers based thiophene; the most common synthetic technique used to achieve low-bandgap polymers is the *donor-acceptor* approach, in which alternating *electron-rich* and *electron-poor* units define the polymer backbone.³⁶⁵

The best examples of this class reported thus far are based almost exclusively on *benzothiadiazole* (or analogues) as the acceptor in combination with several different donor groups.

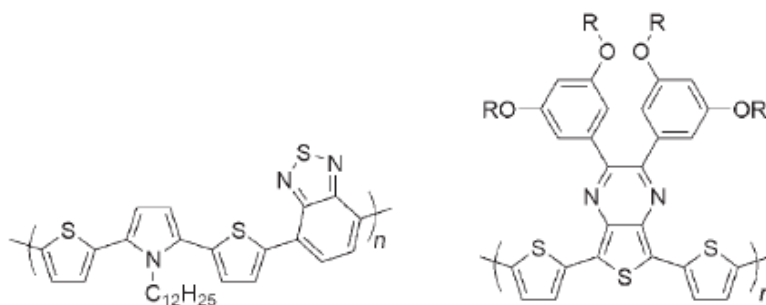


Figure 94. Two different examples of alternative polymers based thiophene.

Obviously it is clear that strategies that focus on optimizing both the polymer and the fullerene structures can afford significant improvement in the ability to harvest light across a broader spectral range.

In this purpose to higher fullerenes, a variety of soluble C_{60} derivatives have been synthesized and employed in BHJ solar cells with varying success (Figure 95).

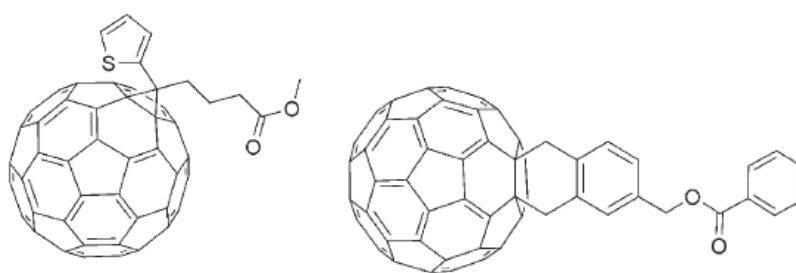


Figure 95. Two different typologies of modified fullerenes.

3.5 Stability of Organic Solar Cells

Apart from the necessity for efficiency improvement, stability is another problem for organic solar cells. Especially under light illumination and by simultaneous exposure to oxygen or water vapor, a rapid photooxidation/degradation occurs. Protection from air and humidity is necessary to achieve long device lifetimes.³⁶⁶ Neugebauer et al.³⁶⁷ showed that the photodegradation of the conjugated oligomers and polymers is significantly decreased when mixed with fullerenes.

The stability of the conjugated polymer-fullerene solar cell mixture, which forms a charge transfer donor and acceptor couple, is higher than the stability of conjugated oligomers and polymers in organic light emitting diodes.³⁶⁸

The stabilization effect of **C₆₀** is presumed to be due to the fast electron transfer. In this process, the highly reactive excited state of the polymer is emptied rapidly, lowering the energy to the more environmentally stable electrochemical potentials of fullerene reduction (LUMO).

In particular **MDMO-PPV/PCBM** solar cells show also a significant nano morphological degradation.³⁶⁹ At elevated temperatures, the **PCBM** molecules can diffuse through the **MDMO-PPV** matrix and form large crystals.³⁷⁰

This nano morphological instability can be fixed by post production cross-linking of the components, to prevent their diffusion.³⁷¹ On the contrary **P3HT/PCBM** blends show much better photostability. The efficiency of solar cells using these components changed less than 20% during 1000 h of light soaking at 70°C under an inert atmosphere.³⁷²

3.6 References

[228] Source <http://www.energy.eu>

[229] A. Shah, R. Tscharner, N. Wyrsh, and H. Keppner, *Science*, **1999**, 285

[230] A. C. Vesterbrogade, *Elektronikbutikken*, **2006**

[231] J. Nelson, *The Physics of Solar Cells. Imperial College Press.*, **2003**

[232] B. A. Gregg, *J. Phys. Chem. B*, **2003**, 107, 4688-4698

[233] J. Xue, S. Uchida, B. P. Rand, S. R. Forrest, *Appl. Phys. Lett.*, **2004**, 84, 3013-3015

[234] N. S. Sariciftci, D. Braun, C. Zhang, V. I. Srdanov, A. J. Heeger, G. Stucky, F. Wudl, *Appl. Phys. Lett.*, **1993**, 62, 585-587

[235] M. Granstrom, K. Petritsch, A. C. Arias, A. Lux, M. R. Andersson, R. H. Friend, *Nature*, **1998**, 395, 257-260

[236] P. Peumans, A. Yakimov, S. R. Forrest, *J. Appl. Phys.*, **2003**, 93, 3693-3723

- [237] J. J. M. Halls, C. A. Walsh, N. C. Greenham, E. A. Marseglia, R. H. Friend, S. C. Moratti, A. B. Holmes, *Nature*, **1995**, 376, 498-500
- [238] G. Yu, A. J. Heeger, *J. Appl. Phys.*, **1995**, 78, 4510-4515
- [239] F. Wudl, *Acc. Chem. Res.*, **1992**, 25, 157161
- [240] J. M. C. R. Nunzi, *Physique*, **2002**, 3, 523
- [241] P. B. Miranda, D. Moses, A. J. Heeger, *Phys. Rev. B*, **2001**, 64, 81201
- [242] A. Mozer, S. C. R. Sariciftci, *Chimie*, **2006**, 9, 568
- [243] C. Brabec, G. Zerza, G. Cerullo, S. De Silvestri, S. Luzatti, J. C. Hummelen, S. Sariciftci, *Chem. Phys. Lett.*, **2001**, 340, 232
- [244] I. Parker, *J. Appl. Phys.*, **1994**, 75, 1656
- [245] P. M. Borsenberger, D. S. Weiss, M. B. Borsenberger, *Organic Photoreceptors for Xerography*; Marcel Dekker Inc.: New York, **1998**
- [246] C. Im, W. Tian, H. A. Bässler, M. D. Fechtenkötter Watson, K. J. Müllen, *J. Chem. Phys.*, **2003**, 119, 3952
- [247] A. Heeger, D. Moses, *Primary Photoexcitations in Conjugated Polymers: Molecular Exciton Versus Semiconductor Band Model*; World Scientific: Singapore, **1997**
- [248] C. J. Brabec, A. Cravino, D. Meissner, N. S. Sariciftci, T. Fromherz, M. T. Rispens, L. Sanchez, J. C. Hummelen, *Adv. Funct. Mater.*, **2001**, 11, 374-380
- [249] A. Gadisa, M. Svensson, M. R. Andersson, O. Inganäs, *Appl. Phys. Lett.*, **2004**, 84, 1609-1611
- [250] P.-M. Allemand, A. Koch, F. Wudl, *J. Am. Chem. Soc.*, **1991**, 113, 1050-1051
- [251] V. I. Arkhipov, H. Bassler, *Phys. Status Solid A*, **2004**, 201, 1152-1187
- [252] C. J. Brabec, C. Winder, N. S. Sariciftci, J. C. Hummelen, A. Dhanabalan, P. A. van Hal, R. A. J. Janssen, *Adv. Funct. Mater.*, **2002**, 12, 709-712
- [253] C. Winder, G. Matt, J. C. Hummelen, R. A. J. Janssen, N. S. Sariciftci, C. J. Brabec, *Thin Solid Films*, **2002**, 403-404, 373-379
- [254] L. J. A. Koster, V. D. Mihailetschi, P. W. M. Blom, *Appl. Phys. Lett.*, **2006**, 88, 093511
- [255] C. Soci, I.-W. Hwang, D. Moses, Z. Zhu, D. Waller, R. Gaudiana, C. J. Brabec, A. J. Heeger, *Adv. Funct. Mater.*, **2007**, 17, 632-636
- [256] M. C. Scharber, D. Muhlbacher, M. Koppe, P. Denk, C. Waldauf, A. J. Heeger, C. J. Brabec, *Adv. Funct. Mater.*, **2006**, 18, 789-794
- [257] Sigma-aldrich., **2006**

- [258] American Dye Source, *Light emitting homopolymer for oled and pled devices*, **2006**
- [259] C. W. Tang, *Appl. Phys. Lett.*, **1986**, *48*, 183
- [260] T. T. Tsuzuki, J. Shirota, J. Rostalski, D. Meissner, *Sol. Energy Mater. Sol. Cells*, **2000**, *61*, 1
- [261] J. X. Uchida, B. P. Rand, S. R. Forrest, *Appl. Phys. Lett.*, **2004**, *84*, 4218
- [262] X. Zhou, J. Blochwitz, M. Pfeiffer, A. Nollau, T. Fritz, K. Leo, *Adv. Funct. Mater.*, **2001**, *11*, 310
- [263] D. Wöhrle, D. Meissner, *Adv. Mater.*, **1991**, *3*, 129
- [264] S. A. Jenekhe, S. Yi, *Appl. Phys. Lett.*, **2000**, *77*, 2635
- [265] A. J. Breeze, A. Salomon, D. S. Ginley, B. A. Gregg, H. Tillmann, H. H. Hoerhold, *Appl. Phys. Lett.*, **2002**, *81*, 3085
- [266] N. S. Sariciftci, D. Braun, C. Zhang, V. I. Srdanov, A. J. Heeger, G. Stucky, F. Wudl, *Appl. Phys. Lett.*, **1993**, *62*, 585
- [267] J. J. M. Halls, C. A. Walsh, N. C. Greenham, E. A. Marseglia, R. H. Friend, S. C. Moratti, A. B. Holmes, *Nature*, **1995**, *78*, 451
- [268] C. Winder, N. S. Sariciftci, *J. Mater. Chem.*, **2004**, *14*, 1077
- [269] M. G. Harrison, J. Gruener, G. C. W. Spencer, *Phys. Rev. B*, **1997**, *55*, 7831
- [270] L. A. A. Petterson, L. S. Roman, O. Inganas, *J. Appl. Phys.*, **1999**, *86*, 487
- [271] J. Rotalsky, D. Meissner, *Sol. Energy Mater. Sol. Cells*, **2000**, *63*, 37
- [272] H. Hoppe, N. S. Sariciftci, *J. Mater. Chem.*, **2004**, *19*, 1924
- [273] J. Hoppe, Ph.D. Thesis, Linz, **2004**
- [274] D. Gebeyehu, B. Maening, J. Drechsel, K. Leo, M. Pfeiffer, *Sol. Energy Mater. Sol. Cells*, **2003**, *79*, 81
- [275] M. Hiramoto, H. Fujiwara, M. Yokoyama, *Appl. Phys. Lett.*, **1991**, *58*, 1061
- [276] W. Geens, T. Aernouts, J. Poortmans, G. Hadziioannou, *Thin Solid Films*, **2002**, *403-404*, 438
- [277] P. Peumans, S. Uchida, S. Forrest, *Nature*, **2003**, *425*, 158
- [278] G. Yu, A. J. Heeger, *J. Appl. Phys.*, **1998**, *78*, 4510
- [279] C. Y. Yang, A. J. Heeger, *Synth. Met.*, **1996**, *83*, 85
- [280] G. Yu, J. Gao, J. C. Hummelen, F. Wudl, A. J. Heeger, *Science*, **1995**, *270*, 1789
- [281] J. J. Dittmer, E. A. Marseglia, R. H. Friend, *Adv. Mater.* **2000**, *12*, 1270

- [282] K. Petritsch, J. J. Dittmer, E. A. Marseglia, R. H. Friend, A. Lux, G. G. Rozenberg, S. C. Moratti, A. B. Holmes, *Sol. Energy Mater. Sol. Cells*, **2000**, *61*, 63
- [283] L. S. Mende, A. Fechtenkötter, K. Müllen, E. Moons, R. H. Friend, J. D. Mackenzie, *Science*, **2001**, *293*, 1119
- [284] F. Padinger, R. Rittberger, N. S. Sariciftci, *Adv. Funct. Mater.*, **2003**, *13*, 85
- [285] J. M. C. R. Nunzi, *Physique*, **2002**, *3*, 523
- [286] S. Shaheen, C. J. Brabec, N. S. Sariciftci, F. Padinger, T. Fromherz, J. C. Hummelen, *Appl. Phys. Lett.*, **2001**, *78*, 841
- [287] M. Wienk, J. M. Kroon, W. J. H. Verhees, J. C. Hummelen, P. A. Van Hal, J. Janssen, *Angew. Chem.*, **2003**, *42*, 3371
- [288] X. Yang, J. Loos, S. C. Veenstra, W. J. H. Verhees, M. Wienk, M. Kroon, M. H. J. Michels, R. A. J. Janssen, *Nano Lett.*, **2005**, *5*, 579
- [289] J. Van Duren, X. Yang, J. Loos, C. W. T. Bulle-Lieuwma, A. B. Sievel, J. C. Hummelen, R. A. J. Janssen, *Adv. Funct. Mater.*, **2004**, *14*, 425
- [290] H. Yokoyama, E. J. Kramer, M. H. Rafailovich, J. Sokolov, S. A. Schwarz, *Macromolecules*, **1998**, *31*, 8826
- [291] A. Pivrikas, G. Juska, A. J. Mozer, M. Scharber, A. Karlauskas, N. S. Sariciftci, H. Stubb, *Phys. Rev. Lett.*, **2005**, *94*, 176806
- [292] A. J. Mozer, N. S. Sariciftci, L. Lutsen, D. Vanderzande, M. Westerling, G. Juska, *Appl. Phys. Lett.*, **2005**, *86*, 112104
- [293] A. J. Mozer, N. S. Sariciftci, A. Pivrikas, R. Osterbacka, G. Juska, L. H. Brassat, *Phys. Rev. B*, **2005**, *71*, 35214
- [294] A. Mozer, N. S. Sariciftci, *Chem. Phys. Lett.*, **2004**, *389*, 438
- [295] A. Mozer, Ph.D. Thesis, Linz, **2004**
- [296] R. Pacios, D. D. Bradley, J. Nelson, C. J. Brabec, *Synth. Met.*, **2003**, *137*, 1469
- [297] V. Mihailetschi, K. K. Van Duren, P. Blom, J. C. Hummelen, R. Janssen, J. Kroon, M. Rispens, W. Verhees, M. Wienk, *Adv. Funct. Mater.*, **2006**, *16*, 699
- [298] H. Hoppe, M. Niggemann, C. Winder, J. Kraut, R. Hiesgh, A. Hinsch, D. Meissner, N. S. Sariciftci, *Adv. Funct. Mater.*, **2004**, *14*, 1005
- [299] D. Gebeyehu, C. J. Brabec, F. Padinger, T. Fromherz, J. C. Hummelen, D. Badt, H. Schindler, N. S. Sariciftci, *Synth. Met.* **2001**, *118*, 1

- [300] T. Martens, J. D. Hoen, T. Munters, Z. Beelen, L. Goris, J. Monca, M. D. Oliesloeger, D. Vanderzende, L. De Schopper, R. Andriessen, *Synth. Met.*, **2003**, *138*, 243
- [301] X. Yang, J. K. J. Van Duren, R. A. J. Janssen, M. A. J.; Michels, J. Loos, *Macromolecules*, **2004**, *37*, 2151
- [302] W. Ma, C. Yang, X. Gong, K. Lee, A. J. Heeger, *Adv. Funct. Mater.*, **2005**, *15*, 1617-1622
- [303] G. Li, V. Shrotriya, J. Huang, Y. Yao, T. Moriarty, K. Emery, Y. Yang, *Nat. Mater.*, **2005**, *4*, 864-868
- [304] (a) N. Noma, T. Tsuzuki, and Y. Shirota, *Adv. Mater.*, **1995**, *7*, 647; (b) A. Mishra, C. Q. Ma, and P. Bäuerle, *Chem. Rev.*, **2009**, *109*, 1141
- [305] Y. Sun, Y. Ma, Y. Liu, Y. Lin, Z. Wang, D. Zhu, et al., *Adv. Func. Mater.*, **2006**, *16*, 426
- [306] T. Taima, K. Saito, et al., *Appl. Phys. Lett.*, **2004**, *85-26*, 6412
- [307] J. Sakai, T. Taima, K. Saito, *Adv. Technol. Dev. Lab.*, Matsushita Electr. Works Ltd., Osaka, **2006**, 291-294
- [308] J. E. Anthony, *Chem. Mater.*, **2010**, *23*, 583
- [309] G. Barbarella, O. Pudova, C. Arbizzani, M. Mastragostino, and A. Bongini, *J. Org. Chem.*, **1998**, *63*, 1742
- [310] G. Barbarella, L. Favaretto, G. Sotgiu, M. Zambianchi, L. Antolini, O. Pudova, and A. Bongini, *J. Org. Chem.*, **1998**, *63*, 5497
- [311] G. Barbarella, L. Favaretto, M. Zambianchi, O. Pudova, C. Arbizzan, A. Bongini, and M. Mastragostino, *Adv. Mater.*, **1998**, *10*, 551
- [312] G. Yu, J. Gao, J. C. Hummelen, F. Wudl, and A. J. Heeger, *Science*, **1995**, *270*, 1789
- [313] C. J. Brabec, A. Cravino, G. Zerza, N. S. Sariciftci, R. Kiebooms, D. Vanderzande, and J. C. Hummelen, *J. Phys. Chem. B*, **2001**, *105*, 1528
- [314] (a) M. Sommer, A. S. Lang, and M. Thelakkat, *Angew. Chem.*, **2008**, *47*, 7901; (b) J. U. Lee, A. Cirpan, T. Emrick, T. P. Russell, and W. H. Jo, *J. Mater. Chem.*, **2009**, *19*, 1483; (c) Q. Zhang, A. Cirpan, T. P. Russell, and T. Emrick, *Macromolecules*, **2009**, *42*, 1079
- [315] L. Bu, X. Guo, B. Yu, Y. Qu, Z. Xie, D. Yan, Y. Geng, and F. Wang, *J. Am. Chem. Soc.*, **2009**, *131*, 13242
- [316] C. K. Chiang, C. R. Fincher, Y. W. Park, A. J. Heeger, H. Shirakawa, E. J. Louis, A. G. MacDiarmid, *Phys. Rev. Lett.*, **1977**, *39*, 1098-1101

- [317] L. S. Roman, M. R. Andersson, T. Yohannes, O. Inganäs, *Adv. Mater.*, **1997**, *9*, 1164-1168
- [318] M. Granstrom, M. Berggren, D. Pede, O. Inganäs, M. R. Anderson, T. Hjertberg, O. Wennerstrom, *Supramol. Sci.*, **1997**, *4*, 27-34
- [319] M. R. Anderson, M. Berggren, O. Inganäs, G. Gustafsson, J. C. Gustafsson-Carlberg, D. Selse, T. Hjertberg, O. Wennerstrom, *Macromolecules*, **1995**, *28*, 7525-7529
- [320] H. Sze On Chan, N. G. Siu Choon, *Prog. Polym. Sci.*, **1998**, *23*, 1167-1231
- [321] B. R. Cho, *Prog. Polym. Sci.*, **2002**, *27*, 307-355
- [322] L. M. Goldenberg, P. C. Lacaze, *Synth. Met.*, **1993**, *58*, 271-293
- [323] X. Yang, J. Loos, S. C. Veenstra, W. J. H. Verhees, M. M. Wienk, J. M. Kroon, M. A. J. Michel, R. A. J. Janssen, *Nano Lett.*, **2005**, *5*, 579-583
- [324] F. C. Krebs, H. Spanggaard, *Chem. Mater.*, **2005**, *17*, 5235-5237
- [325] F. C. Krebs, K. Norrman, *Prog. Photovolt.: Res. Appl.*, **2007**, *15*, 697-712
- [326] M. Bierring, J. S. Nielsen, A. Siu, N. C. Nielsen, F. C. Krebs, *Sol. Energy Mater. Sol. Cells*, **2008**, *92*, 772-784
- [327] E. A. Katz, S. Gevorgyan, M. S. Orynbayev, F. C. Krebs, *Eur. Phys. J.: Appl. Phys.*, **2007**, *36*, 307-311
- [328] J. A. Hauch, P. Schilinsky, S. A. Choulis, R. Childers, M. Biele, C. J. Brabec, *Sol. Energy Mater. Sol. Cells*, **2008**, *92*, 727-731
- [329] M. S. A. Abdou, S. Holdcroft, *Chem. Mater.*, **1994**, *6*, 962-968
- [330] R. J. Waltman, J. Bargon, A. F. Diaz, *J. Phys. Chem.*, **1983**, *87*, 1459-1463
- [331] S. Glenis, G. Horowitz, G. Tourillon, F. Garnier, *Thin Solid Films*, **1984**, *111*, 93-103
- [332] S. Glenis, G. Tourillon, F. Garnier, *Thin Solid Films*, **1984**, *122*, 9-17
- [333] S. Glenis, G. Tourillon, F. Garnier, *Thin Solid Films*, **1986**, *139*, 221-231
- [334] G. Li, V. Shrotriya, J. Huang, Y. Yao, T. Moriarty, K. Emery, Y. Yang, *Nat. Mater.*, **2005**, *4*, 864-868
- [335] W. Ma, C. Yang, X. Gong, K. Lee, A. J. Heeger, *Adv. Funct. Mater.*, **2005**, *15*, 1617-1622
- [336] D. Chirvaze, Z. Chiguvare, M. Knipper, J. Parisi, V. Dyakonov, J. C. Hummelen, *Appl. Phys.*, **2003**, *93*, 3376
- [337] D. Chirvaze, J. Parisi, J. C. Hummelen, V. Dyakonov, *Nanotechnology*, **2004**, *15*, 1314
- [338] R. R. Reyes, K. Kim, D. L. Carroll, *Appl. Phys. Lett.*, **2005**, *87*, 083506

- [339] M. Al Ibrahim, H. Klaus Roth, M. Schroedner, A. Kalvin, U. Zhokhavets, G. Gobsch, P. Scharff, S. Sensfuss, *Org. Electron.*, **2005**, *6*, 65
- [340] T. Ahn, B. Choi, S. N. Ahn, S. N. Han, H. Lee, *Synth. Met.*, **2001**, *117*, 219
- [341] D. Chirvaze, Z. Chiguvare, M. Knipper, J. Parisi, V. Dyakonov, J. C. Hummelen, *Synth. Met.*, **2003**, *138*, 299
- [342] K. Takahashi, K. Tsuji, K. Inote, T. Yamaguchi, T. Kanura, K. Murata, *Synth. Met.*, **2004**, *130*, 177
- [343] H. S. Nalwa, *Handbook of Organic Conductive Molecules and Polymers Vol.3: Conductive Polymers: Spectroscopy and Physical Properties*, ISBN: 0-471-96595-2
- [344] S. Cook, R. Katoh, A. Furube, *J. Phys. Chem. C.*, **2009**, *113*, 2547-2552
- [345] M. Reyes, K. Kim, D. L. Carroll, *Appl. Phys. Lett.*, **2005**, *87*
- [346] X. Yang, J. Loos, S. C. Veenstra, W. J. H. Verhees, M. M. Weink, J. M. Kroon, L. L. Michels, R. A. Janssen, *Nano Letters*, **2005**, *5(4)*, 579-583
- [347] J. Zhao, A Swinnen, G. Van Assche, J. Manca, D. Vanderzande, B. Van Mele, *J. Phys. Chem. B*, **2009**, *113*, 1587-1591
- [348] E. M. J. Johansson, A. Yartsev, H. Rensmo, V. Sundstrom, *J. Phys. Chem. C*, **2009**, *113*, 3014-3020
- [349] M. Campoy-Quiles, T. Ferenczi, T. Agostinelli, P. G. Etchegoin, Y. Kim, T. D. Anthopoulos, P. N. Stavrinou, D. D. C. Bradley, J. Nelsen, *Natural Materials*, **2008**, *7*, 158-164
- [350] J. Kang, et. al; *Electrochemical and solid-State Letters*, **2009**, *12*, 64-66
- [351] A. Colmann, et. al.; *Thin solid Films*, **2009**, *517*, 1750-1752
- [352] R. A. Hatton, et. al.; *Org. Electron.*, **2009**
- [353] Y. Zhao, et. al., *Sol. Energy Mater. & Sol. Cells*, **2009**
- [354] P. D. Andersen, et al., *Opt. Mater.*, **2008**
- [355] R. De Bettingnies, J. Leroy, M. Firon, C. Sentein, *Synthetic Metals*, **2006**, *156*, 510-513
- [356] W. Y. Huang, C. C. Lee, T. L. Hsieh, *Solar Energy Materials & Solar Cells*, **2009**, *93*, 382-386
- [357] DOE office of Science, *Basic Research Needs for Solar Energy Utilization*, **2005**
- [358] J. M. Ding, A. Vornbrock, C. Ting, V. Subramanian, *Solar Energy Materials & Solar Cells*, **2009**, *93*, 459-464
- [359] F. Kerbs, *Solar Energy Materials & Solar Cells*, **2009**, 465-475

- [360] F. Kerbs, M. Jorgensen, K. Norrman, O. Hagemann, J. Alstrup, T. D. Nielsen, J. Fyenbo, J. Kristensen, *Solar Energy Materials & Solar Cells*, **2009**, 422-441
- [361] K. L. Chopra, P. D. Paulson, V. Dutta, *Res. Appl.*, **2004**, 12, 69-92
- [362] H. Hoppe, N. S. Sariciftci, *J. Mater. Res.*, **2004**, 19
- [363] C. Soci, I.-W. Hwang, D. Moses, Z. Zhu, D. Waller, R. Gaudiana, C. J. Brabec, A. J. Heeger, *Adv. Funct. Mater.*, **2007**, 17, 632-636
- [364] S. Gunes, H. Neugebauer, N. S. Sariciftci, *Chem. Rev.*, **2007**, 107, 1324-1338
- [365] H. A. M. Van Mullekom, J. A. J. M. Vekemans, E. E. Havinga, E. W. Meijer, *Mater. Sci. Eng.*, **2001**, 32, 1-40
- [366] J. M. Kroon, S. C. Veenstra, L. H. Sloof, W. J. H. Verhees, M. M. Koetse, J. Sweelssen, H. F. M. Schoo, W. J. E. Beek, M. M. Wienk, R. A. Janssen, X. Yang, J. Loos, V. D. Mihailetschi, P. W. M. Blom, J. Knol, J. C. Hummelen, *Abst. Eur. Sol. Energy Conf.*, **2005**
- [367] H. Neugebauer, *Electrochem. Soc.*, **2002**, 12, 19
- [368] A. J. F. Liedenbaum, J. J. M. Vleggaar, *Philips Journal of Research*, **1998**, 51, 511
- [369] S. Schuler, *Appl. Phys. A*, **2003**, 79, 37
- [370] X. Yang, J. K. J. Van Duren, R. A. J. Janssen, M. A. J. Michels, J. Loos, *Macromolecules*, **2004**, 37, 2151
- [371] M. Drees, H. Hoppe, C. Winder, H. Neugebauer, N. S. Sariciftci, W. Schwinger, F. Schäffler, C. Topf, C. Scharber, R. Gaudiana, *J. Mater. Chem.*, **2005**, 15, 5158
- [372] X. Yang, J. Loos, S. C. Veenstra, W. J. H. Verhees, M. Wienk, M. Kroon, M. H. J. Michels, R. A. J. Janssen, *Nano Lett.*, **2005**, 5, 579

4 *A Successful Chemical Strategy To Induce Oligothiophene Self-Assembly into Fibers with Tunable Shape and Function*

4.1 Introduction

Molecular self-assembly is a key technology for the design and bottom-up fabrication of nano- and microdevices based on soft materials.

Supramolecular structures with controlled shapes, dimensions, and properties are of interest for multi-component systems having defined function in devices for flexible electronics.^{373,374,375,376,377,378}

In this framework, great attention is devoted to the formation of functional nano- and micro-sized fibers self-organizing on surfaces which could be employed as interconnecting modules in integrated molecular circuits.^{379,380,381}

The molecules used as building blocks for such supramolecular structures must exhibit relevant functional properties such as fluorescence, conductivity, photoconductivity, and sensitivity to external stimuli.³⁸²

However, the molecular properties are not automatically transferred into the self-assembled superstructures, which represent novel systems from the point of view of the functional properties.

Aggregation modalities and hierarchical structuring affect light emission, charge transport, and any other property in a way that is still poorly understood. No well established rules are as yet available to relate the molecular structure to the properties of self-assembled systems, hampering the rational design of functional supramolecular architectures.

To induce diverse aggregation modalities, a variety of conjugated oligomers and polymers have been synthesized and several types of non-covalent intermolecular interactions—hydrogen bondings, Van der Waals interactions, solvophobic association between aromatic rings promoting extended π - π stacking—have been exploited.

Results from para-hexaphenylenes bearing groups capable of multiple hydrogen bondings³⁸³ or dyads based on alkyl substituted *hexa-peri-hexabenzocoronene* and *perylene monoimide*³⁸⁴ and *amphiphilic rigid macrocycles*,³⁸⁵ variously substituted *tetrathiafulvalenes*,³⁸⁶ and *oligoanilines*³⁸⁷ have been reported.

Recent research has exploited the gelation properties of functional molecules to induce the formation of electroactive fibers.³⁸⁸

Unfortunately, in most cases, small changes in the choice of the substrate or experimental conditions lead to distinctly different growth behavior and functional properties which are difficult to reproduce.

Thus, the fibers have to be grown on the appropriate substrate and the as grown nano- and microfibers have to be manipulated and mechanically transferred for integration into a device.³⁸⁹

A crucial step forward would be the availability of molecular systems capable to reproducibly self-assemble on any type of surface. Toward this goal, we have explored new molecular design approaches and synthetic patterns to prepare **OTs** which are among the most efficient conjugated materials.³⁹⁰

Owing to the great polarizability of sulfur electrons,^{391,392,393} thiophene is an easily deformable heterocycle that in the solid state is rarely present as a regular pentagon but it is deformed, in bond angles and bond lengths, to adapt its geometry to the environment.

On these grounds, we chose sulfur as the key element to promote the self-assembly and created new 'sulfur-overrich' **OTs**, so named since they have an extra sulfur atom per ring directly attached to one β -carbon of the inner tetrameric core, to induce ordered self-aggregation via *S-S* interactions and weak *CH-S* hydrogen bondings.

On the basis of literature data,³⁹⁴ we envisioned that the directionality of *S-S* and *CH-S* interactions, as well as the large polarizability of sulfur in thioether fragments, would induce the formation of highly anisotropic supramolecular systems.

We show here that sulfur-overrich octathiophenes do indeed self-assemble spontaneously on surfaces affording crystalline fibers combining efficient charge transport with intense fluorescence.

Minor changes in the molecular structure allow the finetuning of fibers morphology which, although the oligomers do not bear chiral substituents, may display helical superstructure with predominance of one type of hand-helicity.

4.2 Results and Discussion

▪ A new platform for the Synthesis of Regioregular Sulfur-Overrich Thiophene Octamers

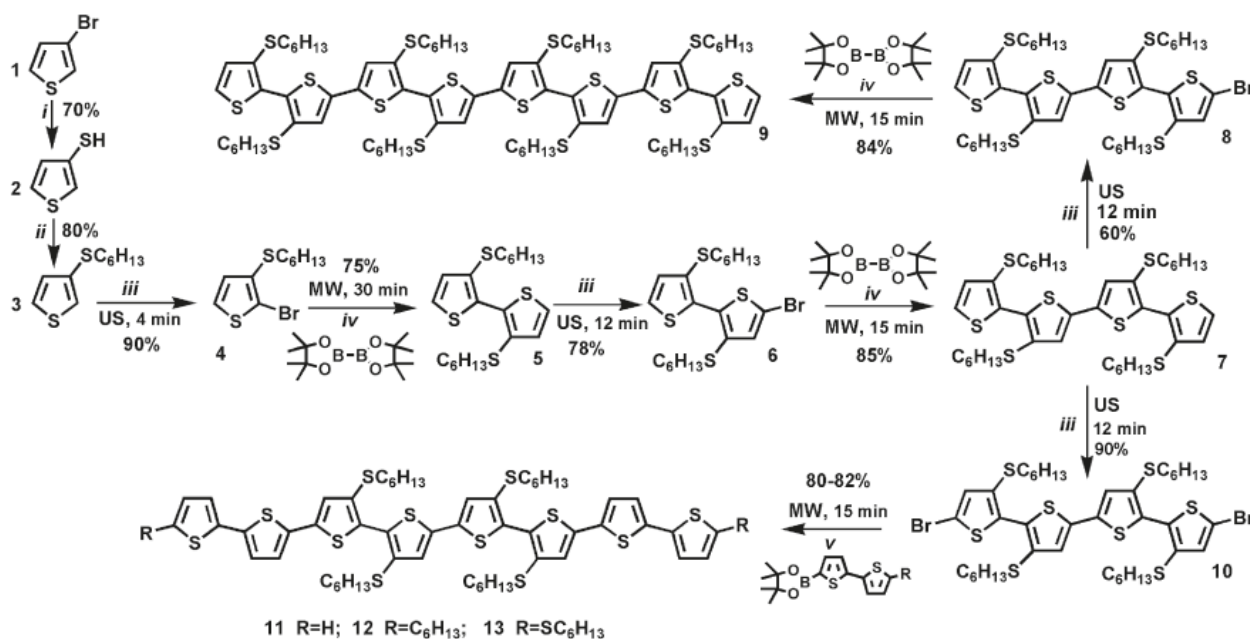
Typically, **OTs** are prepared stepwise by successive *bromination* and *metalation* of intermediates using conventional heating methods for the *palladium catalyzed cross-coupling*.

Here we describe a regiospecific synthesis (**Scheme 12**) based on *Suzuki reaction*^{395,396} enabling the high yield synthesis of sulfur-overrich regioregular thiophene octamers, rapidly prepared making use of *ultrasound* and *microwave irradiation* for the bromination and cross-coupling steps, respectively.

All the octamers are symmetric molecules characterized by an inner core made of two bithiophene subsystems bearing *head-to-head* β -hexylsulphanyl substituents and differing for the type of substitution at both terminal bithiophene subsystems.

Efficient monobromination of *mono-, di-, and quaterthiophenes* was achieved in a few minutes with a single addition of NBS in DMF under ultrasound irradiation, while the formation of the dibromo derivative was negligible.

In the absence of ultrasounds, the monobromination of the same substrates required the slow stepwise addition of NBS in several hours or days leading to sizable amounts of dibromo derivative.



Scheme 12. Ultrasound and microwave assisted synthesis of Sulfur-Overrich Thiophene Octamers starting from commercial 3-Bromo-thiophene; a (i) BuLi, S₈, Et₂O; (ii) (CH₃)₃COK, Hex-Br, EtOH; (iii) NBS (1 or 2 equiv), DMF; (iv) borolane, NaHCO₃, Pd(dppf)Cl₂, THF/H₂O; (v) 2-boropinacolate-2,2'-bithiophene or 2-boropinacolate,5-S-hexyl-2,2'-bithiophene or 2-boropinacolate,5-hexyl-2,2'-bithiophene, NaHCO₃, Pd(dppf)Cl₂, THF/H₂O.

Using commercial 4,4,5,5-tetramethyl-1,3,2-dioxaborolane (**TDB**) in a one pot *borylation-Suzuki* coupling reaction in ethanol/water under microwave irradiation, the doubling of the oligomer skeleton was obtained in high yield and free of byproducts, thus, avoiding long and expensive purifications of the reaction products.

The methodology was successfully extended to the preparation of the regioregular *hexadecamer* and, using the *dibromobithiophene* with **TDB**, also of the corresponding polymers (see Chapter V).

The same methodology was also successfully used for the preparation of *head-to-head* oligomers and polymers bearing *hexyl* instead of *S-hexyl* substituents, such as octamer **6b** (see experimental part).

Thus, the combined use of *ultrasound* and *microwave* irradiation provides a very efficient platform for the rapid, low power, low cost, and environmentally friendly preparation of regioregular *head-to-head* thiophene oligomers and polymers.

▪ **Fibers Formation and Properties**

Of the many newly synthesized sulfur overrich oligothiophenes, octamers **9** and **11-13** displayed the most accentuated tendency to form crystalline aggregates. The octamers achieved the right balance of size, conformation, and shape to self-assemble in ordered fibrillar structures.

The formation of crystalline fibers was induced by dissolving at room temperature the octamers in *toluene*, in which they are very soluble, depositing solution drops on the surface of choice, and exposing it to vapors of *acetonitrile*, in which the octamers are insoluble.

Randomly distributed fibers with high aspect ratio—from 1:1 to 1:2 height versus width and up to hundreds micrometers in length—were spontaneously formed (**Figure 96**, **Figure S7-S8** in experimental part).

The directional molecular self-assembly affording fibers formation was highly reproducible, while drop casting of the octamers without exposition to *acetonitrile* invariably led to the formation of globular aggregates.

The rate of fibers formation varied from minutes to hours, depending on concentration and molecular structure, being slower for **9** than for the other octamers.

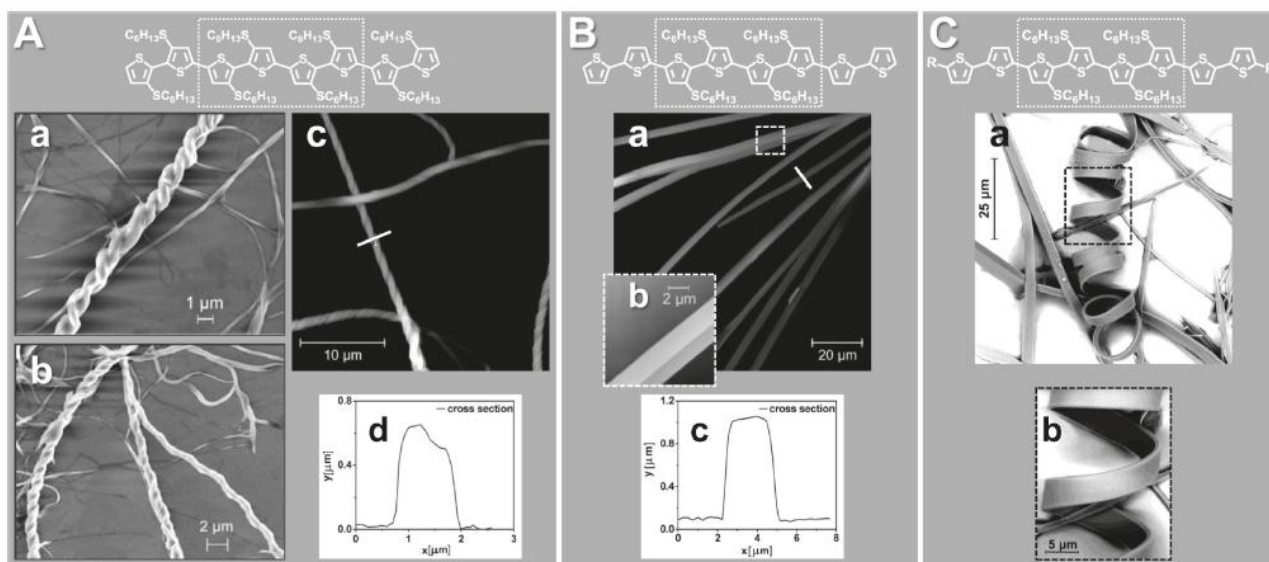


Figure 96. (A) SEM (a and b on SiO₂), AFM (c, on glass) and AFM profile (d) of fibers of **9**; (B) AFM (a, on glass) and AFM profile (b) of fibers of **11**; (C) SEM (a and b on glass) images of fibers of **12**.

Contrary to what is generally observed with thiophene oligomers,^{397,398} the shape and the formation rate of the fibers from **9** and **11-13** were independent of the type of surface employed: *glass, ITO, silicon, and gold* were employed with similar results.

Generally, the aggregates formed on surfaces are the result of a balance between molecule-molecule and molecule-substrate interactions.

Clearly, with octamers **9** and **11-13**, intermolecular interactions are by far more important than molecule-surface interactions and the supramolecular structures that are formed correspond to thermodynamically stable states.

That the presence of the β -sulfurs plays an important role in this process is demonstrated by the fact that octamer **6b** of structure equivalent to **9** but with *hexyl* instead of *S-hexyl* chains (see experimental part) was amorphous in the experimental conditions employed for fibers formation.

Remarkably, secondary helical structure was present in most fibers with the exception of those formed by **11**, the only octamer lacking substituents on terminal bithiophene subsystems. Note that so far a 'secondary structure' has only been assigned to folded **PTs** in solution containing chiral side chains.

Typically, fibers made of **OTs** are rod-like and strong interactions with surfaces are observed affecting film morphology. It is generally assumed that stereocenters in the side chains are required to obtain chirality in oligothiophene fibers.^{399,400}

In our octamers, no chiral substituents are present and the *S-hexyl* groups promote the formation of folded or rod-like fibers depending on molecular structure, independently of the nature of the deposition surface.

Octamer **9**, made of the repetition of four identical bithiophene *head-to-head* substituted subsystems, formed superhelices (helices of helices) and even double helices of superhelices whose periodicity was size independent (**Figure 96**, **Figure S6**).

Bigger fibrils (diameter >1 μm) were formed by several small fibrils wrapped up in themselves to form a multihelical structure, exhibiting a width versus height aspect ratio of 1:1 (**Figure 96**) and length ranging from 100 nm to 5 μm .

On the contrary, octamer **11** formed tapes like fibrils (**Figure 96, Figure S6**) with typical width versus height aspect ratio of 2:1 and length in the same range as **9**, which appeared atomically flat (Rms Roughness < 1 nm) and with typical terraces of crystals.

Finally, octamers **12** and **13**, with α,ω hexyl and *S*-hexyl chains, respectively, formed a complex network of rod-like and folded fibers terminated with astonishing ringlets (**Figure 96, Figure S7-S9**). All fibers exhibited birefringence at optical polarized microscopy regardless of their specific morphology (helices vs tape-like), extinguishing in four positions at intervals of 90° by rotating the polarized light (**Figure S7**).

The reproducibility of morphology on different substrates upon deposition from *toluene* under *acetonitrile* vapors made possible to investigate the fibers with a variety of techniques requiring deposition on *glass, ITO, SiO₂, and gold*.

Below we report a thorough comparative investigation on the electronic, optical, and electrical properties of the helical fibers of **9** with those, rod-like, of **11**.

Circular dichroism (CD) allowed to check the chirality of the films; *cyclic voltammetry (CV)*, the *electrochemical response*; *confocal microscopy* and *space resolved spectroscopy*, the light emission properties; *Tunneling Atomic Force Microscopy* in torsion mode (**Tr-TUNA**) and *conductive Atomic Force Microscopy (C-AFM)*, the charge transport at the nanoscale.

Finally, to test the applicability in devices, the fibers were directly grown on the *SiO₂* surface of a *field-effect transistor* with gold contacts and **FET** charge mobilities were measured.

The helical fibers formed by octamer **9** upon deposition on glass were both left- and right-handed; however, microscopy examinations suggested that one or the other type of hand-helicity was always predominating. **CD** measurements confirmed that the films were chiral and that the sign of chirality was random.

CD plots of two different samples of **9**, deposited on glass, are similar but reversed in sign (**Figure 97**).

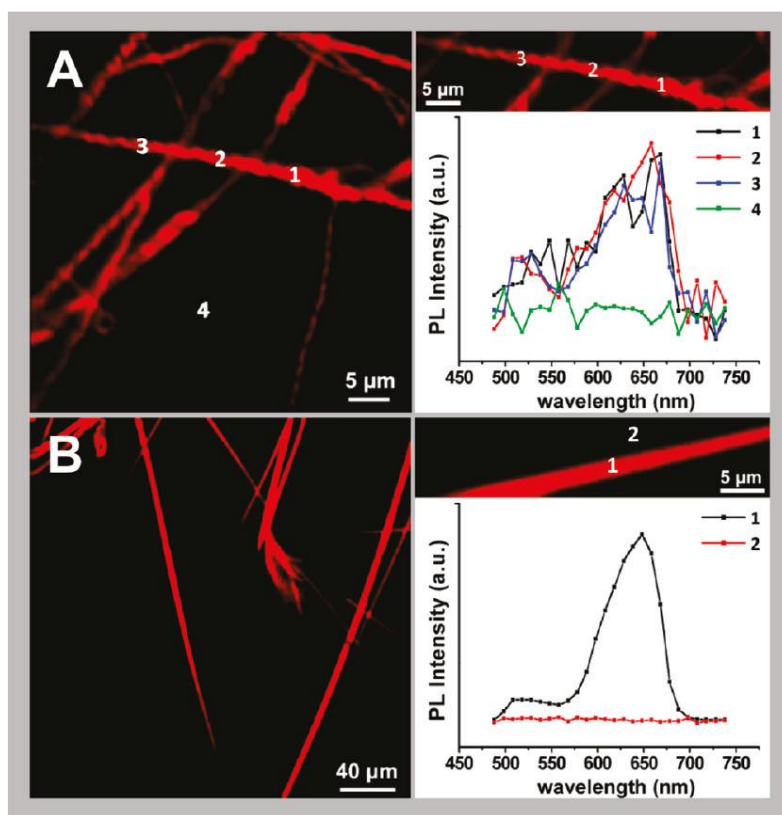


Figure 97. Laser Scanning Confocal Microscopy images and spatially resolved spectral analysis of fibers of **9** (A) and **11** (B) grown on glass.

Considering the thickness of the film (1-2 μm), the signal intensity is rather high. Since octamer **9** has no chiral substituents, no **CD** pattern was detected in solution and the chirality observed in the fibers was a property related to the supramolecular organization in the solid state.

We explain the presence of the **CD** signal and its inversion from one sample to the other by invoking conformational atropisomerism^{401,402} due to restriction of torsional processes about inter-ring C-C bonds in the solid state, which deprives the molecule of all symmetry elements rendering it chiral. Once the first molecule is frozen on the surface in the form of one or the other enantiomer (depending on the ω interring angle, $+\omega$ or $-\omega$ having equal probabilities), the conformation of the following ones is prevalently biased toward the helical sense preferred by that enantiomer causing chirality amplification.^{403,404}

Presumably, the handedness of the major enantiomer also affects the sign of supramolecular helicity (**Figure 98**).

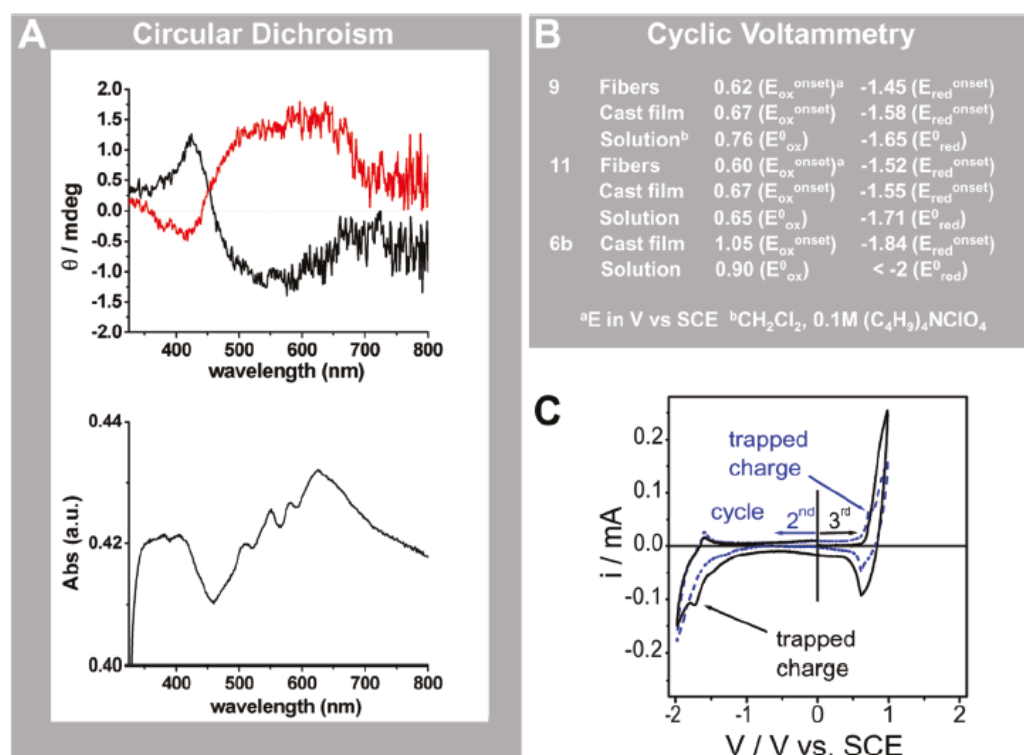


Figure 98. (A) Circular Dichroism and UV spectra of fibers of 9 formed on glass. (B) Onset potentials in PC 0.1M (C₂H₅)₄NBF₄ of films of fibers and cast films (globular aggregates) of 9 and 11 on ITO, together with the redox potentials in CH₂Cl₂, 0.1M (C₄H₉)₄NClO₄. For comparison, the values for 6b (the equivalent of 9 with hexyl instead of S-hexyl substituents) are also reported. (C) Second and third voltammograms of the fibers film of 9 showing charge trapping phenomena.

Solid state electrochemistry on films of **9** and **11** deposited on **ITO** afforded the redox potentials reported as E^{onset} values (**Figure 98**).^{405,406}

For comparison, also the corresponding potentials obtained for films cast from toluene (globular aggregates) and the redox potentials in solution are reported, together with the values for **6b**, the counterpart of **9** with *alkyl* instead of *S-alkyl* chains. The comparison of E^0 values in solution between **9** and **6b** shows the remarkable effect of side chain sulfurs on the oxidation potential, which decreases by 0.14 V, and on the reduction potential, which becomes less negative by more than 0.35 V.

Going from solution to films, an analogous trend was found for both **9** and **11**. Noticeably, the helical fibers displayed the less negative reduction potential, hence the highest electron affinity. Differences in redox potentials were observed for both octamers when the morphology changed from globular aggregates to fibers, in agreement with results from literature indicating that redox potentials depend on morphology.

Interestingly, the oxidation and reduction waves of the fibers film of **9**, after the first conditioning doping, showed prepeaks (**Figure 98**) indicating charge trapping phenomena similar to those observed in some **PTs** and related to the delayed release of the charge stored during the doping process.⁴⁰⁷

All fibers were intensely fluorescent red (**Figure S7-S9**).

The images, with spatial resolution of 500 nm in x-y, reveal the helical morphology of the fibers of **9** and the rod-like arrangement of the fibers of **11**. The **LSCM** images of **9** (**Figure 97**) show spatial modulation of fluorescence along the fibers long axis.

The space resolved spectra show that there is no fluorescence emission from the background and that the maximum emission wavelength of the fibers, around 650 nm for both octamers, is nearly 100 nm red-shifted with respect to the values in solution (**Figure S6**).

The intense fluorescence observed for all fibers, including those from **12** and **13**, plaids in favor of the formation of *J*-type (side-by-side) rather than *H*-type (face-to-face) aggregates. To confirm this point, detailed photophysical studies would be required which are beyond the aim of the present study.

Nevertheless, the similar trend in fluorescence for all fibers suggests that their intimate molecular organization must be very similar despite differences in morphology.

Fibers of **9** and **11** grown on **ITO** were analyzed by **Tr-TUNA**, a new scanning probe technique examining simultaneously surface topography and local current and providing information on nanoscale conductivity within specific domains.⁴⁰⁸

Tr-TUNA images of fibers up to 100 μm long and with an average diameter of approximately 300 nm are reported (**Figure 99**). **Tr-TUNA** current mapping shows a direct correlation with the topography revealing defined conductive domains associated to the fibers.

The variations in conductivity observed for **9** are in agreement with differences in molecules stacking within the nanodomains due to helicity, while the large, homogeneous domains associated to the fibers of **11** are in agreement with a more uniform stacking of the molecules due to the rod-like arrangement.

It is worth noting (**Figure 99**) the wide islands with conductivity lower than that of the fibers have topographic correspondence in amorphous aggregates and impurities whose medium height ranges between 4 and 50 nm, much lower than the average height (300 nm) of the fibers.

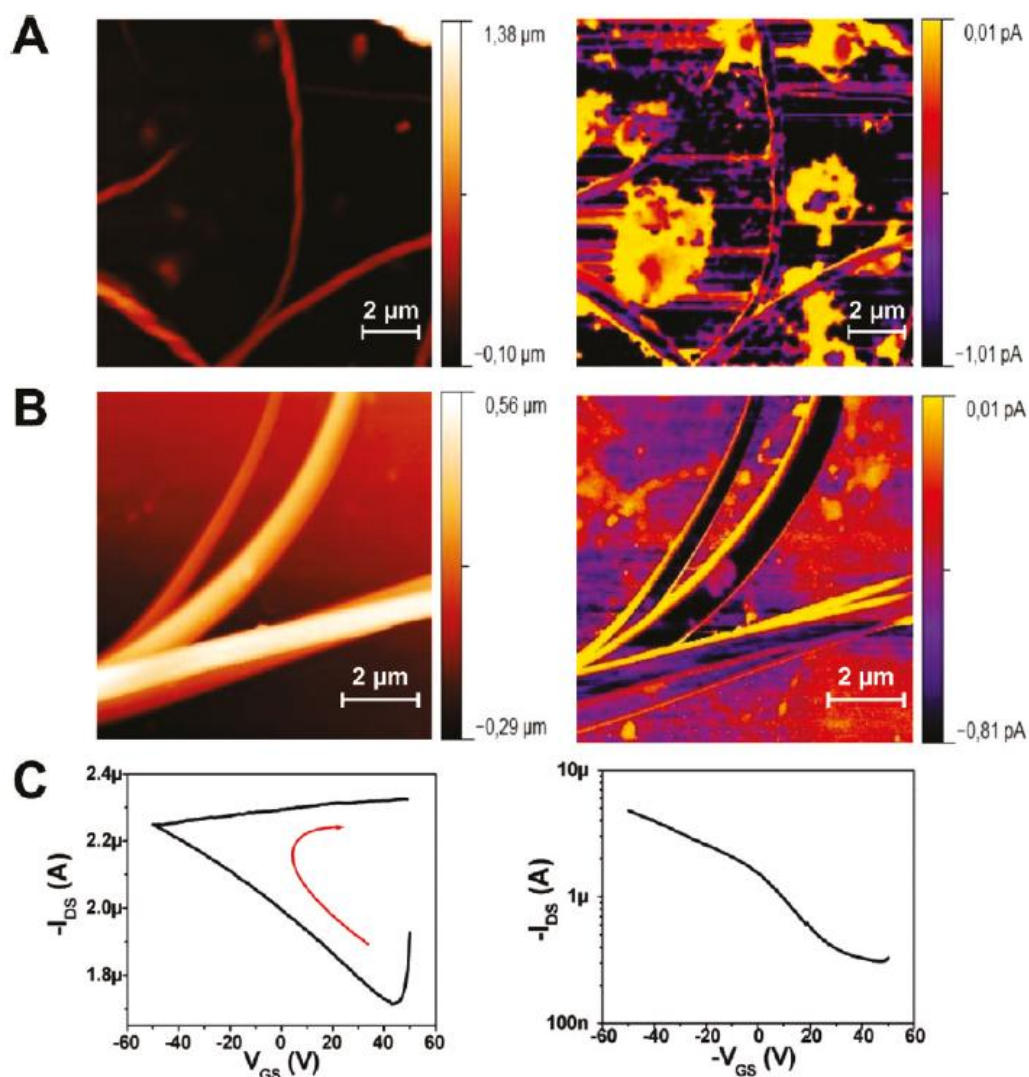


Figure 99. (A) Topography image (left) and hole transportation measurement (right) of helical fibers of 9 grown on ITO obtained using Tr-TUNA with a +5V bias on the tip. (B) The same as panel A for rod-like fibers of 11. (C) Transfer characteristics in saturation regime in air for bottom contact field effect transistors with the active layers made of helical fibers of 9 (left) and rod-like fibers of 11 (right) directly grown on the device. The red arrow indicates the clockwise hysteresis observed on the passage from the on state to the off state, indicating an intrinsic 'memory effect' of fibers of 9.

The islands are visible in topographic images only cutting the upper limit of the height scale suitable to make visible the topographic features of the fibers (**Figure S12-S13**).

The charge (hole) mobility at the nanoscale of the fibers of **9** and **11** was obtained by measuring the charge transport through fibers section by **C-AFM**. The plots current density versus square voltage in a double logarithmic representation are reported (**Figure S14**). The plots showed that **9** and **11** were characterized by different charge mobility values, μ_{holes} , of 9.8×10^{-7} and 5×10^{-6} $\text{cm}^2/\text{V} \cdot \text{s}$, respectively, in agreement with **Tr-TUNA** maps.

Finally, since fibers morphology is independent of the substrate employed, fibers of **9** and **11** were directly grown on the SiO_2 substrate of a **FET** to measure the charge mobility along the fibers in the presence of an electric field.

A standard two probe technique was employed to measure the drain-source current (I_{DS}), versus gate voltage (V_{GS}) for **FET** devices in bottom configuration (experimental part for details).

Typical transfer characteristics in saturation regime, recorded in air, are reported (**Figure 99**). Considering that, owing to the fibrillar morphology, the test patterns were effectively covered for no more than 50% of their nominal surface, μ_{holes} for **9** and **11** were 1×10^{-5} and 4×10^{-4} $\text{cm}^2 \text{V}^{-1} \text{s}^{-1}$, respectively, 2 orders of magnitude higher than the intrinsic mobility measured through a single fiber in the absence of external field, and in the typical range of conductive polymers.⁴⁰⁹

Note that **FET** charge mobility could be significantly improved by assembling the randomly oriented fibers into oriented functional arrays by template-directed growth.

The **FET** based on fibers of **9** shows a peculiar feature of the material represented by the intrinsic "memory effect",⁴¹⁰ observed without recurring to polarizable gate dielectrics.⁴¹¹

The 'memory effect' (**Figure 99**, **Figure S11**) is deduced from the clockwise hysteresis in drain-source current (red arrow), indicating that the device retains the on state in backward gate voltage sweep, corresponding to the passage from the on to the off state. Such an effect, modulated by the gate voltage, is more pronounced in air than in vacuum and is probably related to doping from oxygen, in agreement with **CV** data.

Remarkably, **FETs** based on cast films of **9** and **11** did not show any charge carrier modulation, despite the highly ordered molecular organization displayed by thin film X-ray diffraction (not reported), confirming that charge transport is strongly morphology dependent.

The consistency of the many characterization data reported above allowed us to elaborate a comprehensive model for fibers packing, as described below.

▪ **X-Ray Diffraction and Fibers Packing**

All X-ray profiles of fibers films (**Figure 100**) are dominated by the small angle reflection, other reflections being absent or of very low intensity. The distances indicated by the small angle reflection grow from 1.64 nm for **11**, without substituents on the terminal bithiophene subsystems, to 2.13 nm for **13**, having the longest terminal substituents. On the basis of these data, our hypothesis is that all octamers have a linear backbone with nearly flat conformation and, since the fibers are intensely fluorescent, the supramolecular organization is of the *J-stacking* type.

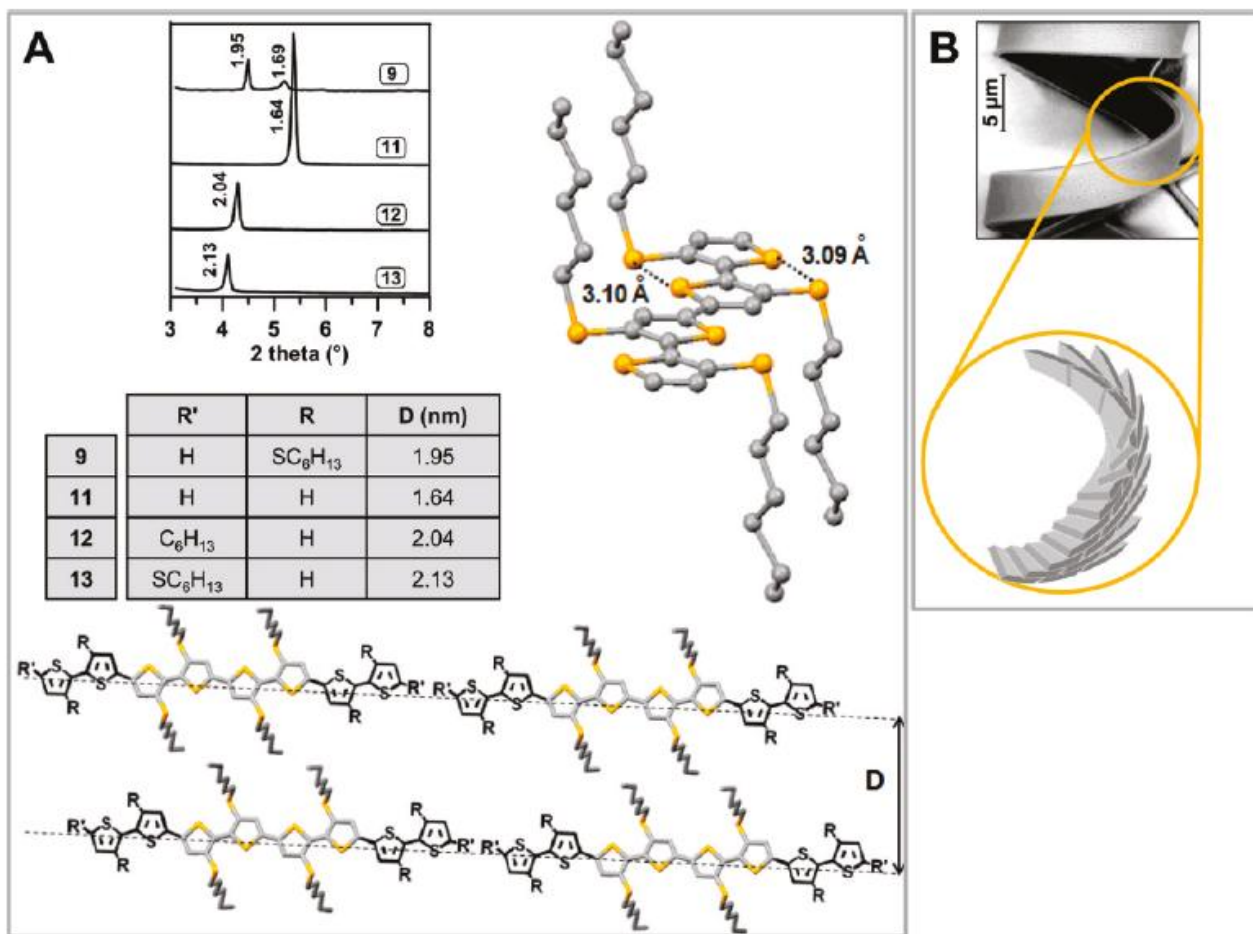


Figure 100. (A) X-ray diffraction pattern of the fibers grown on glass; periodic distances reported in nm; conformation of the inner tetrameric core of the octamers as determined by single crystal X-ray analysis of 11 and model of J-type stacking. (B) A detail of the film from 12 and proposed model for the supramolecular packing.

The β -thioalkyl substitution imposes anti orientation of the thiophene rings of the inner core to reduce steric hindrance and there is a parallel order of the π -conjugated cores, with the alkyl side chains extending almost perpendicularly to the thiophene backbone (**Figure 100**).

In the molecular packing, the *J*-stacked molecules should be parallel to one another in columns at the distance obtained from the X-ray analysis (**Figure 100**).

We anticipate that these hypotheses are nicely confirmed by single crystal X-ray analysis of **11**, also showing that the crystalline form of this compound is the same as in powders and fibers.

The geometry of the tetrameric inner core obtained from single crystal X-ray analysis of **11** is reported (**Figure 100**). The geometry is planar with the sulfur atoms on the same plane and S-S intermolecular distances largely below the sum of Van der Waals radii (3.60 Å).

The presence of substituents in the outermost rings induces disorder effects and distortions at the end points of the molecules that influence the distance between parallel octathiophene rows, making it vary with molecular structure.

Thus, we can describe the supramolecular assembly as lamella-type structure in which the small distortions of the molecular apexes cause a slight disruption of the compact packing of the molecules simply by means of a slightly twist of long molecular axes in the short-range.

The morphology is influenced by the packing order of the molecules and in the long-range ordered helices and curls appear as macroscopic effects of stacking faults during the growth (**Figure 100**).

4.3 Conclusions

In summary, we discovered a new recognition algorithm—Lenh's expression indicating the molecular features driving self-assembly via noncovalent interactions⁴¹²—that causes the spontaneous self-assembly of octathiophenes into nano- and micrometer sized multifunctional fibers on surfaces.

The new recognition algorithm resulted from the combination of thioalkyl substituents and head-to-head regiochemistry of substitution, inducing aggregation of sulfur-overrich octathiophenes mainly via S-S noncovalent interactions. It led to the formation of crystalline superhelices (helices of helices), electroactive and fluorescent, in which one type of hand-helicity was always predominating despite of the absence of chiral substituents in the molecular skeleton.

Contrary to what has been observed so far, fibers morphology was univocally determined by the molecular structure and reproducibly generated on various types of surfaces. Fibers directly grown on the SiO₂ substrate of a field effect transistor displayed efficient charge conduction, indicating their usefulness for application in organic devices.

Taking advantage of X-ray diffraction data, we elaborated a comprehensive model accounting for all the observed properties and interpreting the chirality features on the basis of the interplay of molecular atropisomerism and supramolecular helicity induced by terminal substituents.

Finally, we developed, on one side, a new platform for the rapid and high yield synthesis of the materials in aqueous solvents making use of *ultrasound* and *microwave* irradiation and,

on the other, a new method for fiber formation based on the action of a solvent and a non-solvent to favor crystallization.

For all these aspects, our work represents an important progress in programming and engineering organic functional materials. Because of their crystallinity, charge transport, and fluorescence and due to the control of morphology, hence, of the functional properties, the fibers described here are suited for application in molecular based devices for organic electronics, sensing and mostly photovoltaics.

4.4 Experimental Part

4.4.1 General

▪ *Synthesis*

Unless otherwise noted, all operations were carried out under a dry, oxygen-free nitrogen atmosphere. Organic solvents were dried by standard procedures. TLC was carried out with 0.2-mm thick of silica gel 60 F₂₅₄ (Merck). Visualization was accomplished by UV light or phosphomolybdic acid solution.

Preparative column chromatographies was performed on glass columns of different sizes hand packed with silica gel 60 (particle sizes 0.040-0.063 mm, Merck). Petroleum ether refers to the fraction of bp 40-70°C. 2-thienylboronic acid, 2,2'-bithiophene-5-boronic acid pinacol ester, 5'-hexyl-2,2'-bithiophene-5-boronic acid pinacol ester, 3-hexylthiophene, N-bromosuccinimide, sodium bicarbonate, potassium tert-butoxide, 1-bromohexane 98% were purchased from Sigma-Aldrich Co; 1,1'-bis(diphenylphosphino)ferrocene palladium (II)chloride

dichloromethane complex (PdCl₂dppf), *n*-butyllithium 2.5 M solution in hexane, potassium fluoride were obtained from Acros Organics; sulfur sublimed washed winnowed 99.5% from Carlo Erba; 2-isopropoxy-4,4,5,5-tetramethy-1,3,2-dioxaborolane, Bis(pinacolato)diboron from Alfa Aesar GmbH & Co KG. All reagents and solvents were used as received.

Microwave experiments were carried out in a Milestone Microsynth Labstation operating at 2450 MHz monitored by a proprietary control unit. The oven was equipped with magnetic stirring, pressure and temperature sensors. Reactions were performed in a glass vessel (capacity 10 mL) sealed with a septum. The microwave method was power controlled (100 W maximum power input) and the samples were irradiated with the required power output (setting at the maximum power) to achieve the desired temperature (80°C).

Reactions with ultrasound were performed in a FALC LBS1 50KHz Ultrasonic bath at room temperature. Melting points were determined on Kofler bank apparatus and are uncorrected.

All ¹H-NMR and ¹³C-NMR spectra were recorded on a Varian Mercury-400 spectrometer equipped with a 5-mm probe. Chemical shifts were calibrated using the internal CDCl₃ or benzene-*d*₆ resonance which were referenced to TMS.

Mass spectra were collected on a Finnigan Mat GCQ spectrometer. UV-Vis spectra were recorded using a Perkin Elmer Lambda 20 spectrometer.

Photoluminescence spectra were collected on a Perkin Elmer LS50 spectrofluorometer. Fluorescence measurements were performed using an excitation wavelength corresponding to the maximum absorption lambda.

▪ **Characterization**

Atomic force microscopy

AFM images were taken using a Solver Pro, NT-MDT instrument working in semicontact mode.

Scanning electron microscopy

SEM images of **9** and **11** were obtained with a ZEISS 1530 instrument, those of **12** and **13** were acquired on a desktop Phenom microscope directly on film samples.

Circular Dichroism

CD spectra were recorded using a spectropolarimeter JASCO J-715 under ambient conditions.

X-ray diffraction analysis

Was carried out by means of a PANalytical X'Pert diffractometer equipped with a copper anode ($\lambda_{\text{mean}}=0.15418$ nm) and a fast X'Celerator detector. Films grown on glass cover slips were directly investigated.

Electrochemistry

Oligomer films on ITO electrodes (Balzers) were obtained by drop casting from toluene in air or in acetonitrile saturated air. The films were characterized in PC $0.1 \text{ mol}\cdot\text{L}^{-1}$ $(\text{C}_2\text{H}_5)_4\text{NBF}_4$ purged by Ar bubbling, where they are insoluble (SI for more details).

Confocal Characterizations

The laser scanning confocal microscopy (LSCM) and the spatially resolved photoluminescence (PL) spectra of **9** and **11** samples were collected by a confocal microscope (Fluo-View1000, Olympus) with a spatial resolution of about 200 nm in x-y and 100 nm in z. The excitation source was a Laser Diode at 405 nm (FV5-LD505-2, Olympus) coupled with a 405/488 nm dichroic mirror. The acquisitions were performed with a 60X objective. The optical images were obtained with a charge-coupled device (CCD) color camera coupled to the confocal microscope. Spatially-resolved PL spectra were collected with a wavelength resolution of 2 nm and a spatial resolution of 200 nm.

Tr-TUNA

Tr-TUNA images were obtained with a Veeco Multimode, Nanoscope V Controller microscope equipped with Tr-Tuna module, current amplifier sensitivity 1 pA/V and scanning conductive torsion mode.

4.4.2 Materials

3-Mercapto-thiophene (2)

A solution of 3-bromothiophene (25 mmol, 2.34 mL) in anhydrous diethyl ether (25 mL) was added at -70°C to a 2.5 M solution of *n*-butyllithium in hexane (25 mmol, 10 mL) under a nitrogen atmosphere and the mixture was stirred for 2.5 h at -70°C. To the solution was added sublimed sulfur (25 mmol, 0.804 g) and stirred at -70°C for 2 h before quenching with 100 mL of water.

The resulting mixture was extracted with (3x25 mL) NaOH 1 M. The combined aqueous layers were cooled with ice and acidified with 10% hydrochloric acid to liberate the thiol from its sodium salt. The product was extracted with diethyl ether (3x50 mL). The organic layers were dried over anhydrous sodium sulphate and the solvent was removed under reduced pressure. Yield 86%. Clear yellow oil; EI-MS m/z 116(M⁺); ¹H NMR (400 MHz, CDCl₃, TMS/ppm): δ 7.31 (dd, ³J=5.2 Hz, ⁴J=3.2 Hz, 1H), 7.19-7.17 (m, 1H), 6.99 (dd, ³J=5.2 Hz, ⁴J=1.6 Hz, 1H), 3.39 (s, 1H).

3-(Hexsulphanyl)thiophene (3)

A solution of potassium tert-butoxide (30 mmol, 6.7 g) in anhydrous ethanol (20 mL), was added at 0°C to 3-mercaptothiophene (21 mmol, 2.4 g) under a nitrogen atmosphere and mixture was stirred for 30 min at 0°C. To the solution was slowly added 1-bromohexane (21 mmol, 2.9 mL) and refluxed for 2 h before quenching with 100 mL of water. The product was extracted with diethyl ether (3x30 mL). The combined organic layers were dried over anhydrous sodium sulphate and the solvent was removed under reduced pressure. The residue was isolated by flash chromatography (100% cyclohexane) to give 3.8 g of product. Yield 90%. Colorless oil; EI-MS m/z 200(M⁺); ¹H NMR (400 MHz, CDCl₃, TMS/ppm): δ 7.31 (dd, ³J=4.8 Hz, ⁴J=3.2 Hz, 1H), 7.11 (dd, ⁴J=3.2 Hz, ⁴J=1.2 Hz, 1H), 7.02 (dd, ³J=4.8 Hz, ⁴J=1.2 Hz, 1H), 2.84 (t, 2H), 1.66-1.57 (m, 2H), 1.42-1.39 (m, 2H), 1.31-1.27 (m, 4H), 0.88 (t, 3H); ¹³C NMR (400 MHz, CDCl₃): δ 132.3, 129.6, 126.0, 122.8, 35.3, 31.3, 29.3, 28.4, 22.5, 14.0.

General procedure for the synthesis of bromothieryl-derivatives 4, 6, 8 and 10

To a solution of 3, 5, 7, 9 (1 mmol) in DMF, 1 mmol or 2 mmol of NBS were added. The reaction mixture was sonicated for 12 min at room temperature. The solvent was removed and the products were purified by flash chromatography.

2-Bromo-3-(hexylsulphanyl) thiophene (4)

Yield 90%. Clear yellow oil; EI-MS m/z 278(M⁺); ¹H NMR (400 MHz, CDCl₃, TMS/ppm): δ 7.25 (d, ³J=5.2 Hz, 1H), 6.92 (d, ³J=5.2 Hz, 1H), 2.84 (t, 2H), 1.60-1.54 (m, 2H), 1.40-1.37 (m, 2H), 1.30-1.25 (m, 4H), 0.88 (t, 3H); ¹³C NMR (400 MHz, CDCl₃): d 133.1, 130.1, 125.8, 113.6, 35.1, 31.3, 29.5, 28.3, 22.5, 14.0.

5-Bromo-3,3'-bis(hexylsulphanyl)-2,2'-bithiophene (6)

Yield 78%. Yellow oil; ¹H NMR (400 MHz, CDCl₃, TMS/ppm): δ 7.36 (d, ³J=5.2 Hz, 1H), 7.06 (d, ³J=5.2 Hz, 1H), 7.03 (s, 1H), 2.78 (q, J=7.2 Hz, 4H), 1.58-1.50 (m, 4H), 1.34-1.22 (m, 12H), 0.88-0.84 (m, 6H); ¹³C NMR (400 MHz, CDCl₃): d 134.0, 132.8, 132.35, 132.32, 131.6, 130.7, 126.2, 112.7, 36.1, 31.34, 31.31, 29.5, 29.4, 28.4, 28.3, 22.54, 22.52, 14.0.

5-Bromo-3,3',3''',4''-tetrakis(hexylsulphanyl)-quaterthiophene (8)

Yield 60%. Yellow oil; ¹H NMR (400 MHz, C₆D₆): δ 7.21 (s, 1H), 7.15 (s, 1H), 6.853 (d, ³J=5.2 Hz, 1H), 6.847 (s, 1H), 6.81 (d, ³J=5.2 Hz, 1H), 2.61-2.44 (m, 8H), 1.43-1.31 (m, 8H), 1.16-0.99 (m, 24H), 0.81-0.76 (m, 12H); ¹³C NMR (400 MHz, C₆D₆): d 136.9, 136.5, 134.6, 133.9, 133.8, 133.4, 133.1, 133.0, 132.83, 132.79, 132.0,

131.2, 126.4, 113.5, 36.5, 36.4, 36.36, 36.25, 31.7, 31.68, 31.64, 31.62, 29.9, 29.8, 29.75, 29.72, 28.7, 28.65, 28.63, 22.94, 22.93, 22.92, 14.3.

5,5'''-Dibromo-3,3',3''',4''-tetrakis(hexylsulphanyl)-quaterthiophene (10)

Yield 90%. Orange oil; ^1H NMR (400 MHz, C_6D_6): δ 7.15 (s, 2H), 6.85 (s, 2H), 2.52–2.44 (m, 8H), 1.40–1.31 (m, 8H), 1.15–1.06 (m, 16H), 1.04–0.97 (m, 8H), 0.81–0.76 (m, 12H); ^{13}C NMR (400 MHz, C_6D_6): δ 136.6, 134.5, 133.8, 133.4, 133.2, 132.3, 113.6, 36.5, 36.4, 31.64, 31.62, 29.8, 29.7, 28.6, 22.9, 14.27, 14.26.

General procedure for the synthesis of 5, 7 and 9

A mixture of the bromothiophenyl-derivative **4**, **6**, **8** (1 mmol), bis(pinacolato)diboron (0.6 mmol), PdCl_2dppf (0.05 mmol), NaHCO_3 (2 mmol) in THF/water 2:1 (3 mL) was irradiated with microwaves at 80°C for 30, 15, 15 min respectively. The reaction mixture was brought to room temperature and the solvent was evaporated under reduced pressure. All compounds were purified by flash chromatography with increasing amounts of CH_2Cl_2 in cyclohexane as eluent.

3,3'-Bis(hexylsulphanyl)-2,2'-bithiophene (5)

Yield 75%. Yellow oil; EI-MS m/z 398 (M⁺); TLC (cyclohexane: CH_2Cl_2 , 80:20 v/v): R_f = 0.52; ^1H NMR (400 MHz, CDCl_3 , TMS/ppm): δ 7.36 (d, $^3J=5.2$ Hz, 2H), 7.08 (d, $^3J=5.2$ Hz, 2H), 2.77 (t, 4H), 1.57–1.49 (m, 4H), 1.36–1.20 (m, 12H), 0.86 (t, 6H); ^{13}C NMR (400 MHz, CDCl_3): δ 132.3, 132.1, 130.6, 125.9, 35.9, 31.3,

29.5, 28.4, 22.5, 14.0; UV/Vis: λ_{\max} 275 nm (ϵ 7396 $\text{cm}^{-1}\text{M}^{-1}$), λ_{em} 378 nm in CH_2Cl_2 .

3,3',3''',4''-Tetrakis(hexylsulphanyl)-quaterthiophene (7)

Yield 85%. Orange oil; TLC (cyclohexane: CH_2Cl_2 , 80:20 v/v): Rf = 0.40; ^1H NMR (400 MHz, CDCl_3 , TMS/ppm): δ 7.37 (d, $^3J=5.2$ Hz, 2H), 7.17 (s, 2H), 7.09 (d, $^3J=5.2$ Hz, 2H), 2.82 (t, 8H), 1.59-1.55 (m, 8H), 1.37-1.22 (m, 24H), 0.88-0.84 (m, 12H); ^{13}C NMR (400 MHz, CDCl_3): d 136.2, 132.7, 132.1, 131.8, 130.7, 127.1, 126.0, 36.1, 36.0, 31.34, 31.31, 29.49, 29.44, 28.4, 28.3, 22.51, 22.50, 14.0; UV/Vis: λ_{\max} 384 nm (ϵ 14838 $\text{cm}^{-1}\text{M}^{-1}$), λ_{em} 501 nm in CH_2Cl_2 .

**3,3',3''',3''''',3''''''',3''''''''',4'',4''''',4''''''''-
Octakis(hexylsulphanyl)-octithiophene (9)**

Yield 84%. Red powder, mp 57-59°C; TLC (cyclohexane: CH_2Cl_2 , 80:20 v/v): Rf = 0.27; ^1H NMR (400 MHz, C_6D_6): δ 7.254 (s, 2H), 7.251 (s, 2H), 7.21 (s, 2H), 6.86 (d, $^3J=5.2$ Hz, 2H), 6.82 (d, $^3J=5.2$ Hz, 2H), 2.62-2.55 (m, 16H), 1.46-1.40 (m, 16H), 1.19-1.10 (m, 32H), 1.07-1.00 (m, 16H), 0.82-0.77 (m, 24H); ^{13}C NMR (400 MHz, C_6D_6): d 136.8, 136.69, 136.68, 133.9, 133.7, 133.0, 132.9, 132.8, 132.7, 132.6, 131.3, 126.3, 36.58, 36.56, 36.4, 36.3, 31.70, 31.69, 29.9, 29.8, 28.71, 28.68, 23.0, 22.9, 14.31, 14.29; UV/Vis: λ_{\max} 435 nm (ϵ 39926 $\text{cm}^{-1}\text{M}^{-1}$), λ_{em} 560 nm in CH_2Cl_2 .

General procedure for the synthesis of 11, 12 and 13.

A mixture of the thienylboronic ester (3 mmol), **10** (1 mmol), PdCl₂dppf (0.05 mmol) and NaHCO₃ (2 mmol) in THF/water 2:1 (3 mL) was irradiated with microwaves at 80°C for 15 min. The reaction mixture was brought to room temperature and the solvent was evaporated under reduced pressure. The octamers (**11**, **12**, **13**) were isolated by flash chromatography with increasing amounts of CH₂Cl₂ in cyclohexane as eluent.

3''',3''''',4'',4''''-Tetrakis(hexylsulphanyl)-octithiophene (11)

Yield 82%. Dark-red powder, mp 111-112°C; TLC (cyclohexane:CH₂Cl₂, 85:15 v/v): R_f = 0.36; ¹H NMR (400 MHz, C₆D₆): δ 7.28 (s, 2H), 7.18 (s, 2H), 6.92 (dd, ³J=3.6 Hz, ⁴J=1.2 Hz, 2H), 6.81 (d, ³J=4 Hz, 2H), 6.77 (d, ³J=4 Hz, 2H), 6.66 (dd, ³J=5.2 Hz, ⁴J=1.2 Hz, 2H), 6.59 (dd, ³J=5.2 Hz, ³J=3.6 Hz, 2H), 2.64 (q, J=7.2 Hz, 8H), 1.49-1.45 (m, 8H), 1.20-1.12 (m, 16H), 1.08-1.03 (m, 8H), 0.82-0.77 (m, 12H); ¹³C NMR (400 MHz, C₆D₆): δ 137.4, 137.3, 136.7, 135.6, 133.61, 133.58, 132.8, 132.1, 127.6, 125.3, 124.88, 124.87, 124.3, 36.6, 36.58, 31.7, 31.69, 29.9, 29.8, 28.74, 28.72, 23.0, 22.96, 14.3, 14.28; UV/Vis: λ_{max} 433 nm (ε 47713 cm⁻¹M⁻¹), λ_{em}. 564 nm in CH₂Cl₂.

5,5''''''-Dihexyl-3''',3''''',4'',4''''-tetrakis(hexylsulphanyl)-octithiophene (12)

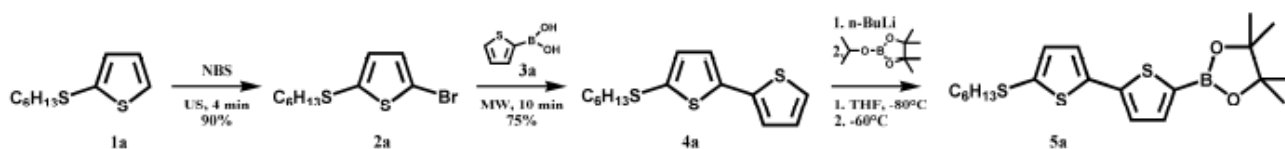
Yield 80%. Purple-red powder, mp 95-97°C; TLC (cyclohexane:CH₂Cl₂, 85:15 v/v): R_f = 0.48; ¹H NMR (400 MHz, C₆D₆): δ 7.28 (s, 2H), 7.19 (s, 2H), 6.88 (d, ³J=3.6 Hz, 2H), 6.84 (d, ³J=3.6 Hz, 2H), 6.81 (d, ³J=3.6 Hz, 2H), 6.65 (d, ³J=3.6 Hz, 2H),

2.64 (q, $J=7.2$ Hz, 8H), 2.51 (t, 4H), 1.50–1.45 (m, 12H), 1.20–1.03 (m, 36H), 0.85–0.78 (m, 18H); ^{13}C NMR (400 MHz, C_6D_6): d 145.9, 138.1, 137.6, 136.6, 135.0, 134.96, 133.55, 133.53, 132.9, 131.9, 127.5, 125.4, 125.35, 124.2, 124.1, 36.6, 36.58, 31.9, 31.89, 31.71, 31.70, 30.4, 29.9, 29.8, 29.0, 28.75, 28.73, 23.0, 14.32, 14.31, 14.29; UV/Vis: λ_{max} 433 nm, λ_{em} 570 nm in CH_2Cl_2 .

3''',3''''',4'',4''''',5,5''''''''-Hexakis(hexylsulphanyl)-octithiophene (13)

Yield 80%. Purple-red powder, mp 85–87°C; TLC (cyclohexane: CH_2Cl_2 , 85:15 v/v): R_f = 0.38; ^1H NMR (400 MHz, C_6D_6): δ 7.28 (s, 2H), 7.18 (s, 2H), 6.83 (d, $^3J=3.6$ Hz, 2H), 6.78 (d, $^3J=3.6$ Hz, 2H), 6.75 (d, $^3J=3.6$ Hz, 2H), 6.72 (d, $^3J=3.6$ Hz, 2H), 2.64 (q, $J=6.8$ Hz, 8H), 2.56 (t, 4H), 1.49–1.44 (m, 12H), 1.21–1.12 (m, 24H), 1.08–1.03 (m, 12H), 0.82–0.77 (m, 18H); ^{13}C NMR (400 MHz, C_6D_6): d 140.1, 137.1, 136.8, 136.5, 135.6, 135.4, 134.2, 133.5, 133.4, 132.6, 132.1, 125.2, 124.8, 124.2, 38.9, 36.44, 36.42, 31.53, 31.51, 31.47, 29.7, 29.6, 28.6, 28.5, 28.3, 22.8, 22.7, 14.11, 14.10, 14.06; UV/Vis: λ_{max} 434 nm, λ_{em} 560 nm in CH_2Cl_2 .

Synthesis of 4,4,5,5-Tetramethyl-2-(5'-hexylthio-2,2'-bithiophen-5-yl)-1,3,2-dioxaborolane (17)



2-(Hexylsulphanyl)thiophene (1a)

Prepared following the same procedure described for **2** and **3**. Yield 90%. Colorless oil; EI-MS m/z 200(M⁺); ¹H NMR (400 MHz, CDCl₃, TMS/ppm): δ 7.32 (dd, ³J=5.2 Hz, ⁴J=1.2 Hz, 1H), 7.10 (d, ³J=3.6 Hz, ⁴J=1.2 Hz, 1H), 6.97 (dd, ³J=5.2 Hz, ³J=3.6 Hz, 1H), 2.79 (t, 2H), 1.65-1.58 (m, 2H), 1.41-1.38 (m, 2H), 1.31-1.26 (m, 4H), 0.89 (t, 3H); ¹³C NMR (400 MHz, CDCl₃): d 135.0, 133.1, 128.7, 127.3, 38.9, 31.3, 29.3, 28.0, 22.5, 14.0.

2-Bromo-5-(hexylsulphanyl)thiophene (2a)

Prepared following the same procedure described for **4**, **6**, **8**, **10**. Yield 95%. Clear yellow oil; EI-MS m/z 278(M⁺); ¹H NMR (400 MHz, CDCl₃, TMS/ppm): δ 6.92 (d, ³J=3.6 Hz, 1H), 6.88 (d, ³J=3.6 Hz, 1H), 2.75 (t, 2H), 1.61-1.56 (m, 2H), 1.40-1.26 (m, 6H), 0.88 (t, 3H); ¹³C NMR (400 MHz, CDCl₃): d 136.3, 134.1, 130.4, 113.8, 39.1, 31.3, 29.3, 28.0, 22.5, 14.0.

5-(Hexylsulphanyl)-2,2'-bithiophene (4a)

A mixture of **2a** (1 mmol), 2-thienylboronic acid (**3a**) (3 mmol), PdCl₂dppf (0.05 mmol), KF (4 mmol) in CH₃CN/water 9:1 (3 mL) was irradiated with microwaves at 85°C for 10 min. The reaction mixture was brought to room temperature and the solvent was evaporated under reduced pressure. The title compound was isolated by flash chromatography on silica gel in cyclohexane as eluent. Yield 75%. Yellow oil; EI-MS m/z 282(M⁺); ¹H NMR (400 MHz, CDCl₃, TMS/ppm): δ 7.21 (dd, ³J=5.2 Hz, ⁴J=1.2 Hz, 1H), 7.14 (dd, ³J=4 Hz, ⁴J=1.2 Hz, 1H), 7.02-7.00 (m, 3H), 2.81 (t, 2H), 1.67-1.60 (m, 2H), 1.43-1.37 (m, 2H), 1.31-1.26 (m, 4H), 0.88 (m, 3H); ¹³C NMR (400

MHz, CDCl₃): δ 140.4, 137.0, 134.1, 133.9, 127.7, 124.5, 123.70, 123.69, 38.9, 31.3, 29.4, 28.1, 22.5, 14.0.

4,4,5,5-Tetramethyl-2-(5'-hexylthio-2,2'-bithiophen-5-yl)-1,3,2-dioxaborolane (5a)

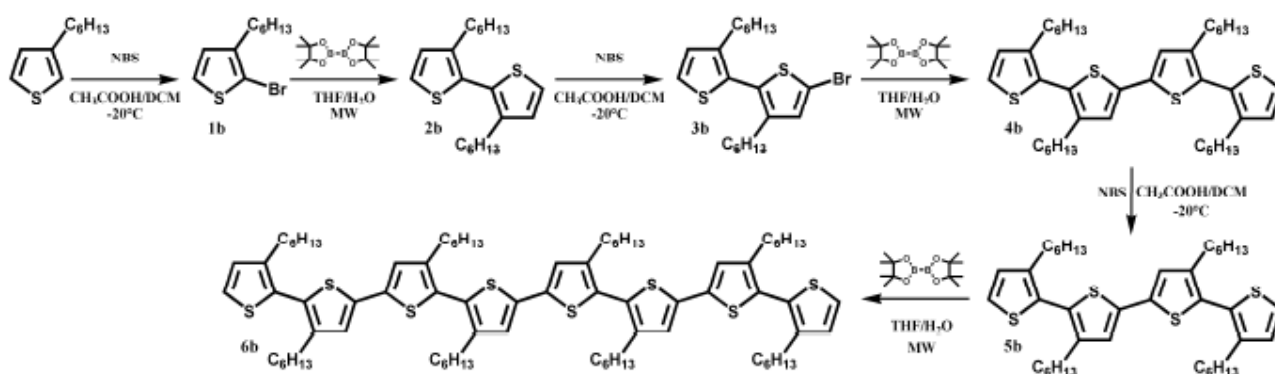
To a stirred solution of **4a** (1 mmol) in dry THF (4 mL) at -80°C was slowly added a 2.5 M solution of *n*-butyllithium in hexane (1.2 mmol). The mixture was allowed to react at this temperature for 1 h, then at room temperature for an additional hour. After cooling at -60°C, 2-isopropoxy-4,4,5,5-tetramethyl-1,3,2-dioxaborolane (2.2 mmol) was added by a syringe.

The resulting mixture was allowed to warm to room temperature and stirred overnight before quenching with water. The product was extracted with ether (2x25 mL).

The combined organic layers were dried over anhydrous sodium sulphate and the solvent was removed under reduced pressure to provide the title compound which was utilized with no further purification. ¹H NMR of the crude product showed a mixture of **5a**/starting material **4a** in the ratio 70:30.

After unsuccessful attempts to purify **5a** (because of instability), the crude product was utilized as obtained for the last synthetic step. Yellow-brown oil; ¹H NMR (400 MHz, CDCl₃, TMS/ppm): δ 7.52 (d, ³J=3.6 Hz, 1H), 7.20 (d, ³J=3.6 Hz, 1H), 7.08 (d, ³J=3.6 Hz, 1H), 6.99 (d, ³J=3.6 Hz, 1H), 2.83-2.78 (m, 2H), 1.67-1.60 (m, 2H), 1.42-1.38 (m, 2H), 1.35 (s, 12H), 1.31-1.26 (m, 4H), 0.89 (t, 3H).

Synthesis of 3,3',3''',3''''',3''''''', 4'', 4''''', 4'''''''-Octahexyl-octithiophene (6b)



Octamer **6b** was prepared following the same procedure described for **9**. Yield 78%. Yellow powder, mp $57\text{--}59^\circ\text{C}$; ^1H NMR (400 MHz, CDCl_3 , TMS/ppm): δ 7.30 (d, $^3J=5.2$ Hz, 2H), 7.03 (s, 6H), 6.97 (d, $^3J=5.2$ Hz, 2H), 2.57–2.46 (m, 16H), 1.60–1.55 (m, 16H), 1.30–1.26 (m, 48H), 0.89–0.85 (m, 24H); ^{13}C NMR (400 MHz, CDCl_3): d 143.41, 143.39, 143.2, 142.5, s 137.0, 136.9, 136.7, 128.6, 128.3, 127.8, 127.4, 127.2, 125.4, 125.1, 125.0, 31.65, 31.64, 31.62, 30.7, 30.61, 30.6, 29.11, 29.10, 29.9, 29.0, 28.93, 28.88, 26.9, 22.6, 22.58, 22.56, 14.08, 14.06; UV/Vis: λ_{max} 369 nm (ϵ 51161 $\text{cm}^{-1}\text{M}^{-1}$), λ_{em} 516 nm in CH_2Cl_2 .

4.4.3 ^1H and ^{13}C NMR Spectra

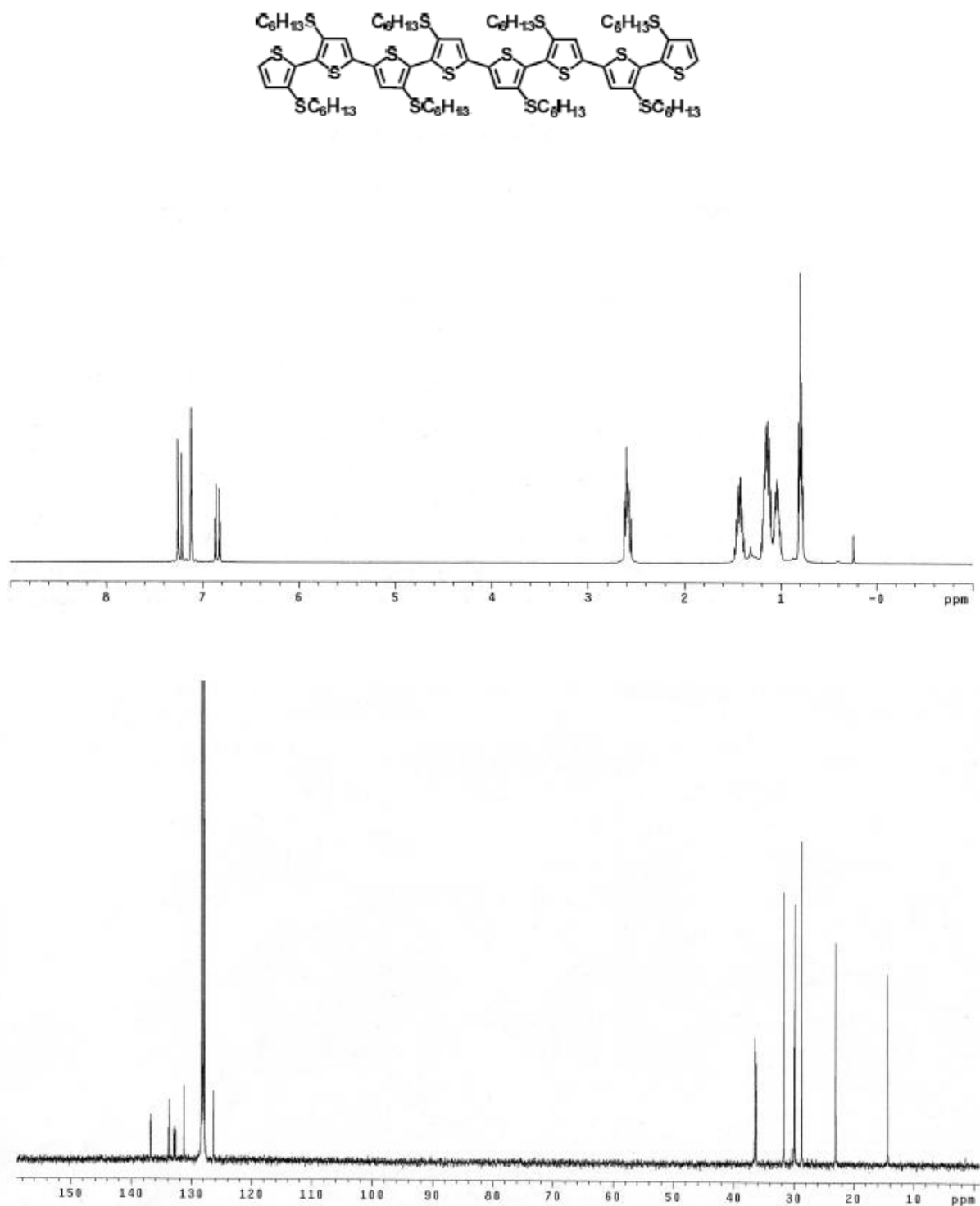


Figure S1. ^1H and ^{13}C NMR spectra of octamer 9.

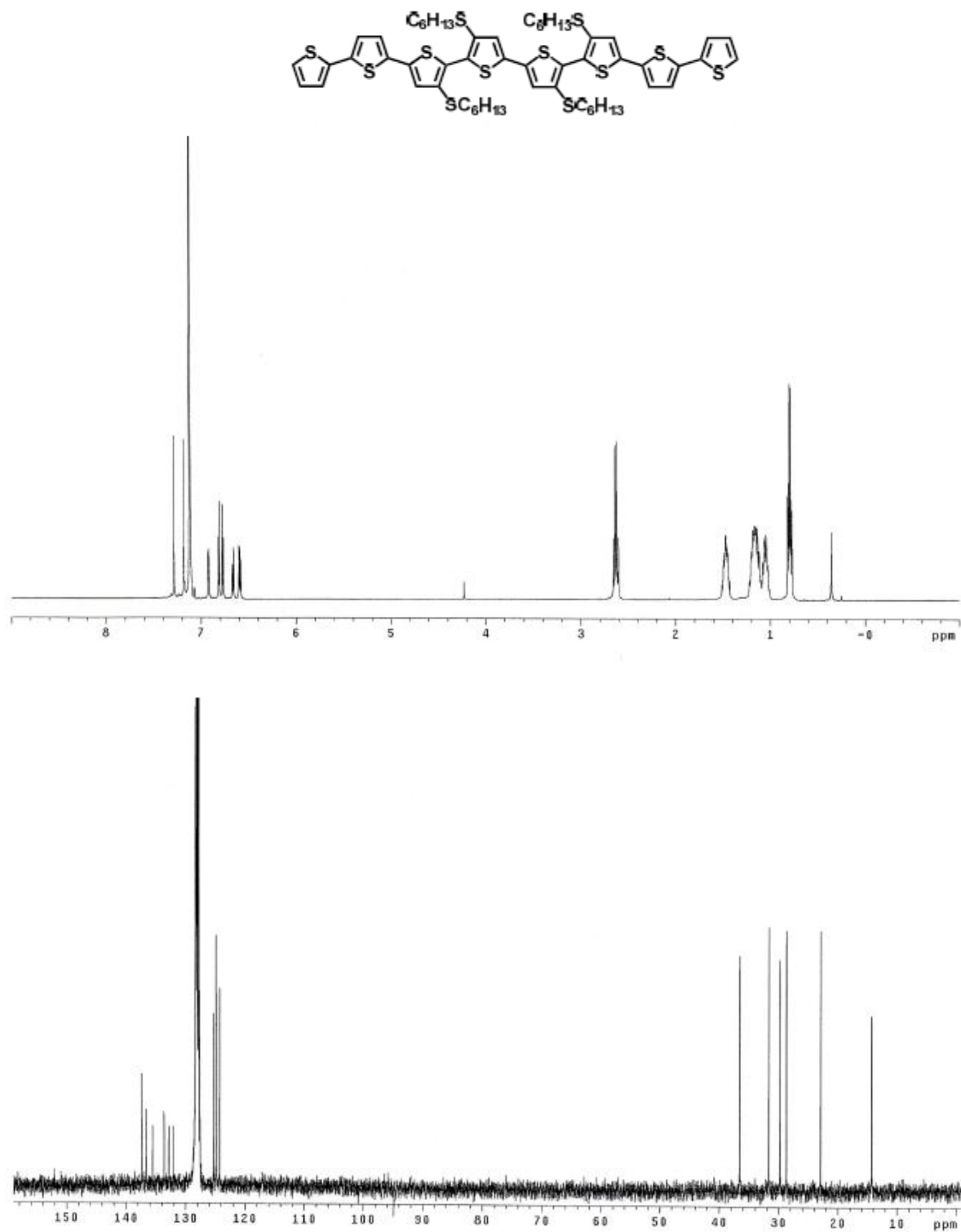


Figure S2. 1H and ^{13}C NMR spectra of octamer 11.

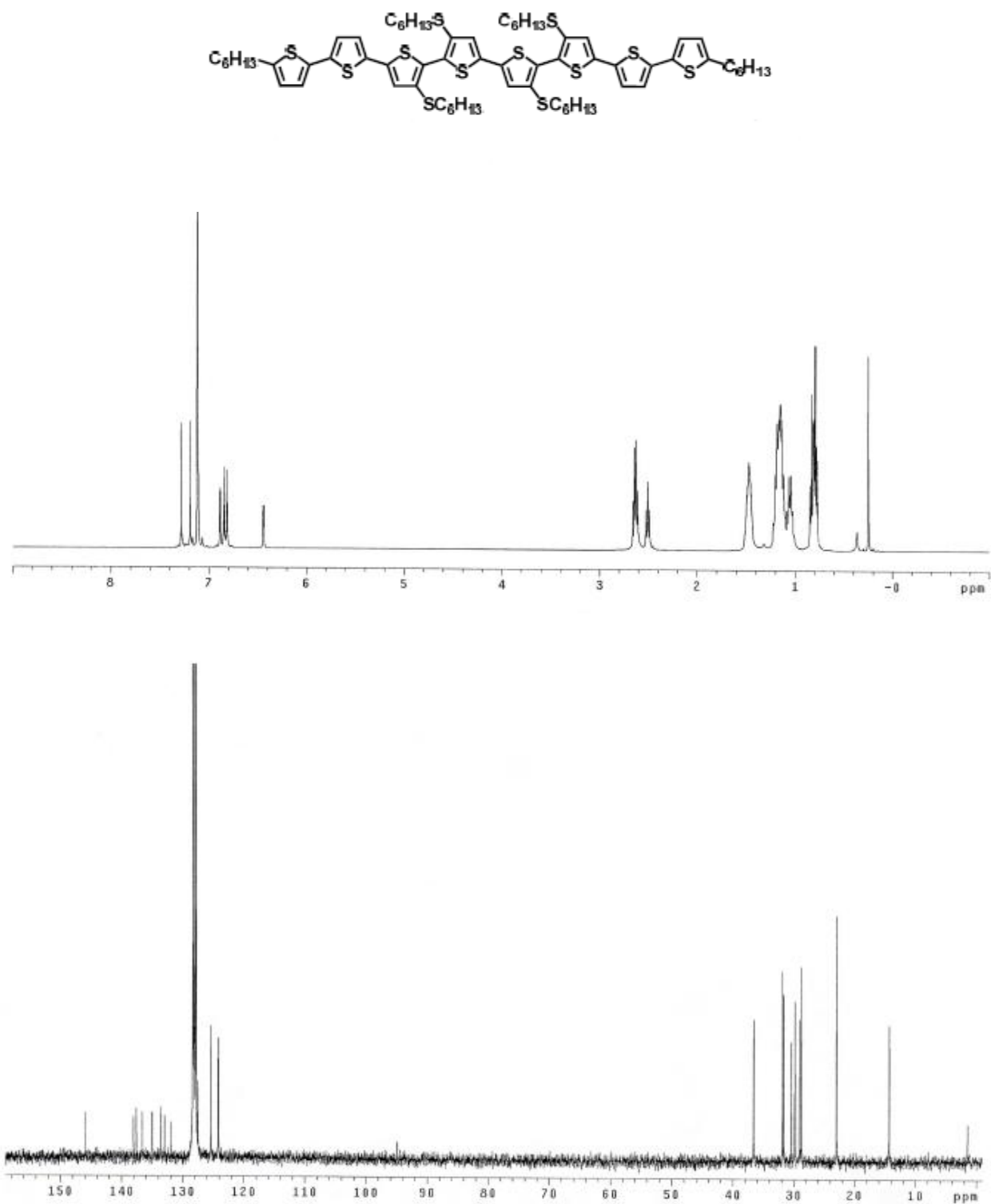


Figure S3. ¹H and ¹³C NMR spectra of octamer 12.

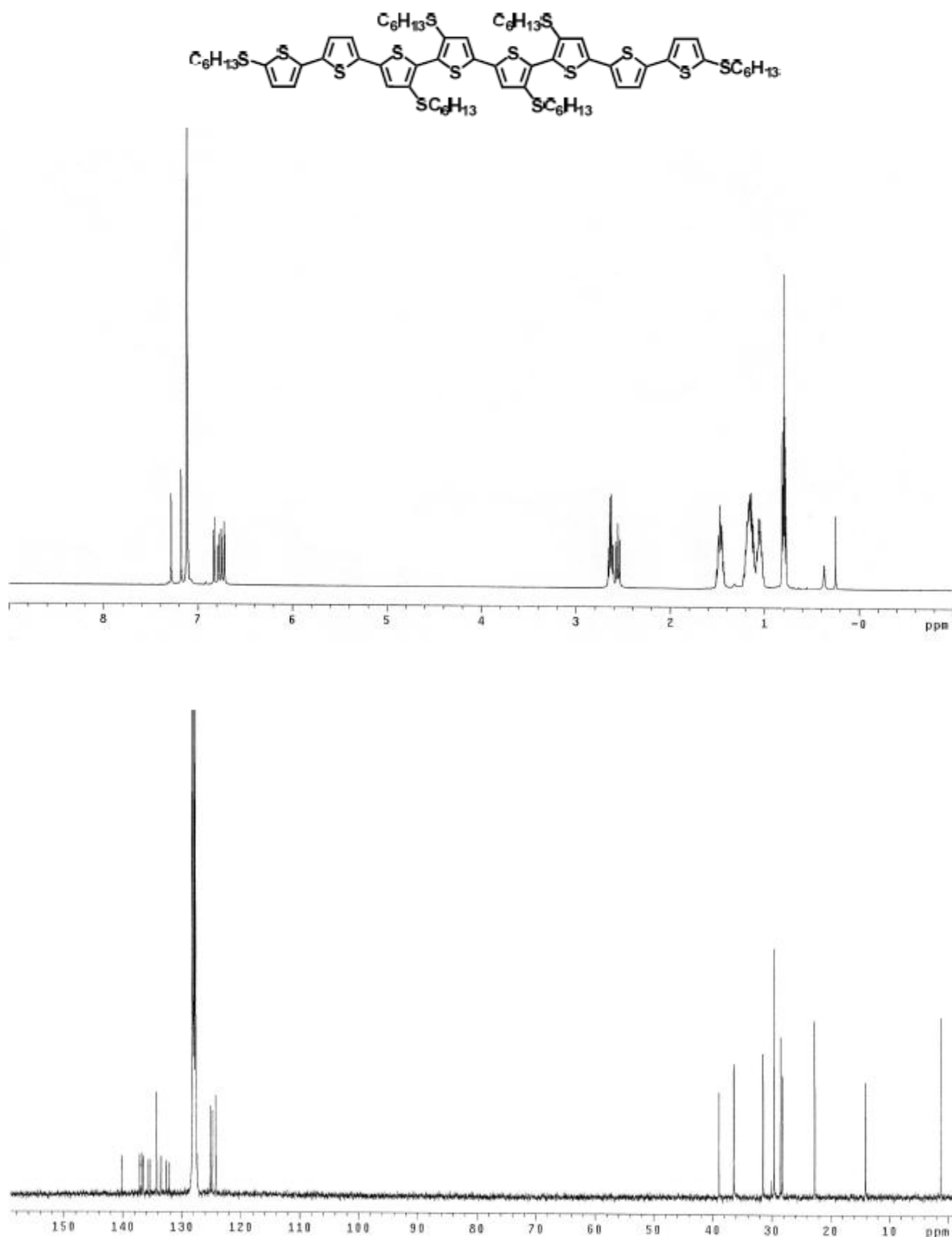


Figure S4. ¹H and ¹³C NMR spectra of octamer 13.

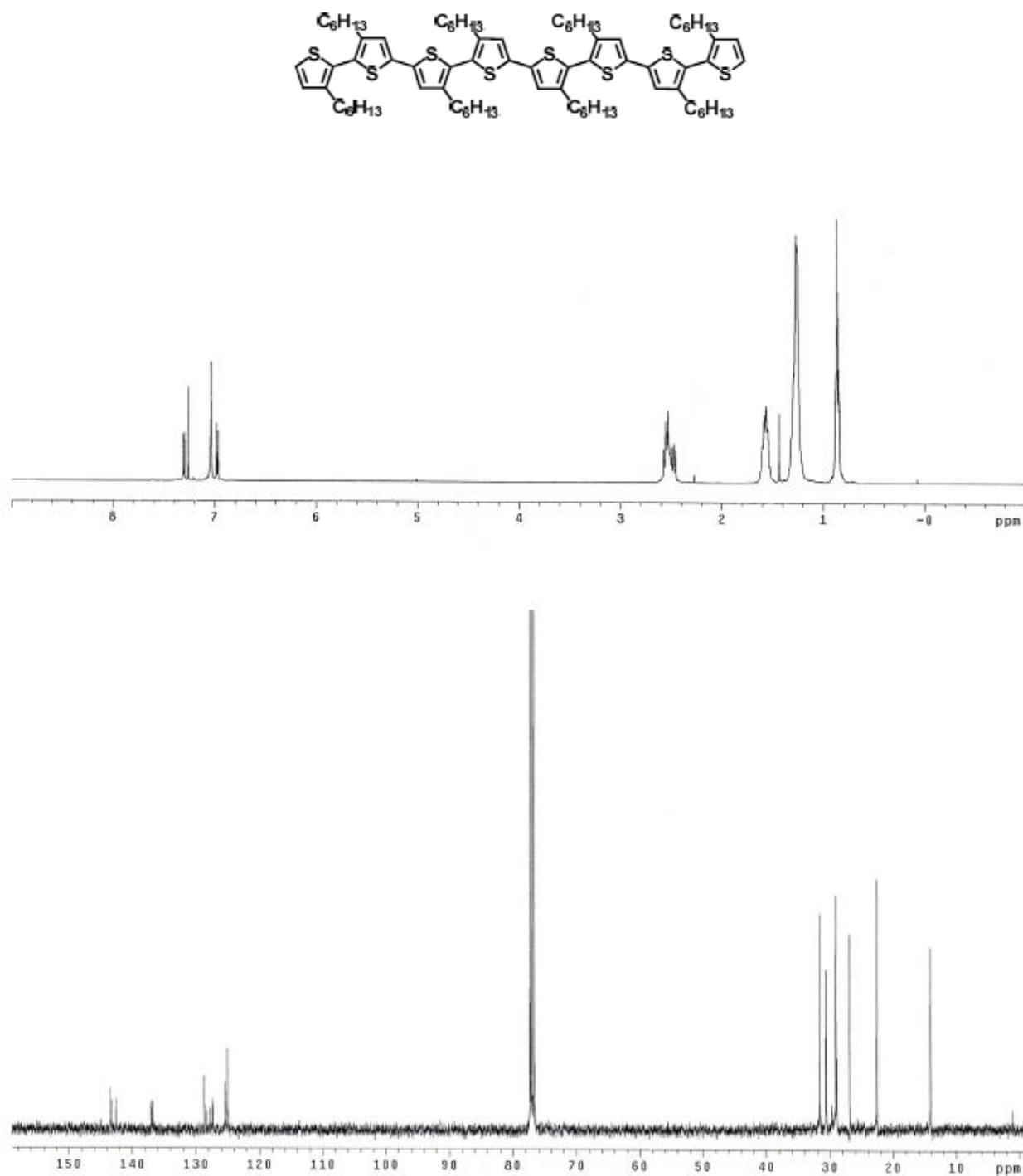


Figure S5. ¹H and ¹³C NMR spectra of octamer 6b.

4.4.4 UV and PL Spectra of Octamers 9 and 11-13

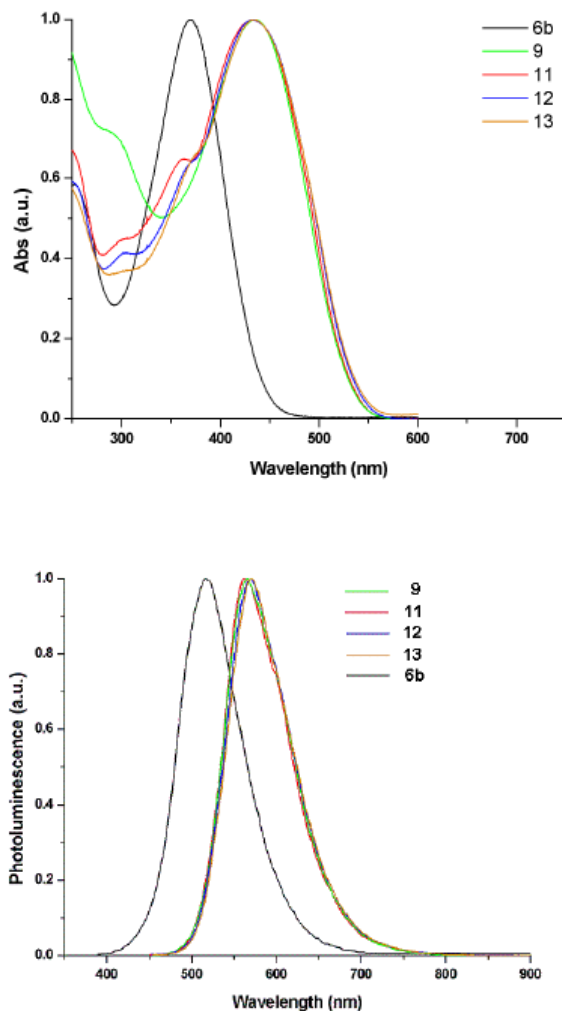


Figure S6. Absorption and photoluminescence spectra of octamers 9, 11-13 and 6b in CH_2Cl_2 .

Item	λ_{max} (nm)	λ_{PL} (nm)
9	434	565
11	433	564
12	433	570
13	434	570

Solvent: CH_2Cl_2

4.4.5 Optical Microscopy of 9,11,12,13 and SEM of 13

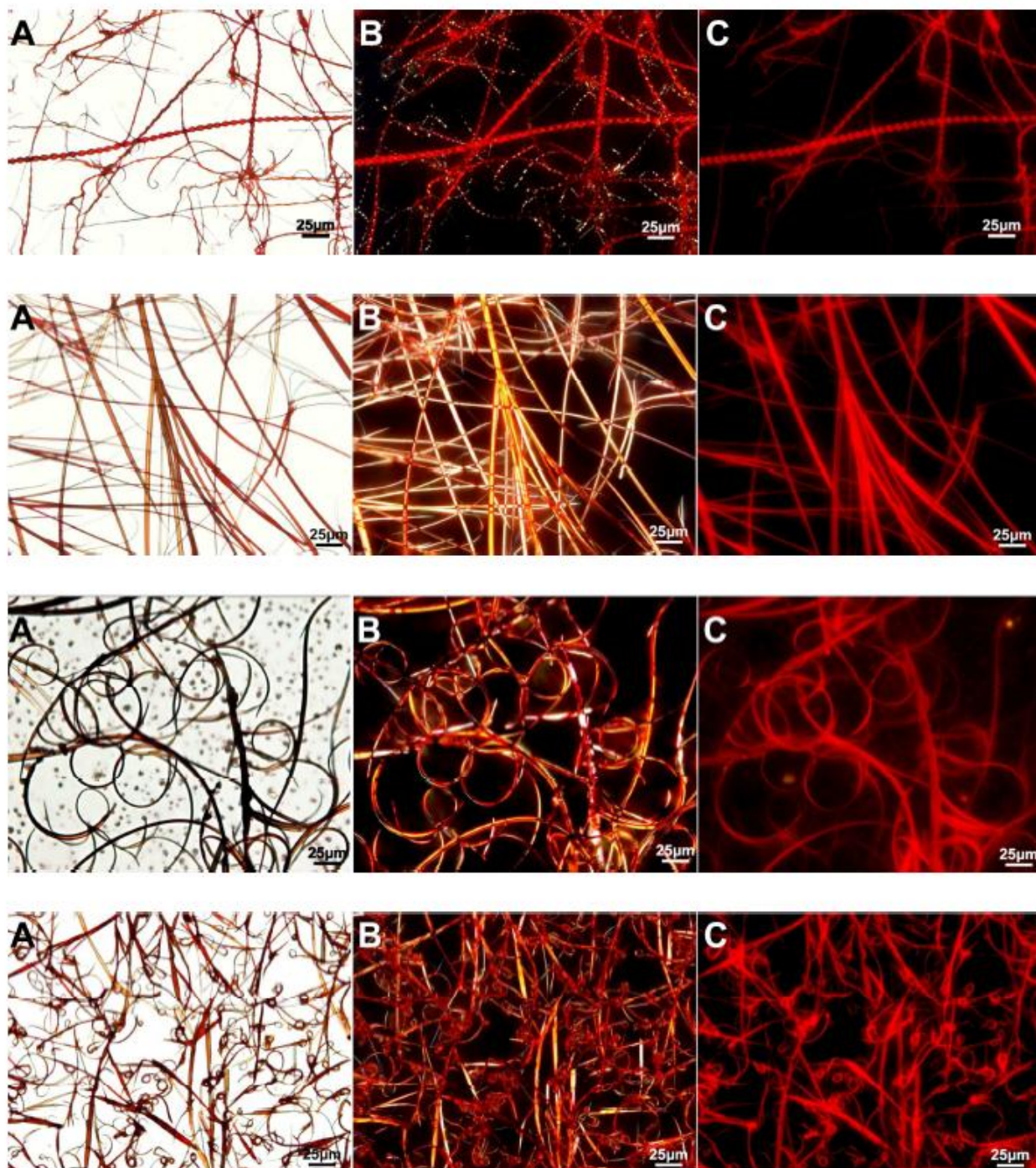


Figure S7. A) Light transmission optical microscopy, B) optical microscopy with cross polars, C) fluorescence microscopy images of octamers 9, 11, 12 and 13 (from top down).

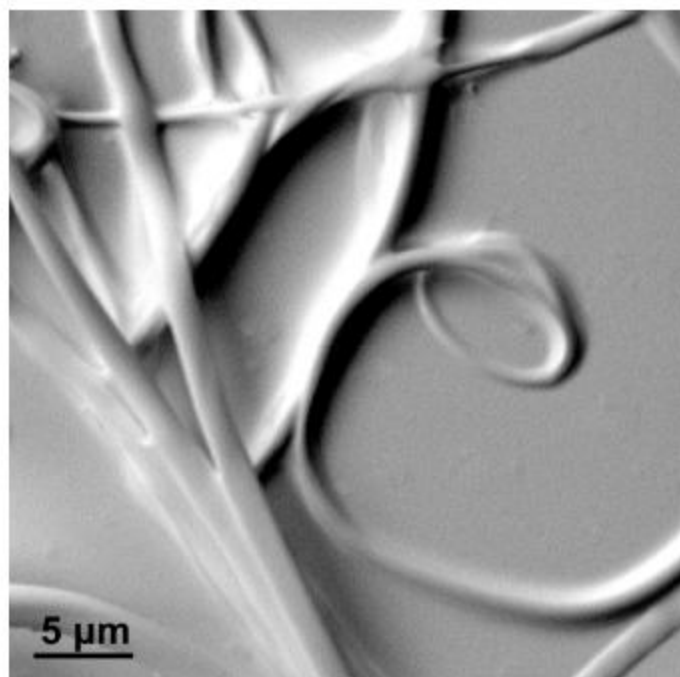


Figure S8. SEM image of octamer 13.

4.4.6 Fluorescence Microscopy and LSCM images of 12

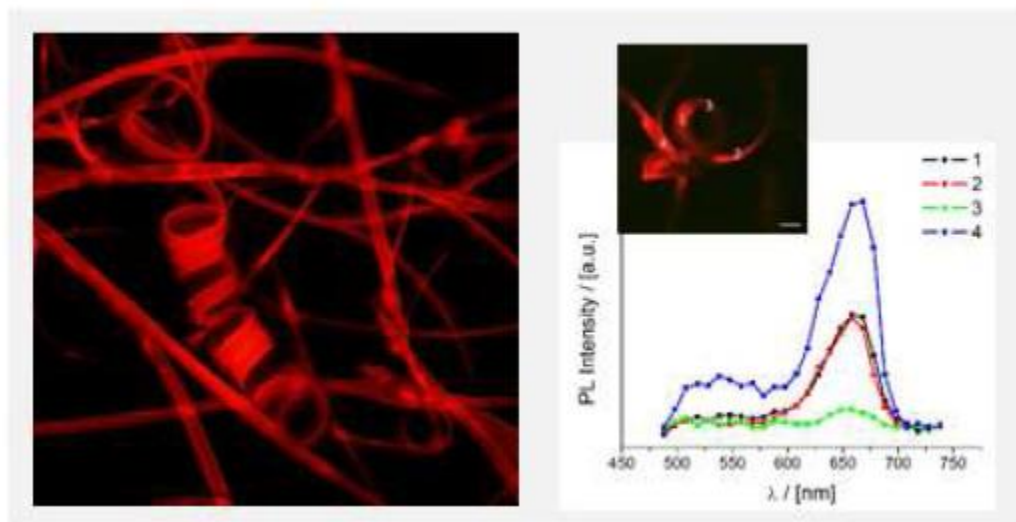


Figure S9. Left: fluorescence microscopy image of fibers of 12 grown on glass. Right: Laser Scanning Confocal Microscopy image and spatially resolved analysis of a detail of 12 grown on glass.

4.4.7 Cyclic Voltametry

Octamer films on ITO electrodes (Balzers) were obtained by drop casting from toluene in air or in acetonitrile saturated air. The films ($\sim 2.3 \text{ cm}^2$) were characterized at room temperature in propylene carbonate (PC, Fluka purum, distilled under reduced pressure and stored over molecular sieves) $0.1 \text{ mol} \cdot \text{L}^{-1}$ $(\text{C}_2\text{H}_5)_4\text{NBF}_4$ (Fluka, puriss.), where they are insoluble.

After Ar bubbling, cyclic voltammeteries (CVs) were performed at scan rates $0.1 \text{ V} \cdot \text{s}^{-1}$, in a home-made three compartment glass cell under Ar pressure, by using an AMEL electrochemical system model 5000. Auxiliary electrode was a Pt wire and reference electrode was aqueous KCl Saturated Calomel Electrode (SCE).

The potential of SCE with the liquid junction to PC $0.1 \text{ mol}\cdot\text{L}^{-1}$ $(\text{C}_2\text{H}_5)_4\text{NBF}_4$ resulted -0.500 V vs. ferrocene/ferricinium redox couple.

After the first doping, the onset of the first oxidation wave appears about 0.1 V less positive than that of the pristine material whereas a reduction wave appears with the onset anticipated about 0.2 V with respect that of the pristine material.^{413,414,415}

The onset of the reduction wave of **6b** clearly grows over the background current but its maximum, and the related reverse wave, are not detectable probably because of the reactions of the radical anion to the environment.

On the other hand, **9** shows a sharp reduction wave at -1.82 V vs. SCE and its reversible one at -1.59 V vs. SCE.

After the second scan the voltammograms remain more or less the same but the current slightly decreases suggesting a progressive dissolution of the film especially in the charged state.

Redox potentials of 1 mM/L **6b**, **9** and **11** have been evaluated at room temperature in CH_2Cl_2 (Carlo Erba RPE, distilled over P_2O_5 and stored under Ar pressure) with 0.1 M/L $(\text{C}_4\text{H}_9)_4\text{NClO}_4$ (Fluka, puriss. crystallized from CH_3OH and vacuum dried).

In this solution SCE potential resulted to be -0.475 V vs. ferrocene/ferricinium.

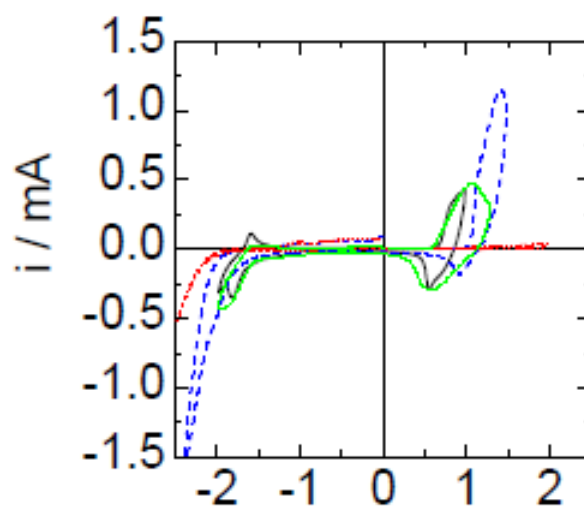


Figure S10. Second cyclic voltammetry of cast films of 6b (blue) and 9 (black) and background current (red) on ITO in PC 0.1 mol L⁻¹ (C₂H₅)₄NBF₄ at 0.1V s⁻¹.

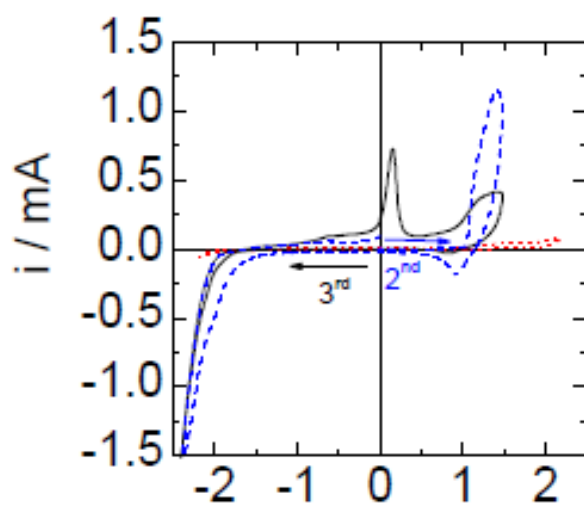


Figure S11. Second (blue) and third (black) voltammogram of 6b on ITO in PC 0.1 mol L⁻¹ (C₂H₅)₄NBF₄ at 0.1V s⁻¹.

4.4.8 Electrical Characterizations

▪ **Tr-TUNA maps**

One of the referees asked the following questions:

1) In "...Tr-TUNA measurements from Fig. 99. A direct comparison between topography and current is not shown (i.e. are the wide conducting islands also visible in topography?.."

The answer is: Wide islands with lower conductivity than fiber (**Figure 99**) have topographic correspondence in amorphous aggregates and impurities the medium height of which ranges between 4 nm and 50 nm much lower than the medium height of 300 nm of the fibers. For this reason islands are visible in the topographic images only reducing the range of the height colored scale (**Figure S12**) cutting the upper limit of the height scale suitable to show the topography features of the fibers (**Figure S13**).

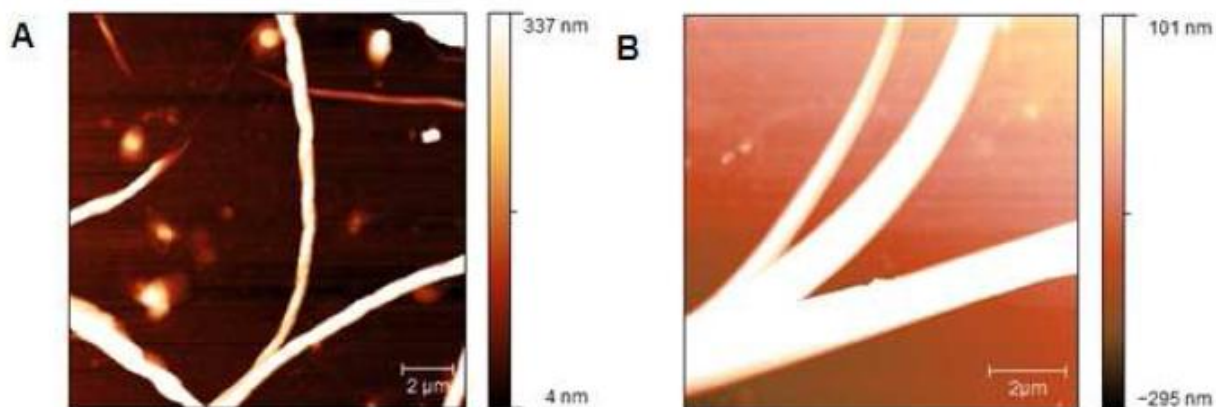


Figure S12. Atomic Force Microscopy images of the fiber of 9 (A) and 11 (B) with reduced z-scale. In both images amorphous aggregates and impurities which are visible with reduced z-scale with respect to the z-scale needed to show the topography of both kinds of fibers are shown. With reduced z-scale the islands with height in the range 4-50 nm are visible, while the topographic features of the fibers cannot be appreciated.

2) "...Why is the conductivity of the fibers larger at one of their edges?..."

The answer is: the reason for this is that the electronic feedback keeping constant the very short distance between the tip and the surface of the sample, typically 1-2 nm, afflicts the measure near close the highest topographic gradient with a lower current felt by the tip.

The high edges of the fibers are an examples. In our case the effect is evident (the spatial extension of the yellow region of **Figure 99**) on one side, because the topographic gradient is different on both sides (**Figure S13**).

In order to minimize this effect, we performed the current detection images at the lower scan velocity available, corresponding to 0.1 Hz.

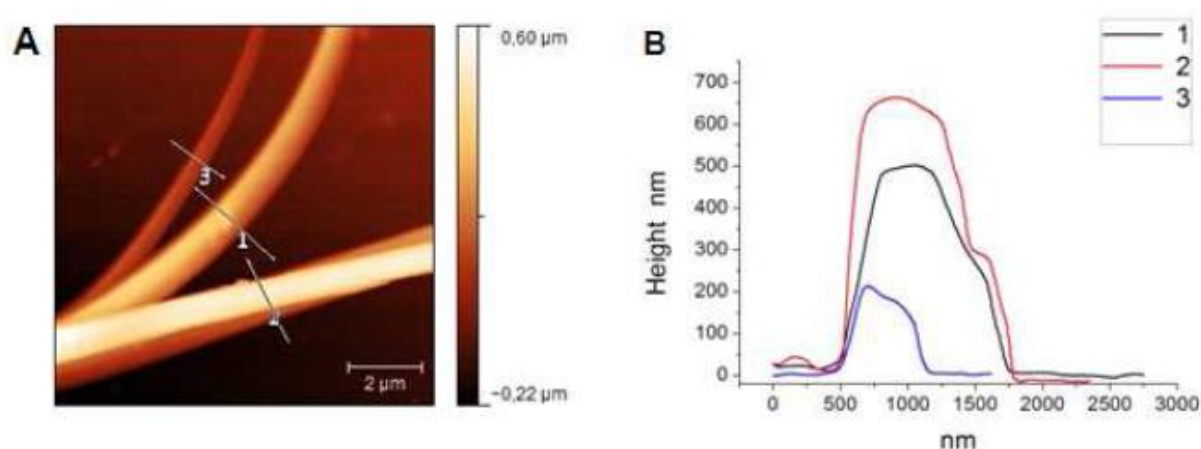


Figure S13. A) Atomic Force Microscopy image of the fiber. B) Cross-sections of the fibers (A) with different heights shows the slope of the sides of the fibers. The topographic gradient of the left side is higher than that of the right side for each fiber.

▪ **Charge Transport Measurement**

In order to study the correlation between the morphology and the transport properties we performed scanning conductive torsion mode microscopy (Veeco Multimode, Nanoscope V Controller equipped with Tr-Tuna module, current amplifier sensitivity 1 pA/V) on semiconductor polymer fluorescent fibers of T_8S_8 and T_8S_4 samples.

Tunneling Atomic Force Microscopy in torsion mode (Tr-TUNA) were used to examine the surface and electronic properties within domains of nanoscale dimensions. Tr-Tuna is a new scanning probe technique combining the torsion mode topography imaging with conductive scanning force microscopy. Tr-TUNA gently examines surface topography and local current simultaneously providing information on the nanoscale charge transport properties within specific domains.⁴¹⁶

In torsion-mode the base of the cantilever is vibrated by a pair of piezoelectric actuators that are driven antiperiodically.^{417,418} Depending on the vibration frequency, a torsional resonance mode can be excited in the cantilever.

When the tip gets close to the sample surface the vibration amplitude is reduced. This damping is caused by surface forces and in-plane interactions with the sample. The decrease in the amplitude is used as a feedback signal for the tip-sample separation. Thus, the feedback loop is sensitive to topography and lateral forces are well controlled. Other than in intermittent contact mode, here the tip vibrates laterally with respect to the sample surface. By applying an electrical potential between the tip and the sample, an electrical current flows.

By scanning the tip, local variations in the conductivity in the sample can be recorded.

A high work-function-metal Pt/Ir tip probe was used to obtain hole-current image. The current measured is expected to be predominantly by hole transport, because the ITO substrate and the Pt/Ir tip have work functions of 4.7 and 5.2 eV, respectively, and the polymer HOMO energy is approximately 5.2-5.3 eV (as estimated from cyclic voltammetry).

However, we note that a rigorous estimate of the energy band gap should also include the exciton binding energy, which is usually a few tenths of an eV. Based on consideration of these energies, there is a higher barrier for hole injection from the Pt/Ir tip (0.1 eV) than from ITO (1.1-1.2 eV).

The ITO/**9** (or **11**)/PtIr device is, therefore, a hole-only device since in both directions of current flow, the hole injection barrier is smaller than the electron injection barrier.

Further insight into the conduction mechanism of fibers of **9** and **11** was obtained studying the charge transport by means of Conductive-AFM technique in contact mode (C-AFM) using hole-only diodes configuration.

The plots of current density vs square voltage [$J(V)$] are reported in a double logarithmic representation for **9** and **11** (**Figure S13**).

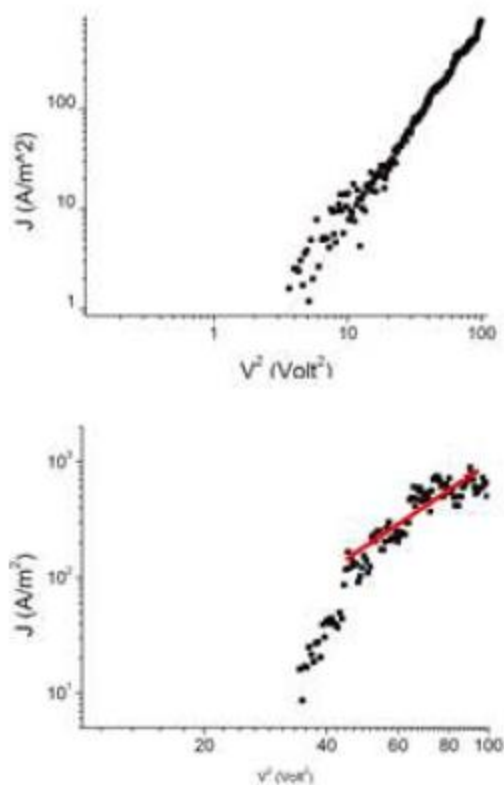


Figure S14. Plots of J vs V^2 on bilogarithmic scale basing on hole-only current and SCLC model fitting for **9** (top) and **11** (bottom).

Analysis of the current density (J) versus bias dependence shows that **9** exhibits a space charged transport regime ($J \sim V^2$) while **11** shows a trap filled regime ($J \sim V^m$, $m > 2$) followed by space charge transport regime ($J \sim V^2$).

It is possible to extract hole mobilities from the SCLC region. For semiconductor polymers the conductivity is often limited by space charge. Space charge limited conduction can approximately be described by a Mott-Gurney Law:⁴¹⁹

$$J = \frac{9}{8} \epsilon \epsilon_0 \mu \frac{V^2}{L^3}$$

where \mathbf{J} is the current density, ϵ is the relative dielectric constant, ϵ_0 is the permittivity of vacuum, μ the charge carrier mobility, \mathbf{V} is the applied bias voltage, and \mathbf{L} is the polymer layer thickness. This method measures the charge mobility in the vertical direction. From these results, one finds hole mobilities (in $\text{cm}^2/\text{V}\cdot\text{s}$) of 9.8×10^{-7} and 5×10^{-6} for **9** and **11**, respectively. Thus the hole mobility for **11** is 5 times greater than the hole mobility of **9**.

▪ **Field Effect Transistor**

Helical fibers of **9** and rod-like fibers of **11** were directly grown on the SiO_2 substrate of a bottom contact field-effect transistor.

A standard two probe technique was employed to measure the transfer, \mathbf{I}_{DS} vs. \mathbf{V}_{GS} (drain-source current versus gate voltage), and output characteristics, \mathbf{I}_{DS} vs. \mathbf{V}_{DS} (drain-source current versus voltage).

Bottom contact test pattern devices were made with Au/Ti interdigitated contacts on SiO_2 200 nm thick, thermally grown on heavily n-doped Si gate electrode.

These electrodes provide two couples of devices with a channel length $L = 20 \mu\text{m}$ and $40 \mu\text{m}$, respectively, and an aspect ratio W/L fixed at 550.

Transfer characteristics were measured at room temperature, in air and in vacuum, both in linear ($V_{\text{DS}} = -10 \text{ V}$) and saturation ($V_{\text{DS}} = -60 \text{ V}$) regime, while output characteristics were measured by sweeping V_{DS} from 0 to -60 V at fixed V_{GS} (from $+10 \text{ V}$ to -60 V with $\Delta V_{\text{GS}} = +10 \text{ V}$).

A strong intrinsic doping effect for all the analyzed devices was shown by the output (not reported) and transfer characteristics. Such effect, deduced from the high value of the off state (the typical magnitude of the current recorded in depletion mode is higher than 0.1 μA), can be ascribed to oxidative reactions. In fact, the off current of the materials can be drastically reduced to few nanoampere by using a hydrazine dedoping procedure.

However, the dedoping procedure is reversible, as the initial off state can be recovered by exposing the devices to the environmental conditions. The charge carrier mobility value (μ assessment in saturation regime) is then affected by this occurrence, as the reduced current modulation for doped devices reflects in the lack of the saturation regime in device response.⁴²⁰

For this reason m was evaluated in linear regime for bottom contact devices, scaling the W/L ratio by a factor 2 as the test pattern is effectively covered by the material for the 50% of its nominal surface.

The most striking feature of FET based on the helical fibrils of **9** is represented by the peculiar memory effect intrinsic to the active material, that is obtained without recurring to polarizable gate dielectrics, as happens for instance in the case of ferroelectric memory field effect resistors.⁴²¹

The memory effect can be deduced from the clockwise hysteresis in drain-source current (red arrow in **Figure 99**), indicating that the device retains the on state in backward gate voltage sweep, which generally corresponds to the passage from the on state towards the off state (**Figure S14**).

Such effect, modulated by the gate voltage, is more pronounced in presence of oxygen (air) and in saturation than in vacuum and in linear regime, respectively.

Surprisingly, the transfer characteristics measured for highly structured cast films of **9** and **11**, with globular instead of fibrillar morphology, do not show any charge carrier modulation, the intrinsic current being comparable in magnitude to the electrometer sensitivity.

This aspect indicates that charge transport is strongly morphology dependent.

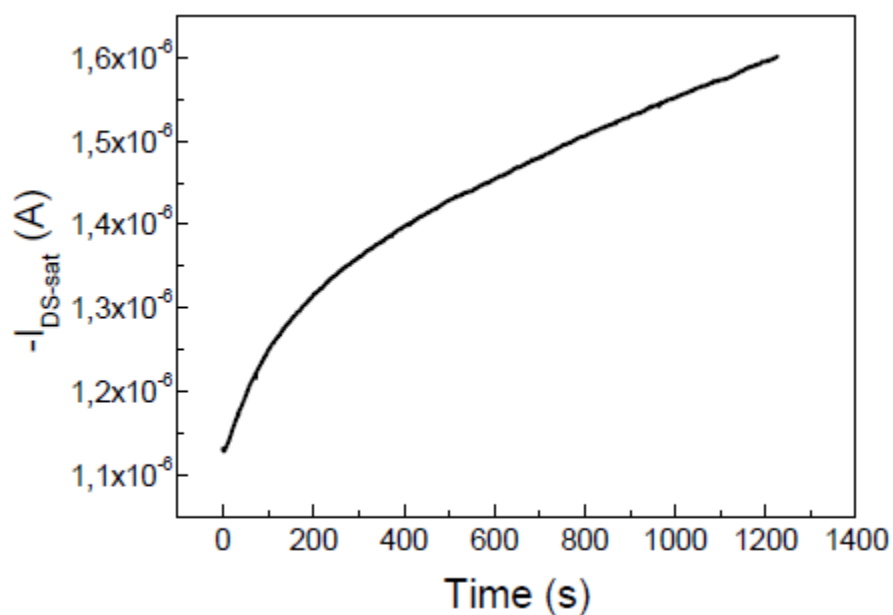


Figure S15. Bottom contact FET device with fibers of **9** directly grown on SiO_2 . I_{DS} vs time recorded in air by fixing $V_{GS} = -60\text{V}$ and $V_{DS} = -60\text{ V}$, indicating charge accumulation with time

4.5 References

- [373] G. M. Whitesides, B. Grzybowski, *Science*, **2002**, *295*, 2418-2421
- [374] L. C. Palmer, S. I. Stupp, *Acc. Chem. Res.*, **2008**, *41*, 1674-1684
- [375] M. Schiek, F. Balzer, K. Al-Shamery, J. R. Brewer, A. Lützen, H.G. Rubahn, *Small*, **2008**, *4*, 176-181
- [376] E. C. P. Smits, S. G. J. Mathijssen, P. A. Van Hal, S. Setayesh, T. C. T. Geuns, K. A. H. A. Mutsaers, E. Cantatore, H. J. Wondergem, O. Werzer, R. Resel, M. Kemerink, S. Kirchmeyer, A. M. Muzafarov, S. A. Ponomarenko, B. De Boer, P. W. M. Blom, D. M. Leeuw, *Nature*, **2008**, *455*, 956-959
- [377] S. Park, K. Hamad-Schifferli, *Curr. Opin. Chem. Biol.*, **2010**, *14*, 616-622
- [378] Y. H. Yun, E. Eteshola, A. Bhattacharya, Z. Dong, G.-S. Shim, L. Conforti, D. Kim, M. J. Schulz, C. H. Ahn, N. Watts, *Sensors*, **2009**, *9*, 9275-9299
- [379] M. Hasegawa, M. Iyoda, *Chem. Soc. Rev.*, **2010**, *39*, 2420-2427
- [380] X. Feng, W. Pisula, T. Kudernac, D. Wu, L. Zhi, S. De Feyter, K. J. Müllen, *J. Am. Chem. Soc.*, **2009**, *131*, 4439-4448
- [381] Y. Wang, H. D. Tran, L. Liao, X. Duan, R. B. J. Kaner, *J. Am. Chem. Soc.*, **2010**, *132*, 10365-10373
- [382] G. M. Whitesides, D. J. Lipomi, *Faraday Discuss.*, **2009**, *143*, 373-384
- [383] M. Durkut, M. Mas-Torrent, P. Hadley, P. Jonkheijm, A. P. H. J. Schenning, E. W. Meijer, S. George, A. J. Ajayaghosh, *Chem. Phys.*, **2006**, *124*, 154704/1-6
- [384] J. M. Mativetsky, M. Kastler, R. C. Savage, D. Gentilini, M. Palma, W. Pisula, K. Müllen, P. Samor, *Adv. Funct. Mater.*, **2009**, *19*, 2486-2494
- [385] J. K. Kim, E. Lee, M. C. Kim, E. Sim, M. J. Lee, *J. Am. Chem. Soc.*, **2009**, *131*, 17768-17770
- [386] K. Tanaka, T. Kunita, F. Ishiguro, K. Naka, Y. Chujo, *Langmuir*, **2009**, *25*, 6929-6933
- [387] Y. Wang, H. D. Tran, L. Liao, X. Duan, R. B. J. Kaner, *J. Am. Chem. Soc.*, **2010**, *132*, 10365-10373
- [388] S. Prasanthkumar, A. Saeki, S. Seki, A. Ajayaghosh, *J. Am. Chem. Soc.*, **2010**, *132*, 8866-8867
- [389] B. K. An, S. H. Gihm, J. W. Chung, C. R. Park, S. K. Kwon, S. Y. Park, *J. Am. Chem. Soc.*, **2009**, *131*, 3950-3957
- [390] G. Barbarella, M. Melucci, G. Sotgiu, *Adv. Mater.*, **2005**, *17*, 1581-1593

- [391] F. Bernardi, I. G. Csizmadia, A. Mangini, H. B. Schlegel, M. H. Whangbo, S. Wolfe, *J. Am. Chem. Soc.*, **1975**, *97*, 2209-2218
- [392] G. R. Desiraju, T. Steiner, *The Weak Hydrogen Bond*, Oxford University Press: Oxford, **1999**
- [393] S. H. Gellman, *Biochemistry*, **1991**, *30*, 6633-6636
- [394] N. Crivillers, M. Mass-Torrent, S. T. Bromley, K. Wurst, J. Veciana, C. Rovira, *Chem. Phys. Chem.*, **2007**, *8*, 1565-1571
- [395] A. Suzuki, *Chem. Commun.*, **2005**, 4759-4763
- [396] S. Alesi, F. Di Maria, M. Melucci, D. J. Macquarrie, R. Luque, G. Barbarella, *Green Chem.*, **2008**, *10*, 517-523
- [397] M. Surin, P. Leclère, S. De Feyter, M. M. S. Abdel-Mottaleb, F. C. De Schrywer, O. Henze, W. J. Feast, R. J. Lazzaroni, *Phys. Chem. B*, **2006**, *110*, 7898-7908
- [398] F. Balzer, M. Schiek, A. Lützen, H. G. Rubahn, *Chem. Mater.*, **2009**, *21*, 4759-4767
- [399] P. Leclère, M. Surin, R. Lazzaroni, A. F. M. Kilbinger, O. Henze, P. Jonkheijm, F. Biscarini, M. Cavallini, W. J. Feast, E. W. Meijer, A. P. H. J. Schenning, *J. Mater. Chem.*, **2004**, *14*, 1959-1963
- [400] O. Henze, W. J. Feast, F. Gardebien, P. Jonkheijm, R. Lazzaroni, P. Leclère, E. W. Meijer, A. P. H. J. Schenning, *J. Am. Chem. Soc.*, **2006**, *128*, 5923-5929
- [401] N. L. Allinger, E. L. Eliel, S. H. Wilen, *Top. Stereochem.*, **1983**, *14*, 1-81
- [402] P. L. Williams, E. Giralt, *Chem. Soc. Rev.*, **2001**, *30*, 145-157
- [403] J. J. Van Gestel, *Phys. Chem. B*, **2006**, *110*, 4365-4370
- [404] K. H. Ernst, *Science*, **2008**, *13*, 54-59
- [405] C. M. Cardona, W. Li, A. E. Kaifer, D. Stockdale, G. C. Bazan, *Adv. Mater.*, **2011**
- [406] J. Heinze, B. A. Frontana-Uribe, S. Ludwigs, *Chem. Rev.*, **2010**, *110*, 4724-4771
- [407] G. Casalbore-Miceli, N. Camaioni, A. Geri, G. Ridolfi, A. Zanelli, M. C. Gallazzi, M. Maggini, T. J. Benincori, *Electroanal. Chem.*, **2007**, *603*, 227-234
- [408] R. Berger, H. J. Butt, M. B. Retschke, S. A. L. Weber, *Macromol. Rapid Commun.*, **2009**, *30*, 1167-1178
- [409] R. J. Kline, M. D. McGehee, *Polymer Rev.*, **2006**, *46*, 27-45

- [410] A. Facchetti, J. Letizia, M.-H. Yoon, M. Mushrush, H. E. Katz, T. J. Marks, *Chem. Mater.*, **2004**, *16*, 4715-4727
- [411] R. C. G. Naber, C. Tanase, P. W. M. Blom, G. H. Gelinck, A. W. Marsman, F. J. Touwslager, S. Setayesh, D. M. De Leeuw, *Nature Mat.*, **2005**, *4*, 243-248
- [412] J. M. Lehn, *Rep. Prog. Phys.*, **2004**, *67*, 249-265
- [413] J. Heinze, B. A. Frontana-Uribe, S. Ludwigs, *Chem. Rev.*, **2010**, *110*, 4724-4771
- [414] T. Johansson, et al., *J. Mater. Chem.*, **2003**, *13*, 1316-1323
- [415] S. Trasatti, *Pure Appl. Chem.*, 1986, *58*, 955-966
- [416] R. Berger, H. J. Butt, M. B. Retschke, *Macromol. Rapid Commun.*, **2009**, *30*, 1167-1178
- [417] T. Kawagishi, A. Kato, Y. Hoshi, *Ultramicroscopy*, **2002**, *91*, 37-48
- [418] L. Huang, *Ultramicroscopy*, **2004**, *100*, 277-285
- [419] O. G. Reid, K. Munechika, *Nano Lett.*, **2008**, *8*, 1602-1609
- [420] M. S. A. Abdou, F. P. Y. Orfino, Y. Son, *J. Am. Chem. Soc.*, **1997**, *119*, 4518-4524
- [421] R. C. G. Naber, et al., *Nature Mater.*, **2005**, *4*, 243-248

5 *BHJ Solar Cells based Head-to-Head Thiophene Hexadecamers*

5.1 Introduction

Thiophene materials—both small organic molecules and polymers—are currently largely employed in *organic photovoltaic devices* (**OPVDs**) owing to their good hole-transporting properties and light absorption ability.^{422,423}

Today, for the development of a low-cost photovoltaic technology, the most widely applied approach to **PVDs** is the *bulk heterojunction* approach (**BHJ**), based on blends of soluble *donor* (D) and *acceptor* (A) components in a bulk volume as photoactive elements.⁴²⁴

The control of the positions of the *HOMO* and *LUMO* energy levels of the donor and acceptor materials is a stringent condition to achieve good performance in **PVDs**.⁴²⁵

The state-of-the-art in the organic photovoltaics field is currently represented by **BHJ** solar cells based on **P3HT** and **PCBM**, with reproducible efficiencies approaching **9%**.^{426,427}

In comparison to the relevant conjugated polymers that are used as active materials in photovoltaic devices, conjugated **OTs** possess some critical advantages (1) well-defined molecular structures lead to their synthetic reproducibility with high purity which is vital to obtain repeatable device performance; (2) crystalline features of oligomers favor the long range order in the solid state and benefit the charge carrier transport; (3) the devices can be readily fabricated by both solution-processable and vacuum-deposited techniques.

Furthermore the introduction of electron-withdrawing or electron-donating building blocks, offer tunable *HOMO* and *LUMO* energy levels; the **OTs** are homogeneous materials, with reproducible physical and chemical properties by different synthetic methodologies.

From the view of these points, thiophene-based p-conjugated oligomers are among the most promising materials for *organic solar cells (OSCs)*,^{428,429} and to synthesize regioregular *head-to-head* hexadecamers based thiophene with a high degree of purity and with reproducible electrical characteristics for application in **BHJ** solar cells was the aim of this project.

Solubility, band-gap and hole transport properties will be tuned via monomer structure and backbone substitution; high purity levels will be achieved via ultrasound and microwave assistance.

Finally the influence of *S-Hexyl* chains was very important on the optical, electrical and morphological properties of these materials (see Chapter IV) thanks to electron-donating properties of the sulfur atom.

5.2 Results and Discussion

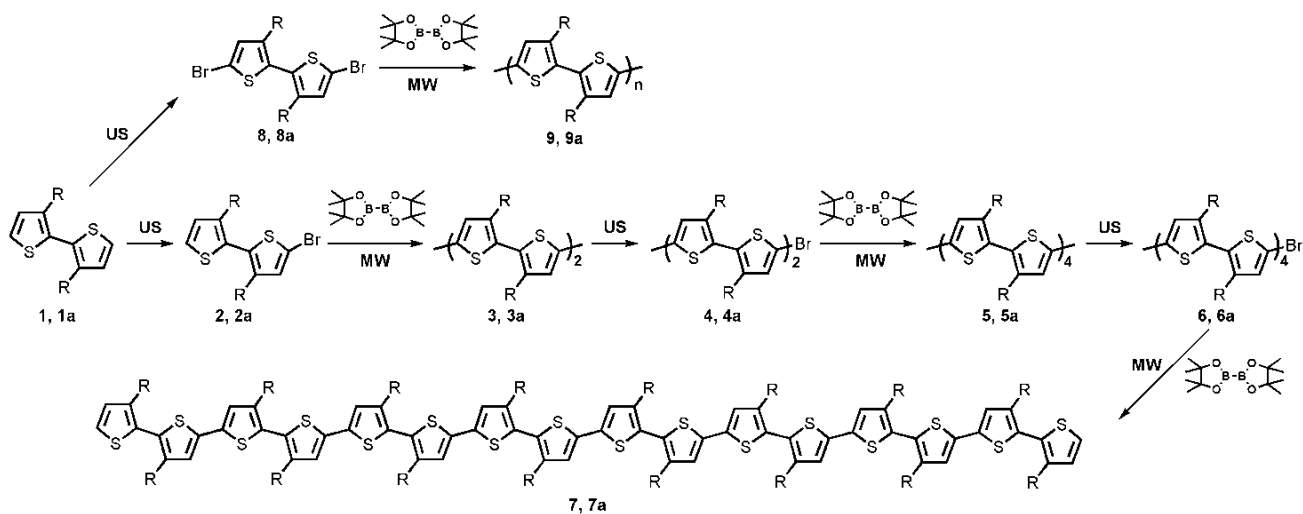
▪ *Synthesis of Regioregular Hexadecamers and Polymers*

Generally, the synthesis of conjugated oligomers is carried out through cross-coupling methodologies under *Pd* or *Ni* catalyses^{430,431} using conventional heating methods.

We described in *Chapter IV* that using commercial *4,4,5,5-tetramethyl-1,3,2-dioxaborolane (TDB)* in a one pot borylation-Suzuki coupling reaction in THF/H₂O under microwave irradiation, the doubling of the oligomer skeleton was obtained in high yield and free of byproducts, thus, avoiding long and expensive purifications of the reaction products.⁴³²

For these reasons the same methodology was successfully extended to the preparation of *head-to-head* regioregular hexadecamer and polymers, with *hexyl* and *S-hexyl* substituents.

Herein we have reported a regiospecific synthetic methodology (**Scheme 13**) based on Suzuki reaction^{433,434} enable to carry out in high yield regioregular **OTs** and **PTs** in short reaction time by taking advantage of *ultrasound* and *microwave* irradiation for the bromination and cross-coupling steps, respectively.



Scheme 13. Synthesis of Hexadecamers and Polymers hexil and S-hexil substituted.

Efficient monobromination and dibromination of quaterthiophenes was achieved in a few minutes with a single or double addition of NBS in DCM under ultrasound irradiation.

Obviously in the absence of ultrasounds, the monobromination and the dibromination of the same substrate would required the slow stepwise addition of NBS in several hours or days leading to decreasing of the yields.

In this manner, the combined use of ultrasound and microwave irradiation provides a very efficient platform for the rapid, low power, low cost, and environmentally friendly preparation of regioregular *head-to-head* hexadecamers and polymers based-thiophene.

▪ Optical Properties

From the optical properties (**Figure 101**), we can observe a red-shift, both in absorption and in emission, passing from materials (hexadecamers and polymers) *alkyl-substituted* to materials *S-alkyl-substituted*, due to inserting of a β -sulfur (which has great electron-donating properties) between the thiophene backbone and the side-alkyl chains.

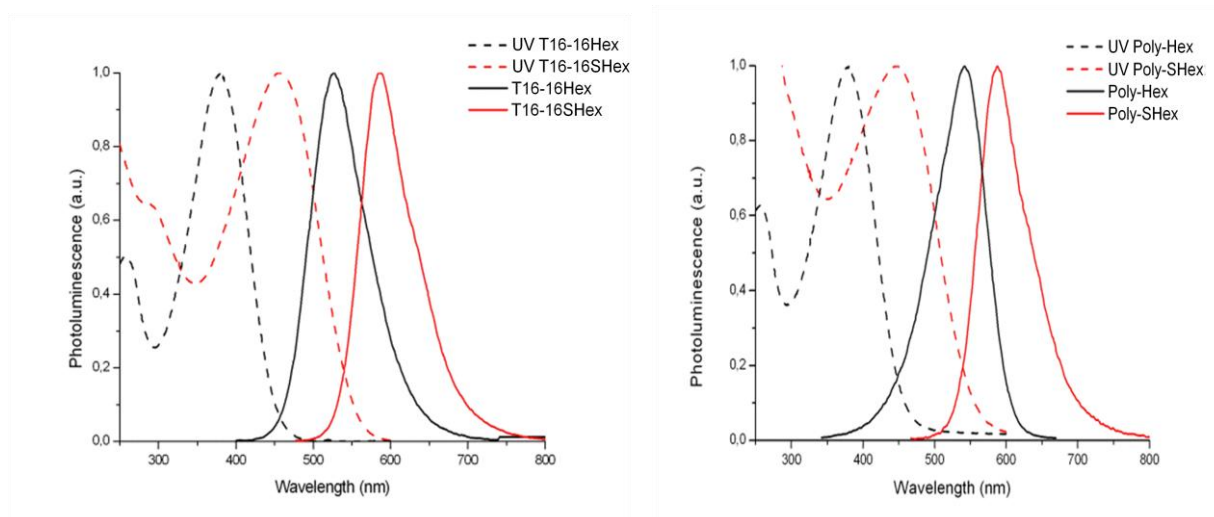


Figure 101. Normalized UV (dash line) and PL (normal line) of hexadecamers- and polythiophenes in CH_2Cl_2 .

Furthermore the UV and PL curves show, that none red-shift is moving from the hexadecamers to the polymers, indicating that these hexadecamers are materials sufficiently long, and therefore able to mime the morphological and optical properties of a polymer.

The same behavior was observed for dimers, tetramers and octamers, red-shift also observed to grow of the dimension of the material for the same type of functionalization *alkyl* or *S-alkyl* (Figure 102 and Table 4)

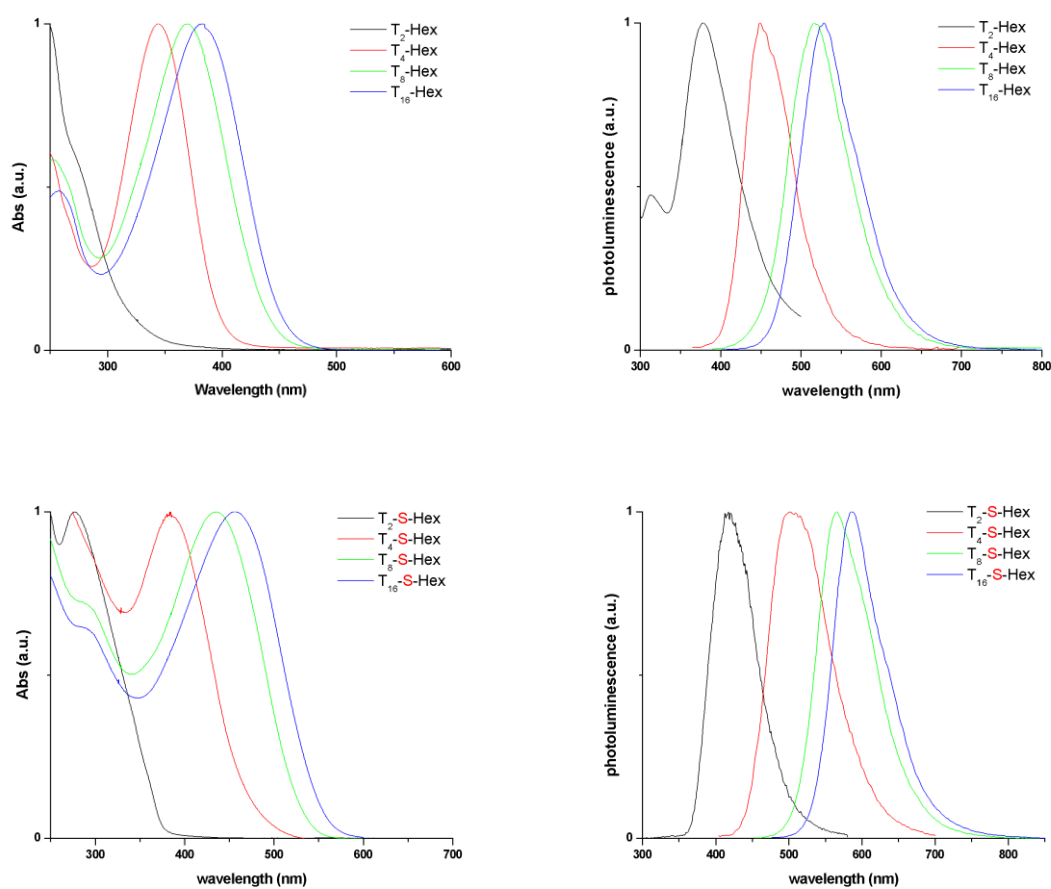


Figure 102. Normalized UV (left) and PL (right) of oligo(alkylthiophenes) and oligo(alkylsulphanylthiophenes) in CH₂Cl₂

Materials	λ_{MAX}	λ_{PL}	ϵ
T2-2Hex / T2-2SHex	275 / 278	378 / 417	11957 / 7396
T4-4Hex / T4-4SHex	345 / 383	448 / 501	24195 / 14839
T8-8Hex / T8-8SHex	369 / 434	516 / 566	51161 / 47713
T16-16Hex / T16-16SHex	382 / 456	529 / 586	98724 / 95069

Table 4. UV, PL and ϵ values for oligo(alkylthiophenes) and oligo(alkylsulphanylthiophenes) in CH_2Cl_2 .

Very interesting is to observe the values of the *molar absorption coefficient* (ϵ) which for the hexadecamers are among the highest reported in the literature, concerning **OTs**-based thiophene; a light decrease of the ϵ for materials *S-alkyl* substituted is probably due to higher distorsion as suggests the bigger stokes-shits of these *S-alkyl* compounds than those *alkyl-substituted*.

Concerning the polymers (**Table 5**), they show discrete values of *polydispersity* (**PDI**); from GPC data we understand the importance to improve our synthetic protocol in order to obtain polymers longer with lower **PDI** values.

Material	λ_{max}^a	λ_{PL}^a	Mn^c	MW^c	PDI^c
<i>Poly-Hex</i>	379	541	8612	14649	1.7
<i>Poly-SHex</i>	457	588	11056	22787	2.06

Table 5. Gel Permeation Chromatography in THF using standard Polystyrene (PS)

▪ Cast-film Morphology of T16-16SHex

In comparison to the octamers (see Chapter IV) in which secondary helical structure was present in most fibers with the exception of the only octamer lacking substituents on terminal bithiophene subsystems, for the hexadecamer T16-16SHex (as well as for the other materials synthesized above by our synthetic protocol) was not observed (in same condition under CH₃CN vapours) supramolecular aggregates but an amorphous morphology (**Figure 103**).

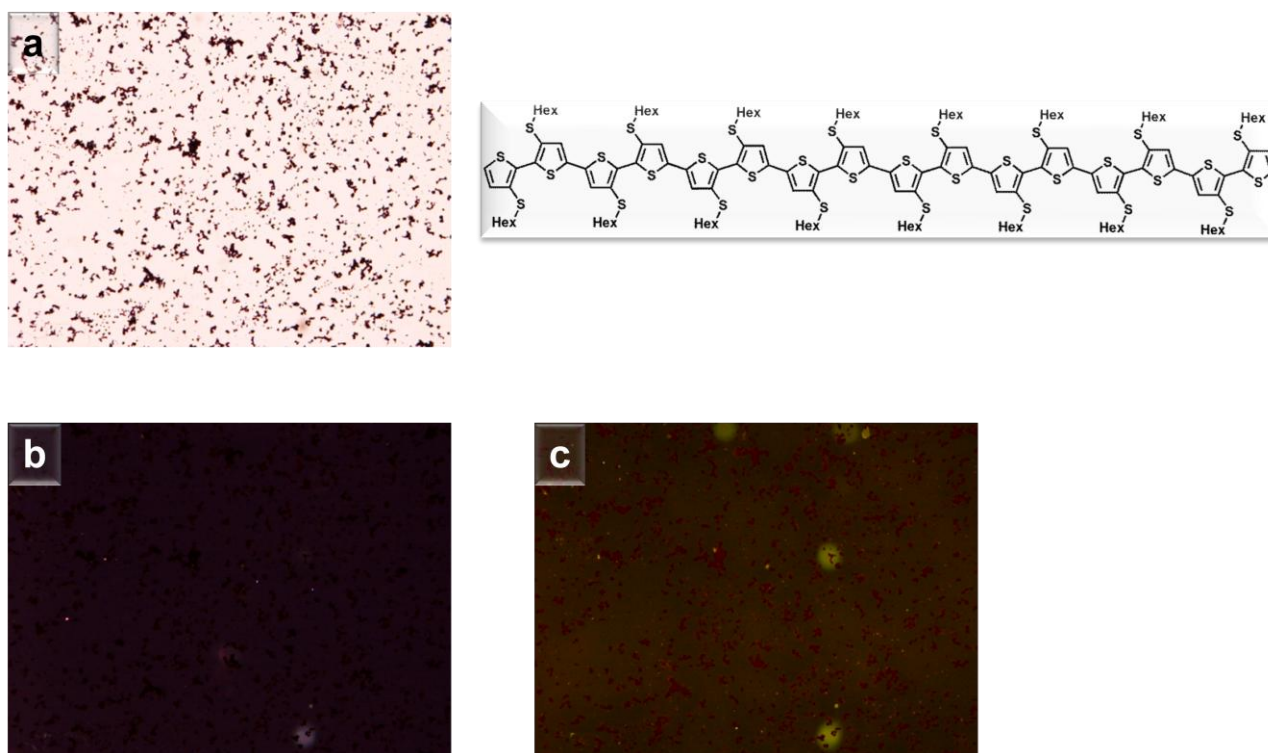


Figure 103. a) Light transmission optical microscopy; b) Optical microscopy with cross polars; c) Fluorescence microscopy

It is very important to emphasize that the morphology of this compound make it particularly useful and usable in the field of organic photovoltaics as *p*-donor material.

In fact the realization of a **BHJ** solar cells requires an intimate mixture between the *donor-material* with the *acceptor-material* (generally **PCBM**), and at this purpose an amorphous morphology, like that of the *T16-16SHex*, allows a better mixing of the two parties *donor-acceptor* (**Figure 104**).

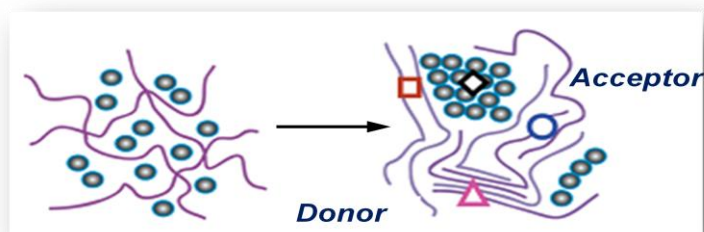


Figure 104. A typical intimate mixing between a donor material and an acceptor material for the building of a BHJ solar cell.

To the contrary when we tried a mixing using the octamers (which present a crystalline morphology, see Chapter IV) as donor-materials, the mixing gave segregation with the acceptor-material not allowing the realization of the blend.

Finally we synthesized, by an eco-friendly synthetic protocol, a new class of head-to-head hexadecamers based thiophene, which are homogeneous materials (monodispersed) with optical and morphological properties easily reproducible, and for these reasons particularly interesting in organic photovoltaic as *p-donor* materials.

▪ T16-16SHex / PCBM BHJ Solar Cells

On the basis of the experimental data obtained, we have realized, in collaboration with the NNL of Lecce, a BHJ solar cell using the *hexadecamers* as *p-donor* materials and the PCBM as *n-acceptor* source.

We note (**Figure 105**) that while for the blend realized with the T16-16Hex no current signal was registered, for the blend realized with the T16-16SHex a flow of electricity both in dark (D) and in illumination (L) was observed.

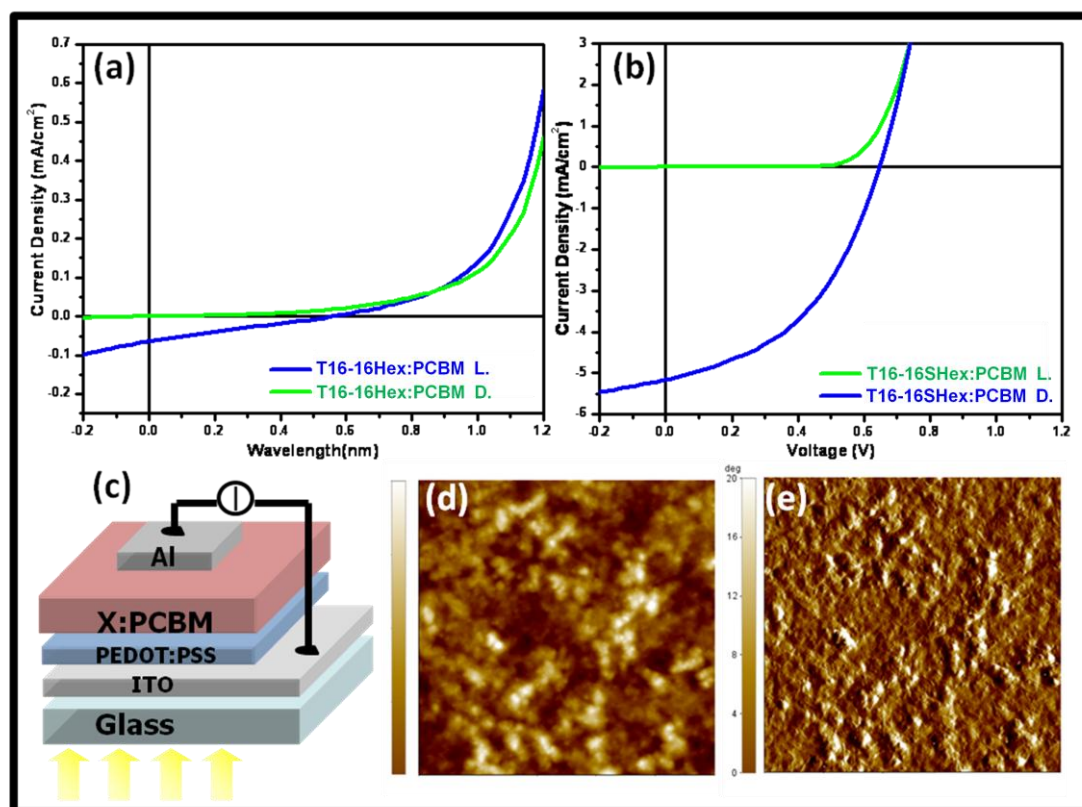


Figure 105. Current density-Voltage characteristics in illumination and in dark of the device with T16-16Hex; a) and with T16-16SHex; b) under 100 mW / cm² A.M. 1.5G conditions; c) Schematic representation of the layer structure; d) AFM topography d) and phase e) of the active layer with T16-16SHex, scan size 5×5µm.

Furthermore the UV curves in solid-state (**Figure 106**), relative to different typologies of blends, show (the green line) how the curve relative to the *PCBM-T16-16SHex* blend covers the whole UV-VIS region and mimics almost completely the curve (the blue line) inherent to the *P3HT-PCBM* blend.

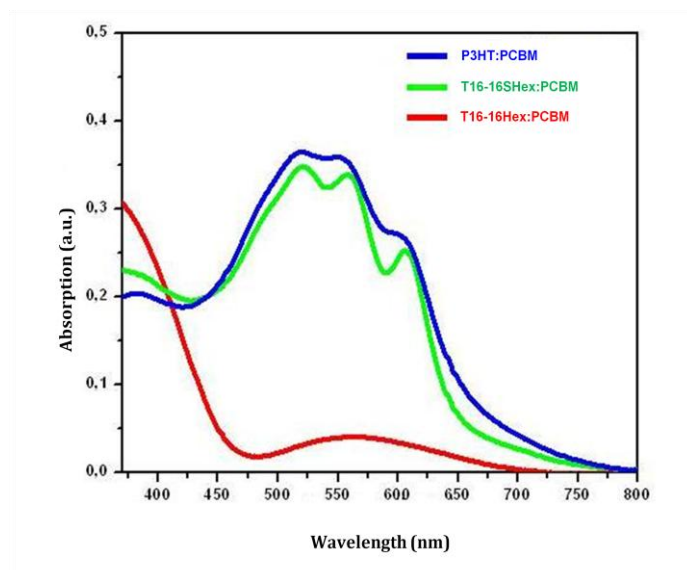


Figure 106. Absorption spectra in solid-state of device with T16-16Hex (red), T16-16SHex (green) and P3HT (blue).

Therefore, preliminary results (**Table 6**) indicate that while for the blend *T16-16Hex:PCBM* the efficiency is c.a. zero, for the blend realized with the hexadecamer *S*-alkyl-substituted efficiency up to 1.5% was recorded.

Materials	η (%)	FF	V_{OC} (V)	J_{sc} (mA/cm ²)	R_p (Ωcm^2)	R_s (Ωcm^2)
T16-16Hex:PCBM	0.01	0.25	0.56	0.06	$0.9 \cdot 10^5$	$1.1 \cdot 10^4$
T16-16SHex:PCBM	1.5	0.46	0.64	5.13	$1.2 \cdot 10^5$	59

Table 6. Summary of Device Properties Prepared for T16-16Hex and T16-16SHex.

Furthermore preliminary x-Ray studies (not reported) highlights that both *T16-16Hex* and *T16-16SHex*, at sub nanometric level, are not completely amorphous, presenting instead a certain degree of supramolecular organization.

Therefore the lower crystallinity degree of the *T16-16SHex* is without doubts an ulterior prove of how this material shows a better blend response in *BHJ-solar cell*, whereas a more amorphous morphology permits a better uniform mixing of the blend constituents.

5.3 Conclusions

We have synthesized new regioregular *head-to-head hexadecamers and polymers based-thiophene* in short reaction times, good yields and environmentally friendly procedure by taking advantage of *ultrasound* and *microwave* assistance.

This new class of *head-to-head hexadecamers* are homogeneous-monodispersed materials, with reproducible physical and chemical properties, with optical and morphological properties similar to those of polymers, and for these reasons particularly interesting in organic photovoltaic field as *p-donor* materials, showing an efficiency up to 1.5% in B_HJ solar cells.

Certainly this first result very important and encouraging, not only can be improved but above all puts on light once again the strong electron-donating properties of *β-sulfur* inserted between the *alkyl-side chains* and the thiophene backbone, important on the optical and electrochemical properties as well as the thin film morphology of these materials.

5.4 Experimental Section

5.4.1 General

▪ *Synthesis*

Unless otherwise noted, all operations were carried out under a dry, oxygen-free nitrogen atmosphere. Organic solvents were dried by standard procedures. TLC was carried out with 0.2-mm thick of silica gel 60 F₂₅₄ (Merck). Visualization was accomplished by UV light or phosphomolybdic acid solution. Preparative column chromatographies was performed on glass columns of different sizes hand packed with silica gel 60 (particle sizes 0.040-0.063 mm, Merck). Petroleum ether refers to the fraction of bp 40-70°C. *N*-bromosuccinimide, sodium bicarbonate were purchased from Sigma-Aldrich Co; 1,1'-bis (diphenylphosphino) ferrocene palladium(II) chloride dichloromethane complex (PdCl₂dppf), potassium fluoride were obtained from Acros Organics; 2-isopropoxy-4,4,5,5-tetramethyl-1,3,2-dioxaborolane, Bis(pinacolato)diboron from Alfa Aesar GmbH & Co KG.

All reagents and solvents were used as received. Compounds **1**, **1a**, **2**, **2a**, **3**, **3a**, **4**, **4a**, **5**, **5a** have already been described.⁴³⁵

Microwave experiments were carried out in a Milestone Microsynth Labstation operating at 2450 MHz monitored by a proprietary control unit. The oven was equipped with magnetic stirring, pressure and temperature sensors.

Reactions were performed in a glass vessel (capacity 10 mL) sealed with a septum.

The microwave method was power controlled (100 W maximum power input) and the samples were irradiated with the required power output (setting at the maximum power) to achieve the desired temperature (80°C).

Reactions with ultrasound were performed in a FALC LBS1 50KHz Ultrasonic bath at room temperature. Melting points were determined on Kofler bank apparatus and are uncorrected.

All ^1H NMR and ^{13}C NMR spectra were recorded on a Varian Mercury-400 spectrometer equipped with a 5-mm probe. Chemical shifts were calibrated using the internal CDCl_3 or benzene- d_6 resonance which were referenced to TMS.

Mass spectra were collected on a Finningan Mat GCQ spectrometer. UV-Vis spectra were recorded using a Perkin Elmer Lambda 20 spectrometer.

Photoluminescence spectra were collected on a Perkin Elmer LS50 spectrofluorometer. Fluorescence measurements were performed using an excitation wavelength corresponding to the maximum absorption lambda.

▪ **Characterization**

X-ray diffraction

Analysis was carried out by means of a PANalytical X'Pert diffractometer equipped with a copper anode ($\lambda_{\text{mean}} = 0.15418 \text{ nm}$) and a fast X'Celerator detector. Films grown on glass cover slips were directly investigated.

Electrochemistry

Oligomer films on ITO electrodes (Balzers) were obtained by drop casting from toluene in air or in acetonitrile saturated air. The films were characterized in PC 0.1 mol·L⁻¹ (C₂H₅)₄NBF₄ purged by Ar bubbling, where they are insoluble (SI for more details).

5.4.2 Materials

General procedure for the synthesis of bromothieryl-derivatives 6, 6a, 8, 8a

To a solution of 5, 5a, 1, 1a (1 mmol) in DMF, 1 mmol or 2 mmol of NBS were added. The reaction mixture was sonicated for 12 min at room temperature. The solvent was removed and the products were purified by flash chromatography.

5-Bromo-3,3',3''',3''''',3''''''', 4'', 4''''', 4'''''''-Octahexyl-octithiophene

Yield 65%. Yellow powder; ¹H NMR (400 MHz, C₆D₆): δ 7.26 (s, 1H), 7.255 (s, 1H), 7.25 (s, 1H), 7.22 (s, 1H), 7.21 (s, 1H), 7.19 (s, 1H), 6.86 (d, ³J=5.2 Hz, 2H), 6.85 (s, 1H), 6.81 (d, ³J=5.2 Hz, 2H), 2.62–2.45 (m, 16H), 1.46–1.37 (m, 16H), 1.20–1.02 (m, 48H), 0.81–0.78 (m, 24H); ¹³C NMR (400 MHz, C₆D₆): δ 136.9, 136.8, 136.78, 136.68, 136.62, 135.5, 134.6, 134.0, 133.9, 133.8, 133.7, 133.69, 133.4, 133.2, 133.0, 132.9, 132.85, 132.82, 132.7, 132.6, 132.5, 132.2, 131.3, 127.6, 126.3, 113.6, 36.57, 36.56, 36.55, 36.52, 36.42, 36.34, 36.26, 31.7, 31.69, 31.65, 31.62, 30.2, 29.9, 29.8, 29.76, 29.72, 29.03, 28.7, 28.66, 28.65, 28.64, 22.96, 22.93, 22.92, 14.3, 14.27.

**5-Bromo-3,3',3''',3''''',3''''''', 4'', 4''''', 4'''''''-
octakis (hexylthio) -octithiophene**

Yield 35%. Yellow powder; ^1H NMR (400 MHz, CDCl_3 , TMS/ppm): δ 7.30 (d, $^3J=5.2$ Hz, 2H), 7.04 (m, 5H), 7.02 (s, 1H), 6.97 (d, $^3J=5.2$ Hz, 2H), 6.94 (s, 1H), 2.56–2.46 (m, 16H), 1.60–1.55 (m, 16H), 1.28–1.26 (m, 48H), 0.89–0.86 (m, 24H); ^{13}C NMR (400 MHz, CDCl_3): δ 143.8, 143.44, 143.4, 143.39, 143.2, 142.5, 137.3, 137.05, 137.0, 136.9, 136.74, 136.70, 131.4, 129.9, 128.6, 128.3, 127.8, 127.5, 127.4, 127.3, 127.2, 126.3, 125.4, 125.2, 125.1, 125.08, 125.0, 124.96, 111.9, 31.64, 31.63, 31.6, 30.7, 30.6, 30.5, 29.7, 29.11, 29.1, 29.09, 29.07, 29.03, 29.0, 28.94, 28.88, 28.83, 22.6, 22.57, 22.58, 22.56, 14.09, 14.08.

General procedure for the synthesis of 7, 7a, 9 and 9a.

A mixture of the bromothiényl-derivative **6**, **6a**, **8** or **8a** (1 mmol), bis(pinacolato)diboron (0.6 mmol), PdCl_2dppf (0.05 mmol), NaHCO_3 (2 mmol) in THF/water 2:1 (3 mL) was irradiated with microwaves at 80°C . The reaction mixture was brought to room temperature and the solvent was evaporated under reduced pressure. All compounds were purified by flash chromatography with increasing amounts of CH_2Cl_2 in cyclohexane as eluent.

3,3',3''',3''''',3''''''', 4'', 4''''', 4'''''''-hexakis(hexylthio)-hexadecanthiophene

Yield 80%. Yellow powder mp 73°C; ^1H NMR (400 MHz, CDCl_3 , TMS/ppm): δ 7.30 (d, $^3J=5.2$ Hz, 2H), 7.05–7.04 (m, 7H), 6.98 (d, $^3J=5.2$ Hz, 2H), 2.58–2.46 (m, 16H), 1.60–1.57 (m, 16H), 1.30–1.26 (m, 48H), 0.89–0.85 (m, 24H); ^{13}C NMR (400 MHz, CDCl_3): δ 143.44, 143.42, 143.4, 143.39, 143.2, 142.5, 137.0, 136.94, 136.9, 128.6, 128.3, 127.8, 127.4, 127.36, 127.35, 127.2, 125.4, 125.1, 125.0, 31.65, 31.6, 30.7, 30.62, 30.6, 29.7, 29.1, 29.08, 29.07, 29.04, 28.94, 28.88, 22.6, 22.58, 22.57, 14.08, 14.06. UV/Vis: λ_{max} 381 nm (ϵ 98724 $\text{cm}^{-1}\text{M}^{-1}$), λ_{em} . 528 nm in CH_2Cl_2 .

3,3',3''',3''''',3''''''', 4'', 4''''', 4'''''''....(hexylthio)-hexadecan thiophene

Yield 60%. Red-purple powder mp 67°C; ^1H NMR (400 MHz, CDCl_3 , TMS/ppm): δ 7.27–7.26 (m, 6H), 7.22 (s, 1H), 6.87 (d, $^3J=5.2$ Hz, 2H), 6.81 (d, $^3J=5.2$ Hz, 2H), 2.63–2.57 (m, 16H), 1.47–1.42 (m, 16H), 1.19–1.02 (m, 48H), 0.83–0.77 (m, 24H); ^{13}C NMR (400 MHz, CDCl_3): δ 136.9, 136.75, 136.71, 136.67, 134.0, 133.8, 133.7, 133.0, 132.9, 132.8, 132.72, 132.7, 132.5, 131.3, 126.3, 36.6, 36.55, 36.4, 36.3, 31.7, 31.68, 30.1piccoacetone, 29.9, 29.8, 28.7, 28.66, 23.0, 22.9, 14.3, 14.28. UV/Vis: λ_{max} 457 nm (ϵ 95069 $\text{cm}^{-1}\text{M}^{-1}$), λ_{em} . 586 nm in CH_2Cl_2 .

Polymers

A mixture of the bromothieryl-derivative **8**, **8a** (1 mmol), bis(pinacolato)diboron (0.6 mmol), PdCl₂dppf (0.05 mmol), NaHCO₃ (2 mmol) in THF/water 2:1 (3 mL) was irradiated with microwaves at 80°C. The reaction mixture was brought to room temperature and the solvent was evaporated under reduced pressure.

Poly-hex

M_w: 14600, M_n: 8600 PDI: 1.7

UV/Vis: λ_{max} 378 nm, λ_{em.} 529 nm in CH₂Cl₂.

Poly-Shex

M_w: 22787 M_n: 11056 PDI: 2.06

UV/Vis: λ_{max} 448 nm, λ_{em.} 588 nm in CH₂Cl₂.

5.4.3 ¹H and ¹³C NMR Spectra

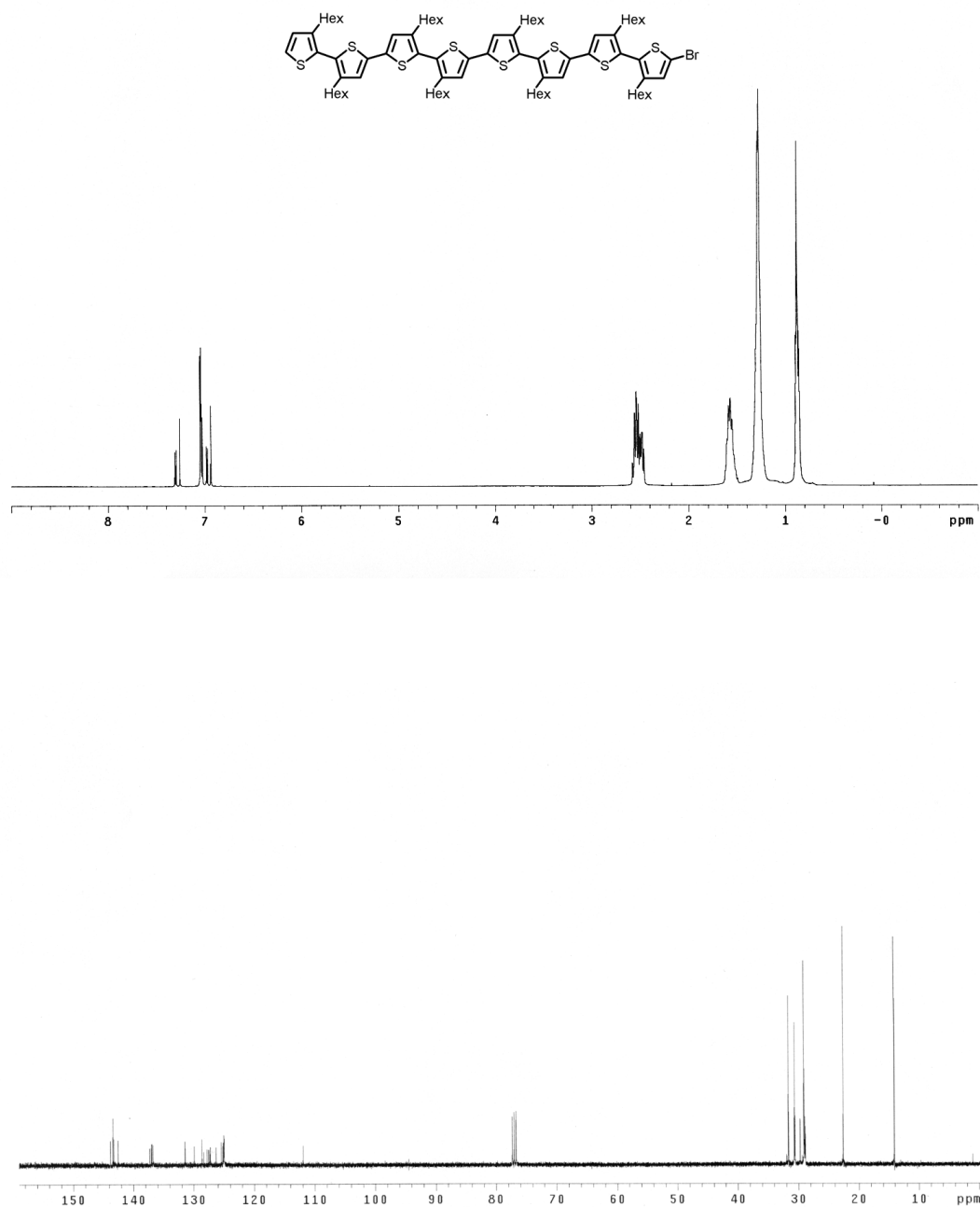


Figure S16. ¹H and ¹³C NMR spectra of compound 6.

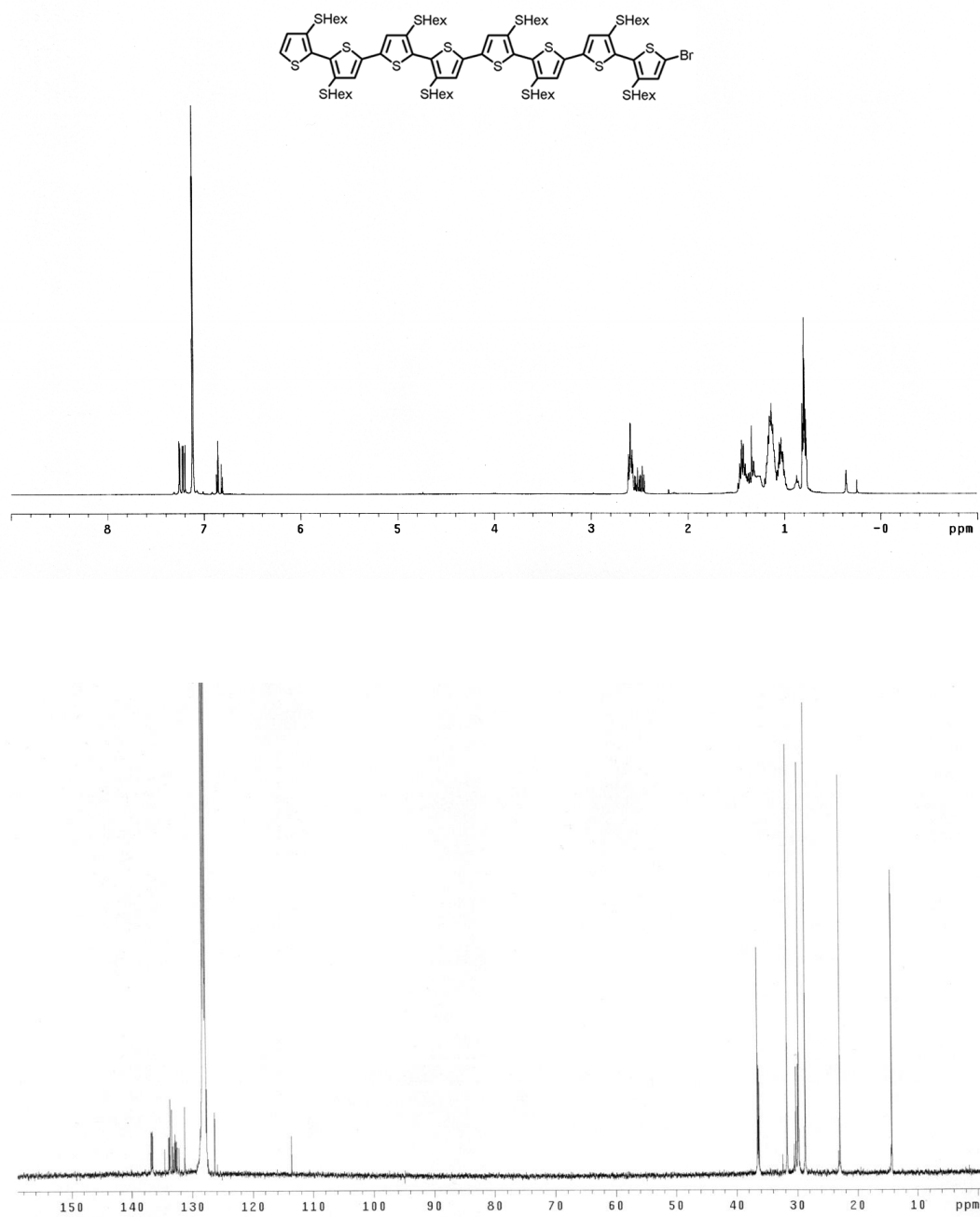


Figure S17. ¹H and ¹³C NMR spectra of compound 6a.

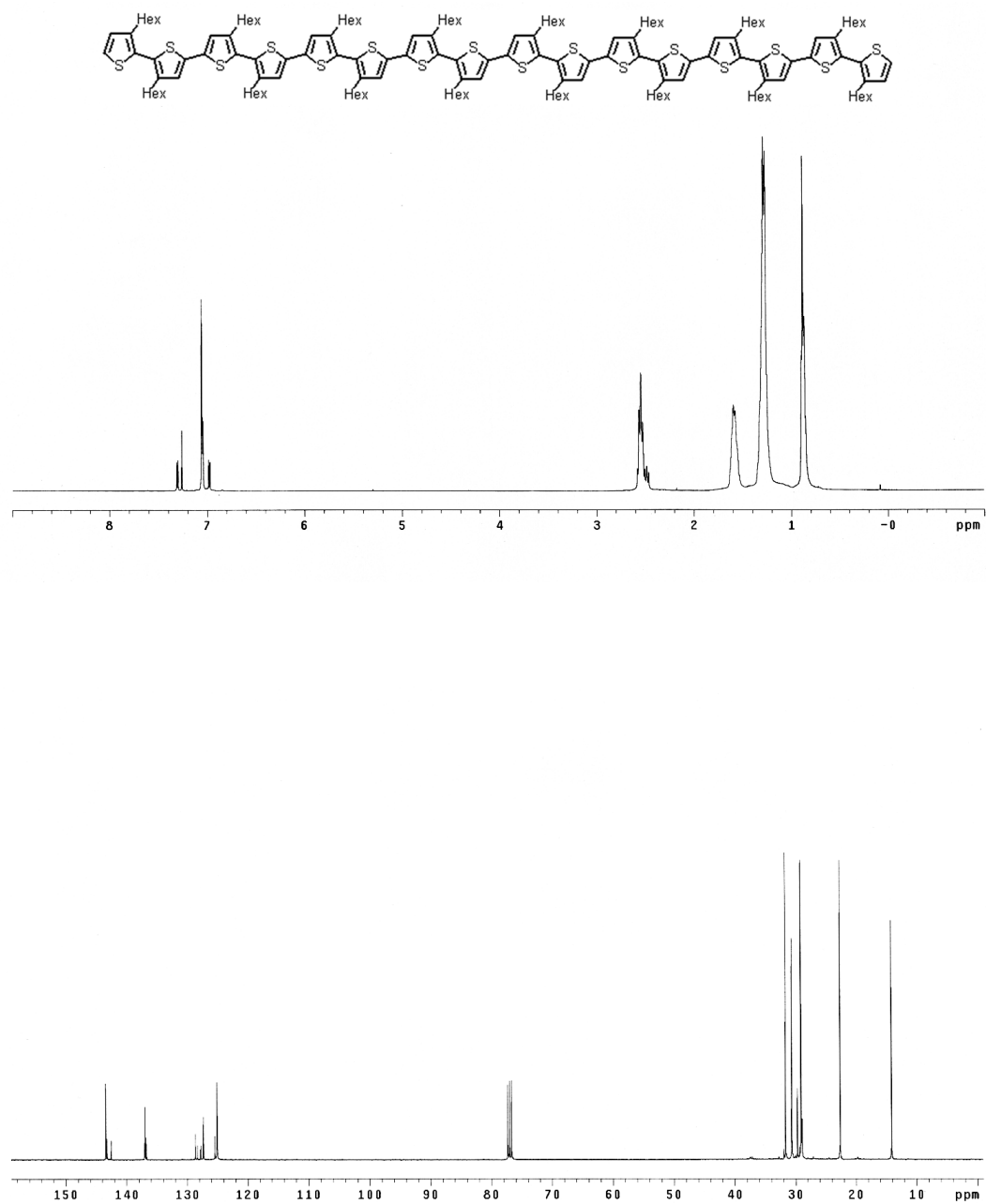


Figure S18. ¹H and ¹³C NMR spectra of compound 7.

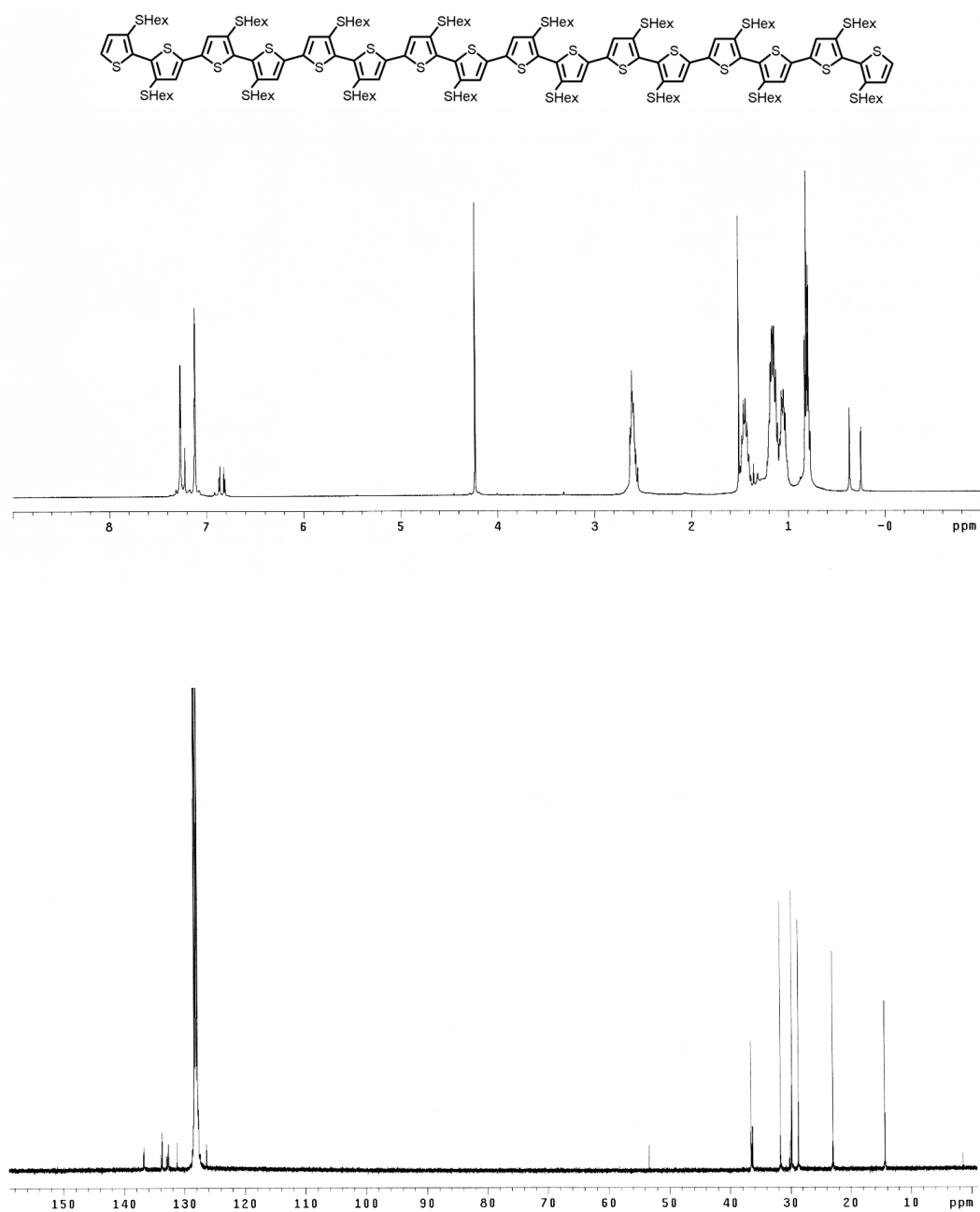


Figure S19. ¹H and ¹³C NMR spectra of compound 7a.

5.5 References

- [422] A. R. Murphy, J. M. J. Fréchet, *Chem. Rev.*, **2007**, *107*, 1066
- [423] B. C. Thompson, J. M. J. Fréchet, *Angew. Chem. Int. Ed.* **2008**, *47*, 58
- [424] B. Kippelen, J. L. Brédas, *Energy Environ. Sci.*, **2009**, *2*, 251
- [425] Y. J. Cheng, S. H. Yang, C. S. Hsu, *Chem. Rev.* **2009**, *109*, 5868
- [426] W. Ma, C. Yang, X. Gong, K. Lee, A. J. Heeger, *Adv. Funct. Mater.*, **2005**, *15*, 1617-1622
- [427] G. Li, V. Shrotriya, J. Huang, Y. Yao, T. Moriarty, K. Emery, Y. Yang, *Nat. Mater.*, **2005**, *4*, 864-868
- [428] N. Noma, T. Tsuzuki and Y. Shirota, *Adv. Mater.*, **1995**, *7*, 647
- [429] A. Mishra, C. Q. Ma, and P. Bäuerle, *Chem. Rev.*, **2009**, *109*, 1141
- [430] F. Babudri, G. M. Farinola, F. Naso, *J. Mater. Chem.*, **2004**, *14*, 11-34
- [431] I. Osaka, R. D. McCulloch, *Acc. Chem. Res.*, **2008**, *41*, 1202-1214
- [432] F. Di Maria, P. Olivelli, A. Zanelli, M. Biasucci, G. Gigli, D. Gentili, P. D'Angelo, M. Cavallini, and G. Barbarella, *J. Am. Chem. Soc.*, **2011**, *133*, 8654-8661
- [433] A. Suzuki, *Chem. Commun.*, **2005**, 4759-4763
- [434] S. Alesi, F. Di Maria, M. Melucci, D. J. Macquarrie, R. Luque, G. Barbarella, *Green Chem.*, **2008**, *10*, 517-523
- [435] F. Di Maria, P. Olivelli, A. Zanelli, M. Biasucci, G. Gigli, D. Gentili, P. D'Angelo, M. Cavallini, and G. Barbarella, *J. Am. Chem. Soc.*, **2011**, *133*, 8654-8661

Conclusions

During this PhD thesis an innovative Suzuki-Miyaura⁴³⁶ synthetic protocol for the preparation of highly pure *head-to-head* oligo- and polythiophenes for application in photovoltaics was developed by taking advantage of *ultrasound (US)* and *microwave (MW)* assistance.^{437,438}

Thanks to this new environmentally friendly procedure, it was possible to synthesize different thiophene-based materials in short times and high purity.

In particular, by our protocol we were able to prepare two new *head-to-head alkyl* and *S-alkyl* substituted oligo- and polythiophene classes.

By comparison of the properties of the two different classes, it was possible to establish that the presence of the β -sulfur inserted between the alkyl-side chains and the thiophene scaffold plays a crucial role in determining the electrical and morphological properties of the compounds.

We found that *S-hexyl* substituted thiophene octamers achieved the right balance of size, conformation, and shape to self-assemble in ordered crystalline *helical fibrils* characterized by intense fluorescence and high charge mobility.

Contrary to *S-alkyl* substituted octamers, the corresponding hexadecamers were amorphous.

Their photovoltaic properties were tested in blend with a fullerene derivative in BHJ solar cell and found to afford a quite significant 1.5% conversion efficiency.

By contrast, the *alkyl* substituted hexadecamer afforded in the same experimental conditions an efficiency of only 0.1%.

[436] N. Miyaura and A. Suzuki, *Chem. Rev.*, **1995**, *95*, 2457-2483

[437] S. Alesi, F. Di Maria, M. Melucci, D. J. Macquarrie, R. Luque, G. Barbarella, *Green Chem.*, **2008**, *10*, 517-523

[438] V. Paul, A. Sudalai, T. Daniel, K. V. Srinivasan, *Synth. Commun.*, **1995**, *25*, 2401-2405